ornl

ORNL6722

OAK RIDGE
NATIONAL
LABORATORY

MARTIN MARIETTA

# SOLID STATE DIVISION

# PROGRESS REPORT
# for Period Ending March 31, 1992

MANAGED BY
MARTIN MARIETTA ENERGY SYSTEMS, INC.
FOR THE UNITED STATES
DEPARTMENT OF ENERGY

ORNL--6722

DE93 003665

# SOLID STATE DIVISION PROGRESS REPORT for Period Ending March 31, 1992

J. B. Roberto, Director
L. A. Boatner, Section Head
J. F. Cooke, Section Head
B. C. Larson, Section Head
R. M. Moon, Section Head
D. M. Zehner, Section Head

*Edited by:*
P. H. Green
L. W. Hinton

*Date Published – September 1992*

Prepared for the
Division of Materials Sciences

Prepared by the
OAK RIDGE NATIONAL LABORATORY
Oak Ridge, Tennessee 37831
managed by
MARTIN MARIETTA ENERGY SYSTEMS, INC.
for the
DEPARTMENT OF ENERGY
UNDER CONTRACT NO. DE-AC05-84OR21400

*Reports previously issued in this series are as follows:*

| | |
|---|---|
| ORNL-1095 | Period Ending April 30, 1951 |
| ORNL-1128 | Period Ending July 31, 1951 |
| ORNL-1214 | Period Ending October 31, 1951 |
| ORNL-1261 | Period Ending January 31, 1952 |
| ORNL-1301 | Period Ending May 10, 1952 |
| ORNL-1359 | Period Ending August 10, 1952 |
| ORNL-1429 | Period Ending November 10, 1952 |
| ORNL-1506 | Period Ending February 10, 1953 |
| ORNL-1606 | Period Ending August 30, 1953 |
| ORNL-1677 | Period Ending February 28, 1954 |
| ORNL-1762 | Period Ending August 31, 1954 |
| ORNL-1851 | Period Ending February 28, 1955 |
| ORNL-1852 | Period Ending February 28, 1955 |
| ORNL-1944 | Period Ending August 31, 1955 |
| ORNL-1945 | Period Ending August 31, 1955 |
| ORNL-2051 | Period Ending February 29, 1956 |
| ORNL-2052 | Period Ending February 29, 1956 |
| ORNL-2188 | Period Ending August 31, 1956 |
| ORNL-2189 | Period Ending August 31, 1956 |
| ORNL-2413 | Period Ending August 31, 1957 |
| ORNL-2414 | Period Ending August 31, 1957 |
| ORNL-2614 | Period Ending August 31, 1958 |
| ORNL-2829 | Period Ending August 31, 1959 |
| ORNL-3017 | Period Ending August 31, 1960 |
| ORNL-3213 | Period Ending August 31, 1961 |
| ORNL-3364 | Period Ending August 31, 1962 |
| ORNL-3480 | Period Ending May 31, 1963 |
| ORNL-3676 | Period Ending May 31, 1964 |
| ORNL-3841 | Period Ending May 31, 1965 |
| ORNL-3935 | Period Ending December 31, 1965 |
| ORNL-4098 | Period Ending December 31, 1966 |
| ORNL-4250 | Period Ending December 31, 1967 |
| ORNL-4408 | Period Ending December 31, 1968 |
| ORNL-4526 | Period Ending December 31, 1969 |
| ORNL-4669 | Period Ending December 31, 1970 |
| ORNL-4779 | Period Ending December 31, 1971 |
| ORNL-4861 | Period Ending December 31, 1972 |
| ORNL-4952 | Period Ending December 31, 1973 |
| ORNL-5028 | Period Ending December 31, 1974 |
| ORNL-5135 | Period Ending December 31, 1975 |
| ORNL-5328 | Period Ending April 30, 1977 |
| ORNL-5486 | Period Ending September 30, 1978 |
| ORNL-5640 | Period Ending February 29, 1980 |
| ORNL-5850 | Period Ending September 30, 1981 |
| ORNL-5975 | Period Ending March 31, 1983 |
| ORNL-6128 | Period Ending September 30, 1984 |
| ORNL-6306 | Period Ending March 31, 1986 |
| ORNL-6453 | Period Ending September 30, 1987 |
| ORNL-6571 | Period Ending March 31, 1989 |
| ORNL-6664 | Period Ending September 30, 1990 |

# Contents

## *BUCKYBALLS, SAND PILES, BAND TAILS, AND MORE*



# 2. *Superconductivity*

## *THEORY*

## *THIN FILMS*

## *BULK MATERIALS*

# 3. *Neutron Scattering*

## *SMALL-ANGLE SCATTERING AND NEUTRON REFLECTOMETRY*

## *NEUTRON DIFFRACTION*



## *INELASTIC NEUTRON SCATTERING*

# 4. Synthesis, Processing, and Characterization of Materials

## SOLID ELECTROLYTES AND THIN-FILM BATTERIES



## PEROVSKITE STRUCTURE OXIDES

## *OPTICAL CHARACTERIZATION OF IMPURITIES AND DEFECTS*

## *MATERIALS PROPERTIES*



# *5. Ion Beam and Laser Processing*

## *ION BEAM PROCESSING*

## *ION IMPLANTATION AND ANALYSIS*

## *LASER AND MOLECULAR BEAM PROCESSING OF THIN FILMS*

# 6. *Structure of Solids and Surfaces*

## *SURFACE PHYSICS*

## *ELECTRON MICROSCOPY*



## *X-RAY DIFFRACTION*

# *Acronyms*

AES – auger electron spectroscopy
ANS – Advanced Neutron Source
APS – Advanced Photon Source
APECS – Auger-photoelectron coincidence spectroscopy
BCA – binary collision approximation
CHESS – Cornell High-Energy Synchrotron Source
CPA – constant-phase angle
CVD – chemical vapor deposition
DSC – differential scanning calorimetry
ECR – electron cyclotron resonance
EDX – energy dispersive x-ray
EELS – electron energy loss spectroscopy
EPR – electron paramagnetic resonance
FWHM – full width at half maximum
HFIR– High Flux Isotope Reactor
HPLC – high-performance liquid chromatography
HREM – high-resolution electron microscopy
HREELS – high-resolution electron energy loss spectroscopy
HRLEED – high-resolution low-energy electron diffraction
HRTEM – high-resolution transmission electron microscopy
HTSC – high-temperature superconductors
IBD – ion beam deposition
IPNS – Intense Pulsed Neutron Source
LDA – local density approximation
LEED – low-energy electron diffraction
MBE – molecular beam epitaxy
MOCVD – metallo-organic chemical vapor deposition
NSLS – National Synchrotron Light Source
PIGE – proton-induced gamma emission
PIXE – particle-induced x-ray emission
PLA – pulsed-laser ablation
PLD – pulsed-laser deposition
QMS – quadrupole mass spectrometer
RBS – Rutherford backscattering spectroscopy
RHEED – reflection high-energy electron diffraction
SANS – small-angle neutron scattering
SAXS – small angle x-ray scattering
SEM – scanning electron microscopy
SPEG – solid-phase-epitaxial growth
STEM – scanning transmission electron microscopy
STM – scanning transmission microscopy
TCR – thermochemical reduction
TDS – thermal desorption spectroscopy
TEM – transmission electron microscopy
TRR – time-resolved reflectivity
UHV – ultrahigh vacuum
UIUC – University of Illinois at Urbana-Champaign
WAND – wide-angle neutron diffractometer
WAXD – wide-angle x-ray diffraction
XDCD – x-ray double-crystal diffraction
XPS – x-ray photoemission spectroscopy
YSZ – yttria-stabilized zirconia

# *Introduction*

This report covers research progress in the Solid State Division from October 1, 1990, to March 31, 1992. During this period, the division conducted a broad, interdisciplinary materials research program with emphasis on theoretical solid state physics, superconductivity, neutron scattering, synthesis and characterization of materials, ion beam and laser processing, and the structure of solids and surfaces. This research effort was enhanced by the return of the High Flux Isotope Reactor (HFIR) to full operation, new emphasis on the synthesis and processing of materials, and increased partnering with industry and universities.

The theoretical effort was broadened to include numerical simulation of surfaces and interfaces, stimulated by recent advances in high-performance computing and by strong interest in related division experimental programs. Superconductivity research continued to advance on a broad front from fundamental mechanisms of high-temperature superconductivity to the development of new conductors and processing techniques. The neutron scattering program was enhanced by a healthy scientific user program and growing diversity represented by new initiatives in colloidal materials, residual stress, and biological materials.

The national emphasis on materials synthesis and processing was mirrored in division research programs in thin-film processing, surface modification, and crystal growth. Research on advanced processing techniques such as laser ablation, ion implantation, and plasma processing was complemented by strong programs in the characterization of materials and surfaces including the continued development and application of Z-contrast scanning transmission electron microscopy. The materials processing research spanned the continuum from basic studies to applications and included more than a dozen cooperative research agreements with industry in superconductivity, thin-film battery materials, and photovoltaic materials.

In addition to the research progress summarized in the report, the division continued a tradition of service and leadership in the scientific community. During this period, 15 division staff members chaired or co-chaired national conferences and workshops, 10 served as national officers or executive committee members for professional societies, 15 served on national or international review committees, 6 served on editorial boards for technical journals, and 7 edited or co-edited books and proceedings.

# 1. *Theoretical Solid State Physics*

This chapter presents an overview of the current research activities of the Solid State Theory Program. As in the past, this research effort covers a diverse range of problems which not only are important from the theoretical perspective but also reflect the division's experimental programs. For purposes of this report, the work is organized into four categories—Superconductivity, Surfaces and Interfaces, Magnetism and Spin Dynamics, and other theoretical research activities. This chapter covers the last three categories. The work on superconductivity, which amounts to about one-third of the Program, can be found in the first section of Chapter 2.

As a result of a recent Exploratory Studies grant, the Solid State Theory Section has developed a molecular dynamics program which initially targeted the study of surfaces and interfaces. Relevant computer hardware was purchased, and scientific software was developed and tested. A version of the molecular dynamics computer code has also been developed to run on massively parallel computers. Results from studies of Si-Ge(001) stepped surfaces and edge dislocations in Si, Ge, and Ge-Si films have been obtained, and a study of ion implantation in buckyballs has been initiated. It is anticipated that this program will expand rapidly and will have a significant impact on many of the division's other experimental programs. In other surface-related work, the theoretical analysis of low-energy electron diffraction data has revealed an anomalous interplanar expansion at the (0001) surface of Be, as well as important structural information about MoRe and TaC(111) surfaces.

Results from research on magnetic systems include an explanation, at long last, of the effects of impurities on the magnetic ordering of Cr, predictions of high-energy spin-wave behavior for arbitrary directions of the wave vector in itinerant ferromagnets, predictions of spin-wave renormalization of a localized hole in a Heisenberg antiferromagnet, and predictions of the spin dynamics of electron-hole droplets in a strong magnetic field. In addition to the work on superconductivity, surfaces and interfaces, and magnetism, the diversity of the Program is reflected in results from studies of the orientational ordering of buckyballs, self-segregation in multicomponent sand piles, thin-film silicon photovoltaics, quasi-Fermi levels in quantum well photoluminescence, band tails and bandwidths in simple metals, impurity doping in inhomogeneous thermoelectrics, current dependence of the van der Waals interactions, and high-energy collision cascades.

# *SURFACES AND INTERFACES*

## ANOMALOUS INTERPLANAR EXPANSION AT THE (0001) SURFACE OF Be[1]

*H. L. Davis, J. B. Hannon,[2] K. B. Ray,[2] and E. W. Plummer[2]*

Oscillatory interplanar relaxation is such a general property of metal surfaces, with obvious repercussions on the static and dynamic properties, that it has attracted considerable theoretical interest. In a key paper, Finnis and Heine[3] applied the concept of surface charge smoothing at the surface, which creates electrostatic forces resulting in a contraction of the first interplanar spacing. Landman, Hill, and Mostoller[4] generalized this model by including a more realistic charge profile normal to the surface, which leads to oscillatory interplanar relaxations. There have been subsequent refinements of this model, but the general picture is the same as that presented by Landman, Hill, and Mostoller.[4] The more open faces have large contractions in the first interplanar spacings while the close-packed faces exhibit small changes, sometimes even expanding slightly. However, a recent LEED I-V analysis of the Be(0001) surface shows an anomalously large interplanar expansion of ~6%.

Beryllium has attracted considerable theoretical attention because of its anomalous nature. Atomic Be has an electronic configuration with completely filled orbitals ($1s^2 2s^2$), so the Be-Be potential might be expected to be weak. In fact, the binding energy of the dimer is only 0.1 eV. In the crystal, Be forms a very strong (3.32 eV/atom) and directional bond due to hybridization of the *s* and *p* bands. A possible explanation of the large interplanar expansion may be the interplay between the degree of hybridization and the number of nearest neighbors. Figure 1.1 illustrates the anomaly of the Be surface by displaying the change in the first

SSDN 4554

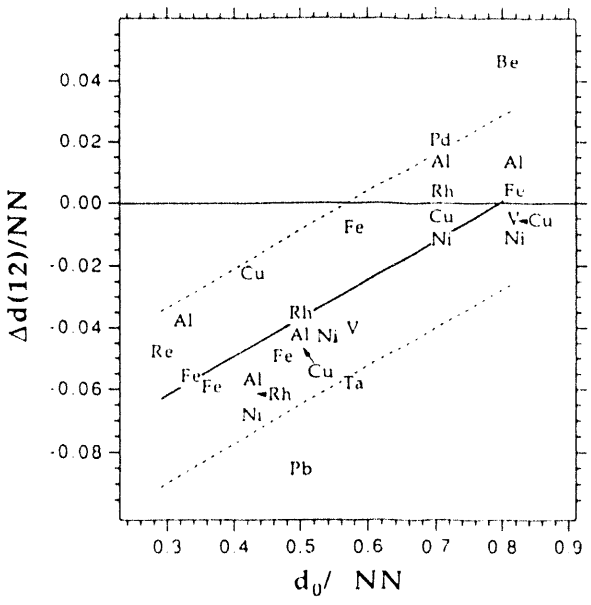


Fig. 1.1. A comparison of the experimentally determined interplanar changes $\Delta d(12)/NN$ as a function of the bulk interplanar spacing $d_0/NN$ for a wide range of metals. *NN* is the nearest neighbor distance in the bulk.

interplanar spacing $\Delta d(12)$ as a function of the bulk interplanar spacing for a large number of metal surfaces. Both first principles[5] and embedded atom[6] calculations of Be(0001) give a 4% expansion of the first interplanar spacing.

---

1. Summary of paper: *Phys. Rev. Lett.* **68**, 2632 (1992).

2. University of Pennsylvania, Philadelphia, Pa.
3. M. W. Finnis and V. Heine, *J. Phys. F* **4**, L37 (1974).
4. U. Landman, R. N. Hill, and M. Mostoller, *Phys. Rev. B* **21**, 448 (1980).
5. P. J. Feibelman, *Phys. Rev. B*, submitted for publication.
6. S. P. Chen, *Surf. Sci. Lett.* **264**, L162 (1992).

## SURFACE SEGREGATION OF RANDOM ALLOYS[1]

*H. L. Davis, B. Dötsch,[2] A. Wimmer,[2] K. Müller,[2] and D. M. Zehner*

Determining the surface composition as a result of surface segregation for random alloys is a necessary requirement for eventually understanding the chemical and physical reactions which take place at the surface. As part of a program concerned with these objectives, low-energy electron diffraction (LEED) has been used to investigate the (100) surfaces of $Mo_{0.75}Re_{0.25}$ and $Mo_{0.85}Re_{0.15}$ samples. Unreconstructed (1 × 1) patterns were observed following cleaning treatments, which involved sputtering, annealing, and heating in oxygen to remove residual carbon. The I-V profile data were collected using video data acquisition techniques with the incident electron beam normal to the surface and the sample maintained at a temperature of 100 K. Analysis of the data base differed from conventional LEED procedures in that a layer-by-layer version of the average *t*-matrix approximation was used to mimic the electron scattering from the randomly occupied sites. An *R*-factor analysis using the $R_2$ factor was used to determine the best agreement between experimental data and results of model calculations. Shown in Table 1.1 are results obtained for the layer-by-layer segregation of Mo and the interlayer relaxations for both samples. In both cases, the outermost layer is terminated almost completely in Mo with a subsequent reduction in the second layer.

**Table 1.1. Comparison of LEED Results for $Mo_{0.75}Re_{0.25}$(100) and $Mo_{0.85}Re_{0.15}$(100).**

| Layer | $Mo_{0.75}Re_{0.25}$ (100) | $Mo_{0.85}Re_{0.15}$ (100) |
|---|---|---|
| Layer-By-Layer Mo Segregation | | |
| 1 | 0.96 | 0.97 |
| 2 | 0.53 | 0.67 |
| 3 | 0.76 | 0.79 |
| 4 | 0.71 | 0.78 |
| 5 | 0.75 | 0.87 |
| 6 | 0.75 | 0.85 |
| Percent Relaxation of Interlayer Spacings | | |
| $\Delta d_{12}$ | -11.0 | -10.6 |
| $\Delta d_{23}$ | +5.2 | +5.1 |
| $\Delta d_{34}$ | -2.7 | -2.7 |
| $\Delta d_{45}$ | +3.3 | +3.0 |
| $\Delta d_{56}$ | -2.1 | -1.8 |
| $\Delta d_{67}$ | +2.4 | +2.6 |
| $\Delta d_{78}$ | -1.3 | -1.8 |
| Bulk spacing | 1.564 Å | 1.567 Å |

The first adsorption studies involved the interaction of hydrogen with the clean surface. Measurements with HREELS show that at 100 K, hydrogen dissociates on the surface and adsorbs in a bridge bond site, and at saturation there are two monolayers present. Results of LEED I-V

investigations of these surfaces show that while the relative elemental concentrations in each layer are virtually unchanged, most interlayer relaxations are reduced to <0.5% of the bulk value.

---

1. Summary of paper to be published.
2. Universität Erlangen–Nürnberg, Erlangen, Germany.

## A LOW-ENERGY ELECTRON DIFFRACTION (LEED) DETERMINATION OF THE TaC(111) TERMINATION[1]

*H. L. Davis, B. Dötsch,[2] and D. M. Zehner*

Since TaC crystallizes in the rock salt structure, bulk (111) planes are composed of either Ta or C atoms only and are stacked such that adjacent planes alternate in composition. Ideally, cleavage of TaC perpendicular to a [111] direction would produce two distinctly different (111) surfaces, one terminated in Ta and the other terminated in C. Although such cleavage is not possible, a TaC(111) surface can be prepared by standard cutting, polishing, sputtering, and annealing techniques. Since this crystal structure is not polar by nature, only one type of termination is expected, reflecting the lowest state of energy. Results of core-level spectroscopy investigations using synchrotron radiation in which a well-defined Ta surface core level is observed indicate that a portion, if not all, of the outermost layer consists of Ta atoms.

In order to determine definitely the composition of this surface, a LEED investigation has been performed. A clean, well-ordered surface was prepared by $Ar^+$ ion sputtering followed by flashing to ~1800°C for ~5 s. With the primary electron beam incident normal to the surface, equivalent beam-averaged I-V profiles were obtained using a computer-controlled video data acquisition system and then compared with profiles calculated for various structural models of the surface. In order to obtain excellent agreement between calculated and experimental profiles, the various nonstructural parameters of the LEED theoretical model were also varied. Structural determinations were made using the $R_2$ factor minimization technique.

Results of the analysis have led to definitive conclusions about the termination of the TaC(111) surface. It is exclusively terminated in Ta, and the layers in the selvedge region have the stacking sequence of the bulk. In addition, the first interlayer spacing, $d_{12}$, is decreased by 9.9% with respect to the bulk value of 1.286Å, the second, $d_{23}$, third, $d_{34}$, and fourth, $d_{45}$, are increased by 0.2, 1.4, and 1.2%, respectively, and the fifth $d_{56}$ decreased by 2.4%.

---

1. Summary of paper to be published.
2. Guest scientist from the University of Erlangen-Nürnburg, Erlangen Germany.

## NUMERICAL SIMULATION OF Si-Ge (001) STEPPED SURFACES[1]

*Majid Karimi,[2] Theodore Kaplan, Mark Mostoller, and David Jesson*

The growth of Si-Ge superlattices by molecular beam epitaxy is of considerable current interest. These superlattices offer the potential of direct band-gap materials for optical electronic devices which could be directly integrated into silicon-based technologies. The study of these materials by Z-contrast scanning transmission electron microscopy (STEM) has revealed additional periodicities in the interfacial structures. Jesson, Pennycook, and Baribeau have suggested a Ge-pump mechanism to explain the growth of these structures.[3]

In the pump model the interchange of Ge and Si atoms at $S_B$ rebonded step edges is an essential part of the growth process. The energetics of this interchange have been investigated by performing atomistic calculations using classical many-body Stillinger-Weber and Tersoff potentials.

An (001) Ge surface with semi-infinite single-layer Si terraces was considered. The terraces terminate in $S_B$ steps that are either rebonded or non-rebonded. Two systems, one with 1428 atoms a ledge separation of 12 Å and a larger one with 4266 atoms and a ledge separation of 52 Å, were constructed. For each system, the energy was minimized by the conjugate gradient method for rebonded and non-rebonded steps with and without Ge and Si interchange at the step edge. The results are presented in Table 1.2. In all cases, it was found that Ge and Si interchange was energetically the most favorable at $S_B$ rebonded steps. This is consistent with the Ge-pump model. Furthermore, despite a difference in the size of the energy changes calculated, both potentials also predict no significant dependence on ledge separation.

**Table 1.2. Formation energy per ledge atom for interchange of Si and Ge at the step edge.**

| Ledge Separation (Å) | Step Structure | Stillinger -Weber DG (eV) | Tersoff DG (eV) |
|---|---|---|---|
| 12 | rebonded | -0.161 | -0.212 |
| 52 | rebonded | -0.162 | -0.220 |
| 12 | non-rebonded | -0.028 | -0.112 |
| 52 | non-rebonded | -0.028 | -0.110 |

1. Summary of paper to be published.
2. Oak Ridge Associated Universities faculty research participant from Alabama A&M University, Normal, Ala.
3. D. E. Jesson, S. J. Pennycook, and J. M. Baribeau, *Phys. Rev. Lett.* **66**, 750, (1991).

## SIMULATION OF (*a*/2)[110] EDGE DISLOCATIONS IN Si, Ge, AND Ge-Si FILMS[1]

*Mark Mostoller, M. F. Chisholm, Theodore Kaplan, and Magid Karimi[2]*

In (001) films of Ge on Si, there is a lattice misfit of about 4% between Ge ($a$ = 5.65 Å) and Si ($a$ = 5.43 Å). The system accommodates the resulting strain by forming a network of $\mathbf{b} = (a/2)[110]$ edge dislocations in the Ge film; this has been observed at atomic scale resolution by Z-contrast scanning transmission elec-

tron microscopy (STEM) in the Solid State Division.[3] These edge dislocations in Si, Ge, and Ge-Si films have been studied using classical simulations.

The dislocations were formed in textbook fashion. Relatively large microcrystals with axes along the $x = [1\bar{1}0]$, $y = [110]$, and $z = [001]$ directions were constructed, and an $xz$ half plane was removed from the bottom half. The microcrystals were usually kept thin along the $[1\bar{1}0]$ (dislocation) direction, where periodic boundary conditions were applied. Typical crystal sizes were 1700–2500 atoms. After removing the half plane, the total energy was minimized by the conjugate gradient method. The interactions between the atoms were modeled with the Stillinger-Weber potential, which includes two- and three-body terms, the latter to stabilize the tetrahedral bonding in these semiconductors.

The core of the resulting dislocations showed the linked pentagon above the heptagon structure seen in perspective in Fig. 1.2. By comparing the simulation results for the total strain energy $V(R)$ as a function of distance $R$ from the core with the predictions of linear elasticity theory, it is clear that the core radius $r_0$ appropriate for use in continuum descriptions of these dislocations is small (~2–5 Å).

The simulations for Ge-Si films seem to indicate that the core will be located at the interface, with the pentagon in Si and the lower five atoms in the heptagon in Ge. However, the energy differences between this and competing alternatives are small, and what the simulations really demonstrate is the need to take another look at the potentials that have been used for nearly a decade. The Stillinger-Weber potential, for example, is too short-range to model a stacking fault accurately and does a poor job on the elastic constants and phonon frequencies, although it does fit the bulk structure and the melting point. Other potentials in the literature suffer from similar drawbacks.

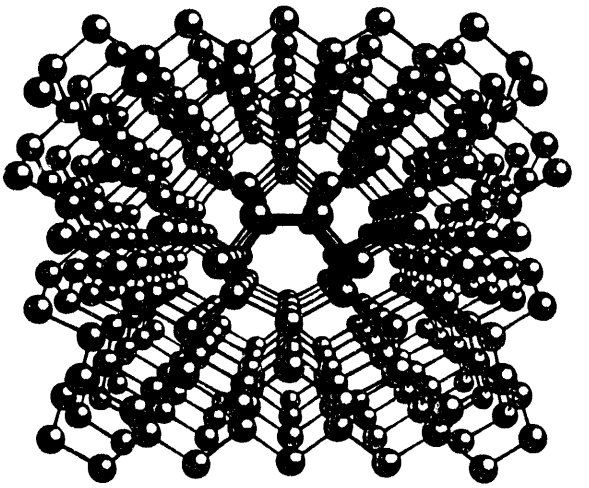

Fig. 1.2. Looking down the core of an $(a/2)[100]$ edge dislocation in silicon.

---

1. Summary of paper to be published.
2. Oak Ridge Associated Universities faculty research participant from Alabama A&M University, Normal, Ala.
3. M. F. Chisholm et. al., "Atomic Structure of Interfacial Misfit Dislocations, this report.

### CHARGING EFFECTS IN SMALL TUNNEL JUNCTIONS[1]

*K. Flensberg,*[2] M. Jonson,[3] *H. O. Frota,*[2] *S. M. Girvin,*[4] *D. R. Penn,*[5] *and M. D. Stiles*[5]

Many interesting effects (e.g., the Coulomb blockade) have been predicted by theory and also observed in tunnel junctions with capacitance $C$ so low that the charging energy $\varepsilon_c = e^2/2C$ associated with a single electron is larger than the energy scale $k_BT$ of thermal fluctuations. The measured blockade is much smaller compared with what is expected from the semiclassical theory. Quantum fluctuations, in addition to thermal fluctuations, must be included in an accurate theory. Two kinds of quantum fluctuations are included. One is the charge fluctuations across a junction, as electrons hop back and forth. The second is the charge fluctuations along the wire leads connecting the current to the tunnel junction. These electromagnetic fluctuations are included by coupling the electrons to a transmission line of impedance $Z(\omega)$. One paper derived the general behavior including these two kinds of fluctuations, and they were found to add in the critical exponent. Another calculation concerned the nature of the impedance $Z(\omega)$ and various physical models which give the behavior observed experimentally.

---

1. Summary of papers: *Phys. Rev. B* **43**, 7586 (1991); *Solid State Comm.* **77**, 917 (1991); *Z. Phys. B* **85**, 395 (1992).
2. Guest scientist from the ORNL/UT Distinguished Scientist Program.
3. Chalmers University of Technology, Göteborg, Sweden.
4. Indiana University, Bloomington, Ind.
5. National Institute of Standards and Technology, Gaithersburg, Md.

# *MAGNETISM AND SPIN DYNAMICS*

### EFFECTS OF IMPURITIES ON THE MAGNETIC ORDERING OF CHROMIUM[1]

*R. S. Fishman*[2] *and S. H. Liu*

It has been found experimentally that impurities profoundly alter the magnetic ordering properties of chromium. In pure chromium the ordered magnetic phase is a spin-density wave whose wave vector is incommensurate with the lattice. Concurrent with the spin-density wave, a charge-density wave has been observed with twice the wave vector as the spin-density wave. Doping with as little as 0.2% vanadium changes the phase transition from weakly first to second order. While vanadium impurities suppress the Néel temperature $T_N$, doping with manganese dramatically enhances $T_N$.

Young and Sokoloff[3] have proposed a model to understand the magnetic ordering in pure chromium. In particular, it was shown that the charge-density wave is a second harmonic of the spin-density wave, and the coexistence of the two causes the phase transition to be first order. The Young-Sokoloff formalism has been defined by examining the subtle balance between spin-density and charge-density terms in the free

energy, including two effects introduced by impurities (i.e., impurity scattering and the change of electron density). It has been found that impurity scattering destroys the charge-density wave and causes the phase transition to be second order. Both scattering and the change of electron density have strong effects on the transition temperature $T_N$; the former always suppresses $T_N$ while the latter can raise or lower $T_N$ depending on whether the electron density is increased or decreased. The theory gives a quantitative account of a complete series of experiments done at ORNL and elsewhere.

---

1. Summary of paper: *Phys. Rev. B* **45**, 12306 (1992).
2. Guest scientist from North Dakota State University, Fargo, N. Dak.
3. C. Y. Young and J. B. Sokoloff, *J. Phys. F* **4**, 1304 (1974).

## ROLE OF EXCHANGE MATRIX ELEMENT ON SPIN-WAVE SPECTRA OF HCP COBALT[1]

*J. M. Bass,[2] J. A. Blackman,[2]*
*J. F. Cooke, and K. N. Trohidou[2]*

Calculations based on the itinerant-electron theory of ferromagnetism have provided a good description of the low-temperature spin-wave spectrum of the cubic transition metals nickel and iron. Multibranch spin-wave spectra which extended to high energies were predicted and subsequently confirmed by neutron scattering experiments.

The prediction of such complex spectra for nickel and iron led to speculation about the nature of magnetic excitations in hcp cobalt. Since there are now two atoms in the unit cell, even more complex spin-wave spectra might be expected. Instead, preliminary calculations based on a highly simplified form of the exchange matrix element predicted the simple two-branch spectra along the $\Gamma$-$A$ direction, shown in Fig. 1.3, which might be expected from simple symmetry arguments.[3]

This work has been extended to include the most general form of the exchange matrix element consistent with hcp symmetry and to determine the corresponding impact on the spin-wave spectra of cobalt.[2] If only $d$-symmetry terms are retained, the exchange matrix element is found to depend on 12 unique symmetry-dependent parameters. These parameters can in turn be divided into four types by virtue of the pairing of their indices. A systematic study of the types of spin-wave spectra which can be generated along the $\Gamma$-$A$ direction by this general form of the exchange matrix has been carried out.

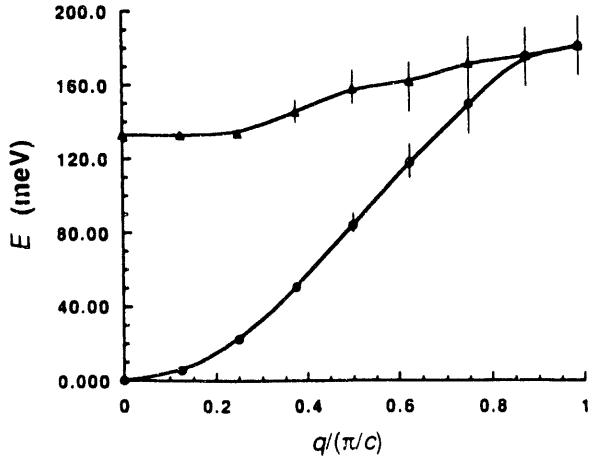


Fig. 1.3. Spin-wave dispersion for $q$ (in units of $\pi/c$) along the $\Gamma$-$A$ direction.

Results of this study have shown that inclusion of the four different types of parameters leads to a wide variety of spin-wave behavior and that the relatively simple result found previously was due to the particularly simple form of the exchange matrix element used. The most complex result found thus far corresponds to four distinct branches, none of which are present along the entire length of the symmetry direction. Work is currently under way to evaluate the parameters using a screened coulomb potential with the screening length taken as the only variable parameter. Results obtained from this approach, combined with more extensive neutron scattering data, will provide the most rigorous test yet of the itinerant-electron theory of ferromagnetism.

---

1. Summary of papers: *Phys. Rev. Lett.* **67**, 2561 (1991); *J. Phys., Condens. Matter* **4**, L275 (1992).
2. University of Reading, Reading, United Kingdom.
3. K. N. Trohidou, J. A. Blackman, and J. F. Cooke, *Phys. Rev. Lett.* **67**, 2561 (1991).

## SPIN SUSCEPTIBILITY OF FERROMAGNETIC NICKEL ALONG ARBITRARY SYMMETRY DIRECTIONS[1]

*J. F. Cooke and J. A. Blackman*[2]

Calculations of the frequency and wave-vector dependent magnetic susceptibility based on the itinerant theory of ferromagnetism have revealed rather complex and unusual behavior of the magnetic excitation spectra in both nickel and iron. For example, the spin-wave spectra in these materials consist of multiple branches along the [100] direction which extend to quite high energies. Because of computer core and time limitations, these calculations were restricted to symmetry directions only and neglected *s*- and *p*-symmetry contributions to the susceptibility. Data from subsequent neutron scattering experiments were found to be in remarkable agreement with predictions from theory except for the persistence of the lower spin-wave branch out to the Brillouin-zone boundary along the [100] direction in nickel. Recent access to computers with significantly greater core and speed combined with improved efficiency of the computer codes have made possible calculations which not only remove essentially all of the strictly numerical approximations in previous calculations but also allow results to be determined along arbitrary directions in the Brillouin zone.

A number of important results have been obtained from calculations based on this more general approach. It has been demonstrated explicitly that the *s*- and *p*-symmetry contributions can indeed be neglected as speculated previously. The behavior of the lower branch of the spin-wave dispersion curve in nickel near the zone boundary has been found to depend on certain of the exchange matrix element parameters and the particular reciprocal lattice vector needed to bring the wave vector being considered into the first Brillouin zone. These two effects can be combined to reproduce the measured

behavior of the spin-wave spectra along the [100] direction in nickel. Finally, the evolution of the spin-wave spectra was investigated as the wave vector was rotated from the [100] direction (where two branches exist) to the [111] direction (where only a single branch exists). It was found that the evolution is not smooth but appears to be abrupt. This result, along with others obtained at off-symmetry wave vectors, will provide a more detailed test of itinerant-electron theory than is possible along symmetry directions.

---

1. Summary of paper to be published.
2. University of Reading, Reading, United Kingdom.

## CURRENT-DENSITY FUNCTIONAL THEORY OF SURFACE PROPERTIES OF ELECTRON-HOLE DROPLETS IN A STRONG MAGNETIC FIELD[1]

*Mark Rasolt, G. Vignale,[2] and P. Skudlarski[2]*

An external magnetic field $B_0$ interacts with a many-Fermion system through both spin and orbital current coupling. For dense Fermi systems (e.g., metals or undoped semiconductors), presently available magnetic fields have a negligible effect. With the exception of calculations of Pauli-spin susceptibility in linear response theory, consideration of magnetic effects has been almost exclusively reserved to spontaneous spin alignment—ferromagnetic and antiferromagnetic—where exchange energies can be sizeable. In low carrier-density semimetals and carrier-doped or carrier-excited semiconductors, accessible laboratory fields can have a profound effect through both spin and orbital current coupling. This occurs when the magnetic length $l = c\hbar/eB_0)^{1/2}$ is comparable to the interparticle separation. In this range of $l$, there is no doubt that the effect of $B_0$ dominates the structure of the ground-state wave function and the corresponding energy.

With the exception of the uniform two-dimensional (2D) electron gas,[3] the effect of orbital currents on ground-state properties has totally been ignored. This is true in nonuniform 2D systems and even more so in three-dimensional (3D) systems. A current-density-functional theory (CDFT),[4] which handles both spin and current related many-body effects rigorously, is now available. Application of the first CDFT has been completed and applied to a nonuniform 3D system of excited electrons and holes and electron-hole droplets (EHD) in semiconductors.

The properties of the EHD most sensitive to the presence of $B_0$ are surface properties. Focus was placed on the effect of $B_0$ on the EHD surface current and surface tension (Fig. 1.4). At cyclotron frequency $\omega_c = 8$, the diamagnetic dependency increases the surface tension by 50%. The effect of the surface diamagnetic current should be readily observed experimentally.

---

1. Summary of paper: *Phys. Rev. B* **45**, 8494 (1992).

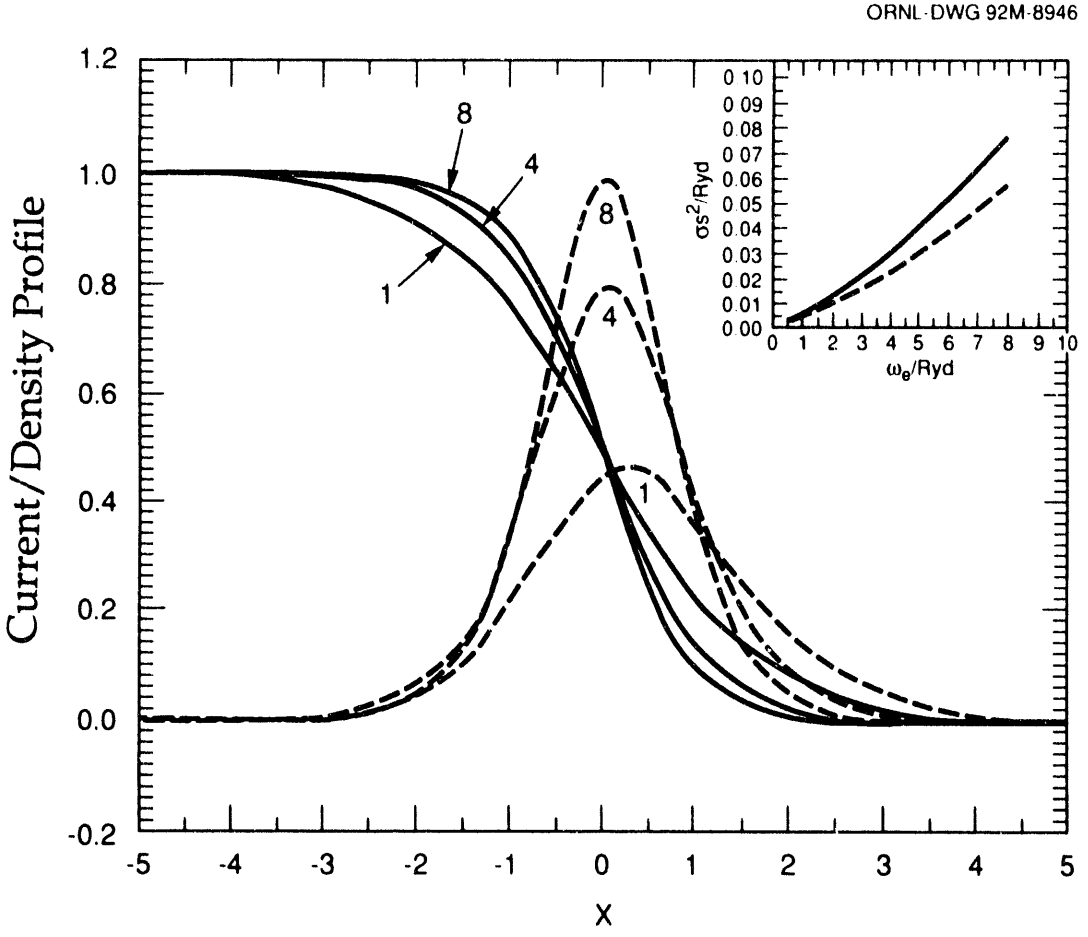


Fig. 1.4. Solid line: surface density profile $n/n_0$ of an EHD. The surface is located at $x = 0$ ($x$ is in units of Bohr radius $a$). Curves are given for $\omega_c = 1, 4$, and 8 Ryd. Dashed line: azimuthal current density. Inset: surface energy of EHD as a function of $\omega_c$.

2. University of Missouri, Columbia, Mo.
3. R. B. Laughlin, *Phys. Rev. Lett.* **50**, 1395 (1983); D. Yoshioka and P. A. Lee, *Phys. Rev. B* **37**, 4986 (1988).
4. G. Vignale and M. Rasolt, *Phys. Rev. Lett.* **59**, 2360 (1987); *Phys. Rev. B* **37**, 10685 (1988); M. Rasolt and G. Vignale, *Phys. Rev. Lett.* **65**, 1498 (1990).

## ANDERSON MODEL[1]

*H. O. Frota[2] and G. D. Mahan[3]*

The Anderson model for a metal describes an impurity with a local spin. The spin can interact with the conduction electrons, and together they generate spin fluctuations. The model cannot be solved exactly, however.

Wilson renormalization group methods were used to obtain two different properties of the single-site case. In one calculation, a charge-fluctuation term was added to the model with a coupling constant $G$. It was found that the Kondo resonance at the Fermi surface could be described by a Doniach-Sunjic line shape, where the exponent was a function of $G$. The orbital energies were also dependent on $G$.

Furthermore, for some values of impurity valence and $G$, it was found that two-electron charge fluctuations were energetically favored over single-electron fluctuations.

In the second calculation, the charge susceptibility of the Anderson model was calculated as a function of frequency. Assuming a set of model parameters where the ground state was an $f^1$ state, the susceptibility showed a two-peak spectra. The two peaks correspond to transitions $f^1 \rightarrow f^0$ and $f^1 \rightarrow f^2$. Their respective oscillator strengths were found to be a function of the model parameters.

---

1. Summary of papers: *Phys. Rev. B* **43**, 10755 (1991); *Phys. Rev. B* **44**, 8433 (1991).
2. Guest scientist from the ORNL/UT Distinguished Scientist Program.
3. ORNL/UT Distinguished Scientist.

### MAGNON RENORMALIZATION OF A LOCALIZED HOLE[1]

*A. G. Mal'shukov[2] and G. D. Mahan[3]*

A problem of current theoretical interest is the behavior of a few holes in a strongly correlated Heisenberg antiferromagnet. An exactly solvable model which describes the behavior of a single hole has been found. The behavior of the hole can be found exactly in the limit where it is assumed to be localized on a single site. Because most other calculations show that it moves slowly, then localizing the hole is a good approximation.

A linearized spin-wave, or magnon, model was used to solve for the correlation functions of the localized hole. Pairs of magnons couple to the hole. The scattering of the magnons, from the spin-impurity caused by the localized hole, can be described by phase shifts. These phase shifts are used to calculate various properties such as the ground state energy and the quasiparticle renormalization. A magnon-bound state was found at zero energy. It strongly renormalizes the values of the phase shifts, which affect all the properties of the localized hole.

---

1. Summary of paper: *Phys. Rev. Lett.* **68**, 2200 (1992).
2. Guest scientist from the ORNL/UT Distinguished Scientist Program.
3. ORNL/UT Distinguished Scientist.

## *BUCKYBALLS, SAND PILES, BAND TAILS, AND MORE*

### FLUCTUATIONS IN HIGH-RANKING TENSOR ORDER PARAMETERS: IMPLICATION TO THE ORIENTATIONAL TRANSITION OF BUCKYBALLS[1]

*Mark Rasolt*

The microscopic icosahedral symmetry of the $C_{60}$ molecules forming a liquid or a solid of buckyballs introduces the additional possibility of an orientational-phase transition (OPT). Such a phase transition has been, in fact, observed in the solid Fullerite at $T_c \approx 249$ K[2], which has generated considerable experimental and theoretical interest.[2-5]

Some issues concerning the general effects of fluctuations in such systems for which this icosahedral high symmetry requires a high-ranking tensor order parameter were studied. Two issues addressed were the effect of such fluctuations on the nature of the OPT in buckyballs, including the order of the OPT which remains in contention,[2,3] and the large low-temperature precursor in the OPT with its strong dependence on pressure which is not conventional.[3]

Following some symmetry considerations, the appropriate Landau-Ginzburg (LG) form for the liquid crystal of buckyballs was derived:

$$F = \frac{1}{1440}\left[(r+\nabla^2)\delta_{\alpha_1\lambda_1} + h\,\frac{\partial}{\partial r_{\alpha_1}}\frac{\partial}{\partial r_{\lambda_1}}\right] \times Q_{\alpha_1\beta_1\gamma_1\rho_1\gamma_1\Delta_1} Q_{\lambda_1\beta_1\gamma_1\rho_1\gamma_1\Delta_1} + t\, Q_{\alpha_1\beta_1\gamma_1\rho 4\gamma_1\Delta_1} Q_{\rho_1\gamma_1\Delta_1\alpha_2\beta_2\gamma_2} \times Q_{\alpha_2\beta_2\gamma_2\alpha_1\beta_1\gamma_1} + \sum_{i=1}^{10} W_\phi Q^4 \qquad (1a)$$

corresponding to $\ell = 6$. There are many constraints which reduce the $3^6$ components of $Q$ to 13. The last term is a shorthand notation for the ten ($\phi = 10$) quartic invariants. For example,

$$W_1\left(Q_{\alpha_1\beta_1\gamma_1\rho_1\lambda_1\Delta_1}\; Q_{\alpha_1\beta_1\gamma_1\rho_1\lambda_1\Delta_1}\right)^2, \qquad (1b)$$

and there are nine more.

For the solid, the LG free-energy density [Eq. (1)] is now broken by a spatial translational modulation with four equivalent $\mathbf{k}^*_1 = \left(\frac{1}{2}\frac{1}{2}\frac{1}{2}\right)\frac{2\pi}{a}$; $\mathbf{k}^*_2 = \left(\bar{\frac{1}{2}}\frac{1}{2}\frac{1}{2}\right)\frac{2\pi}{a}$; $\mathbf{k}^*_3 = \left(\bar{\frac{1}{2}}\bar{\frac{1}{2}}\frac{1}{2}\right)\frac{2\pi}{a}$; $\mathbf{k}^*_4 = \left(\frac{1}{2}\bar{\frac{1}{2}}\frac{1}{2}\right)\frac{2\pi}{a}$. A form of $F$ is written as:

$$F = \sum_{i=1}^{4}\left[\frac{1}{2}(r+\nabla^2)\,\phi_i^2 + t_1\,\phi_i^3 + \sum_{j\neq i=1}^{4} t_2\,\phi_i^2\,\phi_j\right] + t_4\left[\phi_1\phi_2\phi_3 + \phi_1\phi_3\phi_4 + \phi_1\phi_2\phi_4 + \phi_2\phi_3\phi_4\right] + u\left(\sum_{i=1}^{4}\phi_i^2\right)^2 + v\sum_{i=1}^{4}\phi_i^4 + w\phi_1\phi_2\phi_3\phi_4 \qquad (2)$$

where $\phi_i \equiv \phi_i(\mathbf{r})$ ($i = 1 \rightarrow 4$) are the four order parameters for the $\mathbf{k}^*_i$.

Studying both Eqs. (1) and (2) using renormalization group techniques, it was found that the icosohedral OPT of buckyballs must be first order. The unusual behavior of the precursor as a function of temperature and pressure[2,3] to a fluctuation-driven first-order OPT was also explained.

---

1. Summary of paper to be published.
2. P. A. Heiney et al., *Phys. Rev. Lett.* **66**, 2911 (1991).
3. G. A. Samara et al., *Phys. Rev. Lett.* **67**, 3136 (1991).
4. N. W. Ashcroft, *Eur. Phys. Lett.* **16**, 355 (1991).
5. O. Gunnarson et al., *Phys. Rev. Lett.* **67**, 3022 (1991).

## SELF-SEGREGATION IN MULTICOMPONENT SAND PILES[1]

*Theodore Kaplan, S. H. Liu, L. J. Gray,[2] and B. C. Sales*

The flow of granular material composed of more than one type of constituent is common in materials preparation. Typically, various materials are mixed in one container and then poured into another for sintering. Self-segregation under such conditions can severely affect the final form of the treated material. On a larger scale, this phenomenon can be significant in industrial-type processes where granular materials are mixed and then transferred by means which involve granular flow under gravity.

A totally random mixture of two different granular materials was considered. It was assumed that the two kinds of granules have sufficiently different sizes, shapes, or other physical properties such that the critical angles of repose for the materials are different. The critical angle of repose is the maximum slope that any point on a pile of the material can sustain. If this slope is exceeded, the granules will flow. The nonlinear dynamics of this system were modeled by a discrete cellular automaton. Results of simulations showed that pouring a random mixture into another container leads to the almost total segregation of the two constituents. The material with the higher critical angle needs a greater slope to induce motion. As a result, it tends to bunch up around the site at which it is poured, while the more mobile granules with the lower critical slope tend to move away. The final distribution of granules in the new container shows a concentration of the more mobile constituents at the bottom and the periphery of the pile with the less mobile species near the center and top.

This model breaks down when the particles are approximately the same size. The dominate contribution to the angle of repose for different particles is related to the geometry of how they stack. When the sizes are comparable, the differences in angle of repose are small, and the discrete nature of the model becomes unrealistic.

---

1. Summary of paper to be published.
2. Engineering Physics and Mathematics Division, ORNL.

## CANDIDATE FORMATION TECHNOLOGIES FOR THIN-FILM SILICON PHOTOVOLTAICS[1]

*R. F. Wood and D. L. Morel[2]*

An extensive study was carried out to identify and evaluate candidate formation technologies for thin-film, polycrystalline, photovoltaic-quality silicon and to determine research program requirements for any candidates that were judged worthy of pursuit. The study did not cover amorphous Si which is a well-developed field in its own right. Moreover, because of the low absorption coefficient of crystalline Si, the "thin films" considered in the study were 30–50 μm thick and would be more appropriately classified as thick films.

Numerous Si deposition and recrystallization techniques were surveyed. It was concluded that some form of very rapid deposition fol-

lowed by zone-melting recrystallization was the single most promising approach. Recrystallization of the deposited silicon is necessary to achieve the grain sizes required for satisfactory electrical properties. It also became clear during the deposition studies that both liquid-phase epitaxy and electrochemical deposition are techniques that have not been adequately explored for thin-film Si deposition.

In addition to the deposition processes, a vital component of a developmental program must be research on low-cost substrates. It was recommended that initially the major effort in this area be focused on ceramic substrates, including thin-film coatings for diffusion barriers, optical confinement, and passivation. Developments in glass technology should be closely monitored even though it was recognized that glasses able to withstand recrystallization temperatures of ~1410°C are unlikely to be forthcoming. Metallic substrates are not likely to have the correct thermal properties for high-temperature processing, and high-grade graphite is too expensive.

Finally, the program must have the capabilities for extensive in situ and postdeposition diagnostics of the films, substrate evaluation, and device fabrication and testing.

Putting these requirements together, a well-designed research program for establishing the feasibility of thin-film polycrystalline Si solar cells should have the following components: (1) low-cost substrate development, (2) advanced thin-film deposition techniques, (3) recrystallization of small-grained films, (4) liquid-phase epitaxy/electrochemical deposition, and (5) film diagnostics and cell fabrication and testing. Such a program jointly funded by the Electric Power Research Institute (EPRI) and ORNL under a Cooperative Research and Development Agreement has been initiated.

---

1. Summary of a collaborative "White Paper" study carried out by EPRI and ORNL.
2. University of South Florida, Tampa, Fla.

## QUASI-FERMI LEVELS IN QUANTUM WELL PHOTOLUMINESCENCE[1]

*G. D. Mahan[2] and L. E. Oliveira[3]*

The observation of electron-hole recombination radiation has been a standard technique to observe the impurity states in semiconductors. Recently, the method has been applied to semiconductor quantum wells and wires. Here an important variable is the location of the impurity—whether in the center or at the edge of the well/wire. Also, the thickness of the well or wire affects the result. The interpretation of the experiments requires a knowledge of the number of electrons and holes which are temporarily in the conduction and valence bands.

These densities were calculated as a function of laser intensity for typical wells found in GaAS(AlAs) superlattices. Initially, there are negligible electrons and holes, which are excited by photon absorption and then relaxed by various radiative and Auger processes. The

rate for many of these processes was calculated to determine the average number which are temporarily excited during a steady-state laser excitation. A typical laser of 1 W/cm$^2$ gave a quasi-Fermi level of about 1 meV. Most experimental photoluminescence is wider than this, which indicates inhomogeneous broadening due to different positions of the impurities.

---

1. Summary of paper: *Phys. Rev. B* **44**, 3150 (1991).
2. ORNL/UT Distinguished Scientist.
3. Universidade Estadual de Campinas, Campinas, São Paulo, Brazil.

## BAND TAILS AND BANDWIDTHS IN SIMPLE METALS[1]

*H. O. Frota[2] and G. D. Mahan[3]*

Recent experiments on simple metals have been interpreted as indicating excessive narrowing of the occupied conduction bands for electrons. The present calculations were undertaken to see whether excessive band narrowing was due to electron-electron interactions. Past work had discussed band narrowing after calculations of the real part of the quasi-particle self-energy. Here, a complete calculation which included both the real and imaginary self-energy of the electron was performed. The self-energies were used to calculate the complete interacting density of states (DOS). Large band tails were found, in agreement with previous calculations. The extra DOS from these band tails were compensated by fewer states in the regular band, due to quasi-particle renormalization. The resulting band narrowing was found to be less than one or two percent, which is the accuracy of the calculations. Thus, the experimental reports are difficult to explain.

---

1. Summary of paper: *Phys. Rev. B* **45**, 6243 (1992).
2. Guest scientist from the ORNL/UT Distinguished Scientist Program.
3. ORNL/UT Distinguished Scientist.

## INHOMOGENEOUS THERMOELECTRICS[1]

*G. D. Mahan[2]*

Thermoelectric generators and refrigerators occupy a niche market. They are used where reliability is more important than efficiency and where semiconductor chips need to be microcooled. Here, a way to make existing devices slightly more efficient is explained. A computer code was written which permitted the efficiency of these devices to be calculated for any kind of temperature dependence of the device parameters and for any pattern of impurity doping. The devices often operate over large temperature ranges, and the electrical conductivity, thermal conductivity, and Seebeck coefficient all depend upon temperature and doping. It was found that one pattern of doping made these devices more efficient than homogeneous doping. This pattern has the high-conducting material at the cold end.

---

1. Summary of paper: *J. Appl. Phys.* **70**, 4551 (1991).
2. ORNL/UT Distinguished Scientist.

## CURRENT DEPENDENCE OF THE VAN DER WAALS INTERACTION[1]

*A. G. Rojo[2] and G. D. Mahan[3]*

The van der Waals interaction for systems carrying a nonzero current was considered. In simple cases like two parallel wires or sheets, the van der Waals attraction increases quadratically with the difference between the currents in the two subsystems. This implies a nonzero current drag at zero temperature, a new effect that could be detected experimentally.

This effect gives a coupling term between currents that should be distinguished from the classical magnetic interaction that comes from the Biot-Savart law. First, the current drag effect falls off rapidly with distance and is only appreciable for distances in the submicron regime. It is also recognized that for larger distances (in the micron regime), retardation effects are important. In the experiment of Gramila et al.,[4] the 2D electron gas has a Fermi temperature of roughly 60 K, corresponding to a Fermi energy $E_F \sim 10^{-2}$ eV. An estimate of the distance for retardation effects to be important is $R \sim \hbar c/E_F \sim 10^4 \times 137\, a_0$, which is above the micron regime. Since the interlayer distance considered by Gramila et al.[4] is ~240 Å, the zero temperature current drag is expected to be observable for this type of experimental setup. Second, the classical magnetic interaction does not imply a current drag, at least in the stationary regime. If, for example, there are two current loops in the same plane and the current is turned on (e.g., clockwise) in one of them, the induced emf generates a counterclockwise current in the second loop. However, this is a transient effect that is zero in the stationary regime. It should also be noted that this transient current is in the opposite direction from the dragged one.

In summary, it was shown that the van der Waals interaction between the two systems has a current-dependent term, in such a way that the attraction is maximized if the two subsystems have opposite currents. This implies that there should be a current drag between the two subsystems when one of the two is forced to have a finite current. This effect is nondissipative and is nonzero for zero temperature.

---

1. Summary of paper: *Phys. Rev. Lett.* **68**, 2074 (1992)
2. Guest scientist from the ORNL/UT Distinguished Scientist Program.
3. ORNL/UT Distinguished Scientist.
4. T. J. Gramila et al., *Phys. Rev. Lett.* **66**, 1216 (1991).

## COMPUTER SIMULATION STUDIES OF HIGH-ENERGY COLLISION CASCADES[1]

*Mark T. Robinson*

In previous work with the MARLOWE program, it was shown that the binary collision approximation (BCA) may be modified to include an explicit calculation of the time of each collision[2] and that these times may be used to order the collisions in a cascade properly in time.[3] It was shown also that cascade nonlinearities could be approximated by allowing the already stopped cascade atoms to become targets in later encounters. The earlier

work was limited to initial kinetic energies $E_0$ in the low-kilovolt region by the need for frequent searches of the list of atoms in a developing cascade, which made the time to evaluate a single cascade proportional to $E_0^2$.

A so-called "hashing" algorithm has now been developed which enables the stopped cascade atoms to be located much more efficiently than before. With the improved algorithm, the time for a single cascade is proportional to $E_0$, and simulations at much higher initial kinetic energies are feasible. The model was also slightly modified by requiring atoms to surmount a binding energy to be redisplaced. This value was taken as one-tenth of the cut-off energy used in the calculations. It has the effect of slightly reducing the number of redisplacements, but concentrates the attention of the code on the events of most significance.

The revised model was used to generate cascades in Cu and in Au at initial kinetic energies up to 100 keV. Up to 20 keV, 1000 cascades were generated at each energy; 500 were generated at 50 keV, and 250 at 100 keV. In addition to the effects of redisplacements, the effects of thermal disorder were examined. The temporal development of cascades, as well as their overall properties, was examined after the initial energy was dissipated.

The rate of energy dissipation from a developing cascade is increased by the approximate nonlinearity, as well as by thermal disorder. The latter also eliminates long replacement sequences. The cascades are more compact than are those in a linear cascade in a static crystal. Consequently, there tend to be fewer "distant" Frenkel pairs and less damage. Target redisplacements reduce the damage in Cu by 3% at most, but in Au it is reduced by amounts up to 20% at 100 keV. Thermal disorder is also important. By disrupting crystal effects, the damage is reduced significantly.

---

1. Summary of paper: *Nucl. Instrum. and Methods Phys. Res. Sect. B* **67**, 396 (1992).
2. M. T. Robinson, *Phys. Rev. B* **40**, 10717 (1989).
3. M. T. Robinson, *Nucl. Instrum. and Methods Phys. Res. Sect. B* **48**, 408 (1990).

# 2. *Superconductivity*

The Solid State Division research programs in superconductivity encompass a broad range of topics, extending from fundamental theoretical advances in understanding the mechanisms of high-temperature superconductivity (HTS) to the development of filamentary HTS conductors capable of carrying technologically useful electric currents at liquid nitrogen temperatures. The strong diversity in this research results from collaborations among the theoretical and experimental groups in the division and with outside academic and industrial scientists including base support of the ORNL Superconducting Technology Program. This chapter is divided into three sections: Theory, Thin Films, and Bulk Materials.

In the Theory Section, several new results are presented which reflect unique properties arising from the layered structure of the HTS oxide materials. A number of different single and multilayer mechanisms of HTS in layered materials are investigated. The effects of two dimensionality on the current carrying states, upper critical field and magnetic behavior, and superconductive transitions are summarized. In the field of fractional statistical quasiparticles, the theory of anyons has been extended to account both for coulomb coupling between two-dimensional planes and for exact finite temperature effects.

In the Thin-Films Section, several contributions summarize advances in understanding the lattice stability, defect structure, and crystal growth mechanisms in HTS materials through a variety of microstructural studies. Interfaces in superlattices and in ion beam amorphized films, as well as films at early stages of deposition, have been characterized by x-ray diffraction, Z-contrast scanning transmission electron microscopy, and scanning tunneling microscopy techniques. Detailed x-ray studies have elucidated the role of heteroepitaxial near-coincidence lattice matching on the properties of HTS films deposited on various oxide and metallic substrates. Through systematic studies conducted on both thin films and bulk materials, the effects of oxygen content on the superconducting properties and magnetic flux pinning have been clarified.

In the bulk materials section, several contributions describe studies of enhanced loss-free response in materials that have undergone heavy and light ion irradiations to produce tailored defect structures for flux pinning. Much of this work has significant ramifications for practical applications. Neutron scattering has provided new insights into HTS materials, including evidence for increased electron-phonon coupling at the superconducting transition and structural imaging of the magnetic vortex lattice.

# THEORY

## SPONTANEOUSLY BROKEN CURRENT-CARRYING STATES IN HIGH-$T_c$ SUPERCONDUCTORS [1]

*Mark Rasolt and F. Perrot*[2]

The issue addressed is whether spontaneously broken current-carrying states (SBCCS) ("analog" for spontaneous ferromagnetic alignment[3]) are a realistic possibility in such itinerant 2D systems. Prejudice against such SBCCS in favor of spin-polarized ground states originates in the Landau diamagnetic[4] response, $\chi_L$, vs. the Pauli susceptibility, $\chi_p$. For strong inhomogeneities, however, things can be quite different. Also, aside from strong inhomogeneities, 2D is also very important for SBCCS.[5]

The SBCCS was calculated using the theory of Vignale and Rasolt. The energy, $E$, of the inhomogeneous Fermi liquid is written as

$$E\Big(n(\mathbf{r}),\, \nabla x(j_p(\mathbf{r})/n(\mathbf{r}))\Big) = E_i(n(\mathbf{r}),j_p(\mathbf{r}))$$

$$+\left[+n(\mathbf{r})V(\mathbf{r}) - \frac{e}{c} j_p(\mathbf{r}) \cdot A(\mathbf{r}) + \frac{e^2 n(\mathbf{r})}{2mc} |A(\mathbf{r})|^2\right] \tag{1a}$$

where

$$E_i(n(\mathbf{r}),j_p(\mathbf{r})) = T_c(n(\mathbf{r}),j_p(\mathbf{r})) + E_H(n(\mathbf{r}))$$

$$+ E_{xc}(n(\mathbf{r}),\nabla x(j_p(\mathbf{r})/n(\mathbf{r}))) . \tag{1b}$$

$T_c$ is the kinetic energy of a noninteracting Fermion liquid with density $n(\mathbf{r})$ and paramagnetic current $j_p(\mathbf{r})$, $E_H(n(\mathbf{r}))$ is the Hartree energy, and $E_{xc}$ is the exchange and correlation energy. The effect of inhomogeneity [i.e., $V(\mathbf{r})$] as reflected in larger effective mass $m^*$ was determined. For $m^*/m \simeq 1.8$ no SBCCS was found. As the depth of the wells to $m^*/m \simeq 3.3$, $m^*/m \sim 6.4$ and $m^*/m \sim 12.4$ continued to increase, SBCCS clearly appear. Figure 2.1 details the current pattern of $j_p(\mathbf{r})$. A wide variety of patterns are observed. For relatively small $m^*/m \sim 3.3$ (first panel of Fig. 2.1) $j(\mathbf{r})$ has not yet stabilized to a clear-cut vortex antivortex structure observed in the other two panels.

---

1. Summary of paper: *Physical Review Letters* (in press).
2. Commissariat á l'Energie Atomique, Villeneuve-Saint-Georges, France.
3. D. Ceperley, *Phys. Rev. B* **18**, 3126 (1978).
4. G. Vignale, M. Rasolt, and D. J. W. Geldart, *Phys. Rev. B* **37**, 2502 (1988).
5. Y. Hasegawa et al., *Phys. Rev. Lett.* **63**, 907 (1989).

## UPPER CRITICAL FIELD OF LAYERED SUPERCONDUCTORS[1]

*S. H. Liu*

All high-$T_c$ copper oxide superconductors have stratified crystal structures. The charge carriers move freely in the CuO layers but hop weakly between the layers. As a result, the effective mass in the direction perpendicular to the layers is usually much larger than that within the layers. The mass anisotropy causes the fluxoid structure to be flattened when the applied magnetic field is parallel to the layers; and with sufficiently high field, the

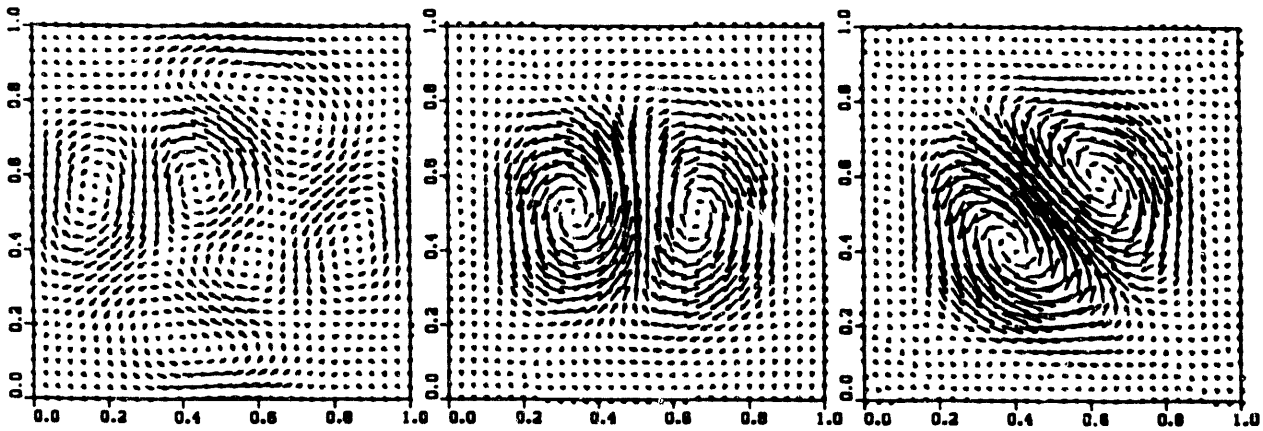

Fig. 2.1. The current patterns in a unit cell of a symmetry-broken current-carrying state in a two-dimensional nonuniform interacting electron gas. The panel on the left has the smallest density nonuniformity with $\frac{m^*}{m} \approx 3.3$ the center panel has $\frac{m^*}{m} \approx 6.4$ and the right panel $\frac{m^*}{m} = 12.4$ (see text).

fluxoid can fit inside the space between adjacent layers. This effect is known as "dimensional crossover," and at this point the magnetic field ceases to have any further deleterious effect on superconductivity. Typically, the effect is expected to occur at a realistic magnetic field strength in systems in which the hopping strength between the layers is exceedingly weak, much weaker than that found in CuO systems.

In systems with more than one layer in a unit cell, a new dimensional crossover phenomenon becomes possible. If the layers have unequal pair coupling strengths, a sufficiently strong magnetic field can quench the superconductivity in one layer and leave the other layer less affected. The same can happen if the two hopping strengths are far apart. A set of critical field vs. temperature curves is shown in Fig. 2.2. These are calculated for a two-layer model with intralayer pairing interactions in

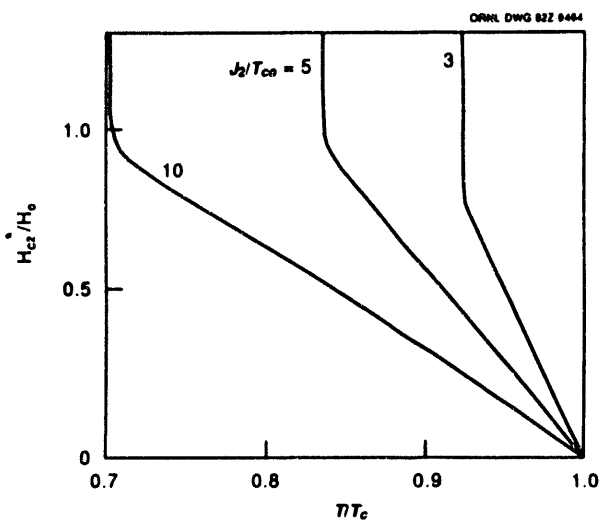


Fig. 2.2. Upper critical field curves for a two-layer model which shows the new kind of dimensional crossover, as indicated by the sharp upturn of the curves. The model parameters are given in the text.

the ratio $\lambda_{02}/\lambda_{01} = 0.5$ and the hopping strengths in the ratio $J_1/J_2 = 0.1$. Fig. 2.3 shows how the order parameter in the layer with weaker pairing is quenched by the magnetic field. A superconductor in this state may be

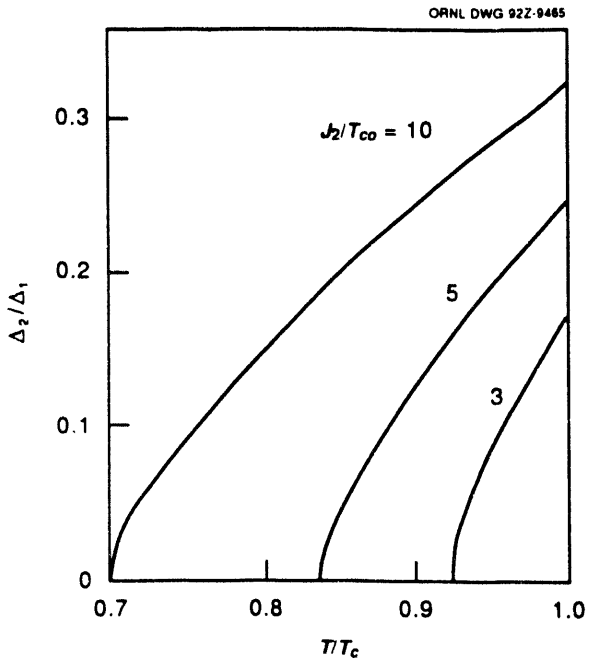


Fig. 2.3. The ratio of the order parameters of the two kinds of superconducting layers plotted as a function of the magnetic field, demonstrating that the weakly paired layers become nonsuperconducting at the dimensional crossover field.

able to withstand a high current because the current can flow in the strongly superconducting layers while the accompanying magnetic field can penetrate the weakly superconducting layers. The flux lattice consists of parallel sheets which are rigidly pinned. Such a state, if realized, could be of technological importance.

1. Summary of paper to be published.

## $d^9$ SPIN POLARON THEORY OF HIGH-$T_c$ SUPERCONDUCTIVITY[1]

*R. F. Wood and J. F. Cooke*

The results of further studies of a $d^9$ spin-polaron model of high-$T_c$ superconductivity are reported. Calculations of their formation energies suggest that spin polarons involving the Cu $d^9$ configuration and O $2p\sigma$ orbitals in the $CuO_2$ planes should form readily in the new high-$T_c$ superconductors. Estimates of their radii and effective masses indicate that they are small spin polarons with masses approximately four times the band effective mass. Formation of spin polarons destroys the long-range antiferromagnetic (AFM) ordering, but repair, or healing, of the AFM order locally provides a pairing mechanism.

Parameterized AFM band calculations for a $CuO_2$ plane show how a Mott-Hubbard (M-H) gap opens as a consequence of an electron repulsion energy U at the Cu sites. The parameters are chosen to give agreement with measured density of states, the magnetic moment per Cu site, and other data. In contrast to our earlier band calculations,[2] self-consistency on the Cu spin density has now been introduced. In a typical calculation, using ~200 points in the irreducible sector of the magnetic Brillouin zone, convergence to the final up- and down-spin densities at a Cu site is rapid. Convergence in less than ten iterations occurs even when starting with nearly equal values of $\rho_\alpha$ and $\rho_\beta$ (e.g., for an $\alpha$-spin site, $\rho_\alpha$ = 0.52 and $\rho_\beta$ = 0.48). The converged values differ little from those

obtained from the nonself-consistent calculation (i.e., for a single iteration when starting with $\rho_\alpha = 1.0$ and $\rho_\beta = 0.0$). Moreover, an increase of ~20% in the value of U (from 4.0 to 4.8 eV) brings the results of the two calculations into close coincidence. Variation of the hole concentration by Sr doping in $La_{2-x}Sr_xCuO_4$ and O depletion in $YBa_2Cu_3O_{7-x}$ moves the Fermi level relative to the M-H band edge. The band calculations are in agreement with a number of recently measured quantities.

Approximate expressions for the gap and $T_c$ within the framework of a Cooper-pairing approach are derived and then solved using information from the band calculations. The proximity of the Fermi level to the M-H band edge and the interplay of O $2p\sigma$ and $2p\pi$ bands and/or localization effects can provide good fits to the variations of $T_c$ with $x$ in $La_{2-x}Sr_xCuO_4$ and $YBa_2Cu_3O_{7-x}$. In the latter case, the fitting provides clear evidence for the role of electron trapping in the chain plane as $x$ is increased. The in-plane gap is either *s*- or *d*-like but anisotropic in either case. A discussion of various aspects and implications of the model is given. The main features of our spin-polaron model are contrasted to those of a more recently proposed spin bipolaron model by Mott.[3]

---

1. Summary of paper: *Phys. Rev. B* **45**, 5585 (1992).
2. R. F. Wood, M. Mostoller, and J. F. Cooke, *Physica C* **165**, 97 (1990).
3. N. F. Mott, *Adv. Phys.* **39**, 55 (1990).

## RESISTIVE TRANSITION AND NORMAL-STATE CONDUCTIVITY IN $YBa_2Cu_3O_7/PrBa_2Cu_3O_7$ SUPERLATTICES

*R. F. Wood*

Fiims containing varying numbers $N_Y$ and $N_P$ respectively of YBCO ($YBa_2Cu_3O_7$) and PBCO ($PrBa_2Cu_3O_7$) unit cells in a "supercell" have shown interesting superconducting properties whose understanding may shed light on the basic pairing mechanism and on interplanar coupling. The resistance as a function of temperature, $R(T)$, from the onset of the resistive transition to 300 K has been fit for ~15 such superlattices fabricated and measured at ORNL. In the resistive-transition region, expressions based on Kosterlitz-Thouless (K-T) vortex-antivortex unbinding theory and Aslamazov-Larkin (A-L) fluctuation theory are used.[1] In the normal state, conductivity ($\sigma$) terms associated with bulk YBCO and PBCO are introduced. For bulk YBCO, $\sigma$ is assumed to be $\alpha T^{-1}$, as observed experimentally, while for bulk PBCO a fit to the measured conductivity of thin PBCO films is used. In addition, it was found necessary to introduce a hopping-type term, which is tentatively associated with the YBCO/PBCO interface and/or charge transfer. Overall, this fitting procedure gives quite good fits to $R(T)$ for all 15 superlattices.

Samples with $N_P$ fixed at 16 and $N_Y$ varied illustrate the type of results that are obtained. As $N_Y$ is increased from 1 to 8 while holding $N_P = 16$, $R(T)$ shows evolution from a broad resistive region and an activated normal-state

conductivity to a narrow resistive region and bulk normal state YBCO conductivity. The bulk PBCO term contributes only at temperatures $\gtrsim$200 K.

Although the combination of K-T and A-L theories appears to provide a good fit to the data on a linear scale, caution is needed in interpreting the results. The quality of the fit, as determined from the least-squares fitting criterion, is not good in the K-T region, particularly for the $N_Y = 1$, $N_P = 16$ structure. This suggests that while the basic K-T mechanism may be operative, other effects also enter. Values of the Ginzburg-Landau "bulk" transition temperature, $T_c^0$, used as a fitting parameter in the A-L term must be chosen well below the ~92 K value for $T_c^0$ in bulk YBCO samples. This strongly suggests that charge transfer from PBCO to YBCO or hole trapping at the interface is an important effect, as was concluded in a recent publication.[2] In fact, the values of $T_c^0$ derived here are in good agreement with those calculated in Ref. 2. Also, the weight of the interface term appears to correlate with the amount of charge transfer found in Ref. 2, but further study of this is required.

---

1. Numerous authors have recognized the potential importance of K-T dimensionality effects in both high-$T_C$ bulk and thin-film samples. See, for example, S. Martin et al., *Phys. Rev. Lett.* **62**, 677 (1989); Q. Y. Ting and H. S. Kwok, *Phys. Rev. B* **42**, 2242 (1990); D. Aniosa and H. Beck, *Phys. Rev. B* **43**, 344 (1991); T. Schneider, Z. Gedik, and S. Ciraci, *Europhys. Lett.* **14**, 261 (1991); M. Rasolt, T. Edis, and Z. Tešanović, *Phys. Rev. Lett.* **66**, 2927 (1991). The role of fluctuation effects has been much less studied.

2. R. F. Wood, *Phys. Rev. Lett.* **66**, 829 (1991).

## POLARONS IN THE LAYERED ELECTRON GAS[1]

*G. D. Mahan*[2]

High-temperature superconductors are layered electron gases (LEG). The conduction electrons in the planes of copper-oxygen are in two-dimensional layers, which are stacked parallel to each other. Previously, the electron-phonon interaction for a simple LEG was derived. This work has been extended to calculate the electron-phonon coupling constant for simple analytical models of the electrons and phonons. This project relates to possible mechanisms of high-temperature superconductivity. One possible mechanism has the electrons pairing because of the coupling to the phonons. Previously, calculations of this coupling did not properly account for the layered nature of the conducting electrons. This calculation is the first to do so correctly.

Several new items of physics were found. The screening of the interaction from the electron-electron interactions is quite anisotropic. The anisotropy causes a dimensional crossover. For phonons of long wavelength, the screening is three-dimensional. However, for phonons of short wavelength, the screening causes the electron-phonon interaction to become two-dimensional. Then, it depends only upon the vibrations within the cuprate plane of the conduction electrons. The crossover occurs at $qc > 1$, where $q$ is the wave vector of the phonon, while $c$ is the interlayer spacing. Since $c$ is large, most of the phonons in the Brillouin zone contribute to the coupling in the two-dimensional limit. Thus, the electron-

phonon coupling for the cuprates should be nearly the same for all of them, since only the in-plane behavior matters.

Another feature of the anisotropic interaction is that phonon vibrations with polarization components perpendicular to the plane (and parallel to the c axis) contribute little. Since the electron density oscillations can only vibrate within the plane, they can only strongly couple to phonons which vibrate in the same direction. Vibrations perpendicular to the plane have a negligible electron-phonon interaction and are unscreened. This result agrees with polarized infrared absorption. The anisotropy tends to weaken the total electron-phonon coupling.

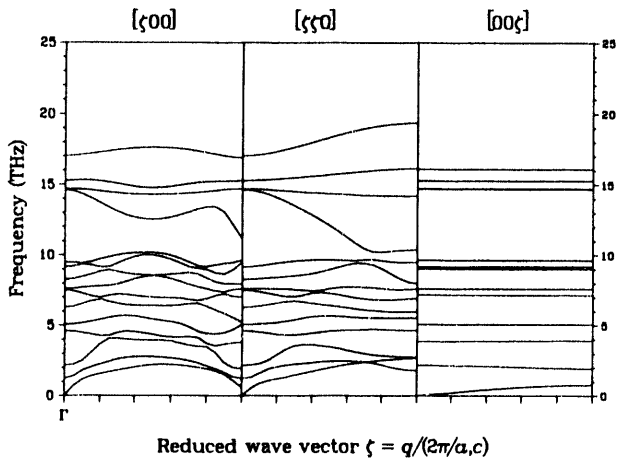


Fig. 2.4. Calculated quasi-longitudinal modes in Bi 2212.

---

1. Summary of paper: *Phys. Rev. B* **43**, 2934 (1991).
2. ORNL/UT Distinguished Scientist.

## LATTICE DYNAMICS OF HIGH-$T_c$ SUPERCONDUCTORS[1]

*Mark Mostoller*

Previously, shell model calculations have been reported[2] for the 35-K superconductor $La_2CuO_4$, which has one $CuO_2$ plane per layer and a seven atom basis in the body-centered tetragonal (bct) unit cell. In connection with recent neutron scattering experiments,[3] the computer programs have been extended to treat $Bi_2CaSr_2Cu_2O_8$ (Bi 2212), for which $T_c \geq 80$ K. The bct 2212 structure has 2 $CuO_2$ planes per layer and 15 atoms in the bct cell. Figure 2.4 shows calculated quasi-longitudinal modes for Bi 2212. As in other high-$T_c$ layered perovskites, the high-frequency modes are vibrations of the in-plane oxygen atoms.

Preliminary calculations for the cubic perovskite $Ba_{1-x}K_xBiO_3$, in connection with current neutron scattering experiments[4] which have $T_c = 30$ K for $x = 0.4$, have been carried out. This material is interesting because it is cubic rather than layered and does not exhibit any antiferromagnetic behavior.

---

1. Summary of paper to be published.
2. M. Mostoller et al., *Phys. Rev. B* **41**, 6488 (1990).
3. H. A. Mook et. al., "Phonons and Superconductivity in $Bi_2CaSr_2Cu_2O_8$," this report; *Physical Review Letters* (in press).
4. R. M. Nicklow et. al., "Phonons in Superconducting $Ba_{0.6}K_{0.4}BiO_3$," this report.

## SIGN OF THE COUPLING BETWEEN *T*-VIOLATING SYSTEMS IN SECOND-ORDER PERTURBATION THEORY[1]

*A. G. Rojo*[2] *and A. J. Leggett*[3]

There is current interest in time-reversal ($T$) violating systems, mostly because of the realization that the charge carriers in the CuO planes of the high-$T_c$ superconductors may be fractional statistics quasiparticles. Other $T$-violating possibilities in this context are the so-called "flux-phases,"[4] or $^3$He "ABM"-type phases.[5] Theoretical treatments of this problem concentrate mainly on a single plane, whereas in predicting observable quantities in the bulk system, it is important to have a picture of the ordering of the signs of the (spontaneous) symmetry breaking in different planes. With this motivation, the general situation of two distinguishable systems, each of them breaking $T$ and coupling via a $T$-even interaction, was considered. It was shown that up to second-order perturbation theory, the AFM configuration has lower energy in most physically interesting cases. In second order, the degeneracy between the two configurations is lifted if the spectral function of the coupling operator (density in the case of the Coulomb interaction) is different from its time-reversed value ($\chi_{\mathbf{k}} - \chi_{-\mathbf{k}} \neq 0$). To get an order-of-magnitude estimate, it was assumed that the "asymmetry" in $\chi$ is of order one ($\chi_{\mathbf{k}} - \chi_{-\mathbf{k}} \sim \chi_{\mathbf{k}}$) corrected by an "edge-effect factor" $d/R$, where $d$ is the interparticle distance and $R$ is a typical domain-size perimeter. Using the fact that the main weight of $\chi_{\mathbf{k}}(\omega)$ is the plasmon pole and that $d$ is of order or the interplane distance $D$, it was calculated that $\Delta E/\text{particle} \sim (D/R)\,\omega_P$, with $\omega_P$ the three-dimensional plasma frequency. Typical twin-domain widths are $R \sim 5000$ Å.[6] If the "domains" corresponding to coherent $T$ violations with the twin domains are identified, then it is estimated that $\Delta E/\text{particle} \sim 10^{-3}$ eV.

---

1. Summary of paper: *Phys. Rev. Lett.* **67**, 3614 (1991).
2. Guest scientist from the ORNL/UT Distinguished Scientist Program.
3. University of Illinois, Urbana, Ill.
4. G. Kotliar, *Phys. Rev. B* **37**, 3664 (1988).
5. A. J. Leggett, *Rev. Mod. Phys.* **47**, 331 (1975).
6. C. Chen, p. 124 in *Physical Properties of High-$T_c$ Superconductors*, Vol. II, ed. by D. Ginsberg, World Scientific, 1991.

## TWO PHASES OF THE ANYON GAS AND BROKEN *T* SYMMETRY: SOME EXACT RESULTS[1]

*G. S. Canright*[2] *and A. G. Rojo*[3]

The first exact finite-temperature studies of anyons are reported. This method is an extension to finite $T$ of earlier numerical work with small numbers of anyons on a lattice. The spontaneous magnetization $M_0(T)$ was studied, since this signature has been identified as a key signature of broken $T$ symmetry for anyon models. These results confirm the two-phase picture suggested by earlier work in which a low-temperature regime, where $M_0$ is very small or zero, and a high-temperature regime, where $M_0$ is of $O(0.1\ \mu_B)$ per particle, were found. In the high-temperature regime, an excellent estimate of $M_0(T)$ in the thermodynamic limit (which we will call $M_0^\infty$) can be

obtained, since our finite-size results extrapolate smoothly with little scatter. Values for $M_0^\infty$ can then be compared with the results of μSR experiments on high-temperature superconductors, which set an upper experimental bound on the internal fields from such moments. $M_0^\infty$ in a bulk material of many planes almost certainly will give a signal well above this threshold if (and only if) the planes are ordered ferromagnetically. In the antiferromagnetic case (which is strongly favored energetically), the signal from $M_0^\infty$ is probably undetectable. Finally, it is estimated that the transition temperature $T_c$ from our finite-size studies will obtain a value on the order of a few hundred Kelvins.

---

1. Summary of paper: *Int. J. Mod. Phys. B* **5**, 1553 (1991).
2. Guest scientist from The University of Tennessee, Knoxville, Tenn.
3. Guest scientist from the ORNL/UT Distinguished Scientist Program.

## SOME CONSEQUENCES OF *PT* SYMMETRY FOR OPTICAL ROTATION EXPERIMENTS[1]

*G. S. Canright[2] and A. G. Rojo[3]*

A number of optical experiments have been carried out on various samples of high-temperature superconductors (HTSC) to search for signs of spontaneously broken time-reversal $T$ symmetry. The results from these experiments appear to support both positions on this question—that there is, or is not, such spontaneous symmetry breaking in the HTSC. Of two sets of experiments specifically constructed to select only nonreciprocal effects, one gave a null result, while another set gave unambiguous positive results. A third set of experiments strongly suggested broken $T$; these experiments were not constructed, however, in such a way as to rule out reciprocal effects.

The "*PT* state" has been defined, and its consequences were examined for experiments on optical rotation. Optical rotation in transmission is forbidden in the *PT* state only if the additional requirement of rotational symmetry is imposed. The experiments of Weber et al.[4] on (2212) show large optical rotation in transmission, which is not allowed if the *PT* model plus tetragonal symmetry for the material is assumed. In fact, however, (2212) is only pseudotetragonal, as there is usually an incommensurate modulation of the lattice along the a or b axis. The experiment of Spielman et al.[5] measures $\arg(T^{\ell}_{--}/T^{r}_{++})$. Interestingly, this quantity may be nonzero for the general *PT* state, but is strictly zero for orthorhombic symmetry or higher—and hence for the HTSC in the *PT* state.

---

1. Summary of paper: *Phys. Rev. Lett.* **68**, 1601 (1992).
2. Guest scientist from The University of Tennessee, Knoxville, Tenn.
3. Guest scientist from the ORNL/UT Distinguished Scientist Program.
4. H. J. Weber et al., *Solid State Commun.* **76**, 511 (1990).
5. S. Spielman et al., *Phys. Rev. Lett.* **65**, 123 (1990).

## ORDERING OF CHIRALITY FOR MANY PLANES OF ANYONS[1]

*A. G. Rojo*[2] *and G. S. Canright*[3]

In quantum mechanics it is known that the indistinguishability of the (identical) particles imposes symmetry constraints on the wave function and on the observables. Thus, the wave functions can be either symmetric or antisymmetric with respect to the interchange of two-particle coordinates, whereas the observables must be invariant under such operations.

Identical anyons are particles that give an arbitrary complex phase $e^{i\theta}$ upon interchange which is neither +1 (Bose) nor -1 (Fermi); and for simple topological reasons, they can live only in two dimensions. The high-temperature superconductors are based on copper-oxide planes, which are, in a useful approximation, two-dimensional. It has been argued that particles doped over the insulating phase of these compounds become dressed quasi-particles that obey fractional statistics. One essential feature of the anyon models is the violation of time-reversal symmetry $T$. In predicting observable quantities in the $m$ bulk system, it is of crucial importance to have a picture of the ordering of the signs of the spontaneous symmetry breaking (statistical angles) in different layers. It has been shown that if a two-body Coulomb interaction $V$ between anyons in different planes is included, the antiferromagnetic (AFM) configuration of statistical angles in different planes is favored. The ground state energy was calculated for many planes of anyons $p$ = 2–4, were $p$ is the number of coupled planes. All planes were identical (small lattices with free-boundary conditions and $N$ particles per plane) except for the sign of the statistics angle $\theta$. Ordering schemes for sgn$\theta$ included strictly alternating order (AFM: e.g., + − + for $p$ = 3), uniform order (FM: + + +), and intermediate schemes for $p > 2$. The quantity $\Delta E \equiv E$(FM) - (AFM) was calculated; thus, $\Delta E > 0$ implies that alternating order is favored energetically. It is found that this $\Delta E > 0$ for a wide variety of cases—for either sign of $V$, for the entire range of $\theta$, and for either sign of an in-plane near-neighbor coupling $U$. It was concluded that the bulk system does not break time-reversal symmetry. A possible experimental test of this picture will be the dichroism for transmission in which it is predicted that the rotation angle should be independent of the sample thickness.

---

1. Summary of paper: *Phys. Rev. Lett.* **66**, 949 (1991).
2. Guest scientist from the ORNL/UT Distinguished Scientist Program.
3. Guest scientist from The University of Tennessee, Knoxville, Tenn.

## ANTIFERROMAGNETIC ORDERING OF SYMMETRY BREAKING IN MULTIPLE PLANES[1]

*A. G. Rojo*[2] *and G. S. Canright*[3]

A multiplane model for the anyon problem is presented. Anyons on different planes are coupled via a Coulomb-type interaction. The model solves exactly finite clusters and shows that the antiferromagnetic order of the chirality is favored for both attractive and repulsive

interplane coupling. A simple model has been studied which can be treated analytically and has the same qualitative behavior as the exact results. This model consists of free particles on a ring geometry enclosing fluxes that can be either parallel or antiparallel. The results of this solution are in remarkable agreement with the computer simulations for small clusters. The fact that the dependence of energy bias on the different parameters of the problem (statistics or interplane repulsion) for two-dimensional (2D) systems is very similar to the case of one-dimensional (1D) rings has been explained in a different publication,[4] where it was shown that this mechanism, at least in second-order perturbation theory, is an edge effect. In that sense, the basic relevant dynamics of the 2D system is included in the edges of the sample, and this can be modeled by a 1D system. These results apply to the low-density limit, in which finite currents exist in each plane. These currents also occur in the high-temperature (nonsuperfluid) phase of the anyon system, and so these results should apply also to that regime. It has been shown[5,6] that these currents should vanish in the low-temperature regime in the thermodynamic limit. At lower temperatures a superfluid transition with a time-reversal symmetric-order parameter is likely to occur, and it seems plausible that in this regime the FM and the AFM configurations would be degenerate. A question then arises as to what extent thermal fluctuations in the normal (high-temperature) regime might affect the AFM order.

If only the relative signs of the statistical angles in different planes are considered, the energetics of the system are that of a 1D Ising model. The effective coupling $J$ between different planes is, however, proportional to the number of particles in each plane; thus it is plausible that the AFM order would not be destroyed by thermal fluctuations.

---

1. Summary of paper: *Int. J. Mod. Phys. B* **5**, 1565 (1991).
2. Guest scientist from the ORNL/UT Distinguished Scientist Program.
3. Guest scientist from The University of Tennessee, Knoxville, Tenn.
4. A. G. Rojo and A. J. Leggett, *Phys. Rev. Lett.* **67**, 3614 (1991).
5. G. S. Canright and M. D. Johnson, *Phys. Rev. B* **42**, 7931 (1990).
6. Y. Kitazawa, *Phys. Rev. Lett.* **65**, 1275 (1990).

# *THIN FILMS*

## GROWTH OF UNIFORM-THICKNESS THIN FILMS BY PULSED-LASER ABLATION

*D. H. Lowndes, J. W. McCamy,*[1] *Shen Zhu,*[1] *and D. B. Poker*

Pulsed-laser ablation (PLA) has advantages for thin-film growth that include stoichiometric (congruent) deposition of complex, multi-element materials from a single solid target, epitaxial growth at reduced substrate temperatures, and precise, "digital" control for atomic layer-by-atomic layer construction of artificial phases. However, a disadvantage of PLA is that the angular distribution of ablated

material from a "point" ablation source is strongly peaked in the forward direction, so that the film thickness varies rapidly with position (~$|\cos \vartheta|^n$, with $n$ ~1.5–10).

Two new PLA film-deposition geometries to overcome this limitation were recently designed and tested. For compound semiconductor growth, it was found that film thickness variations could be nearly eliminated by using a rotating substrate heater and rotating ablation target with coincident rotation axes, but offsetting the laser beam on the target by an amount ρ from the rotational center line. The "plume" of ablated material then is most intense at some radial distance away from the center line; by adjusting the ratio ρ/Δ (where Δ is the target-substrate separation), the deposition profile can be varied continuously from a central peak to a central minimum (saddle shape). Figure 2.5 (top) shows that this offset geometry produced epitaxial ZnS films that were completely uniform (±1%) in thickness over areas ~75 mm$^2$ and with good thickness uniformity (±3%) over areas ~300 mm$^2$.

The second uniform-thickness geometry involved scanning the focused pulsed-laser beam in a nearly circular path, near the outer edge of a 5-cm-diam $YBa_2Cu_3O_{7-x}$ (YBCO) target, thus simulating a "ring source" of material. By adjusting the ratio ρ/Δ, where ρ now is the radius of the ring source, the deposition thickness profile was controlled. Figure 2.5 (bottom) shows that YBCO films were deposited over a ~20-mm × 20-mm area with the thickness constant to within ±5%. The figure also shows that the deposition could have been more uniform over a larger area had a larger ρ been used (resulting in a slightly saddle-shaped profile). This suggests that annular ablation targets with large inner and outer radii may be the most economical for future applications of this geometry.

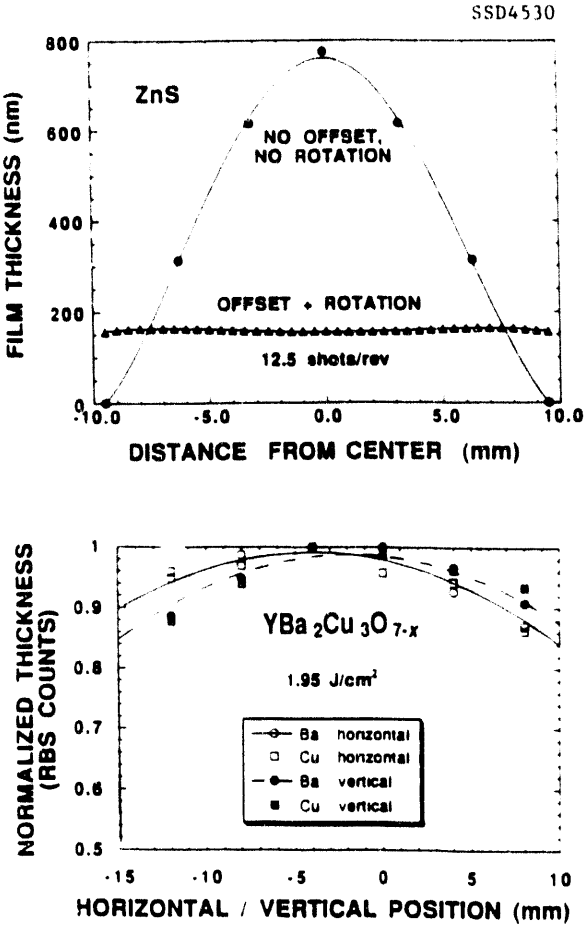


Fig. 2.5. (Top) ZnS film thickness uniformity, either with no substrate rotation or offset (1200 total laser shots) or with 12.5 laser shots/substrate revolution and ρ = 5 mm (2000 total shots). (Bottom) Film thickness uniformity, as measured by total RBS counts for Ba and Cu, for both vertical and horizontal scans of a YBCO film.

---

1. Graduate student from The University of Tennessee, Knoxville, Tenn.

## EARLY STAGES OF $YBa_2Cu_3O_{7-\delta}$ EPITAXIAL GROWTH ON (001) MgO AND $SrTiO_3$[1]

*Douglas H. Lowndes, X.-Y. Zheng,[2] Shen Zhu,[3] J. D. Budai, and R. J. Warmack[4]*

The vortex pinning centers responsible for the high $J_c$ of $YBa_2Cu_3O_{7-\delta}$ (YBCO) films are believed to be related to film-growth defects, since bulk YBCO single crystals have much lower $J_c$. Consequently, studies of the initial film-growth mechanism and of the formation and evolution of dislocations and other defects are expected to identify the source of vortex pinning.

Recently STM studies of the initial stages of the epitaxial growth of very thin $c_\perp$ YBCO films on (001) $SrTiO_3$ and (001) MgO were reported.[1] For MgO, it was found that YBCO clearly grows by an island mechanism, even at very small film thicknesses. Figure 2.6 (top) shows the high density of islands observed even in an ~8 unit-cell (~9.4-nm) YBCO film on MgO. While most island sites appear to be developing screw-growth features, a few islands already have formed well-developed spirals of a half to one turn. A side view of the images shows that the edges of many of the islands are slightly higher than their centers, indicating that the planes of growth at each YBCO island are tilted relative to the MgO substrate surface. This small tilt may be responsible for the formation of the screw dislocations; the origin of the tilt may be the large (~9%) lattice mismatch between YBCO and MgO.

In contrast, Fig. 2.6 (bottom) shows that films of the same thickness grown on (001) $SrTiO_3$ have a smooth, planar appearance, consistent with a layer-by-layer growth mechanism. However, formation of 3D islands was

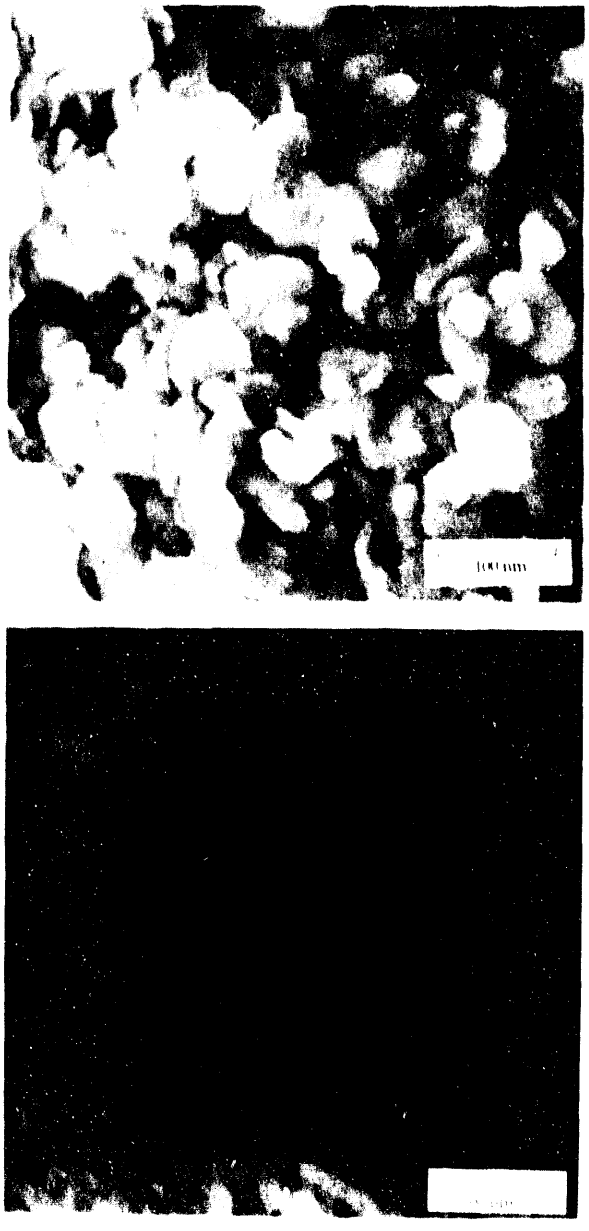

Fig. 2.6. STM images of $c_\perp$ YBCO films ~8 unit cells thick grown at 720°C on (001) MgO [top] and (001) $SrTiO_3$ [bottom].

observed for thicker films grown on (001) $SrTiO_3$, beginning at ~16 $c_\perp$ unit cell thicknesses (~19 nm). Thus, these studies indicate that YBCO films grow on (001) $SrTiO_3$ in a Stranski-Krastanov-like mode.

A second, striking result was that no screw-growth features were found in thin films grown on (001) $SrTiO_3$, until the film thickness increased to 32 unit cells, when screw-growth features, including several turns of the screw, appeared. This demonstrates that there is a critical thickness for the introduction of screw dislocations into YBCO on (001) $SrTiO_3$, with screws first appearing at a slightly greater film thickness than the changeover from layer-like to island growth. This suggests that the generation of a high density of screw dislocations could be due to island coalescence, after the switch of the growth mode, or may be due to the release of built-up strain caused by the ~1% YBCO/$SrTiO_3$ lattice constant mismatch. Observations do not rule out the possibility that YBCO films undergo similar transitions on (001) MgO. However, on MgO the critical film thickness may be only 1 or 2 unit cells, due to the much larger lattice mismatch.

---

1. Summary of paper: *Phys. Rev. B: Rapid Communications* (in press).
2. Postdoctoral fellow from The University of Tennessee, Knoxville, Tenn.
3. Graduate student from The University of Tennessee, Knoxville, Tenn.
4. Health and Safety Research Division, ORNL

## SUPPRESSION OF THE SPIRAL-GROWTH MECHANISM IN EPITAXIAL $YBa_2Cu_3O_{7-\delta}$[1]

*Douglas H. Lowndes, X.-Y. Zheng,[2] Shen Zhu,[3] J. D. Budai, and R. J. Warmack[4]*

Scanning tunneling microscopy (STM) studies have been made of the effects of small changes of substrate orientation on the crystalline alignment, growth mechanism, and defect microstructure of epitaxial YBCO films. The principal finding is that the spiral-growth features that are so prominent in YBCO films grown on well-aligned (001) substrates[5,6] can be completely eliminated by growing YBCO on a nearly lattice-matched substrate that is miscut only 2–3 degrees away from (001).

Figure 2.7 shows the striking effect that the substrate miscut has in modifying the microstructure and growth mechanism of a nominally 16-cell (~188-Å)-thick YBCO film grown at 720°C on a $LaAlO_3$ substrate with $\theta_m = 2.7°$. In this figure $\theta_m$ is the miscut tilt angle of the surface normal away from <001>, and $\varphi_m$ is the in-plane angle, between the projection of the surface normal onto the (001) plane and the nearest in-plane <100> direction. The film is seen to consist of a high density of overlapping tilted platelets. An STM line-scan profile of the film surface (Fig. 2.7) shows that each platelet is one c-axis lattice constant (~1.17 nm) thick, and x-ray measurements of $\theta_m$ and $\varphi_m$ reveal that the YBCO platelets are fully epitaxially aligned with the $LaAlO_3$ crystal lattice within measurement error. For a

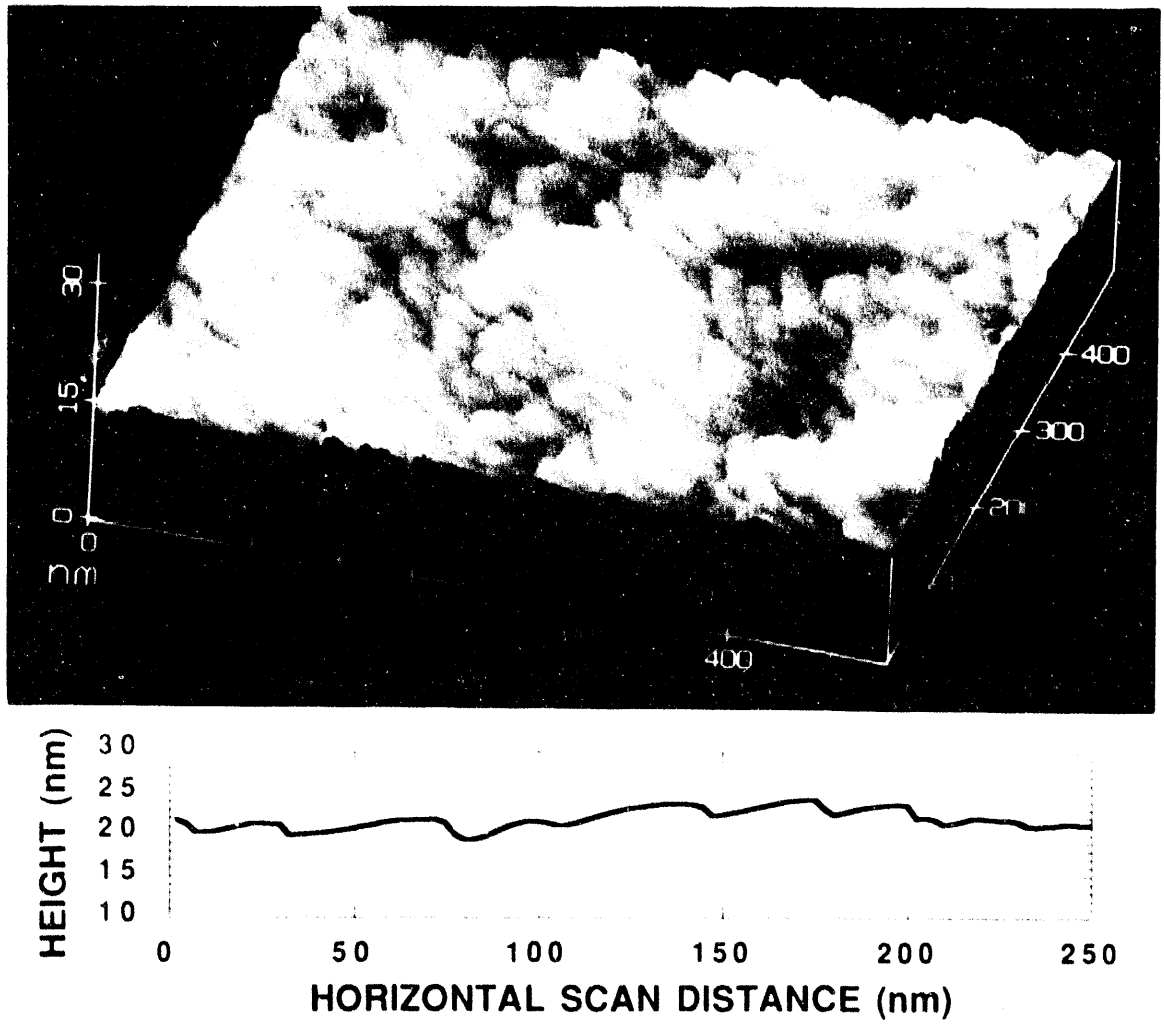


Fig. 2.7. (Top) STM image of the surface microstructure of a YBCO film grown on a miscut $LaAlO_3$ substrate. (Bottom) Line scan surface-height profile.

miscut angle $\theta_m = 2.7°$, the spacing between successive 0.39-nm-tall surface steps is expected to be ~8.3 nm, which should result in a horizontal separation of ~25 nm between successive single-cell YBCO layers. This is in excellent agreement with the actual ~28-nm average width of the exposed terraces seen in the line scan of Fig. 2.7. Very similar results were obtained for YBCO films of various thicknesses grown on miscut $LaAlO_3$ and $SrTiO_3$, demonstrating that this morphology is a general consequence of growth on miscut near-(001) substrates.

The reason that miscut-aligned growth so easily supplants screw-mediated growth is believed to be that a significantly miscut surface simultaneously exposes a large number of steps that nucleate and position in rows (i.e., align) the rapid-growth *a-c* and *b-c* crystal faces so that simultaneous growth occurs on many terraces. Thus, the miscut-aligned

growth mechanism results in grains that are stacks of terraces one unit cell in height and is a rapid-growth mechanism in that numerous terrace-edge sites continuously are made available for growth.

It was also found that the tilted-plate microstructure produced by the miscut-aligned growth mechanism persists to the surface of even thick YBCO films. The film grains were found to be slightly sinuous "strands" of tilted plates, which gave the grains a "rope-like" appearance at low STM resolution. No spiral-growth features were apparent. Thus, the miscut-aligned growth mechanism is remarkably stable, once established.

---

1. Summary of paper to be published.
2. Postdoctoral fellow from The University of Tennessee, Knoxville, Tenn.
3. Graduate student from The University of Tennessee, Knoxville, Tenn.
4. Health and Safety Research Division, ORNL.
5. M. Hawley et al., *Science* **251**, 1587 (1991).
6. C. Gerber et al., *Nature* **350**, 279 (1991).

## SCANNING TUNNELING MICROSCOPY OF PULSED-LASER DEPOSITED $YBa_2Cu_3O_{7-\delta}$ EPITAXIAL THIN FILMS: SURFACE MICROSTRUCTURE AND GROWTH MECHANISM[1]

*David P. Norton, Douglas H. Lowndes, X.-Y. Zheng,[2] Shen Zhu,[3] and R. J. Warmack[4]*

Scanning tunneling microscopy (STM) has been used to investigate the surface of microstructures in epitaxial YBCO thin films grown by pulsed-laser deposition (PLD). The STM images suggest that c-axis-oriented YBCO films grow by a terraced-island mechanism in which the islands consist of flat terraces with step heights that are multiples of the c-axis lattice parameter. Figure 2.8 shows a STM image of a c-axis-oriented epitaxial YBCO thin film grown at $T_{sub}$ ~ 680°C on (100) $SrTiO_3$. Well-defined islands are clearly evident with each island composed of stacks of terraces. The terrace step heights are multiples of the c-axis unit cell height (1.17 nm). The island-like appearance seen in Fig. 2.8 was common to c-axis-oriented films, with the most symmetric, well-defined, and largest grains obtained at higher growth temperatures.

For some of the films, spiraling growth patterns, similar to those reported for sputter-

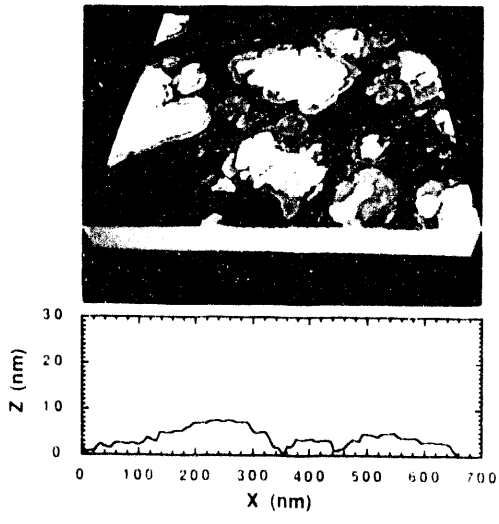


Fig. 2.8. STM image (upper) and line-scan profile (lower) of a c-axis-oriented YBCO epitaxial thin film grown on (100) $SrTiO_3$ at $T_{sub}$ ~ 680°C. The dimensions of the STM image are 670 × 670 $nm^2$.

deposited epitaxial YBCO films, were observed. However, it has not been possible to identify these spiral structures unambiguously in YBCO films that were grown at high temperatures on nearly lattice-matched substrates [i.e., (100) $SrTiO_3$ and (100) $LaAlO_3$] for which the superconducting properties and c-axis growth are optimized. The fact that our smoothest c-axis YBCO films exhibit a surface roughness on the order of 10 nm implies that undulations and/or step discontinuities should exist in the connectivity of ultrathin YBCO layers within $YBa_2Cu_3O_{7-\delta}/PrBa_2Cu_3O_{7-\delta}$ (YBCO/PBCO) superlattice structures. This has important implications for the interpretation of superlattice electrical transport properties and can be interpreted as direct evidence of the structural defects that are needed to justify a weak-link model, where the ultrathin YBCO layers in these structures act as an array of in-plane Josephson-coupled superconducting grains.

---

1. Summary of paper: *Phys. Rev. B* **44**, 9760 (1991).
2. Postdoctoral fellow from The University of Tennessee, Knoxville, Tenn.
3. Graduate student from The University of Tennessee, Knoxville, Tenn.
4. Health and Safety Research Division, ORNL

## KINETIC ROUGHENING DURING a⊥ AND c⊥ GROWTH OF $YBa_2Cu_3O_{7-x}$[1]

*S. J. Pennycook, M. F. Chisholm, S. Zhu,*[2] *D. P. Norton, and D. H. Lowndes*

The surface morphology of $YBa_2Cu_3O_{7-x}$ films is important for device characteristics and microwave properties and seems generally to be controlled by kinetic factors. In the case of c⊥ growth, once the film has relaxed and threading dislocations of screw character are present, they act as favorable nucleation sites in the growing crystal surface. Provided no other competing nucleation sites exist within the radius of a critical nucleus (i.e., the step density due to substrate misorientation is not too high), then the well-known spiral growth patterns, as seen by scanning transmission microscopy (STM), will develop.

However, c⊥ growth is kinetically rather inefficient (although thermodynamically preferred), because it requires a large amount of surface diffusion to grow a layer one unit cell thick. If the crystal orientation were to change to a⊥, then practically no surface diffusion would be necessary. The incoming flux would automatically find itself at the active crystal growth sites, as indicated schematically in Fig. 2.9. Therefore, this growth mode occurs under conditions of high surface supersaturation (e.g., low substrate temperatures or high deposition rates.

However, the surface morphology changes radically with a⊥ growth. Because there is no long-range surface diffusion, the lateral scale of the roughness decreases sharply. Instead of the

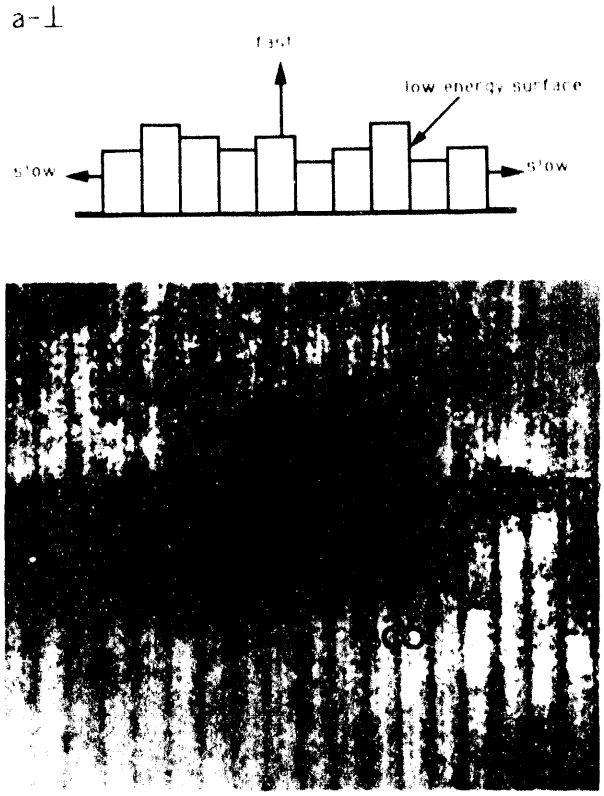


Fig. 2.9. Schematic and Z-contrast image showing microscopic roughness associated with a⊥ growth.

macroscopic waviness seen with c⊥ growth, a microscopic roughness develops, as preserved by the a⊥ superlattice imaged in Fig. 2.9. This can only be distinguished from interdiffusion in the very thin regions of the sample, so that the image is rather noisy. However, the change in composition from $PrBa_2Cu_3O_{7-x}$ to $YBa_2Cu_3O_{7-x}$ and back can just be discerned in each individual unit cell column.

The anisotropy in surface energies, which leads to the relatively smooth interfaces found for c⊥ growth (and c⊥ amorphization), indicates that there is now rather little driving force for smoothing an a⊥ film; roughness only increases the surface area of the low-energy planes (Fig. 2.9). Obviously, microscopic roughness could significantly affect the characteristics of any device structure requiring thin insulating layers, particularly a tunnel junction.

---

1. Summary of paper to be published.
2. Graduate student from The University of Tennessee, Knoxville, Tenn.

## NUCLEATION AND GROWTH OF $YBa_2Cu_3O_{7-x}$ ON MgO[1]

*S. J. Pennycook, M. F. Chisholm, S. Zhu,[2] and D. H. Lowndes*

Initial nucleation and growth processes critically determine the eventual microstructure and properties of a superconducting film. This connection was investigated in the case of ultrathin films of $YBa_2Cu_3O_{7-x}$ on MgO for which scanning tunneling microscopy (STM) has shown the presence of spiral-topped islands in films only a few unit cells thick.[3] In order to distinguish Stranski-Krastanov growth (strain-driven islanding in the presence of a wetting layer of $YBa_2Cu_3O_{7-x}$ on the substrate) from Volmer-Weber growth (islanding with no wetting layer), dark-field plan-view electron microscopy was performed using the {100} reflections of $YBa_2Cu_3O_{7-x}$, which are forbidden in MgO. As can be seen in Fig. 2.10, no wetting layer is present between the islands, and in fact the image intensity is seen to be quantized corresponding to thicknesses of 1, 2, or more unit cells of $YBa_2Cu_3O_{7-x}$.

Fig. 2.10. Dark field Moiré fringe image showing relaxed islands of $YBa_2Cu_3O_{7-x}$ on MgO.

The Moiré fringes visible in the image show directly that even the single unit cell regions of the film have relaxed close to their bulk lattice parameter. Although small regions of the film show fringes having twice the periodicity of the Moiré fringes (indicating the presence of interfacial dislocations and the formation of strong chemical bonds with the substrate), most of the film shows no localized strain fields. This indicates an incommensurate interface with the substrate so most islands were essentially floating on the substrate surface and presumably acquired their epitaxial alignment (cube-on-cube) by nucleating graphoepitaxially at atomic steps in the MgO substrate.

The islands tend to have small angular misalignments. Therefore, as individual islands coalesce on further film deposition, low-angle grain boundaries are formed, which can be seen clearly in the Moiré patterns. In addition, islands nucleating on substrate terraces of different heights may produce c/3 stacking faults as they coalesce. The removal of such a fault requires the nucleation of a screw dislocation, which is presumably the origin of the high density of growth spirals observed by STM (~$10^{10}$ $cm^{-2}$). The total dislocation density determined from the Moiré patterns was found to be ~$10^{11}$ $cm^{-2}$, which is sufficient to account for the strong flux pinning seen in $YBa_2Cu_3O_{7-x}$ thin films.[4]

---

1. Summary of paper to be published.
2. Graduate student from The University of Tennessee, Knoxville, Tenn.
3. S. Zhu et al., *Materials Research Society Symposium Proceedings* (in press).
4. J. Mannhart et al., *Z. Phys. B* **86**, 177 (1992).

## DEFECT STRUCTURE OF SUPERCONDUCTING $YBa_2Cu_3O_x$ FILMS PREPARED AT LOW OXYGEN PRESSURES

*H. Fujita,*[1] *J. D. Budai, J. Z. Tischler, R. Feenstra, and D. P. Norton*

Studies of $YBa_2Cu_3O_x$ (YBCO) films grown on oxide substrates have revealed systematic correlations between the in situ oxygen pressure and the measured film properties. For instance,

as the oxygen pressure during growth is reduced below the typical value of ~100 mTorr, the measured c-lattice parameter increases and the superconducting transition temperature, $T_c$, decreases. The purpose of the present study was to identify the structural modifications responsible for these changes, specifically to consider a proposal that cation disorder (in the form of substitutions between Y and Ba atoms) is quenched in at low oxygen pressures.[2]

X-ray diffraction and resistivity measurements were made on YBCO films grown on MgO substrates at oxygen pressures ranging from 200 mTorr down to 2 mTorr. Over this range of oxygen pressures, it was found that the measured c-lattice parameters varied from 11.7 to 11.8 Å and $T_c$ varied from 89 to 58 K. Reliability factor (*R* factor) comparisons between the measured and calculated x-ray integrated intensities of (00ℓ) reflections revealed that the structures of the YBCO thin films differed systematically from published structures for bulk YBCO crystals. It was found that the suggested model incorporating exchanges between Y and Ba sites does not provide an accurate description of the pressure-induced defect structure in these films; and comparisons with other model structures showed the *R* factors to be relatively insensitive to changes in the oxygen content of the film and to the Y-Ba stoichiometry. These results suggest that more complex structural modifications are introduced during growth at lower oxygen pressures.

1. Great Lakes Colleges Association Science Semester Program student from Monmouth College, Monmouth, Ill.

2. V. Matijasevic et al., *J. Mater Res.* **6**, 682 (1991).

## CELL-BY-CELL GROWTH AND AMORPHIZATION OF $YBa_2Cu_3O_{7-x}$[1]

*S. J. Pennycook, M. F. Chisholm, D. E. Jesson, D. P. Norton, D. H. Lowndes, R. Feenstra, H. R. Kerchner, and J. O. Thomson*[2]

The Z-contrast imaging of an amorphous/crystalline interface formed by room-temperature implantation of oxygen ions into a thin film of $YBa_2Cu_3O_{7-x}$ provides significant insights into the thermodynamically preferred growth mechanism. In Fig. 2.11, the interface is seen to be atomically abrupt, containing discrete interface steps; the height of each step is the full 11.8-Å c-axis lattice parameter.

The most remarkable feature of this image is an overwhelming tendency for the interface to reside at the Cu-chain planes in the crystal,

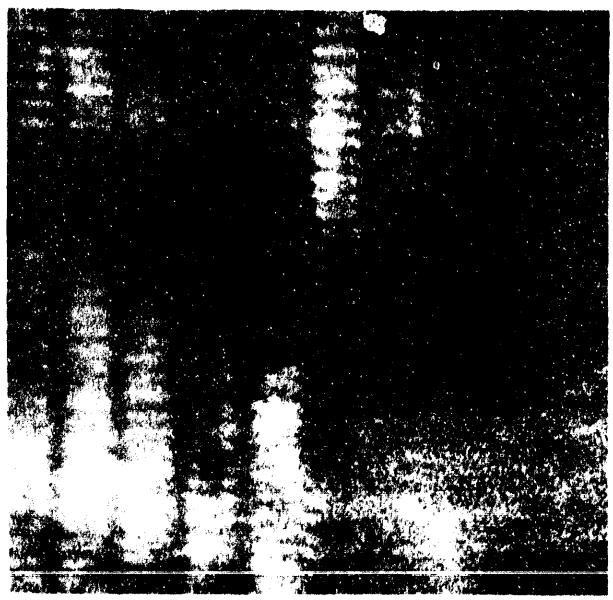

Fig. 2.11. Cell-by-cell amorphization of a c⊥ $YBa_2Cu_3O_{7-x}$ film by oxygen ion implantation.

which are seen as the dark vertical lines in the image. This implies that the surface energy of the Cu-chain plane must be substantially lower than that of the many other possible termination planes of the crystal. Therefore, the Cu-chain plane is the thermodynamically preferred crystal termination and the reason for the cell-by-cell amorphization. It also explains why the c⊥ growth mode is thermodynamically preferred, and why it too proceeds on a cell-by-cell basis to maintain the same low-energy terminating plane. Reflection high-energy electron diffraction (RHEED) oscillations have shown a periodicity of 11.8 Å, although no indication of the termination plane was given.[3] The lattice image in Fig. 2.11 indicates the location of the terminating plane within the unit cell, but the image resolution is not sufficient to determine the number and arrangement of Cu atoms on this plane.

Images from $YBa_2Cu_3O_{7-x}/PrBa_2Cu_3O_{7-x}$ superlattices have also shown that c⊥ growth proceeds on a cell-by-cell basis through sequential nucleation and coalescence of islands, which is the origin of the RHEED oscillations. Investigations of superlattices with single-unit cells of one component show clearly that each layer is almost perfectly completed before the next layer is nucleated and that the intrinsic height of these single-layer islands under the nonequilibrium conditions of actual growth is 20–30 nm.

---

1. Summary of paper: *Phys. Rev. Lett.* **67**, 765 (1991).
2. The University of Tennessee, Knoxville, Tenn.
3. T. Terashima et al., *Phys. Rev. Lett.* **65**, 2684 (1990).

## DEPRESSION AND BROADENING OF THE SUPERCONDUCTING TRANSITION IN $YBa_2Cu_3O_{7-\delta}$-BASED SUPERLATTICES: INFLUENCE OF THE BARRIER LAYERS[1]

*David P. Norton, Douglas H. Lowndes, S. J. Pennycook, and J. D. Budai*

The superconducting properties of $YBa_2Cu_3O_{7-\delta}/PrBa_2Cu_3O_{7-\delta}$ (YBCO/PrBCO) superlattices are a function of both the superconducting (YBCO) and the barrier (PrBCO) layer thicknesses $d$. The zero-resistance transition temperature, $T_c$, decreases as the YBCO layer thickness is decreased or as the PrBCO layer thickness is increased, but for all YBCO layer thicknesses, the $T_{co}$ values appear to saturate at nonzero values. Several theoretical explanations have been suggested for the resistive transitions observed in these superlattice structures. However, fundamental questions concerning the role of the barrier layers in these structures must be answered experimentally before specific mechanisms can be considered. In particular, are the transition temperatures and transition widths for ultrathin YBCO layers, isolated by relatively thick PrBCO layers, determined intrinsically by the YBCO layer thickness or are they largely determined by the electronic properties of the isolating matrix?

In this study, it was determined that the superconducting properties of an isostructural set of $YBa_2Cu_3O_{7-\delta}$-based superlattices depend strongly on the electronic properties of the barrier layers. The resistive transition [$R(T)$] width decreases significantly (i.e., $T_{co}$ increases) as the hole-carrier density in the barrier layers is increased. However, $T_c$(onset)

does not change, contrary to predictions of hole filling models. Figure 2.12 shows the $R(T)$ behavior for 1 × 16 superlattices with either PrBCO, $Pr_{0.7}Y_{0.3}Ba_2Cu_3O_{7-\delta}$ (PrYBCO), or $Pr_{0.5}Ca_{0.5}Ba_2Cu_3O_{7-\delta}$ (PrCaBCO) utilized as the barrier layer material. The $R(T)$ of the

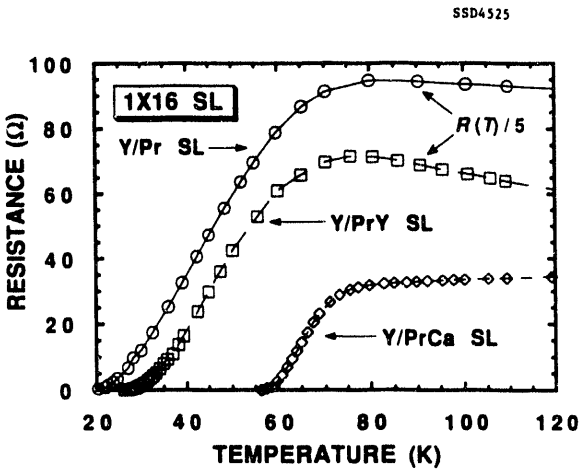


Fig. 2.12. $R(T)$ for 1 × 16 YBCO/PrBCO (o), YBCO/PrYBCO (□), and YBCO/PrCaBCO (◊) superlattice structures.

superlattices clearly depends on the carrier density of the barrier layers. The most interesting effect is a significant increase in $T_{co}$ with increasing barrier layer carrier density (i.e., decreasing Pr content). For the 1 × 16 superlattices, $T_{co}$ increases from ~20 K for the YBCO/PrBCO structure to >50 K for the YBCO/PrCaBCO structure. $T_c$(onset) apparently is determined by the $YBa_2Cu_3O_{7-\delta}$ layer thickness, while the transition width, determined by long-range phase coherence of the superconducting wave function, depends on the electronic properties of the isolating barrier layers.

---

1. Summary of paper: *Phys. Rev. Lett.* **67**, 1358 (1991).

## TRANSPORT-CURRENT RESISTIVITY AND INDUCTIVE IMPEDANCE OF $YBa_2Cu_3O_7/PrBa_2Cu_3O_7$ SUPERLATTICE FILMS[1]

*H. R. Kerchner, D. K. Christen, C. E. Klabunde, J. O. Thomson,[2] Y. R. Sun,[3] and J. R. Thompson[4]*

Experimental measurements of four-terminal transport-current resistivity of certain superlattice films show broad resistive transitions to the superconductive state. Through dynamic ac magnetic response measurements, these films show frequency-dependent, step-like transitions in the inductive impedance just below the temperature where resistivity reaches zero. As an example, Fig. 2.13 shows such data for a superlattice film of 2-unit-cell-thick layers of $YBa_2Cu_3O_7$ and 4-cell-thick layers of $PrBa_2Cu_3O_7$. Such a superconductive critical transition is not described by mean-field theory. Epitaxial superlattice films of $YBa_2Cu_3O_7/PrBa_2Cu_3O_7$ were grown in situ by laser ablation in the Solid State Division Semiconductor Physics, Thin Films, and Photovoltaic Materials Program.[5] Layer thicknesses of each compound ranged from two to four atomic cells. While material inhomogeneity can produce such a broad resistive transition, it

ORNL-DWG 92-8172

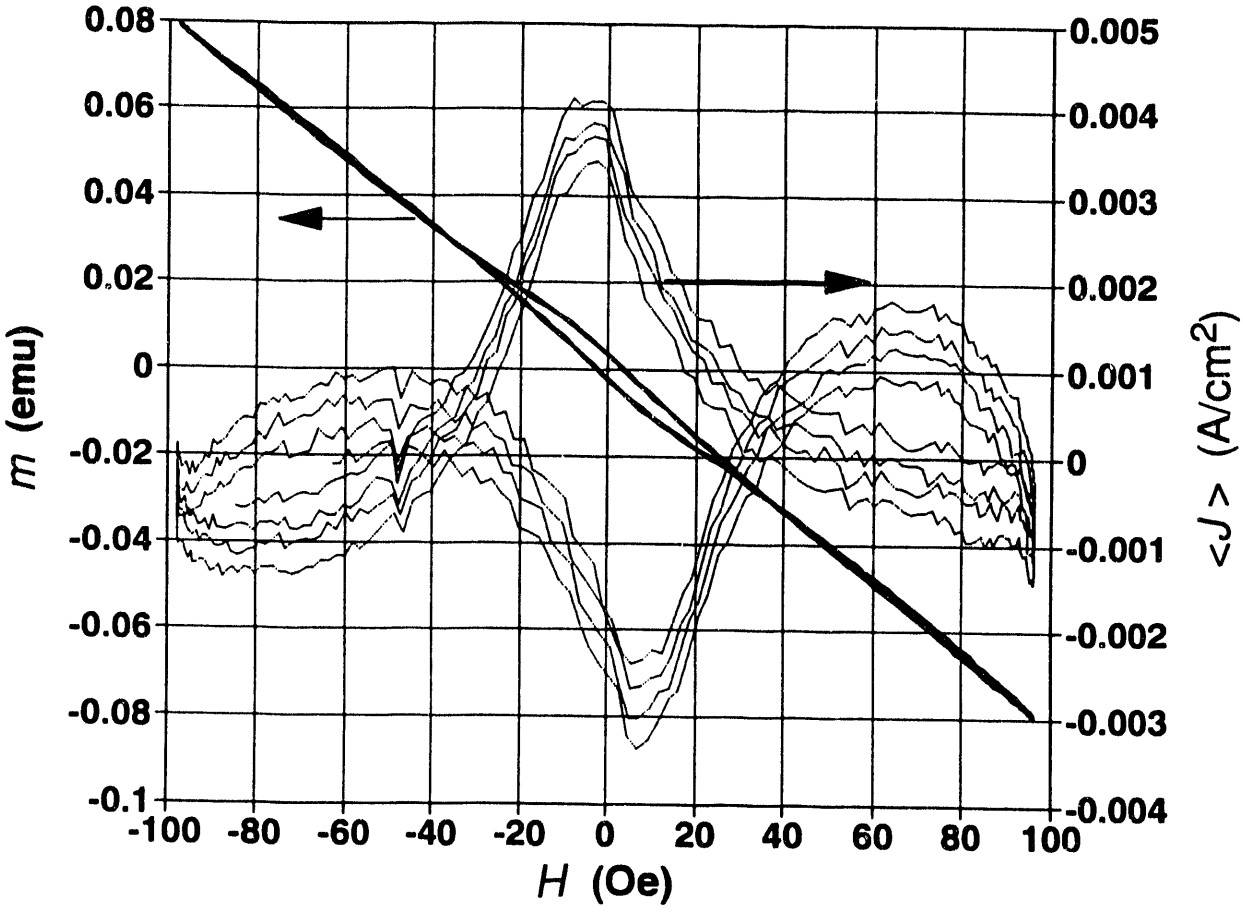


Fig. 2.13. Both transport-current sheet resistance (bulk resistivity $\rho$ divided by film thickness $d$) data (solid line) and ac shielding-current data (□-inductive phase, O-resistive or lossy phase) of a 2 × 4 superlattice film are shown as functions of temperature. The temperature at which the transport-current $\rho = 0$ is near the high-temperature onset of the audio-frequency, ac-inductive-signal step and of the corresponding loss peak. These ac data are at 918 Hz. The apparent Kosterlitz-Thouless critical temperature $T_c$ and the onset $T_c^0$ of the transport-current transition are indicated by arrows. The inset shows the resistance plot used to deduce $T_c$ and $T_c^0$

would prevent observation of a sharp step-like transition in the inductive impedance. Such a response must arise due to vibrations of pinned and bound supercurrent vortices. Observation of the Kosterlitz-Thouless (K-T) transition of bound vortices is expected to occur in a two-dimensional system.[6] Apparent K-T transitions are seen only in films of thin (two or three atomic-lattice cells) Y-compound layers and thick Pr-compound layers. This systematically implies that extreme anisotropy of Cu-O superconductors can be tied to observations of two-

dimensional physical phenomena. Magnetic hysteresis measurements imply quite high critical current density and, therefore, strong vortex pinning, within the $YBa_2Cu_3O_7$ material.

---

1. Summary of paper: *Physics C* (in press).
2. Guest scientist from The University of Tennessee, Knoxville, Tenn.
3. Graduate student from The University of Tennessee, Knoxville, Tenn.
4. Adjunct research and development participant from The University of Tennessee, Knoxville, Tenn.
5. Douglas H. Lowndes, David P. Norton, and J. D. Budai, *Phys. Rev. Lett.* **65**, 1160 (1990).
6. B. I. Halperin and D. R. Nelson, *J. Low Temp. Phys.* **36**, 599 (1989).

## SUPERCONDUCTIVITY AND HOLE DOPING IN $Pr_{0.5}Ca_{0.5}Ba_2Cu_3O_{7-\delta}$ THIN FILMS[1]

*David P. Norton, D. H. Lowndes, B. C. Sales, J. D. Budai, and B. C. Chakoumakos*

The superconducting properties of the material $RBa_2Cu_3O_{7-\delta}$ are nearly independent of the rare-earth element, $R$. The exceptions to this behavior are Ce, Tb, and Pr, which do not form superconductors, with only Pr forming a single-phase "123" structure. Substitution of Pr for Y in $Y_{1-x}Pr_xBa_2Cu_3O_{7-\delta}$ suppresses $T_c$, with superconductivity disappearing at $x \sim 0.5$. Two mechanisms have been proposed for the suppression of $T_c$ by Pr in the "123" phase. The first involves superconducting pair breaking by local moments, due to spin-dependent exchange scattering of the holes in the $CuO_2$ planes, with hybridization between the Pr 4*f* states and the $CuO_2$ valence band states contributing as well. The second mechanism involves the filling and/or localization of holes available for conduction in the $CuO_2$ planes due to a Pr valency greater than +3.

Pulsed-laser deposition has been used to grow $Pr_{0.5}Ca_{0.5}Ba_2Cu_3O_{7-\delta}$ epitaxial thin films that exhibit a superconducting onset temperature of 43 K with $T_c(R = 0) = 34.9$ K. This result is interesting because it is the first time that "123"-phase superconductivity has been achieved by substituting Ca for Pr without the presence in the alloy of Y or any other rare-earth element for which $RBa_2Cu_3O_{7-\delta}$ is superconducting. Also, superconductivity has not been achieved in bulk materials of the same nominal composition. Figure 2.14 shows the superconducting transition for a $Pr_{0.5}Ca_{0.5}Ba_2Cu_3O_{7-\delta}$ epitaxial thin film. These results support the view that hole

SSD4523

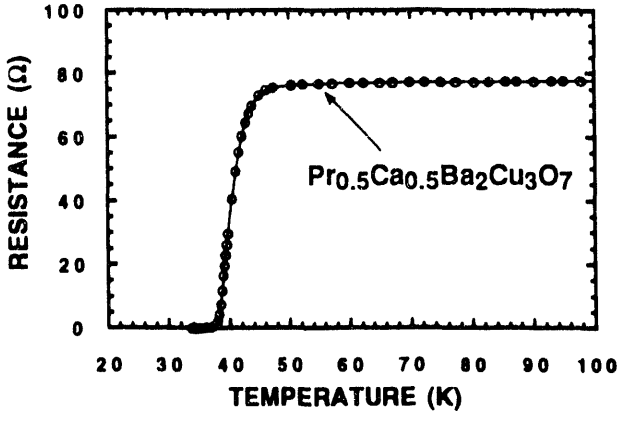


Fig. 2.14. Resistance vs. temperature for a $Pr_{0.5}Ca_{0.5}Ba_2Cu_3O_{7-\delta}$ epitaxial thin film grown at 640°C on (001) $SrTiO_3$; film thickness is ~300 nm.

localization/filling contributes substantially to the suppression of superconductivity by Pr in $PrBa_2Cu_3O_{7-\delta}$ and clearly demonstrate that this suppression can be compensated by appropriate hole doping divalent with Ca on the Pr site.

---

1. Summary of paper: *Phys. Rev. Lett.* **66**, 1537 (1991).

## ROLE OF OXYGEN VACANCIES IN THE FLUX- PINNING MECHANISM AND HOLE-DOPING LATTICE DISORDER IN HIGH CURRENT DENSITY $YBa_2Cu_3O_{7-x}$ FILMS [1]

*R. Feenstra, D. K. Christen, C. E. Klabunde, and J. D. Budai*

The effects of initial and residual oxygen content on the superconductive transport properties were investigated on a series of high-$J_c$ epitaxial thin films. The films were produced either ex situ by postannealing in wet oxygen of Y, $BaF_2$, and Cu coevaporated precursor films or in situ by laser ablation of YBCO onto single-crystal (001) $SrTiO_3$ or $LaAlO_3$ substrates. Initially, the postannealed films were reacted either at low oxygen partial pressure and low temperatures (e.g., $P_{O2} \approx 200$ mTorr, 730°C) or at $P_{O2} = 1$ atm, 850°C. All films possessed high critical current densities, with systematically higher $J_c$ in the range 4–5 MA/cm$^2$ at 77 K in zero-applied magnetic field for the low $P_{O2}$-reacted films. The O(1) (chain-site) oxygen nonstoichiometry $x$ was varied by low-temperature anneals below 550°C in various $P_{O2} \leq 1$ atm. Relative to the nominally fully oxygenated state ($P_{O2} = 1$ atm), it was found that the initially low $P_{O2}$-reacted films display a maximum in $T_c$ at slightly reduced O content, while the usual plateau and gradual reduction of $T_c$ are observed in the high $P_{O2}$-reacted and in the laser-ablated films. A similar peak in $T_c$ with oxygen deficit $x$ was also observed in a laser-ablated film of $(Y_{0.9}Ca_{0.1})Ba_2Cu_3O_{7-x}$. These results suggest that fully oxygenated, postannealed films initially formed at low $P_{O2}$ behave as hole-doped materials. Strikingly, all films show a monotonic decrease in $J_c$ with increasing $x$. The combined effects on $T_c$ and on $J_c$ are shown in Fig. 2.15. These results are consistent with a

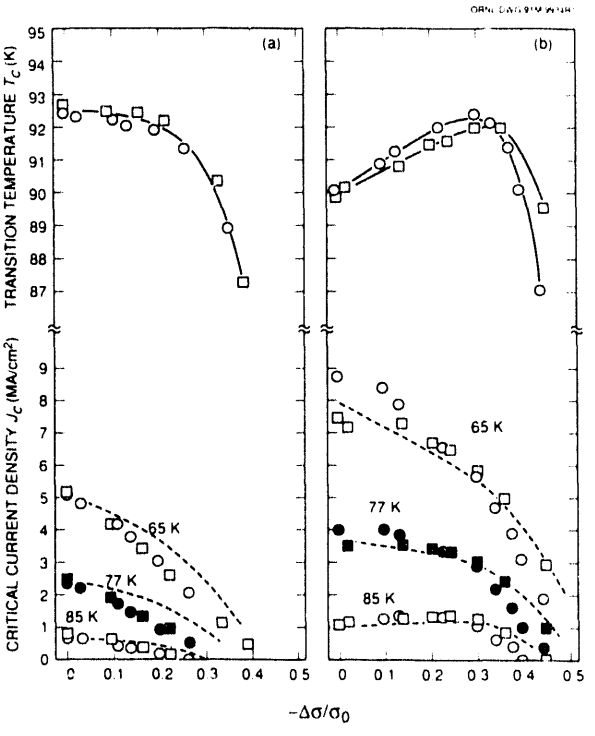


Fig. 2.15. Variation of $T_c$ and $J_c$ with the relative change in the normal state conductivity due to oxygen content.

simple model (dashed lines in Fig. 2.15) based on the effects of carrier density on near-optimal flux pinning.[2,3]

---

1. Summary of paper: *Phys. Rev. B (Rapid Communications)* **45,** 6569 (1992).
2. D. K. Christen and R. Feenstra, *Physica C* **185–189,** 2225 (1991).
3. J. G. Ossandon et al. *Phys. Rev. B* **45,** 12534 (1992).

## EPITAXIAL ORIENTATIONS FOR $YBa_2Cu_3O_x$ FILMS ON SILVER SUBSTRATES

*J. D. Budai, D. K. Christen, E. C. Jones,[1] and R. T. Young[2]*

Although epitaxial $YBa_2Cu_3O_x$ (YBCO) films with critical current densities, $J_c$, exceeding $10^6$ A/cm$^2$ can be grown routinely on a variety of oxide single-crystal substrates (e.g., $SrTiO_3$), the resulting samples generally are limited in size and flexibility and are not suitable for many superconducting applications. On the other hand, the transport capabilities of high-$T_c$ films produced on more suitable flexible, polycrystalline substrates are severely limited by weak-link coupling between misoriented grains. In light of these limitations, the structure and the epitaxial relationship for YBCO films grown by laser ablation on textured Ag foils and on Ag single-crystal substrates have been investigated.

The results of four-circle x-ray diffraction measurements show that YBCO films can be grown textured with the ⟨00ℓ⟩ axis aligned predominantly along the surface normal. More significantly, samples grown on single-crystal surfaces exhibit in-plane alignment between the film and the substrate, as well as alignment along the surface normal. Figure 2.16 shows x-ray diffraction $\phi$ scans through the YBCO (205) c⊥ reflections for films grown on three different Ag single-crystal surfaces. Peaks are observed every 45° for films on Ag(100) surfaces, indicating the presence of two types of domains

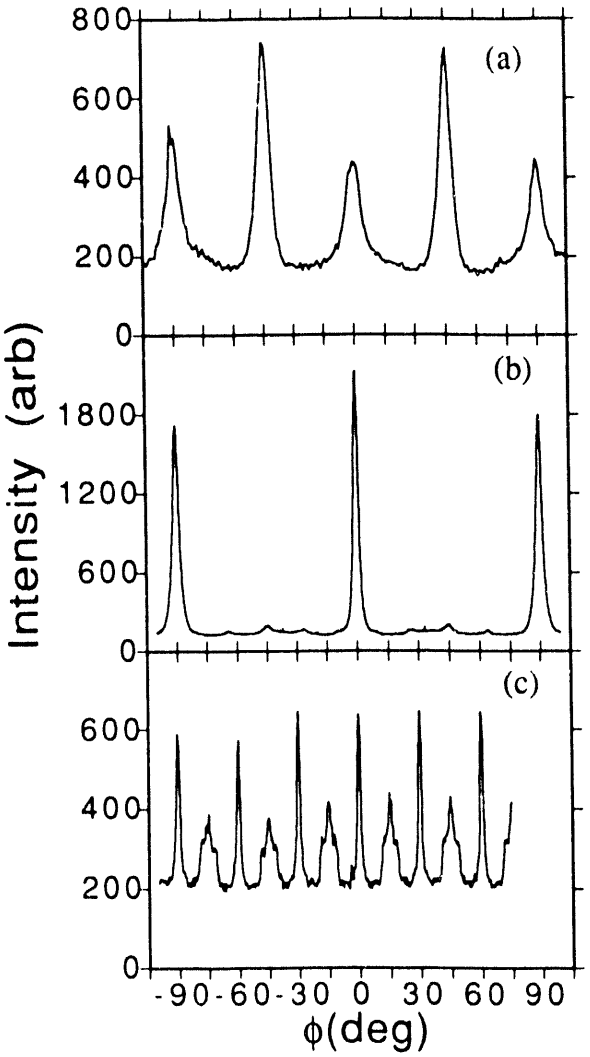


Fig. 2.16. X-ray diffraction $\phi$ scans for c-axis-oriented YBCO films on (a) Ag(100), (b) Ag(110), and (c) Ag (111) surfaces. Peaks indicate the in-plane directions of the a or b axes of the films.

rotated by 45°. In Fig. 2.16(b), the presence of large peaks separated by 90° reveals that the YBCO grains on the Ag (110) surface are aligned in essentially a single orientation, eliminating the weak-link current transport limitations associated with high-angle grain boundaries. On the other hand, the YBCO grains on the Ag(111) surface are shown in Fig. 2.16(c) to be oriented in several possible in-plane orientations. The YBCO-Ag interfaces were geometrically analyzed using near-coincidence lattice models, and for each of the three Ag surfaces, the observed orientations were found to correspond to interfaces with high atomic coincidences and relatively small lattice mismatches. These structural results are currently being correlated with $T_c$ and $J_c$ measurements with complementary goals of understanding and exploiting epitaxy of superconducting films on metal substrates.

---

1. Graduate student from The University of Tennessee, Knoxville, Tenn.
2. Energy Conversion Devices, Inc., Troy, Mich.

## HIGH-QUALITY EPITAXIAL YBCO(F) FILMS DEPOSITED DIRECTLY ON SAPPHIRE[1]

*R. T. Young,*[2] *K. H. Young,*[2] *M. D. Miller,*[2]
*S. R. Ovshinsky,*[2] *J. D. Budai,*
*C. W. White, and J. S. Martens*[3]

Research on applications of high-$T_c$ superconductors in microwave devices has shown that performance is critically dependent on the quality of the film and the dielectric loss of the substrate. Although sapphire substrates possess excellent dielectric and mechanical properties, epitaxial $YBa_2Cu_3O_{7-\delta}$ (YBCO) films have a poor lattice match and react chemically with sapphire at the growth temperature, resulting in inferior microwave properties. In this study, high-quality epitaxial YBCO(F) films were grown directly on r-plane $(1\bar{1}02)$ sapphire by a pulsed-laser deposition technique using a multiphase fluorinated target.

X-ray diffraction measurements show that the orthorhombic YBCO films are three-dimensionally epitaxial with the c-axis oriented near the surface normal and that the in-plane YBCO ⟨110⟩ directions are aligned with the orthogonal $Al_2O_3$ $[\bar{1}101]$ and $[11\bar{2}0]$ directions. The c-axis and in-plane mosaic spreads were measured on one film to be 1.1 and 2.4°, respectively. Rutherford backscattering/ion channeling measurements along the (001) film axis revealed that values for the minimum yield, $\chi_{min}$, are ~50% at the film surface and increase to ~75% at the substrate interface. This behavior is qualitatively similar to that observed for aligned spectra of silicon on sapphire films, where the defect density decreases as a function of distance from the film-sapphire interface. Scanning electron microscopy photos revealed that while the YBCO(F) films appeared free of cracks, films deposited under the same conditions from YBCO targets without fluorine frequently contained cracks along the a and b axes.

Microwave measurements made using a con-focal resonator configuration showed the surface resistance to be 56 mΩ at 94.1 GHz and 77 K, which is the best value reported for a YBCO film on sapphire that is known at this time. It is speculated that the improved film quality can be attributed to fluorine transported to the growing surface of the film and acting as an etching and/or catalytic agent to remove the defects and second-phase impurities preferentially.

---

1. Summary of paper to be published.
2. Energy Conversion Devices, Inc., Troy, Mich.
3. Sandia National Laboratories, Albuquerque, N. Mex.

## FLUX CREEP IN THE JOSEPHSON MIXED STATE OF GRANULAR-ORIENTED $YBa_2Cu_3O_{7-x}$ THIN FILMS [1]

*E. C. Jones,[2] D. K. Christen, C. E. Klabunde, J. R. Thompson,[3] D. P. Norton, R. Feenstra, D. H. Lowndes, and J. D. Budai*

A self-consistent critical current model in the Josephson mixed state is proposed for a series of c-oriented polycrystalline and for a series of epitaxial triaxially oriented YBCO thin films. The flux-pinning activation energies were experimentally determined from electrical transport measurements over a wide range of temperatures and were found to behave quite differently for the two types of granular films. With these activation energies applied to a superconductor-normal metal-superconductor weak-link system, thermally activated flux motion is shown to reproduce the experimentally measured critical current densities, as shown in Fig. 2.17.

---

1. Summary of paper: *Appl. Phys. Lett.* **59**, 3183 (1991).
2. Graduate student from The University of Tennessee, Knoxville, Tenn.
3. Adjunct research and development participant from The University of Tennessee, Knoxville, Tenn.

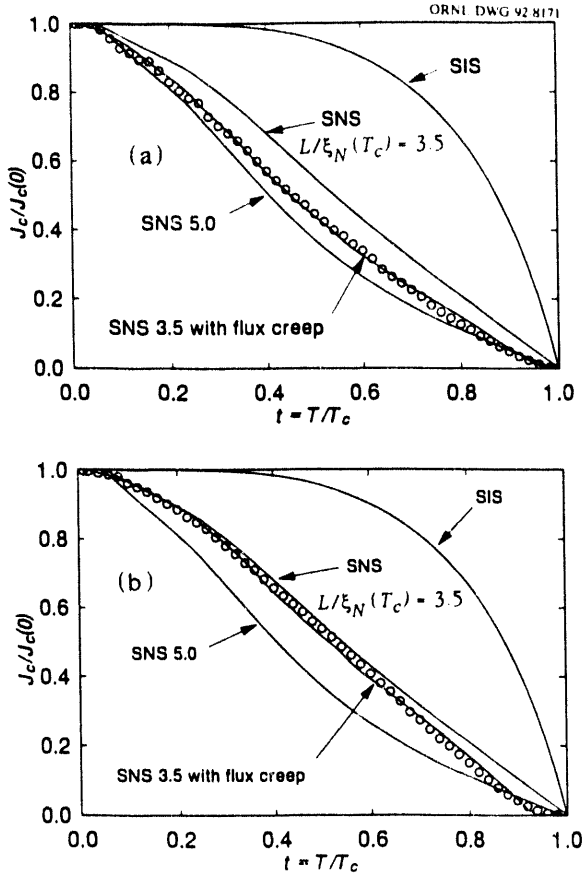


Fig. 2.17. Normalized critical current density $J_c(T)/J_c(0)$ vs. reduced temperature. Symbols are the data for (a) c-axis oriented and (b) triaxial films. Curves are conventional weak-link models and the SNS model including flux creep.

## THERMALIZATION AND ATTENUATION OF YBCO LASER ABLATION PLUMES BY BACKGROUND GASES[1]

*D. B. Geohegan*

The slowing and attenuation of the laser-induced plasma formed by KrF irradiation of $Y_1Ba_2Cu_3O_7$ have been studied in background pressures of oxygen and argon similar to those used for thin-film growth. The ion current transmitted through the background gases was recorded as a function of distance along the normal to the irradiated pellet in order to measure the decrease in velocity and plasma current due to collisional slowing and attenuation of the laser plume. As shown in Fig. 2.18(a), the ion transmission is found to drop exponentially with distance and background pressure, in agreement with a simple scattering model that yields general scattering cross sections for ion-argon, $\sigma_{i\text{-}Ar} = 2.1 \times 10^{-16}$ cm$^2$, and ion-oxygen, $\sigma_{i\text{-}O_2} = 2.3 \times 10^{-16}$ cm$^2$, interactions in background pressures up to 300 mTorr. Inelastic scattering leads to increased recombination and reactive conversion of ions, as indicated by increased fluorescence of all species, which become dominated by fluorescence of YO and BaO. Spatially resolved fluorescence measurements indicate that the luminous boundary to the plasma follows a weak shock front, which coincides with the ion flux propagation. As the background pressure increases, the plasma plume becomes delayed behind this expansion front, relative to the plume in vacuum, as recorded by digitized ion current waveforms. Time-resolved and spatially resolved fluorescence measurements indicate that the different species are slowed together behind the common expansion front. The decreasing velocity of the plasma plume was measured by recording the arrival time of the ion probe signal peak at various distances. The slope of the *R-t* curves yields the instantaneous velocity of the plume at a given distance and indicates, for example, that the most probable kinetic energies for $Ba^+$ ions change from 70 eV in vacuum to 0.1 eV in 200-mTorr oxygen at a typical film-growth distance of 5.0 cm.

---

1. Summary of paper: p. 557 in *Surface Chemistry and Beam-Solid Interactions*, ed. by Harry A. Atwater, Frances A. Houle, and Douglas H. Lowndes, Materials Research Society, Pittsburgh, Pa., 1991.

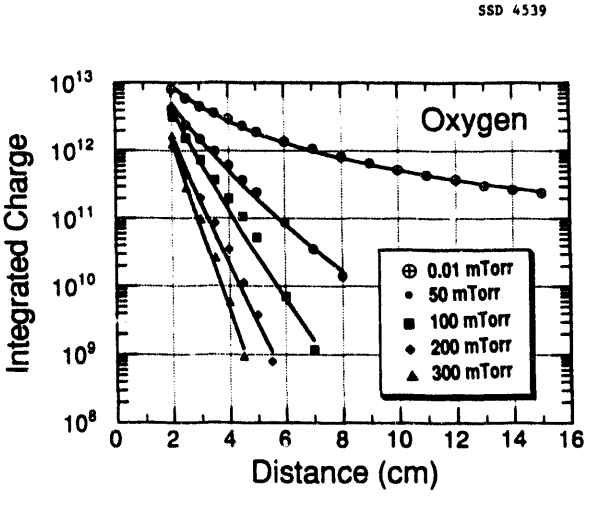


Fig. 2.18. Integrated positive ion-probe current transmitted through oxygen back pressures of 0.01, 50, 100, 200, and 300 mTorr. Fits to the data follow the form $d^{-1.8}e^{-bd}$, where $b$ is the attenuation coefficient and $d$ is the distance from the pellet.

# BULK MATERIALS

## ENHANCED CURRENT DENSITY $J_c$ AND EXTENDED IRREVERSIBILITY OF SINGLE-CRYSTAL $Bi_2Sr_2CaCu_2O_8$ BY LINEAR DEFECTS FROM HEAVY ION IRRADIATION[1]

*J. R. Thompson,[2] Y. R. Sun,[3] H. R. Kerchner, D. K. Christen, B. C. Sales, B. C. Chakoumakos, A. D. Marwick,[4] L. Civale,[4] and J. O. Thomson[5]*

There were large enhancements in the critical current density $J_c$ that were produced in single crystals of the high-temperature superconductor $Bi_2Sr_2CaCu_2O_8$ by irradiation with high-energy Sn ions. Furthermore, the irreversibility line was moved to considerably higher magnetic fields. In contrast with analogous studies on $YBa_2Cu_3O_7$, there was little, if any, selective pinning when the magnetizing field was applied parallel to the linear, ion-damage-produced tracks.

For many applications envisioned for high-temperature superconductors (HTSCs), it is necessary to conduct large electric currents in the presence of high magnetic fields. Consequently, enhancing the critical current density $J_c$ in high-$T_c$ materials and gaining insight into the motion of their vortices have considerable scientific and technological importance. In previous experiments in which single crystals of $YBa_2Cu_3O_7$ were irradiated with heavy ions (Sn ions with 580-MeV energy), it was shown that the resulting linear damage tracks are quite effective in pinning vortices, particularly when the magnetic field is applied parallel to the microscopic columns of damaged material (~50 Å in diam). In this study, the efficacy of heavy ion damage was examined in enhancing $J_c$ and extending the region of magnetic irreversibility to higher temperatures and magnetic fields in the Bi-based superconductor $Bi_2Sr_2CaCu_2O_8$, which contains two adjacent Cu-O superconducting layers. Total ion fluences were 2.4 and $4.8 \times 10^{11}$ ions/cm$^2$; by multiplying these fluences by the flux quantum $\phi_0 = 2.07 \times 10^{-11}$ T-cm$^2$, the area density of damage tracks was written as an equivalent area density of vortices, with damage flux density $B_\phi = 5$ and 10 T, respectively. Very large enhancements in $J_c$ were produced. In Fig. 2.19, results are shown for the temperature dependence of $J_c(T)$ for one crystal, measured magnetically in fields of 1, 2, and 4 T, respectively. For comparison and contrast, the open symbols in Fig. 2.19 show $J_c$ for the same crystal prior to irradiation. It is apparent that the region of potentially useful current densities has been extended to substantially higher temperatures and fields. These increases in $J_c$ were accompanied by an elevation of the irreversibility line to higher temperatures. However, the angularly selective pinning of vortices, which was observed in studies of $YBa_2Cu_3O_7$ single crystals with fields parallel to the damage columns, is notably absent in this more strongly layered and two-dimensional material. Enhancements in the thermal operating range for Bi-based HTSCs for configurations with a magnetic field $H$ perpendicular to the Cu-O planes are particularly promising, since the problem of intergrain weak links appears to be more amenable to solution in

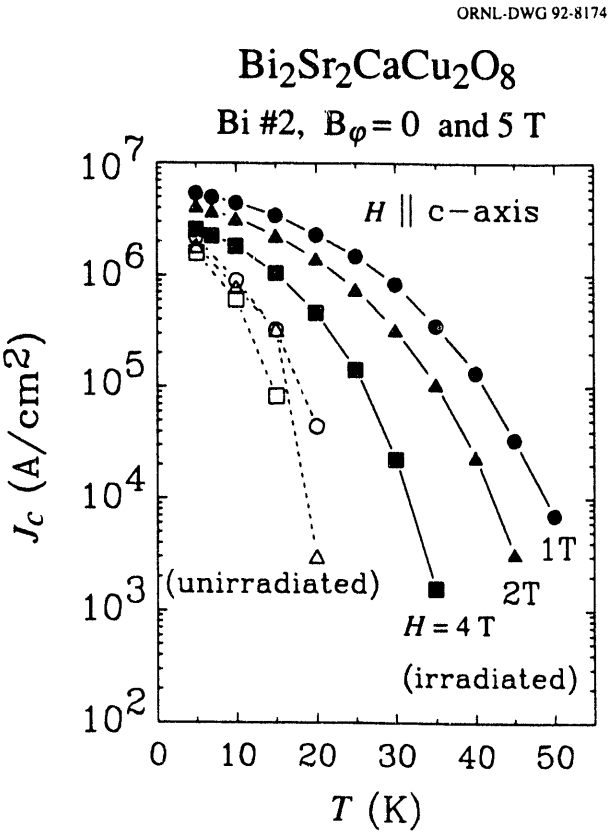


Fig. 2.19. Critical current density $J_c$ vs. temperature $T$ for a $Bi_2Sr_2CaCu_2O_8$ single crystal before and after irradiation with heavy ions to a fluence $B_\phi = 5$ T. The magnetic field was applied parallel to the crystalline c-axis.

these materials than in the case of Y-Ba-Cu-O superconductors.

---

1. Summary of paper: *Appl. Phys. Lett.* **60**, 2306 (1992).
2. Adjunct research and development participant from The University of Tennessee, Knoxville, Tenn.
3. Graduate student from The University of Tennessee, Knoxville, Tenn.
4. IBM Thomas J. Watson Research Center, Yorktown Heights, N.Y.
5. Guest scientist from The University of Tennessee, Knoxville, Tenn.

## VORTEX CONFINEMENT BY COLUMNAR DEFECTS IN $YBa_2Cu_3O_7$ CRYSTALS: ENHANCED PINNING AT HIGH FIELDS AND TEMPERATURES [1]

*L. Civale,[2] A. D. Marwick,[2] T. K. Worthington,[2] M. A. Kirk,[3] J. R. Thompson,[4] L. Krusin-Elbaum,[2] Y. R. Sun,[5] J. R. Clem,[6] and F. H. Holtzberg[2]*

The properties of many superconducting materials, including the high-$T_c$ superconductor $YBa_2Cu_3O_7$, can be modified by suitable defect structures. In this work, tailored defects were created by irradiating thin crystals of the superconductor with energetic heavy ions (580-MeV $Sn^{+30}$ ions) at the Holifield Heavy Ion Facility accelerator at ORNL. In passing through the crystal (e.g., perpendicular to the highly conductive copper-oxygen planes), the Sn ions created discontinuous but linear columns of highly damaged material, as confirmed by transmission electron microscopy. These columns act as "pinning" regions for vortices and are particularly effective in immobilizing them, since both the damage columns and the vortices are linear structures. The effects are most striking at high temperatures in large fields. For example, the $J_c$ at 77 K exceeded $10^5$ A/cm$^2$ in a field of 4.5 T, with $H \parallel$ c-axis. These results are vastly superior to those obtained previously with point-like defects in proton-irradiated crystals, even in the best cases. There, only vanishingly small current densities were obtained under these conditions.

The efficacy of aligned defects for pinning vortices was verified by irradiating additional

crystals at angles of 30 and 45 degrees from the crystalline stacking direction, the c-axis. When the field was applied parallel to the damage tracks, the current density was significantly larger than in the opposite case, where the field was approximately perpendicular to the tracks (but maintained in the same orientation relative to the copper-oxygen planes). These experiments confirmed that the linear columns are the source of the enhanced material properties.

Complementary flux-creep experiments on materials processed with heavy ions showed that the temporal stability of supercurrents and fractional losses are comparable to or less than ion-irradiated YBCO, even though $J_c$ (and the associated driving force for flux motion) in the heavy ion-irradiated material are greater, especially at high temperatures.

Developments with columnar defects demonstrate that the potential operating range of $YBa_2Cu_3O_7$ can be extended to substantially greater fields at 77 K or higher. Altogether, the experimental results are promising and help to remove one more impediment from technological applications of this material.

---

1. Summary of paper: *Phys. Rev. Lett.* **67**, 648 (1991).
2. IBM Thomas J. Watson Research Center, Yorktown Heights, N.Y.
3. Argonne National Laboratory, Argonne, Ill.
4. Adjunct research and development participant from The University of Tennessee, Knoxville, Tenn.
5. Graduate student from The University of Tennessee, Knoxville, Tenn.
6. Ames Laboratory, Iowa State University, Ames, Iowa.

## SYSTEMATICS OF SUPERCONDUCTIVE PROPERTIES AND FLUX PINNING VS. OXYGEN DEFICIENCY δ IN ALIGNED $YBa_2Cu_3O_{7-\delta}$ MATERIALS[1]

*J. R. Thompson,[2] J. G. Ossandon,[3] D. K. Christen, Y. R. Sun,[4] B. C. Sales, H. R. Kerchner, J. E. Tkaczyk,[5] and K. W. Lay[5]*

Magnetization studies were made on a series of oxygen-deficient $YBa_2Cu_3O_{7-\delta}$ materials to determine the role of oxygen deficiency δ on intragrain superconductive properties. The samples were magnetically aligned, sintered materials with an x-ray rocking curve linewidth of 7° FWHM. The relative porosity (78% of theoretical density) allowed the oxygen content (7 - δ) to be adjusted homogeneously and measured in situ by processing under reduced oxygen pressure at relatively low temperatures in a thermogravimetric apparatus (TGA). For internal consistency, all measurements were made on one specimen having constant grain size and morphology. The materials had oxygen deficiency δ in the range 0–0.20 (±0.005) (i.e., from full oxygenation with $\delta = 0$) through the "$T_c$ plateau" with $\delta < 0.12$, where $T_c$ remains near 90 K, and into the compositional range in which $T_c$ steadily decreases with δ. Magnetic studies were made with SQUID-based and vibrating sample magnetometers and an ac response apparatus, mostly with applied magnetic field $H \parallel$ c axes. The properties investigated include $T_c$; magnetization $M(H,T)$; intragrain $J_c$; irreversibility line; superconducting condensation energy $F_c$, London penetration depth λ; coherence length ξ from analysis of the mixed-state magnetization; and

flux-creep behavior. The essential findings are: (1) $J_c$ and pinning decreased steadily as oxygen was removed, even where $T_c$ was nearly constant; (2) the irreversibility line, which moved with δ to progressively lower temperatures and magnetic fields, was well correlated with $J_c(\delta)$; (3) both the irreversibility line and $J_c$ at low temperatures scaled very well with the parameter $F_c\xi_{ab}$, as provided by a simple, single-site model for vortex pinning; (4) both λ and ξ increased as oxygen was removed, and (5) their ratio κ and the superconductive anisotropy parameter $\gamma = (\lambda c/\lambda ab) \approx 5$ were affected very little by oxygen depletion in the range investigated.

Further studies of the time dependence of the vortex-state magnetization were made using the SQUID magnetometer with applied field $H\|c = 1$ T at temperatures $T = 5 \sim 75$ K. These flux-creep studies showed that to lowest order, the decay was logarithmic in time over the observation period (4.5 h). As a function of $T$, the normalized flux creep rate $S \equiv d\ln(M)/d\ln(t)$ showed a small initial peak at low $T$ and a higher temperature plateau with $S \approx 0.02$, for all δ. From a "Maley analysis," values for the $J$-dependent flux-pinning barrier

$$U_{eff}(J,T) = k_BT[\ln(dM/dt) - C] \approx U_{eff}(J,0)g(T/T_c)$$

were obtained, with the fitting parameter $C$ determined by the low-temperature data. Estimates for $U_{eff}(J,0)$ [obtained by using the thermal function $g(T/T_c) = [1 - (T/T_c)^2]^{3/2}$ were compared with the model function $U_{eff}(J) = (U_o/\mu)[(J_{c0}/J)^\mu - 1]$ from vortex-glass and collective-pinning theories. This relation for $U(J)$ describes the data relatively well, especially at low temperatures. The best value $\mu \approx 0.9$ was nearly independent of δ, while $J_{c0}$, the critical current density without flux creep, decayed strongly with δ. The systematics of $U_o(\delta)$ were consistent with recent theory for collective flux creep. This analysis was possible only through the availability of δ-dependent material parameters from the equilibrium state studies described above.

---

1. Summary of papers: *Phys. Rev. B* **45**, 12534 (1992); *Physical Review B* (in press).
2. Adjunct research and development participant from The University of Tennessee, Knoxville, Tenn.
3. Graduate student from The University of Tennessee, Knoxville, Tenn. Present address: Universidad de Talca, Talca, Chile.
4. Graduate student from The University of Tennessee, Knoxville, Tenn.
5. General Electric Corporate R&D Laboratory, Schenectady, N.Y.

## SCALING OF THE HYSTERETIC MAGNETIC BEHAVIOR IN $YBa_2Cu_3O_7$ SINGLE CRYSTALS[1]

*L. Civale,[2] M. W. McElfresh,[2] A. D. Marwick,[2] F. H. Holtzberg,[2] C. Feild,[2] J. R. Thompson,[3] and D. K. Christen*

A study was performed on the pinning force density $F_p(B,T)$ in $YBa_2Cu_3O_7$ single crystals, as a function of flux density $B$ and temperature $T$. The properties of the crystals, particularly the critical current density $J_c$, were modified by irradiation with 3-MeV protons, which created

controlled densities of point-like defects. For a given level of ion damage, all $F_p$ data could be reduced onto a single function of reduced field $b = B/B^*$, where the scaling field $B^*(T)$ was much smaller than the upper critical field $H_{c2}(T)$. Rather, it was shown that the scaling field is related to the irreversibility line, which is the boundary in the $B$-$T$ plane at which $J_c \to 0$. This scaling result rules out the possibility that the vortex lattice matches some distribution of lattice defects. Thermally activated flux creep was shown to be very influential in determining the behavior of pinning-force density in $YBa_2Cu_3O_7$ materials (Fig. 2.20).

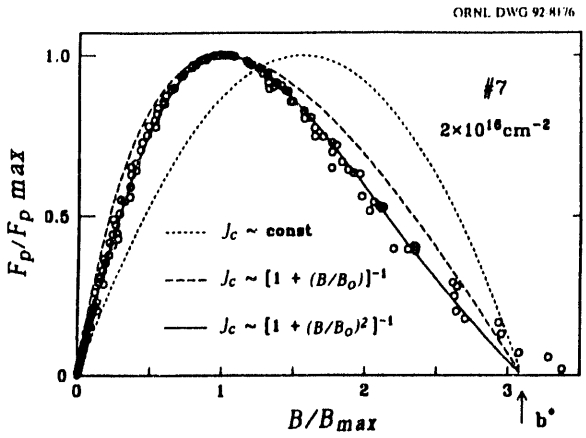


Fig. 2.20. Scaled experimental results for $F_p(B,T)$ at various temperatures vs. $B$ for a crystal irradiated with $2 \times 10^{16}$ protons/cm$^2$ are shown; this fluence approximately maximizes $J_c$. For comparison, the lines show predictions for some simple pinning models. It is evident that quite good modeling can be obtained over nearly all of the region, with some deviations remaining near the maximum $b$ values. Overall, the results underscore the dominating influence of flux-creep effects in limiting the current transport properties of $YBa_2Cu_3O_7$ superconductors.

---

1. Summary of paper: *Phys. Rev. B (Rapid Communications)* **43**, 13732 (1991).
2. IBM Thomas J. Watson Research Center, Yorktown Heights, N.Y.
3. Adjunct research and development participant from The University of Tennessee, Knoxville, Tenn.

## LONG-TERM, NONLOGARITHMIC MAGNETIC RELAXATION AND FLUX CREEP ANNEALING IN HIGH-$J_c$, SINGLE-CRYSTAL SUPERCONDUCTOR[1]

*J. R. Thompson,[2] Yang Ren Sun,[3] A. P. Malozemoff,[4] D. K. Christen, H. R. Kerchner, J. G. Ossandon,[5] A. Marwick,[4] and F. H. Holtzberg[4]*

The time dependence of the irreversible superconductive magnetization (flux creep) has been studied in a high-$J_c$, proton-irradiated $YBa_2Cu_3O_{7-x}$ single crystal for long periods, up to $3.5 \times 10^5$ s. A nonlogarithmic decay of magnetization $M$ with time was observed. In this study, the deviation from a conventional logarithmic time dependence cannot be interpreted as an approach of the system to the equilibrium state. These experiments show that the decay is described extremely well by the expression

$$M(t) = M_o/[1 + (\mu kT/U_o)\ln(t/t_o)]^{1/\mu}. \qquad (1)$$

This expression for $M(t)$ is provided by vortex glass and collective pinning theories, which have an effective energy barrier for vortex motion, $U_{eff}(J)$, that depends on the instantaneous current density. The resulting thermally activated flux creep deviates from the classical Anderson-Kim time dependence $M(t) \propto \ln(t)$.

An example is shown in Fig. 2.21, a semilogarithmic plot of $M$ vs. $t$ for a $YBa_2Cu_3O_7$ crystal at 30 K in a magnetic field $H$ = 1 T applied parallel to the crystalline c-axis. The nonlogarithmic character of the decay is quite clear. More importantly, the theoretical expression in Eq. 1 (solid line in Fig. 2.21) provided an excellent description of $M(t)$, thereby giving strong experimental evidence for the validity of these

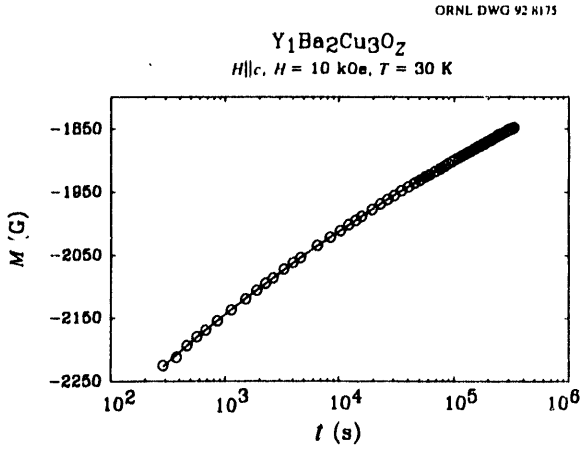


Fig. 2.21. Magnetization $M$ vs. log($t$) for a proton-irradiated $YBa_2Cu_3O_7$ single crystal at $T$ = 30 K, with 1-T field applied perpendicular to the a-b plane. Curvature is apparent everywhere. Here (■) represents the experimental data, and the solid line is fitted to Eq. 1, with $\mu$ = 1.9.

controversial theories. Additional support comes from the fact that the temperature and field dependence of the characteristic exponent $\mu$ follows the predictions of collective pinning theory to a semiquantitative level. Flux creep annealing experiments provided still further evidence for the $J$-dependent pinning and showed that the supercurrents could be greatly stabilized in time by operating with somewhat subcritical current densities.

---

1. Summary of papers: *Phys. Rev. B (Rapid Communications)* **44,** 469 (1991); *Appl. Phys. Lett.* **59,** 2612 (1991).
2. Adjunct research and development participant from The University of Tennessee, Knoxville, Tenn.
3. Graduate student from The University of Tennessee, Knoxville, Tenn.
4. IBM Thomas J. Watson Research Center, Yorktown Heights, N.Y.
5. Graduate student from The University of Tennessee, Knoxville, Tenn. Present address: Universidad de Talca, Talca, Chile.

## GRAIN BOUNDARY FACETING IN $YBa_2Cu_3O_{7-\delta}$[1]

*M. F. Chisholm and S. J. Pennycook*

Understanding the intrinsic mechanism responsible for the weak-link nature of grain boundaries is crucial both for improvement of the critical current density in polycrystalline materials and for development of reproducible Josephson junction devices. While it has been demonstrated that the critical current density of polycrystalline samples of $YBa_2Cu_3O_{7-\delta}$ is determined by the relative orientations of the grains[2] and by the coupling between grains,[3] the microscopic origin of this behavior must be related to the grain-boundary chemistry, stress state, and/or structure. High-resolution Z-contrast imaging, which combines strong compositional sensitivity with atomic-scale resolution, has been used to obtain detailed characterization of the grain-boundary region to deter-

mine the relative importance of these factors. For low-angle boundaries, compositional variations at grain boundaries are not necessarily present, and the stress state of the boundary provides a consistent and physical explanation of the observed critical current behavior.[4]

For high-angle [001] tilt boundaries, grain boundaries normally contain asymmetric structures involving (100)/(010) faceting of one of the adjoining grains (Fig. 2.22). The image clearly demonstrates the material's propensity to form only complete unit cells. This property restricts the material's ability to accommodate the misfit between the misoriented grains, which based on the low-angle results, should severely depress the critical current density. However, some combinations of misorientation and boundary plane have been shown to produce symmetric boundaries. It has been proposed that these boundaries undergo further relaxation to reduce the strain energy at the boundary. Work in progress will investigate this hypothesis by cor-

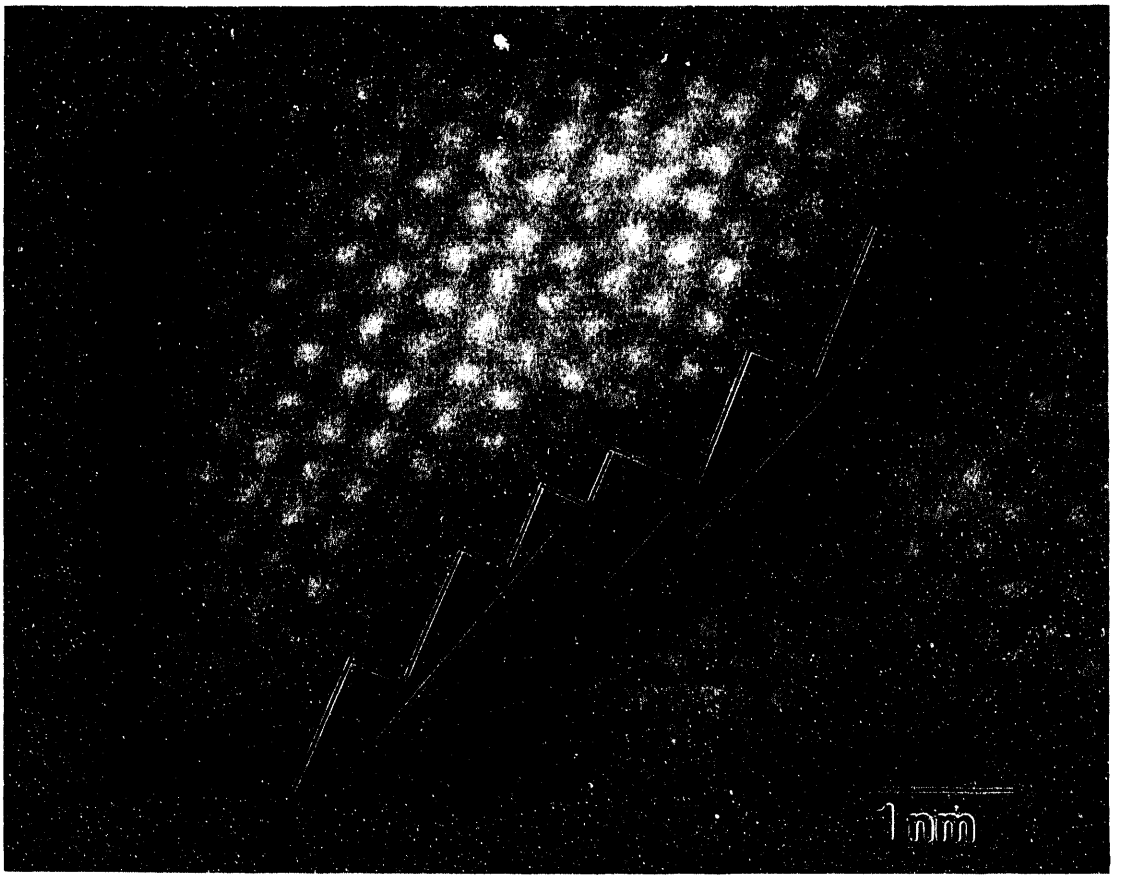


Fig. 2.22. Z-contrast image of a section of a grain boundary between two grains misoriented by an ~67° rotation about their common [001] direction. The boundary is seen to consist of short segments of (100)/(010) facets.

relating grain-boundary structures with measured transport properties of selected bicrystal films.

---

1. Summary of paper to be published.
2. D. Dimos et al., *Phys. Rev. B* **41**, 4038 (1990).
3. R. Gross et al., *Phys. Rev. B* **42**, 10735 (1990).
4. M. F. Chisholm and S. J. Pennycook, *Nature* **351**, 47 (1991).

## THE PRODUCTION AND PROPERTIES OF MELT-ZONE-TEXTURED $YBa_2Cu_3O_{7-\delta}$ FILAMENTS

*D. K. Christen, C. E. Klabunde, D. B. Chandler,[1] M. J. Neal,[1] M. V. Parish,[2] B. C. Chakoumakos, A. Goyal,[2] and D. M. Kroeger[2]*

In comparison to the other classes of high-temperature oxide superconductors, $YBa_2Cu_3O_{7-\delta}$ (YBCO) materials are known to possess superior flux-pinning properties at high temperatures and in large magnetic fields. The development of practical YBCO conductors, however, has been limited severely by the existence of "weak links" at the grain boundaries. It is now well established that strongly linked, high-$J_c$ YBCO materials can be produced in the form of bulk masses by a variety of melt-processing techniques. Reported here are electrical transport properties of YBCO materials that are formed by a continuous fiber-spinning process combined with zone melt processing to produce long lengths of high-quality YBCO filaments that have microstructures similar to those of melt-textured bulk materials.

Present furnace configurations limit filament lengths to 1 m, but the process is considered "continuous" based on achieved steady state growth conditions. Metallographic examination over a 40-cm length of fiber has revealed a uniform crystal morphology and microstructure.

The transport properties of two 190-μm-diam filaments were measured as a function of temperature and orientation of the fiber in the transverse applied magnetic field. High values of the temperature- and magnetic field-dependent dc transport critical current density $J_c(T,H)$ were determined in the temperature range of pumped liquid nitrogen (63–77 K) with the sample immersed in liquid. In self-field conditions, $J_c$ exceeded $10^5$ A/cm$^2$ at 77 K, requiring a total current of about 32 A. Both samples exhibited a strong and complicated angular dependence with respect to rotation about the fiber axis. The observed anisotropy most likely results from a combination of the highly textured growth morphology and flux-pinning microstructure. Microscopic analysis on one of the samples revealed virtually single-crystal structure over the entire length (~2.5 cm), with the YBCO c-axis oriented nearly orthogonal to the fiber, resulting in a desired basal plane conduction along the fiber axis. In the optimal orientation and at an 8-T applied field, $J_c \approx 27{,}000$ A/cm$^2$ at 77 K and 75,000 A/cm$^2$ at 65 K (pumped liquid nitrogen), establishing current density levels approaching those of conventional NbTi wire operating at 4.2 K. These results confirmed strongly linked

materials with high flux pinning and established the existence of technologically useful current density levels at high temperatures and magnetic fields in YBCO materials that can be produced continuously over long lengths.

---

1. CPS Superconductor Corporation, Milford, Mass.
2. Metals and Ceramics Division, ORNL.

## MAGNETIZATION AND CRITICAL CURRENT DENSITY RELATED TO MICROSTRUCTURE IN $YBa_2Cu_3O_{\sim 7}$-Ag COMPOSITES[1]

*H. R. Khan,*[2] *J. R. Thompson,*[3] *and J. G. Ossandon*[4]

A magnetization study has been performed for temperatures in the range 4.5–60 K and magnetic induction fields up to 6.5 T on a series of $YBa_2Cu_3O_7$-Ag (YBCO-Ag) composite materials prepared by powder sintering techniques. The temperature dependence of the intragrain critical current density $J_{c\text{-}intra}$ was determined from the irreversible magnetization, which was measured using a vibrating sample magnetometer. The $J_c(T)$ exhibited a quasi-exponential decay with temperature, and this result was interpreted using a flux-creep model. This analysis yielded estimates for the flux-pinning potential in magnetic fields of 0.27 and 3.8 T near 40 meV. Comparative studies on similarly processed YBCO materials with no Ag additions led to very similar values for the pinning potential. These results indicate that the intragrain properties were not affected significantly by the addition of Ag in these composites. Comparison of the intergrain critical current density from transport studies with these intragrain $J_c$ values shows that with Ag additions weakly linked behavior still dominates the intergrain transport of current.

---

1. Summary of paper: *Supercond. Sci. Technol.* **4,** 133 (1991).
2. Forschungsinstitut für Edelmetalle und Metallchemie, Schwaebisch-Gmuend, Germany.
3. Adjunct research and development participant from The University of Tennessee, Knoxville, Tenn.
4. Graduate student from The University of Tennessee, Knoxville, Tenn. Present address: Universidad de Talca, Talca, Chile.

## DEPENDENCE OF THE CRITICAL CURRENT DENSITY ON THE ADDITION OF ALUMINUM TO CERAMIC $J_c$ $YBa_2Cu_3O_{7-\delta}$

*H. R. Kerchner, J. O. Thomson,*[1] *Jennifer Paul,*[2] *and H. R. Khan*[3]

This experiment investigates the relationship between the critical current density, $J_c$, and the variation in composition of $YBa_2Cu_3AlO_{7-\delta}$ produced at FEM in Schwaebisch-Gmuend, Germany. Each sample contains a different percentage of Al which substitutes for the Cu in $YBa_2Cu_3O_{7-\delta}$. The critical current density was deduced from magnetic hysteresis measurements carried out in a mutual inductance bridge with $10^{-6}$ Oe-cm$^3$ sensitivity. This study determined that Al substitution increases the current barriers due to the grain boundaries.

Electrical current induced by application of a magnetic field gives an ac magnetic moment sensed by pickup coils. The pickup voltage is digitized at 1024 points of time during a few cycles of the ac field and is integrated numerically over time in order to deduce magnetic moments as functions of applied magnetic field. One low-temperature magnetic hysteresis loop is shown in Fig. 2.23 for the sample with $\varepsilon = 0.1$.

In each case, the most dominant effect is the shielding of the interiors of superconductive grains (intragranular current flow). The magnitude of this signal corresponds to the exclusion of applied field from about 70% of the interior of each sample. In addition to the granular shielding (straight-line data), the data show magnetic hysteresis loops arising due to intergranular current flow. The critical intergranular current density $J_c$ equals the geometrical average $\langle J \rangle$ when it all flows in the same direction. No such loop is visible for sample #816 ($\varepsilon = 0.2$), indicating that the intergranular critical current density is below the measurement sensitivity.

It is immediately evident that increasing Al content from 0.05 to 0.10 decreases the intergranular critical current density (and resulting magnetic hysteresis) by roughly a factor of 10. Also evident is the sensitivity of intergranular critical current density to magnetic fields. The current density decreases with increasing magnetic field, reaching zero near 30 Oe for each material.

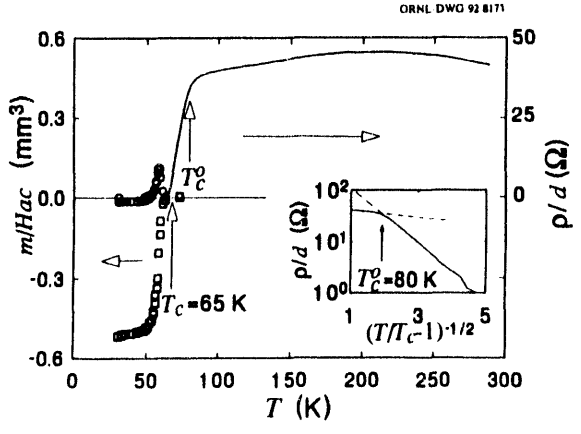


Fig. 2.23. Magnetic moment $m$ as a function of applied magnetic field $H$ for sample #815 of $YBa_2Cu_3Al_{0.05}O_{7-\delta}$. For $H > 30$ Oe, the moment is due solely to intragranular shielding currents. Subtracting the straight line fit to this latter moment allows one to deduce the average circular current density $\langle J \rangle$.

---

1. Guest scientist from The University of Tennessee, Knoxville, Tenn.
2. Boston College, Chestnut Hill, Mass.
3. Forschungsintitut für Edelmetalle und Metallchemie, Schwaebich-Gmuend, Germany.

## MEASUREMENT OF THE KINETIC ENERGY FOR Cu IN $YBa_2Cu_3O_{7-\delta}$ BY NEUTRON RESONANCE ABSORPTION SPECTROSCOPY

*H. A. Mook, J. A. Harvey, N. W. Hill, and N. Hecker*[1]

The phonon spectra for the high-temperature superconductors are very complicated as the large number of atoms per unit cell result in a dense energy spacing of the phonon branches. This is particularly true in the energy region for the Cu vibrations. However, the kinetic energy (KE) was determined at the Oak Ridge Electron Linear Accelerator for Cu in

$Bi_2Sr_2CaCu_2O_8$ (2212) using the 230-eV absorption resonance in $^{65}Cu$.[2] Measurements of KE for motion in the *a,b* planes showed a sudden decrease just above $T_c$ and then no further decrease as the temperature was lowered below $T_c$.

The Cu KE measurements have now been extended to $YBa_2Cu_3O_{7-\delta}$ (123) for δ values of 0 and 0.5. It is expected that the measurements will differ from $Bi_2Sr_2CaCuO_8$ as the Cu resides in the chain sites as well as the planes for the (123) compound. Figure 2.24 shows the KE for Cu in (123) divided by the KE for $La_2CuO_4$. $La_2CuO_4$ is an insulator with the same Cu-O planes as (123); thus, the division removes the normal temperature-dependent lattice effects. For the superconductor (δ = 0), the normalized KE falls off slightly as the temperature is lowered toward $T_c$, but then rises again at low temperatures. For the non-superconductor (δ = 0.5), little temperature dependence is observed. The rise in the normalized KE at low temperatures means the Cu phonons stiffen below $T_c$. This effect is also observed for the normalized KE for (2212). This also agrees with ion channeling measurements[3] and suggests the presence of a lattice instability in these materials.

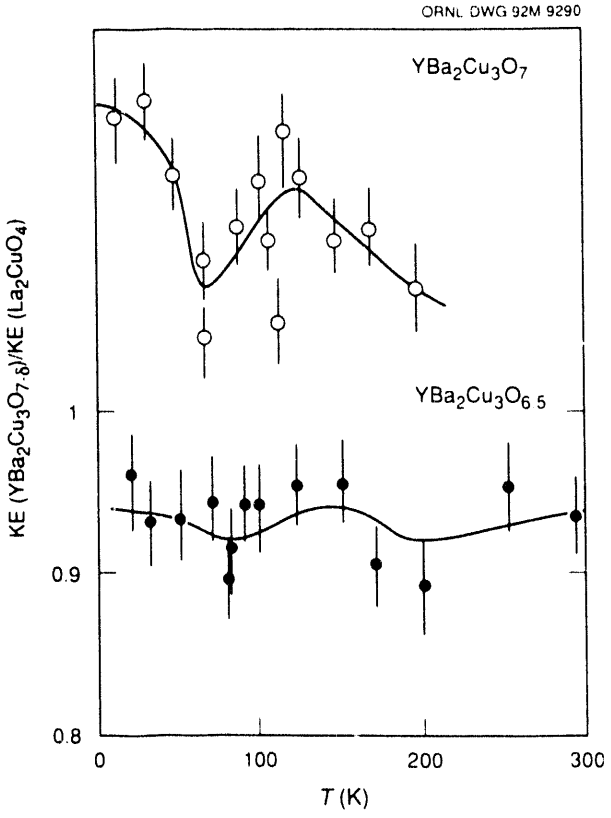


Fig. 2.24. Normalized KE plotted as a function of temperature for $YBa_2Cu_3O_{7-\delta}$ for δ = 0 and 0.5.

1. Harvard University, Boston, Mass.
2. H. A. Mook et al., *Phys. Rev. Lett.* **65** 2712 (1990).
3. T. Haga et al., *Phys. Rev. B* **41**, 826 (1990).

## PHONONS IN SUPERCONDUCTING $Ba_{0.6}K_{0.4}BiO_3$

*R. M. Nicklow, Mark Mostoller, C.-K. Loong,[1] and M. L. Norton[2]*

Among the materials that do not contain copper, $Ba_{1-x}K_xBiO_3$ exhibits the highest superconducting transition temperature, $T_c$ = 30 K for $x$ = 0.4. This material displays none of the antiferromagnetism common to other high-$T_c$ materials, and it is cubic in the superconducting phase in contrast to the anisotropic planar Cu-O structures in the other compounds. With no evidence for magnetic fluctuations in

$Ba_{1-x}K_xBiO_3$, it is quite possible that standard electron-phonon coupling is responsible for superconductivity in this material. To investigate this further, a study of the phonons in $Ba_{0.6}K_{0.4}BiO_3$ as a function of temperature using neutron scattering has been initiated.

The results obtained so far are shown in Fig. 2.25. The acoustic branches in the three principal directions have been measured at room temperature to the zone boundary except for the longitudinal branch in the [111] direction. That branch has been difficult to observe for unknown reasons. The lines are the results of a preliminary fit to the data based on a shell model for the interatomic forces. At present there are too few data for the optic modes to provide a definitive test of the model.

The temperature dependences of the transverse acoustic modes in the [100] and [110] directions have been measured, and only small effects on the phonon energies have been observed. However, a fairly large (15%) temperature dependence of the energy widths of transverse phonons with small $q$ in the [110] direction has been seen just at $T_c$, indicating that a significant change occurs at that tem-

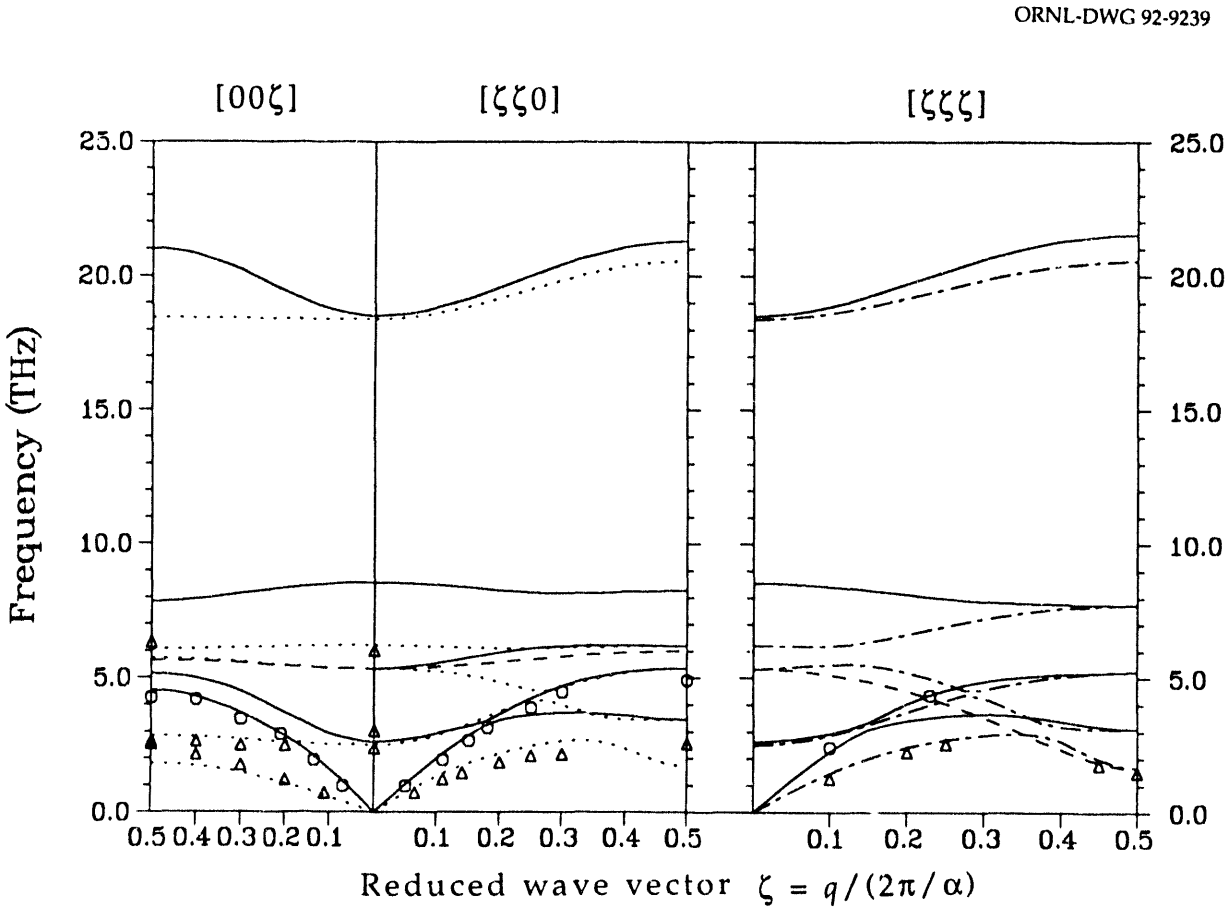


Fig. 2.25. Phonon dispersion curves for $Ba_{0.6}K_{0.4}BiO_3$ at room temperature.

perature in the electron-phonon coupling for those modes.

---

1. Argonne National Laboratory, Argonne, Ill.
2. Marshall University, Huntington, W. Va.

## PHONONS AND SUPERCONDUCTIVITY IN $Bi_2Sr_2CaCu_2O_8$

*H. A. Mook, B. C. Chakoumakos, M. Mostoller, A. T. Boothroyd,[1] and D. Mck. Paul[1]*

Detailed neutron scattering measurements have been made for selected phonons for $Bi_2Sr_2CaCu_2O_8$ at temperatures above and below $T_c$ in order to measure the effect of superconductivity on the phonon linewidths. The measurements were made using triple-axis spectrometers at the HFIR and by time-of-flight spectrometry at the ISIS facility at the Rutherford Appleton Laboratory. Large single crystals are not available, but it was possible to grow boules of the material by the floating-zone technique in which the a or b direction alternated in being well oriented along the rod. Using these rods, it was possible to measure longitudinal phonons along the rod axis or the $(\pi,\pi)$ direction, using square lattice notation. Three modes that could be clearly isolated from the rest of the phonon spectra have been emphasized. These are the two highest energy in-plane oxygen vibrations and the longitudinal acoustic mode at the 0.5 $(\pi,\pi)$ position.

Figure 2.26 shows the temperature dependence of the measured phonon widths. The top

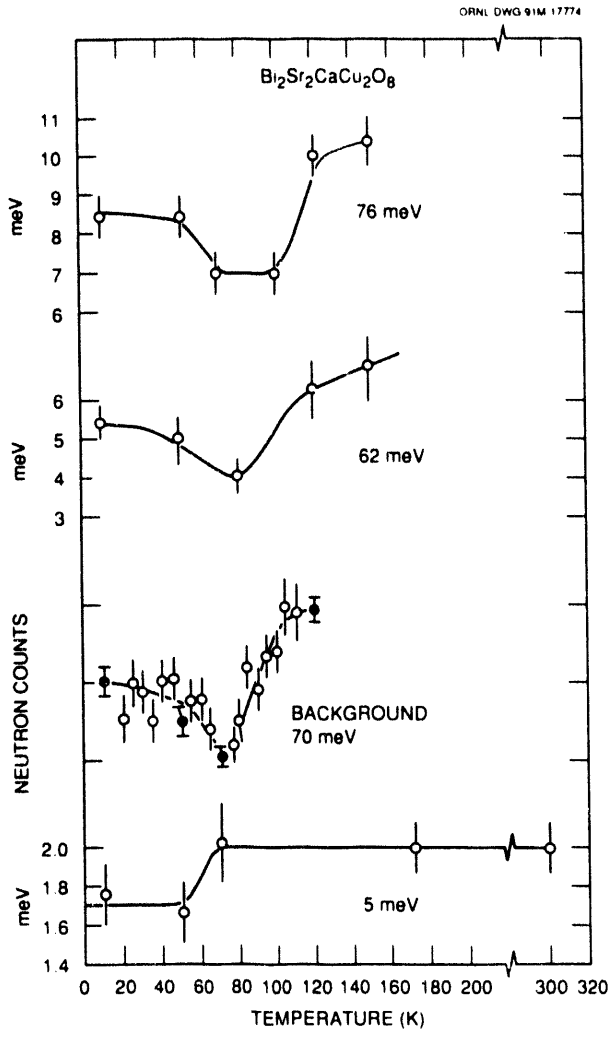


Fig. 2.26. The top two curves show the phonon widths for the in-plane oxygen vibrations as a function of temperature. The third curve shows the background between the oxygen modes which effectively samples their width. The bottom curve is for the acoustic mode at half the zone boundary.

curve is for the mode measured at 0.8 $(\pi,\pi)$ and 76 meV, which is essentially the breathing mode in which the in-plane oxygen atoms move directly toward the Cu atoms. The modes are found to be very wide at high temperatures and narrow as the temperature is lowered toward

$T_c$, which is about 83 K. Below $T_c$, the width of the mode increases as the temperature is reduced. Similar behavior is found for the 0.6 $(\pi,\pi)$ 62-meV mode, for which the in-plane oxygen atoms move along the a(b) axis, as shown in the second curve on Fig. 2.26. The third curve shows that the behavior of the phonon widths can also be determined by measuring the intensity of a point between them, as when the widths are large, the modes overlap to some degree. The lower curve shows the width measurement for the acoustic mode which is fairly temperature independent, perhaps narrowing somewhat as the superconducting gap opens. The oxygen modes display considerable anharmonicity that reduces as the temperature is lowered near $T_c$. Below $T_c$, these phonons widen as quasiparticles are pushed upward into their energy region as the gap opens. This broadening is consistent with an electron-phonon coupling constant of about 0.05 for each of these modes. If all phonon modes contributed equally, this would result in an overall electron phonon coupling of 2.25. However, it is more likely that Fermi surface nesting occurs near $(\pi,\pi)$ resulting in an unusually large electron-phonon contribution for the measured modes.

## MAGNETIC DYNAMICS OF SUPERCONDUCTING $La_{1.86}Sr_{0.14}CuO_4$[1]

*T. E. Mason,*[2] *G. Aeppli,*[2] *and H. A. Mook*

Neutron inelastic scattering has been used to determine the general magnetic response function $\chi''(Q,\omega)$ of a superconducting single crystal of $La_{1.86}Sr_{0.14}CuO_4$ ($T_c$ = 33 K). It was found that the magnetic fluctuations are incommensurate in this material, peaking at the points $(\pi,\pi) \pm \delta\ (\pi,0)$ and $(\pi,\pi) \pm \delta\ (0,\pi)$ using square lattice notation, where $\delta = 0.245 \pm 0.004$. The measured spectra are broad at high temperatures but narrow and increase in strength as the sample is cooled to the superconducting temperature. As the temperature is lowered below $T_c$, superconductivity suppresses the magnetic fluctuations for energies below 6.0 meV, which is about the value for the gap energy for the superconductor. Figure 2.27 shows that $\chi''(Q,\omega)$ at the incommensurate position peaks at $T_c$ and then reduces at lower temperatures in greater proportion as the energy transfer is reduced. This implies that this is not an ideal BCS superconductor, where at low temperatures, no excitations are expected below the pair condensation energy. Also, because $\chi''(Q,\omega)$ has a sharp peak rather than merely a break in slope at $T_c$, superconductivity is not due to Bose condensation of preformed pairs.

For the normal state, it was found that the shape of $\chi''(Q,\omega)$ can be described in terms of models proposed for conventional metals near a

1. University of Warwick, Warwick, United Kingdom.

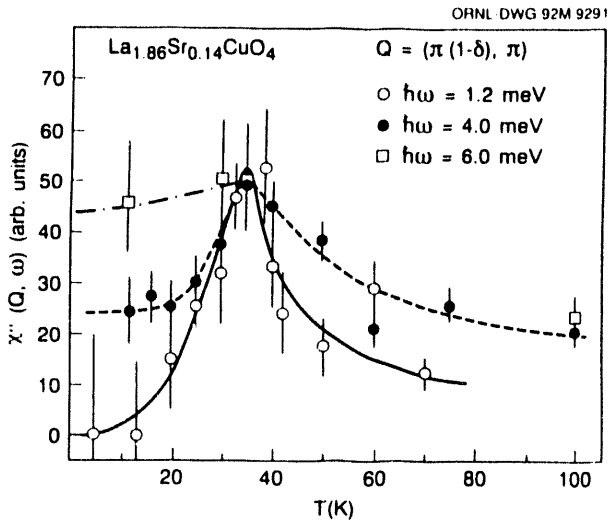


Fig. 2.27. The generalized susceptibility $\chi''(Q,\omega)$ plotted as a function of temperature for different energy transfers.

Fermi surface nesting instability. The superconductor should be compared with the appropriate Lindhard function for a superconductor with the Fermi surface of our sample. However, because of the complexity of such a calculation, the data were fit by including a real term in $\chi''(Q,\omega)$ that represents the energy difference between the singlet and triplet states for pairs of carriers with relative momentum $Q$. This gives a good fit to the measurements and results in a low-temperature spin correlation length of about 25 Å. It was found that the two-fluid form $2\Delta\ (T) = 2\Delta_0(1-(T/T_c)^{1/2}$, with $2\Delta_0 = 6$ meV and $T_c = 33$ K, gives a good description of the pairing energy.

---

1. Summary of paper: *Phys. Rev. Lett.* **68**, 1414 (1992).
2. AT&T Bell Laboratories, Murray Hill, N.J.

## PRESSURE EFFECTS ON THE CRYSTAL STRUCTURE OF $La_{2-x}Ba_xCuO_4$

*S. Katano*[1] *and J. A. Fernandez-Baca*

The study of the role of structural transformations in the high-$T_c$ superconductors is of considerable interest. $La_{2-x}Ba_xCuO_4$ (for $0.05 < x < 0.2$), for example, undergoes a peculiar sequence of structural transformations upon cooling: from tetragonal ($I4/mmm$) to orthorhombic ($Bmab$) to a mix of tetragonal ($P4_2/ncm$) and orthorhombic ($Bmab$) phases.[2] The fraction of the system that transforms into the low-temperature tetragonal (LTT) phase varies with the Ba concentration $x$ and seems to be largest for $x = 0.125$, when the bulk superconductivity is suppressed. It has also been noted that the application of pressure to this system leads to the recovery of the superconductivity.[3] These observations have led to the suggestion that there is a correlation between the LTT phase and the suppression of superconductivity and that the effect of pressure is to suppress the LTT phase and thus to recover the superconductivity. In order to test this suggestion and to investigate the correlation between superconductivity and the crystal structure in this system, a neutron diffraction experiment on $La_{2-x}Ba_xCuO_4$ ($x = 0.125$) at ambient pressure and at 7 kbar has been performed. The neutron diffraction measurements were performed at the HB-4 multidetector powder diffractometer at the HFIR using a clamp-type high-pressure cell with a sapphire window[4] and a standard closed-cycle refrigerator The diffraction patterns for the ambient pressure case were consis-

tent with the structural changes reported by Axe et al.[2] with an orthorhombic-to-tetragonal transition at a temperature $T \approx 80$ K. Below this temperature the LTT peaks have Gaussian shapes slightly broader than the instrumental resolution, with little or no evidence of the low-temperature orthorhombic phase. The diffraction patterns for the 7-kbar case, on the other hand, suggest that the orthorhombic structure persists down to the lowest temperature studied ($T$ = 14 K) and that the LTT phase has been suppressed in this temperature range. This finding seems to confirm that there is a correlation between the low-temperature orthorhombic phase and the onset of superconductivity in this system and that the transformation to the LTT phase results in the loss of superconductivity.

---

1. Guest scientist from Japan Atomic Energy Research Institute, Tokai, Japan.
2. J. D. Axe et al., *Phys. Rev. Lett.* **62**, 2751 (1989).
3. N. Yamada et al., *Solid State Commun.* **70**, 1151 (1989).
4. A. Onodera et al., *Jpn. J. Appl. Phys.* **26**, 152 (1987).

## SMALL-ANGLE NEUTRON SCATTERING STUDY OF THE FLUX LINE LATTICE IN $YBa_2Cu_3O_7$

*M. Yethiraj,*[1] *H. A. Mook, and G. D. Wignall*

In type-II superconductors, when an applied field is above $H_{c1}$ but below $H_{c2}$, quanta of flux penetrate the superconductor forming a two-dimensional flux line lattice (FLL). Since neutrons have a magnetic moment, they are sensitive to the field distribution because of the penetration of the sample by flux vortices. Small-angle neutron scattering (SANS) techniques have been used successfully in the past to study the flux lattice in traditional superconductors.

The FLL in the high-$T_c$ superconductor $YBa_2Cu_3O_7$ was investigated via SANS at the HFIR. It was observed that with the applied field parallel to the c axis, the lattice was square rather than triangular and aligned along the orthorhombic (110) crystal axes. Spots, rather than a ring, were observed in the 2-D data as shown in Fig. 2.28, indicating that long-range orientational order exists in this

ORNL-DWG 92-8199

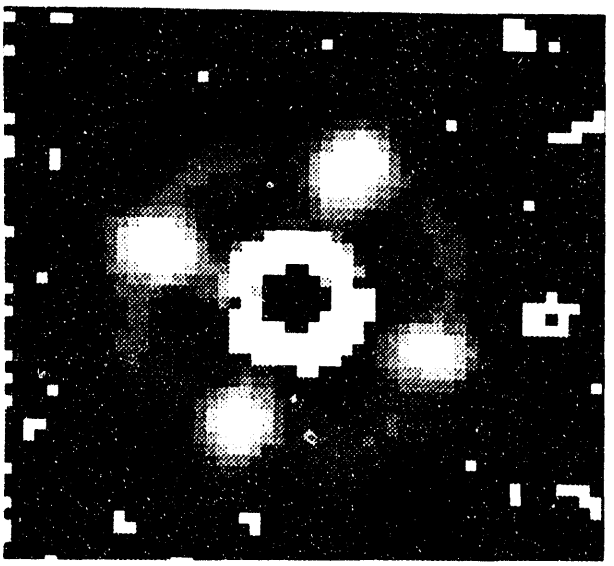

Fig. 2.28. When a magnetic field is applied along the c axis of $YBa_2Cu_3O_7$, a square vortex lattice is observed in the difference between 11- and 100-K data.

lattice. The mosaic width of the FLL was comparable to that of the c-axis mosaic in the sample. This strongly suggests the influence of pinning by twin plane defects, known to exist in the sample, in the formation of a square lattice.

Extremely curious behavior resulted when the field was applied at an angle to the c axis. A varying fraction of the lattice tended to form along the c axis irrespective of the field direction till the angle between the c axis and the applied field was almost 40°. The reason for this is not understood.

The temperature dependence of the FLL intensity was measured both for the field applied along the c axis of the crystal and for a direction 30° away from the c axis. There is no substantial difference in the temperature dependence between the two directions, and it deviates markedly from the two-fluid behavior observed via muon spin relaxation for polycrystalline samples of the compound.

---

1. Oak Ridge Associated Universities postgraduate research participant.

# 3. *Neutron Scattering*

The High-Flux Isotope Reactor (HFIR) operated routinely through this reporting period with an availability of about 64%. A major milestone was passed early in 1992 when a second periodic hydrostatic test to assure the integrity of the pressure vessel was completed successfully.

A total of 11 neutron scattering instruments are now operational, some of which are still under development or are in a reactivation process. The Neutron Scattering Program is growing in new directions, thanks to several successful funding initiatives. These new directions include anisotropic colloidal materials (in collaboration with Los Alamos and The University of Tennessee), residual stress (in collaboration with the ORNL Metals and Ceramics Division), and biological materials (in collaboration with the ORNL Biology Division). The latter two initiatives are part of a conscious effort to involve other ORNL research divisions in neutron scattering at HFIR as a prelude to the Advanced Neutron Source (ANS).

The user program is healthy; during FY 1991 there was a total of 137 users (95 neutron and 42 SAXS users). The vitality of the U.S.–Japan Cooperative Program on Neutron Scattering was reaffirmed at a Planning Committee meeting held in January 1992. Funds are being requested from the Japan Atomic Energy Research Institute for a major upgrade of the wide-angle neutron diffractometer.

With the completion of the ANS conceptual design, this project is entering a crucial stage where the established scientific need is balanced against the estimated cost in an atmosphere of growing concern about the federal debt. Work with the project team will be continued to try to plan a first-class facility at a reasonable cost.

The work described in this section is of growing diversity. Our traditional interest in magnetic materials remains strong, and there is a variety of results on phase transitions. Small-angle studies using both neutrons and X rays are dominated by polymer results, but also include work on micelles, gels, and metallurgical samples. Entirely new areas include neutron reflectometry and residual stress measurements of welds. There is a full array of neutron scattering experiments on high-$T_c$ superconductors, which is reported in the Bulk Materials Section of Chapter 2 entitled "Superconductivity."

# SMALL-ANGLE SCATTERING AND NEUTRON REFLECTOMETRY

## MOLECULAR WEIGHT SCALING IN CRITICAL POLYMER MIXTURES BY SANS[1]

*G. D. Wignall, M. Gehlsen,[2] F. S. Bates,[2] L. Hansen,[3] and K. Almdal[3]*

Over 50 years ago, Flory and Huggins (FH) derived similar mean-field theories which describe the mixing of two polymer species in the undiluted (bulk) state. These led to a critical scaling condition $\chi_c N = 2$ for phase separation where $N$ is the number of segments on each chain and $\chi$ is an interaction parameter accounting for the contact energy between dissimilar segments. Although the FH theory is a relatively crude approximation which neglects chain self-avoidance, self-contact, and intra- and interchain segment correlations, it has had great success in terms of qualitative predictions. Only recently have fundamental modifications been proposed, as for example the reference interaction site model (RISM) integral equation theory.[4] The contention that local correlations are amplified for large molecular weight (MW) due to self-avoidance leads to a renormalization of $\chi$ and produces the provocative conclusion that the critical point in symmetric mixtures should scale as $\chi_c \sim N^{-\delta}$ (where $\delta = 0.5$), which contrasts with the FH prediction ($\delta = 1$). Experimentally establishing scaling relationships is surprisingly difficult as both components should have equal, monodisperse MW as well as structurally equivalent segments. Furthermore, because the temperature window is relatively narrow (above the glass transition but below the onset of thermal degradation), only a limited range of $N$ could hitherto be assessed. A strategy to circumvent these limitations has been developed, based on the isotopic $\chi$ parameter observed between H- and D-labeled segments of the same species.[5] By tuning the degree of deuteration, $X_D$ ($\chi \sim X_D^2$), the magnitude of $\chi$ can be systematically varied without perturbing the structure, as would be the case with mixtures of chemically different polymer species. Thus, SANS has been used to verify the scaling behavior over a wide range of $N$ with the result $\delta = 1.01 \pm 0.05$ (Fig. 3.1).

This result confirms the remarkably simple FH prediction and rules out modifications based on RISM theory as currently formulated. Polymer-polymer thermodynamics is used extensively in materials science, and hence the

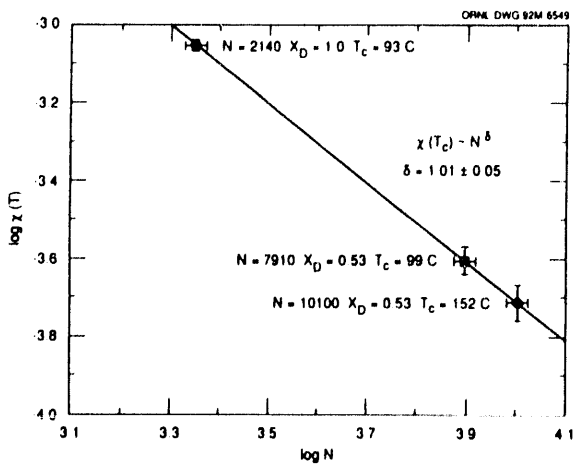


Fig. 3.1. Log $\chi(T_c)$ vs. log $N$ for critical isotopic polymer mixtures.

development of improved theory has important practical applications. The experimental verification of the mean-field scaling behavior ($\delta = 1$) was made possible by the discovery of polymer isotope effects at ORNL via SANS.[5] The use of polymer isotopes circumvents complications due to structural asymmetry and provides an ideal model to test revisions of FH theory.

---

1. Summary of paper: *Phys. Rev. Lett.* **68,** 2452 (1992).
2. University of Minnesota, Minneapolis, Minn.
3. Risø National Laboratory, Roskilde, Denmark.
4. K. S. Schweizer and J. Curro, *Phys. Rev. Lett.* **60,** 809 (1988).
5. F. S. Bates, G. D. Wignall, and W. C. Koehler, *Phys. Rev. Lett.* **55,** 2425 (1985); ibid., **57,** 1429 (1986).

## SMALL-ANGLE NEUTRON SCATTERING FROM POLY(VINYL ALCOHOL) GELS[1]

*G. D. Wignall, T. Kanaya,[2] K. Kaji,[2] and H. Yamaoka[3]*

It is well known that solutions of poly(vinyl alcohol) (PVA) show a transition from sol to gel on cooling. The gels exhibit interesting mechanical properties and have important industrial applications. Recently, it was reported[4] that PVA gels formed in mixtures of dimethylsulfoxide (DMSO) and water show very interesting features (e.g., the mixtures are transparent, and the elasticity is very high). Below -20°C, gelation occurs without phase separation, while above -20°C, the phase separation can play an important role, though the structure of the gels is not well understood. Therefore small-angle neutron scattering (SANS) measurements on the PVA gels in mixtures of DMSO and water to elucidate the structure have been carried out. PVA is a crystalline polymer, and the cross-linking points in this gel are believed to be crystallites. This hypothesis has recently been confirmed by wide-angle neutron scattering[5] and is used as the basis for interpreting the SANS data.

For PVA gels in DMSO-$d_6$/$D_2O$ (60/40 = v/v) at 23°C, the phase separation is known to occur. In the $Q$ range above 0.05 Å$^{-1}$, the scattering intensity $I(Q)$ is proportional to $Q^{-4}$. This $Q$ dependence corresponds to the Porod law and indicates that the surfaces of the crystallites are smooth. In the $Q$ range between 0.008 and 0.03 Å$^{-1}$, the $Q$ dependence of $I(Q)$ can be described by $I(0)/(1 + \xi^2Q^2)$, where $\xi$ is a correlation length, ($\xi$ = 151, 141, and 135 Å for PVA concentrations, $C_p$ = 2, 5, and 10 g/dl, respectively). These values of the correlation length may be related to the intercrystallite spacings. Below $Q$ = 0.008 Å$^{-1}$, this functional form is no longer valid; there is excess scattering observed in systems which show a phase separation. It is believed that the excess scattering is related to the structure of the separated phase. Figure 3.2 shows the contrasting low-$Q$ behavior for a system which phase separates (60/40) and a system which does not phase separate (80/20). Further exper-

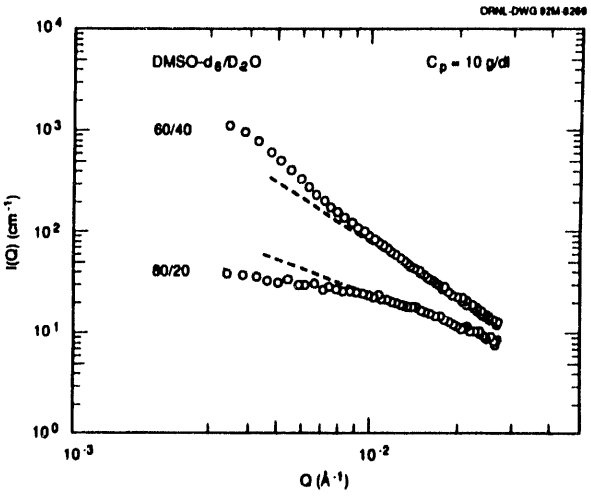


Fig. 3.2. Small-angle neutron scattering intensities $I(Q)$ of PVA gels in DMSO-$d_6$/$D_2O$ (60/40) and in DMSO-$d_6$/$D_2O$ (80/20) for $C_p$ = 10 g/dl.

iments are in progress to quantify this phenomenon via SANS and light scattering.

---

1. Summary of paper to be published.
2. Kyoto University, Kyoto, Japan.
3. Kyoto University, Kumatori, Osaka, Japan.
4. S.-H. Hyon, W.-I. Cha, and Y. Ikada, *Polym. Bull.* **22**, 119 (1989).
5. Y. Ishikawa et al., *Appl. Cryst.* **19**, 229 (1986).

## SANS STUDIES OF POLYMERIZABLE OIL-IN-WATER MICROEMULSION[1]

*Andy P. Full,[2] Eric W. Kaler,[2] and G. D. Wignall*

Polymerization of microemulsions can result in latexes with higher molecular weights ($10^6$–$10^7$ daltons) and smaller particle radii (<500 Å) than those produced by conventional emulsion polymerization. However, analysis of strongly interacting systems is difficult, and with one exception,[3] no small-angle neutron scattering (SANS) studies have been done on polymerizable microemulsions. Since SANS probes the appropriate length scales, details about colloidal interactions are quantified. Dynamic light scattering data have been reported previously for a three-component cationic microemulsion consisting of dodecyltrimethylammonium bromide (DTAB), styrene, and water[4] and are consistent with a bimodal system of empty micelles coexisting with monomer-swollen micelles. An attempt is currently being made to determine for this system the microstructure and the particle interactions that exist in the microemulsion before polymerization and thereby complement the light scattering behavior. SANS data have been obtained for microemulsions of DTAB, styrene, and $D_2O$ with and without added electrolyte.

The coherent scattered intensity is modeled as $I(Q) = n\,P(Q)\,S'(Q)$, where $n$ is the number density of particles, $P(Q)$ is the average particle form factor, and $S'(Q)$ is an average interparticle structure factor. $P(Q)$ is calculated assuming a spherical core consisting of a homogenous mixture of styrene and DTAB tails, surrounded by a shell consisting of hydrated head groups and bound counterions. D'Aguanno et al.[5] outline a method for calculating structure factors for colloidal systems that are polydisperse both in size and charge, and this method has been used in our studies to model a bimodal population.

Representative scattered neutron intensity curves for microemulsions containing DTAB, styrene, and brine are shown in Fig. 3.3. Increasing the styrene content while holding the surfactant/solvent ratio constant in the microemulsion causes the $Q$ value where the maximum intensity occurs ($Q_{max}$) to shift to lower $Q$ and increases the peak height ($I_{max}$). This trend is consistent with an increase in particle size. Preliminary fits of the data, assuming monodisperse spherical particles, indicate that particle volume increases linearly with total particle volume fraction upon the addition of styrene. This is strong evidence in favor of a monomodal population. Adding salt does not shift $Q_{max}$, but reduces $I_{max}$ slightly (Fig. 3.3). The more dramatic increase of intensity at low $Q$ is consistent with an increase of the system's isothermal compressibility. This effect is expected when the electrostatic potential between colloidal particles is screened with added electrolytes.

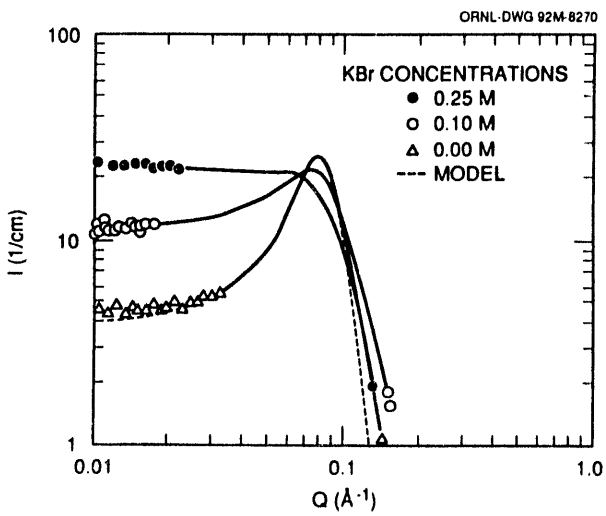


Fig. 3.3. SANS spectra of 4 wt.% styrene, 14.4 wt.% DTAB, 81.6 wt.% brine (KBr in $D_2O$) oil-in-water microemulsions at different salt concentrations. The line represents the calculated spectra due to charged monodispersed spheres with a radius of 31.7 Å, particle volume fraction of 0.236, and a fraction of bound counterions of 0.888.

By modeling experimental SANS data, it has been possible to describe particle interactions successfully. This analysis should give some insight into the perplexing light scattering behavior. Details of the complete analysis, including the degree of ion binding and trends in particle size, will be published in the near future.

---

1. Summary of paper to be published.
2. University of Delaware, Newark, Del.
3. C. Holtzscherer, F. Candau, and R. H. Ottewill, *Progr. Colloid Polym. Sci.* **81**, 81 (1990).
4. V. H. Perez-Luna et al., *Langmuir* **6**, 1040 (1990).
5. B. D'Aguanno, R. Klein, and N. J. Wagner, *Mat. Res. Soc. Symp. Proc.* **177**, 219 (1990).

## SANS STUDIES OF MIXED MICELLES OF NONIONIC AND ANIONIC SURFACTANTS AS A FUNCTION OF TEMPERATURE AND COMPOSITION[1]

*C. Brent Douglas,[2] Eric W. Kaler,[2] and G. D. Wignall*

Nonionic surfactants of the poly alkyl glycol monoether ($C_iE_j$) family present intriguing phase behavior in aqueous solution. Depending upon the lengths of the head-group and tail-group portions, the phase behavior can be dominated by liquid crystalline regions,

a liquid-liquid miscibility gap, or a complex combination of both. In the two-phase region a concentrated micellar phase exists in equilibrium with excess water containing dilute surfactant. However, micelle growth and micelle interactions mask each other within a scattering experiment to the extent that neither can be uniquely determined. Studies of aqueous surfactant mixtures of $C_iE_j$ surfactants with relatively small amounts of added ionic surfactant (sodium alkyl sulfonates) have been initiated. The incorporation of a small amount of electrostatic charge within the surfactant aggregates greatly reduces the extent of the miscibility gap and stabilizes liquid crystalline phases, and various models for the aggregate interactions are being tested using small-angle neutron scattering (SANS) from mixed micellar solutions.

A combination of SANS and static light scattering experiments were performed on mixtures of $C_{12}E_6$ and $C_{12}SO_3Na$ at various molar mixing ratios, *R*. The data for pure nonionic surfactant solution ($R = 0$) are shown in Fig. 3.4(a), and the dependence on *R* is shown in Fig. 3.4(b). The solid lines are attempted fits using models based on micelles of various shapes and interactions. All of the fits are of equal quality, but the parameters appear physically unreasonable for all models attempted initially.

These results and calculations indicate that for low concentrations of added anionic surfactant, attractive interactions due to the nonionic surfactant must be treated accurately. Currently, fits to the spectra using an integral equation approach containing an interaction potential that consists of two different Yukawa potentials are being evaluated.

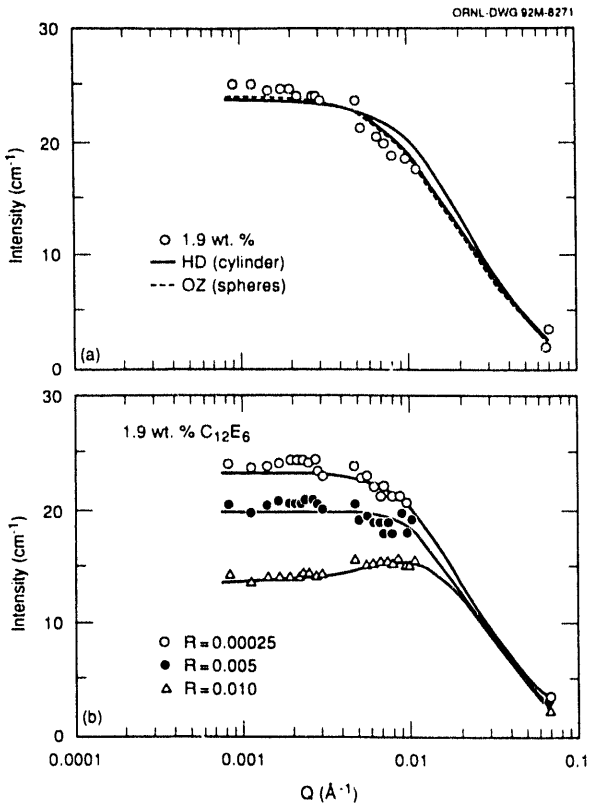


Fig. 3.4. Combined static light scattering and SANS spectra for (a) 1.9 wt.% $C_{12}E_6$, and (b) 1.9 wt.% $C_{12}E_6$ with added $C_{12}SO_3Na$ as indicated by the molar mixing ratio, *R*. The two fits in (a) correspond to cylindrical micelles of length 270 Å and radius 20 Å interacting through a hard core repulsion and spherical micelles of radius 21.5 Å under the influence of critical fluctuations. The fits in (b) were produced using prolate ellipsoidal micelles interacting through a coulombic potential. The major radius of the ellipsoid decreases from 160 to 124 Å with increasing *R* for a minor radius of 21.5 Å.

---

1. Summary of paper to be published.
2. University of Delaware, Newark, Del.

## SMALL-ANGLE X-RAY SCATTERING STUDY OF FLUCTUATING LAMELLAE IN A TERNARY SYSTEM[1]

*E. Y. Sheu,[2] Sow-Hsin Chen,[3] Bruce L. Carvalho,[3] J. S. Lin, and Malcolm Capel[4]*

The existence of a lamellar neat phase in surfactant-water mixtures and in surfactant-water-alcohol mixtures is well-known and extensively documented. The phase consists of coherent double layers of amphiphilic molecules with the polar groups in the interfaces with intervening layers of water molecules. The microscopic structural description of one-dimensional layer-type ordering is characterized by the observation of the well-defined Bragg spacing of ratios 1/2/3. Depending on the type of surfactant used in the mixtures, the addition of water results in one-dimensional swelling of the interlayer spacing. Diffuse scattering around the Bragg peaks shows that the structure of this lamellar phase deviates from the periodic stacking of infinite homogeneous lamellae of water and amphiphilic molecules.

A ternary surfactant-water-alcohol liquid mixture (sodium octyl sulfate-water-decanol) has been studied by small-angle x-ray scattering, particularly in its lamellar neat phase. By constructing a Debye correlation function[5] for a fluctuating lamella, the line shape of the small-angle scattering (SAS) has been considered. The density fluctuation was treated within a lamellar sheet as a superposition of propagating cosine waves having random phases and having a distribution of wave numbers centered around a most probable wave number $k_o$. By fitting the theory to the data, $k_o$ was obtained, and by making the assumption that $2\pi/k_o$ is equal to the DeGennes-Taupin persistence length,[6] the bending rigidities constant for the bilayers was obtained. The magnitude of bending rigidity obtained is of the order $k_BT$ and decreases along both water and alcohol dilution lines.

It should be emphasized that by focusing on the SAS near the origin, it was possible to avoid dealing with the interlayer correlations which are subject to the Landau-Peierls effect. This effect leads to a power law decay of the density correlation function giving rise to a characteristic line shape for the Bragg peaks at higher $Q$ values, which can only be studied by using high-resolution x-ray scattering.

---

1. Summary of paper: *Langmuir* **7**, 1895 (1991).
2. Texaco Research Center, Beacon, N.Y.
3. Massachusetts Institute of Technology, Cambridge, Mass.
4. Brookhaven National Laboratory, Upton, N.Y.
5. P. Debye, H. R. Anderson, and H. Brumberger, *J. Appl. Phys.* **28**, 679 (1957).
6. P. G. DeGennes and C. Taupin, *J. Phys. Chem.* **86**, 2294 (1982).

## SMALL-ANGLE X-RAY SCATTERING OF ZIRCONIUM(IV) ION HYDROLYSIS AND AGGREGATION[1]

*L. M. Toth,[2] J. S. Lin, and L. K. Felker[2]*

Long-lived radioactive components of nuclear wastes consist mainly of Th and/or Pu ions. By adjusting the acidity of the waste

solution, these ions tend to aggregate or polymerize, forming clusters of size 10–20 Å, which is an appropriate size range for small-angle x-ray scattering (SAXS) characterization. The clusters may then be removed from the organic phase by solvent extraction. The aggregates are linked by hydroxyl or oxo bridges, and during the aggregation process large polymeric networks are formed that can attain colloidal dimensions and are either suspended in the aqueous medium as sols or settle out in gel form.[3] Following the aggregation process, aging of the hydroxyl-bridged polymers often occurs with the resulting formation of oxygen-bridged species. Ultimately, the aggregates can reach the thermodynamically stable metal oxides. The heavy tetravalent cations [e.g., Th(IV), Pu(IV), and Zr(IV)0 are analogous in many aspects of their hydrolysis chemistry. The primary difference is that Th(IV) and Pu(IV) hydrolyze and aggregate to form extensive polymer networks; therefore, it is initially difficult to identify any simple intermediate aggregates in these systems. Zr(IV) hydrolyzes and aggregates initially as tetrameric units that are formed at relatively high acidities. Because of radiation safety concerns, most of the work to date has centered on Zr aggregates to simulate nuclear waste behavior. SAXS data were collected for 0.035–1.0 M Zr(IV) in aqueous solution where species present were hydroxyl-bridged tetramers. Modeling calculations for spheres, ellipsoids of revolution, and cylinders have been performed with adjustable parameters, and the scattering data were fitted best with a cylindrical model with a radius of 4.8 Å and an aspect ratio of 2.3.

The aging effects and dispersion effect in relevant organic solvents of these tetravalent heavy-metal ions are under investigation.

---

1. Summary of paper: *J. Phys. Chem.* **95,** 3106 (1991).
2. Chemical Technology Division, ORNL.
3. C. F. Baes, Jr., and R. E. Mesmer, *The Hydrolysis of Cations,* John Wiley and Sons, New York (1976).

## STRUCTURAL DEVELOPMENT OF CRYSTALLITES IN STRETCHED POLYANILINE AND THE EFFECT OF DOPING[1]

*B. K. Annis,[2] J. S. Lin, E. M. Scherr,[3] and A. G. MacDiarmid[3]*

The drawing or stretching of polymers has often been used to enhance selected physical properties, such as tensile strength or, more recently, the electrical conductivity. The processing of materials results in microstructural changes that, in turn, may correlate with the property of interest. These changes may be investigated via small-angle x-ray scattering (SAXS), as for example in studies of drawn films of the emeraldine base ($[\text{-NHC}_6\text{H}_4\text{NHC}_6\text{H}_4\text{N} = \text{C}_6\text{H}_4 = \text{NC}_6\text{H}_4\text{-}]_n$) form of polyaniline. The results indicate the development of a periodic array of crystalline regions alternating with amorphous regions along the draw axis. The spacing is 160 ± 30 Å, and the size of the crystallites is ~60–70 Å. The latter parameter results from a standard

Scherrer peak-width analysis of wide-angle x-ray diffraction data. Such dimensional sizes are comparable to those obtained by SAXS analysis of drawn polypropylene[4] and nylon 6.[5]

The effect on the structural change of doping the polyaniline films with HCl-conducting salt was also investigated. For draw ratios <4, no significant changes in the scattering pattern were observed. However, for samples with a draw ratio >4, the evidence for a periodic structure disappeared. Doping the material with chloride ions causes a reduction of electron contrast either by chloride ions entering the amorphous regions or by the expansion of the unit cell volume of the crystallites.[6]

---

1. Summary of paper: *Macromol.* **25,** 429 (1992).
2. Chemistry Division, ORNL.
3. University of Pennsylvania, Philadelphia, Penn.
4. E. Ferracini and A. Ferrero, *J. Macromol. Sci.-Phys.* **B10,** 97 (1974).
5. E. Ferracini and A. Ferrero, *Makromol. Chem.* **189,** 1957 (1988).
6. J. P. Pouget et al., to be published.

## SCALING BEHAVIOR IN THE PRECIPITATION OF AN ALUMINUM-LITHIUM ALLOY

*Steve Spooner*

In the long time during alloy decomposition, it is expected that the characteristic scale of the microstructure should coarsen with time in a power law with the exponent -1/3. Studies of precipitation in Al-Li alloys have shown this behavior in plots of the average $R^3$ vs. time. These plots appear to be linear but do not always go through zero at time zero, which raises the question as to whether or not the system is truly in the coarsening regime. In a series of in situ small-angle x-ray scattering experiments, scattering was measured at temperatures between 100 and 200°C for times on the order of 10 h. The scattering curves showed an interference peak characteristic of a high density of precipitates, and curve fitting was used to determine the scattering vector for the interference peak ($Q_{MX}$). A test of dynamic scaling was performed by plotting $(Q_{MX})^3 \times I(Q)$ vs. $Q/Q_{MX}$. At 180°C the data conform closely to dynamic scaling, while a similar scaling test for data at 100°C indicates the failure of scaling.

The test for scaling behavior was extended by using the hypothesis that a common adjusted time scale can be defined to examine the kinetics at different temperatures. Specifically, the time was adjusted by the factor $\exp(-E/RT)/T$ where $E$ is an activation energy, $T$ the absolute temperature, and $R$ the gas constant. By this adjustment, more than three orders of magnitude in effective time are covered in these experiments. The plot of $Q_{MX}$ vs. time shown in Fig. 3.5 indicates that there is an asymptotic approach to a power law, $t^{-1/3}$, in this time range. The success of this exploration of scaling depends on the insensitivity of the form of the scattering function to temperature, and this seems assured in circumstances where the equilibrium volume fraction of precipitate does not change significantly over this small temperature range.

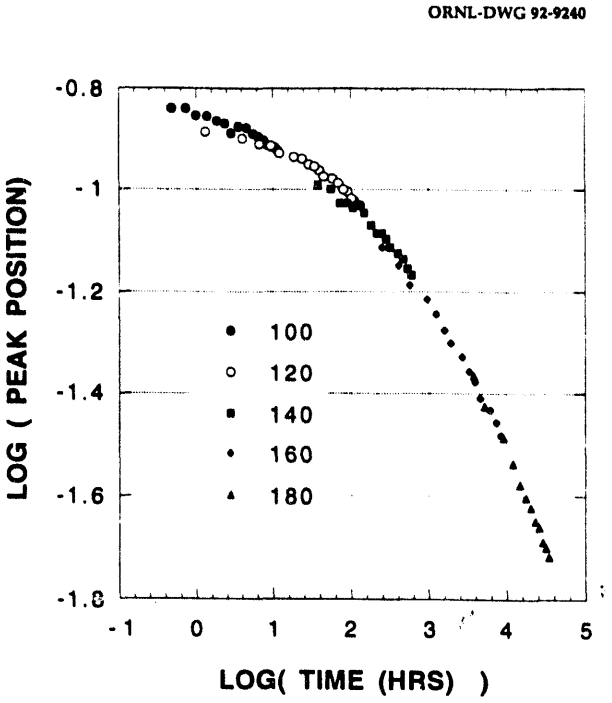


Fig. 3.5. The peak position in the small-angle scattering pattern, $Q_{MX}$, decreases with time as the precipitate structure coarsens. Log ($Q_{MX}$) vs. log (time) curves for the alloy at six different temperature with adjusted times appear to fall on a master curve.

## A TEST OF THE LANGER-SCHWARTZ MODEL OF NUCLEATION AND GROWTH

*J. J. Hoyt,*[1] *G. Sundar,*[1] *and S. Spooner*

The classical interpretation of alloy decomposition is based on separate nucleation and growth processes. The formation of nuclei in a supersaturated alloy is driven by the lowering of chemical-free energy with the formation of a new phase, but the formation of an interface between the old and new phases raises the energy of the system. Upon achieving a balance between these two factors, a nucleus, formed by thermodynamic fluctuation, will have sufficient stability to grow. The supersaturated condition where nucleation can be seen experimentally is the cloud point. Until recently, nucleation and growth were assumed to operate independently. The classically calculated supersaturation required for the cloud point was lower than experiments indicated. The nonclassical approach of Langer and Schwartz[2] treats nucleation and growth as concurrent processes. The cloud point is predicted to occur at higher initial supersaturations than for the classical model.

Observation of the nucleation and growth was undertaken in Al-Zn alloys with the use of small-angle x-ray scattering (SAXS), which is sensitive to the small-scale fluctuations associated with the cloud point. The integrated intensity from a decomposing alloy saturates when nucleation is complete and the alloy has decomposed into precipitate and matrix having their respective equilibrium compositions. In experiments at the 10-m SAXS instrument, the time to achieve half-completion of decomposition was determined for a range of temperatures representing different initial supersaturations. The results shown in Fig. 3.6 agree with a modified Langer-Schwartz model where time-dependence in the nucleation rate is incorporated into the theory (dotted line). The original Langer-Schwartz model prediction is shown in the solid line. The dashed line is the prediction of classical nucleation and growth.

---

1. Washington State University, Pullman, Wash.

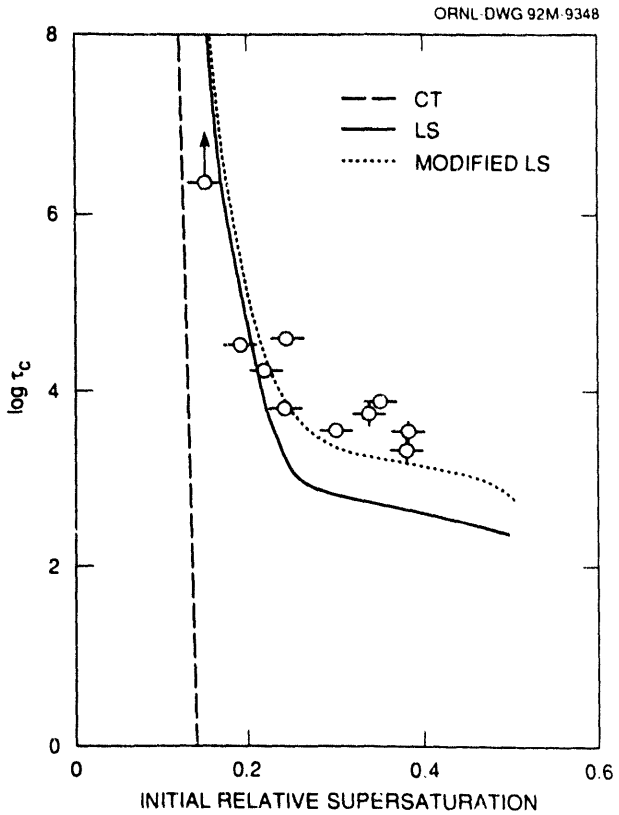


Fig. 3.6. The experimental times for half-completion of decomposition are compared with classical theory (dashed line), Langer-Schwartz theory (solid line), and the modified Langer-Schwartz theory (dotted line). The modified theory which takes into account the time-dependent nucleation rate represents a significant improvement in the fit to experiment.

## SURFACE STRUCTURE OF A VISCOELASTIC FLUID UNDER SHEAR

*J. B. Hayter, R. Pynn,*[1] *L. J. Magid,*[2]
*G. S. Smith,*[1] *W. A. Hamilton, and P. Butler*[3]

Many complex fluids exhibit viscoelastic (VE) behavior which is widely exploited in a multitude of industrial processes and products. Despite their importance, there is still little fundamental understanding of such systems at a molecular level. A study of surface-shear structure at interfaces using neutron reflectometry has been initiated,[4] and initial experiments in a short run on SPEAR, the neutron reflectometer at the Manuel Lujan Jr. Neutron Scattering Center, Los Alamos National Laboratory, have been performed.

The samples used were the very different 20-mM solutions of hexadecyltrimethylammonium 3.5 and 2.6 dichlorobenzoate in $D_2O$ (for neutron contrast). The 3.5-chlorinated material solution is strongly VE, while the 2.6-chlorinated surfactant solution behaves as a nearly Newtonian fluid. Neutron reflectivity measurements of the quartz-fluid interface in a sample cell were made for the Newtonian and VE fluids, as well as pure $D_2O$ (Fig. 3.7). The critical edges for both the VE and Newtonian fluid samples are very close to that of quartz-$D_2O$ ($Q$ = 0.011 Å$^{-1}$), indicating the same bulk scattering length densities and low concentrations. However, both show much stronger reflectivities than the $D_2O$ reference at higher $Q$; apparently due to near-surface solute alignments (at length scales <100 Å), which are either more pronounced or at longer length scales for the VE fluid. The Newtonian fluid also shows a small scattering peak at $Q$ = 0.016 Å$^{-1}$ indicating a possible long-range accommodation to the surface (length scale ~500 Å).

After these static measurements, a preliminary attempt to observe shear effects was made by displacing the quartz crystal along the beam direction to apply a shear force to the VE fluid. Reflection measurements were then repeated

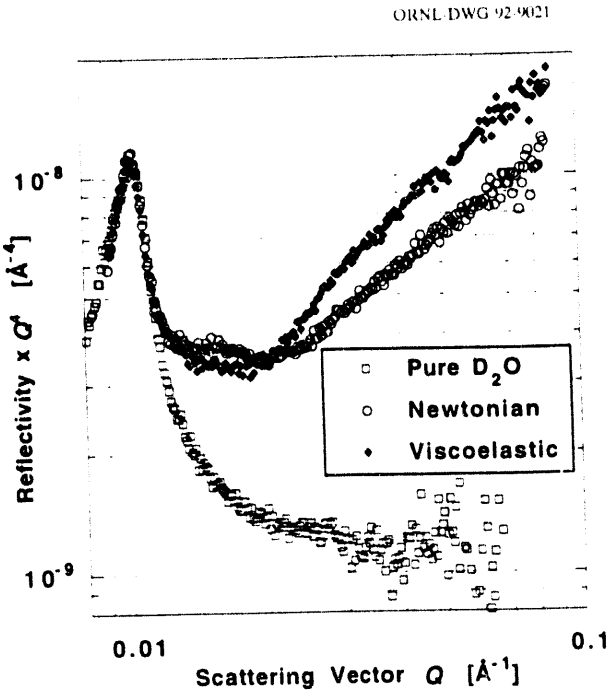


Fig. 3.7. Variation of reflectivity × $Q^4$ vs. scattering vector, $Q$, for the unsheared fluid samples. (Errors are of the same order as the scatter in the data.) The reflectivity limit on SPEAR for these 15-m runs is about $10^{-4}$, which was only reached for the $D_2O$ reference sample.

every quarter hour for 7 h. Over this limited time period (the relaxation time for this sample is on the order of days), there were no apparent changes in the observed scattering.

So, as yet, no effects of shear have been observed. Currently, a shear cell for reflection geometry, which will apply a larger constant shear rate to the fluids, is being designed and built. This new apparatus and longer runs over a wider $Q$ range should help to explain the features observed and to study the effect of shear on the structures causing them.

---

1. Los Alamos National Laboratory, Los Alamos, N. Mex.
2. University of Kentucky, Lexington, Ky.
3. The University of Tennessee, Knoxville, Tenn.
4. W. A. Hamilton and J. B. Hayter, "The Neutron Reflectometer at the HFIR," this report, and references therein.

## THE NEUTRON REFLECTOMETER AT HFIR

*W. A. Hamilton and J. B. Hayter*

In recent years, measurement of the reflection of neutrons from surfaces has emerged as a new probe of surface and interface structures on length scales ranging from a few to a few thousand angstroms.[1,2] The reflection coefficient for neutrons at a surface is an optical transform in the scattering vector of the gradient of the scattering length density profile (approximately as modulus-squared Fourier by $1/Q^4$ at high $Q$). Neutron reflectometry and the complementary technique of x-ray reflectometry have been used in studies of a diverse variety of surface structures including: thin-film superconductors, multilayers in semiconductors and polymers, and model biological lipid membranes. As in small-angle scattering and diffraction, the neutron technique has major advantages over its x-ray counterpart—manipulation of isotopic contrast to highlight regions within a larger structure without altering chemistry and in sensitivity to magnetic structures.

As part of the DOE research initiative "Structure of Anisotropic Colloidal Materials," a 6-m neutron reflectometer has been designed and built beside the High-Flux Isotope Reactor 30-m small-angle neutron scattering (SANS) instrument. The instrument, currently under

test, is primarily intended to study nanoscale structures in liquid-state colloidal phases, with particular emphasis on the anisotropic structures which occur naturally in fibrous or magnetic colloids or which may be induced under shear.

The reflectometer employs a 4.75-Å neutron beam, which is skimmed from the edges of the SANS beam by double pyrolytic graphite crystal reflection. The beam cross section is ~5-mm wide × 20-mm high. Operating with a horizontal reflection plane (vertical sample surface), the beam is reflected onto a 1-D position-sensitive detector with 2-mm resolution and 100-mm active length. (Position-sensitive detection allows measurement of off-specular diffuse scattering and also faster data collection by relaxed incident beam collimations.) The machine is run under personal computer (PC) control using a new version of the in-house software developed for the SANS and small-angle x-ray scattering instruments (Fig. 3.8). To

ORNL-DWG 92-9022

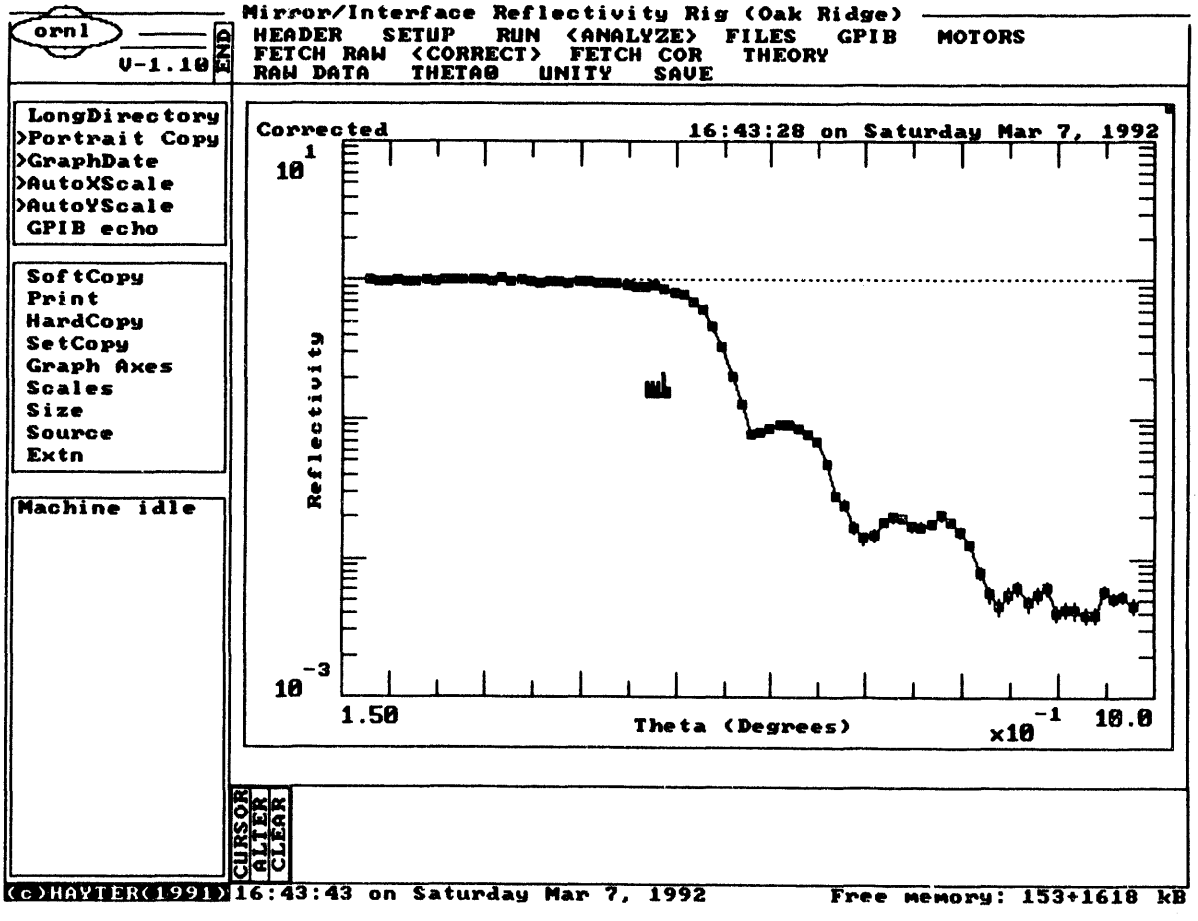


Fig. 3.8. Black and white copy of a standard screen from the PC data collection and analysis software. The graph shows the variation of the reflectivity of 4.75-Å neutrons with incident angle; the sample was a 7-cm section of neutron guide. Below the critical angle for the sample, the reflectivity is unity; while above this angle, interference fringes due to the sample's layered structure are seen. This data set has been reduced from the instrument's raw 2-D (position-angle) data set.

date, the instrument has been tested over reflection angles from 0.1 to 1.5° (a $Q$ range from 0.005 to 0.07 $Å^{-1}$) and reflectivities down to a few parts in $10^4$. Work is continuing to improve instrument backgrounds and data collection.

---

1. J. B. Hayter et al., *J. Chem. Soc. Faraday Trans.* 77, 1437 (1981).
2. T. P. Russell, *Mater. Res. Repts.* 5, 171 (1990).

# *NEUTRON DIFFRACTION*

## ATOMIC SHORT-RANGE ORDER AND SPIN DENSITY WAVE PROPAGATION IN CuMn

*Y. Tsunoda[1] and J. W. Cable*

Although Cu-Mn alloys have long been regarded as prototypical spin glasses, recent neutron scattering studies[2] carried out at ORNL show that this spin-glass concept is not correct for these alloys. Instead, there are spin density waves (SDW) that are incommensurate with the lattice and essentially static below a concentration-dependent freezing temperature. Long-range order does not develop for these SDW, and this lack of order has been attributed to topological problems associated with the multiple magnetic domains usually observed in these alloys. Quite recently a very unusual Cu-35% Mn alloy was obtained after a heat treatment designed to enhance the atomic short-range order (ASRO). Not only does this sample have a much higher degree of ASRO than previous samples, but this ASRO develops mostly in a single tetragonal domain. The diffuse peaks arising from the SDW also show a distinctly noncubic distribution which is readily correlated with the single-domain ASRO. This allows for a direct determination of the SDW propagation direction relative to that of the ASRO. The SDW diffuse peaks were found only at $(1 + \eta, 1, 0)$ and $(1, 1 + \eta, 0)$-type positions, and this corresponds to SDW propagating only in the c plane of the tetragonally based ASRO. This propagation direction could not be unambiguously established in previous studies because of equally populated ASRO and SDW domains. The temperature dependence of the SDW peaks yields a transition temperature of about 400 K, which is approximately a factor of 3 higher than that for a quenched alloy of the same Mn concentration. Thus, the high degree of ASRO and single-domain character of this carefully heat-treated sample produces an unusually stable SDW with a high transition temperature and a large, but not infinite, correlation length. Since SDW stability depends on structural features in the conduction electron susceptibility and on flat, parallel sections of the Fermi surface,[3,4] these observations suggest that the degree of ASRO and/or the presence of single-domain ASRO influences the sharpness of the relevant Fermi surface features in Cu-Mn alloys.

---

1. Guest scientist from Osaka University, Osaka, Japan.
2. J. W. Cable et al., *Phys. Rev. Lett.* **49**, 829 (1982).

3. S. A. Werner, *Cond. Matt. Phys.* **15**, 55 (1990).

4. A. W. Overhauser, *J. Phys. and Chem. Solids* **13**, 71 (1960).

## MAGNETIC AND STRUCTURAL PHASE TRANSITION IN $Ce(Fe_{1-x}Al_x)_2$

*Y. S. Yang,*[1] *J. A. Fernandez-Baca, N. Ali,*[2] *and B. D. Gaulin*[1]

The Laves-phase intermetallic compound $CeFe_2$ is a ferromagnet with a Curie temperature $T_c$ = 225 K. It has been observed that the substitution of small amounts of Al for Fe in this system leads to a degradation of the ferromagnetism: $T_c$ decreases when increasing the concentration of Al, and there is a new low-temperature phase that has been described by different authors as a re-entrant spin-glass phase[3] or as an antiferromagnetic phase.[4] In order to elucidate the nature of this low-temperature phase, a neutron diffraction experiment has been performed on a powder specimen of $Ce(Fe_{1-x}Al_x)_2$ for $x$ = 0.06. The diffraction measurements were carried out at the HB-3 triple-axis spectrometer and at the HB-4 powder diffractometer at the HFIR at temperatures between 14 K and room temperature. These measurements show that this low-temperature phase is antiferromagnetic with a Néel temperature $T_N \approx$ 100–110 K and that at this temperature, there is a structural transformation from the Laves phase to a trigonal structure (Fig. 3.9), as reported by Kennedy and Coles.[4] Further analyses and measurements on samples of other Al concentrations are in progress.

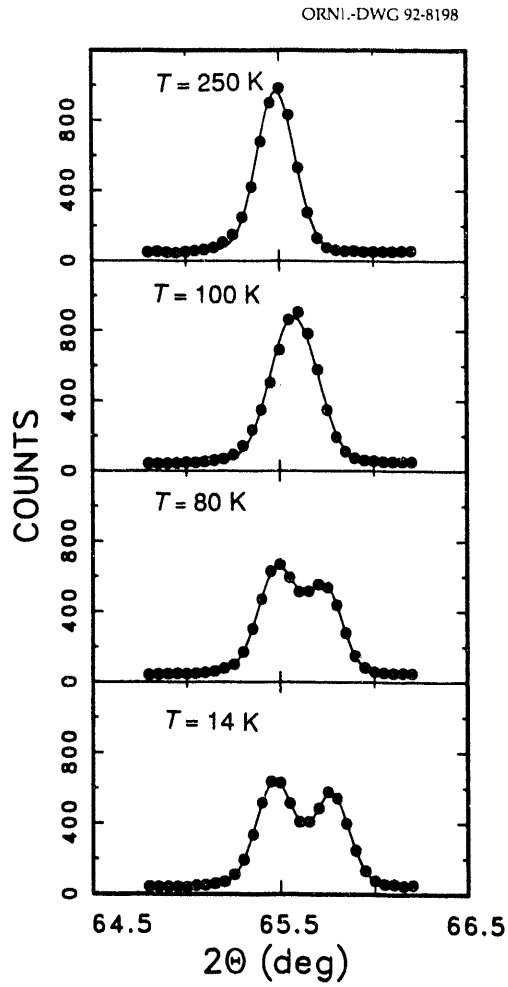


Fig. 3.9. Partial HB-4 powder diffraction patterns for $Ce(Fe_{1-x}Al_x)_2$ for $x$ = 0.06 showing the (4 4 0) reflection of the Laves phase at $T$ = 250 K and the (4 2 2) and (-2 2 0) reflections of the trigonal phase below about 100 K. The trigonal distortion is largest at the lowest temperature ($T$ = 14 K). The solid lines in this figure are fitted Gaussian line shapes.

---

1. McMaster University, Hamilton, Ontario, Canada.

2. Southern Illinois University, Carbondale, Ill.

3. J. Eynon and N. Ali, *J. Appl. Phys.* **63**, 4094 (1988).

4. S. J. Kennedy and B. R. Coles, *J. Phys., Condens. Matter* **2**, 1213 (1990).

## THE STRUCTURES OF SODIUM METAL[1]

*R. Berliner,[2] H. G. Smith, J. R. D. Copley,[3] and J Trivisonno[4]*

The martensitic transformation in sodium metal has been studied using neutron diffraction and neutron inelastic scattering techniques. In two separate experiments the transformation was observed on cooling near 32 K. Measurements of the diffuse scattering, diffraction linewidths, quasielastic scattering, and the temperature dependence of the $\Sigma_4$ [hh0] phonon energies above the transformation show no evidence of transformation precursors. The sodium martensite appears as 24 rhombohedral variants, 4 about each bcc (110), with reflections from their planes at (1.018, 0.92, ±0.06), (0.92, 1.018, ±0.06), and equivalent points. The layer stacking order of the variants is fixed by their relationship to the host bcc materials. The crystallography of the low-temperature phase is shown to be a complex mixture of stacking fault affected, rhombohedral polytypes of a particular "almost-hexagonal" structure. These form a ladder of structures connected, one to another, by stacking faults. As the martensite is warmed and before the complete reversion to a bcc structure, the relative fraction of the different martensite phases changes. Near 55 K, the longest period polytypes are the most stable.

---

1. Summary of paper: *Physical Review B* (in press).

2. University of Missouri, Columbia, Mo.

3. National Institute of Standards and Technology, Gaithersburg, Md.

4. John Carroll University, Cleveland, Ohio.

## NEUTRON SCATTERING STUDIES OF THE STRUCTURES AND LATTICE DYNAMICS OF THE ALKALI METALS[1]

*H. G. Smith, R. Berliner,[2] and J. Trivisonno[3]*

Early x-ray diffraction studies by Barrett[4] and his coworkers on the crystal structures of the alkali metals revealed that lithium and sodium transformed to close-packed structures at low temperatures and ambient pressures, while the heavier alkali metals did not. The effects of cold working on the metals were also studied, and particularly in the case of Li, it was shown that the type and amount of close-packed structures (hcp and fcc) were influenced by cold work. It was demonstrated that stacking faults were also introduced. These were difficult experiments then, which did not reveal the finer details of the transformations, except to show that they were of martensitic origin.

The neutron scattering technique, with its penetrating power, permits large samples to be used in cryostats at low temperatures. Neutron scattering is also unique in that the dynamical properties of crystals can readily be measured

and can be used to determine whether these properties are associated directly or indirectly with any martensitic transformations. This article is, necessarily, a very brief review of neutron scattering studies of the crystal structures, phonon behavior, and premartensitic behavior of Li, Na, K, Rb, and Cs as a function of temperature and pressure (Li, Na, Rb, and Cs) by the authors, their colleagues, and other workers in the field.

Li has been shown to transform partially to the 9R (Sm-type) structure in the vicinity of 75 K and then partially to fcc on annealing. There is an increase in $T_c$ with applied pressure. Na, on the other hand, partially transforms to a mixture of 9*R* and nearly hexagonal *R* polytypes, which approach hcp on annealing. Its $T_c$ is rapidly suppressed by application of modest pressures. No martensitic or premartensitic phenomenon, or phonon anomaly, has been observed in K down to 5 K. Also, a search for charge-density waves in the vicinity of (110) has been inconclusive. Similar negative results have been obtained for Rb. The absence of precursor effects are consistent with the more sensitive ultrasonic attenuation studies.

---

1. Summary of paper to be published.
2. University of Missouri, Columbia, Mo.
3. John Carroll University, Cleveland, Ohio.
4. C. S. Barrett, *Phys. Rev. B* **72**, 245 (1947).

## REFINEMENT OF THE STRUCTURES OF $Sr_3Al_2O_6$ AND THE HYDROGARNET $Sr_3Al_2(O_4D_4)_3$ BY RIETVELD ANALYSIS OF NEUTRON POWDER DIFFRACTION DATA[1]

*B. C. Chakoumakos, G. A. Lager,[2] and J. A. Fernandez-Baca*

The conversion of $Ca_3Al_2O_6$ to the hydrogarnet $Ca_3Al_2(O_4H_4)_3$ is one of the principal hydration reactions in the setting of Portland cements. The density decrease for this reaction is 16% for the Ca analogs and 24% for the Sr analogs. A comparison between the Sr and Ca analogs is being made to elucidate the reactivity of the aluminate and the stability of the $(O_4H_4)$ unit. In addition, structural systematics and Al-O bond length and Al-O-Al angle variations among the tetrahedral aluminates are being examined. The crystal structures of the Ca analogs have been determined and studied extensively. The structure of the Sr hydrogarnet has been refined only from single-crystal x-ray data whereas that of the $Sr_3Al_2O_6$ has not been reported.

The strontium aluminate was prepared by solid state reaction of high-purity $Al_2O_3$ and $SrCO_3$ at 1573 K. The hydrogarnet was prepared by adding $D_2O$ to the finely powdered strontium aluminate. For these samples, neutron powder diffraction data were collected at the HFIR on the HB-4 diffractometer, and their crystal structures were refined by Rietveld analysis methods. For $Sr_3Al_2O_6$, which is cubic, $Pa3$, $a$ = 15.8556 (4) Å, and $R_{wp}$ = 0.0447. The noteworthy feature of the strontium aluminate structure is a puckered 6-membered $AlO_4$ tetrahedral ring, with the

average bridging Al-O bond length, 1.768(8) Å, slightly greater than the average nonbridging Al-O bond length, 1.746(5) Å. For $Sr_3Al_2(O_4D_4)_3$ (Fig. 3.10), which is also cubic, $Ia3d$, $a$ = 13.0319 (1) Å, and $R_{wp}$ = 0.0464. $Sr_3Al_2(O_4D_4)_3$ has the hydrogarnet structure, which in contrast to the silicate garnets, has the $D_4O_4$ unit in place of the $SiO_4$ unit. The O-D distance is 0.914(4) Å, and the refined D content of the H position is 90%. Both the Sr hydrogarnet and the aluminate are isostructural with the Ca analogs. The enhanced reactivity of the $Sr_3Al_2O_6$ to form the hydrogarnet as compared with that of $Ca_3Al_2O_6$ is ascribed to the increased cell size and strain caused by the substitution of the larger size Sr for Ca.

---

1. Summary of paper: *Acta Crystallogr. C* **48**, 414 (1992).
2. University of Louisville, Louisville, Ky.

## PHASE TRANSITION OF METASTABLE TETRAGONAL $ZrO_2$ TO MONOCLINIC PHASE

*Y. Ishii,[1] S. Katano,[1] H. R. Child, N. Igawa,[1] and R. M. Nicklow*

The phase transition rate of metastable tetragonal zirconium oxide ($ZrO_2$) to the mono-

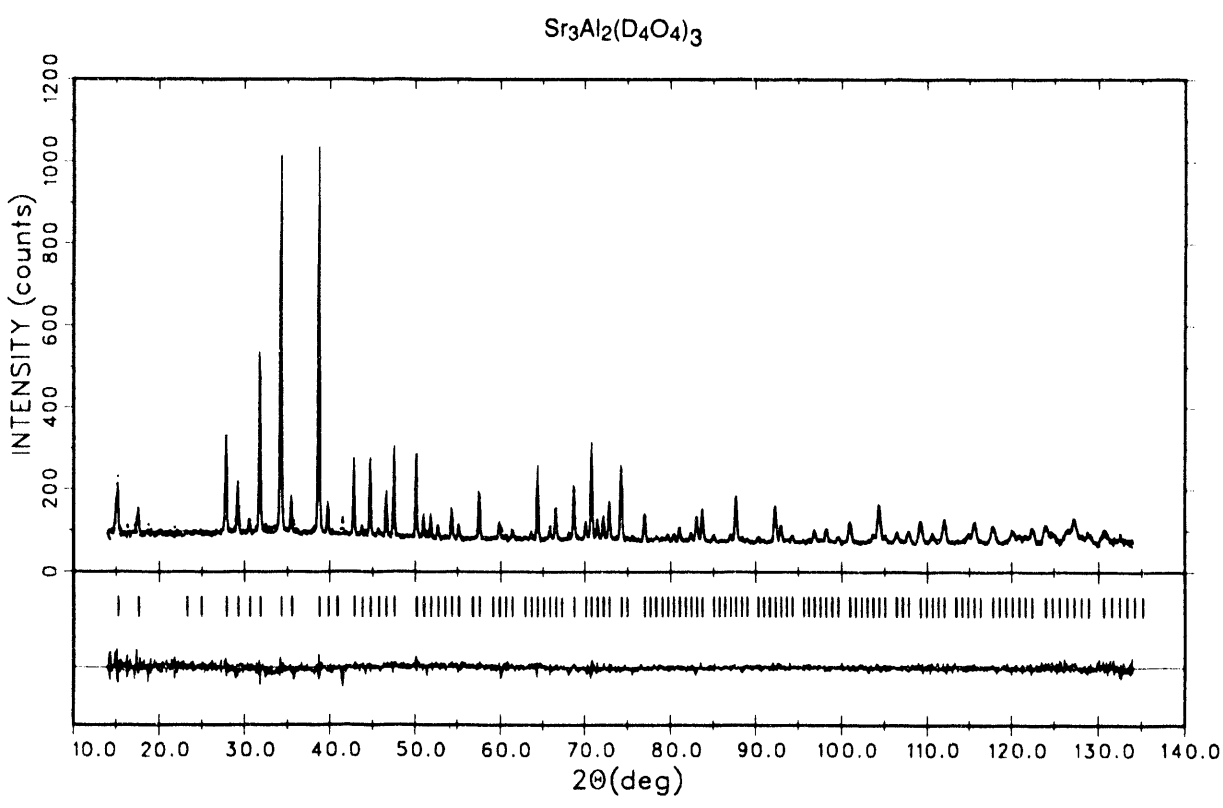


Fig. 3.10. Observed, calculated, and difference neutron powder diffraction profiles for $Sr_3Al_2(Da_4O_4)_3$. The short vertical lines below the profiles mark the positions of all possible Bragg reflections, and the bottom curve is the difference between the observed and calculated intensities.

clinic phase is substantially influenced by its crystallite size, partial oxygen pressure, and temperature. The phase transitions of $ZrO_2$ have been studied with x-ray diffraction by many workers. Neutrons are diffracted by the bulk specimen while X rays are only scattered near the surface of a specimen. The transition from the metastable tetragonal phase to the monoclinic phase was measured over the temperature range 800–950°C by neutron diffraction.

The powder used in this experiment was produced from $Zr(O_nC_4H_9)_4$ starting material by an alkoxide method, which is usually used to obtain fine-particle powder. This powder was in an amorphous state. To get the crystalline $ZrO_2$ specimen, the powder was heated at 700°C for 10 min in air. The specimen obtained has a metastable tetragonal structure.

Diffraction measurements were carried out utilizing the wide-angle neutron diffractometer (WAND) with a high-temperature furnace. The volume fraction of the monoclinic $ZrO_2$ was obtained from the intensity ratio of $(I_{111m} + I_{11\bar{1}m})/(I_{111m} + I_{111t} + I_{11\bar{1}m})$ where suffixes of $m$ and $t$ indicate the monoclinic and tetragonal phases, respectively.

Some typical diffraction patterns for $ZrO_2$ measured with a time-sliced method are shown in Fig. 3.11 for an annealing temperature of 900°C. At 800°C, the initial stage of the transformation seems to be a nucleation process. A precise analysis is being conducted based on an Avrami-type equation.

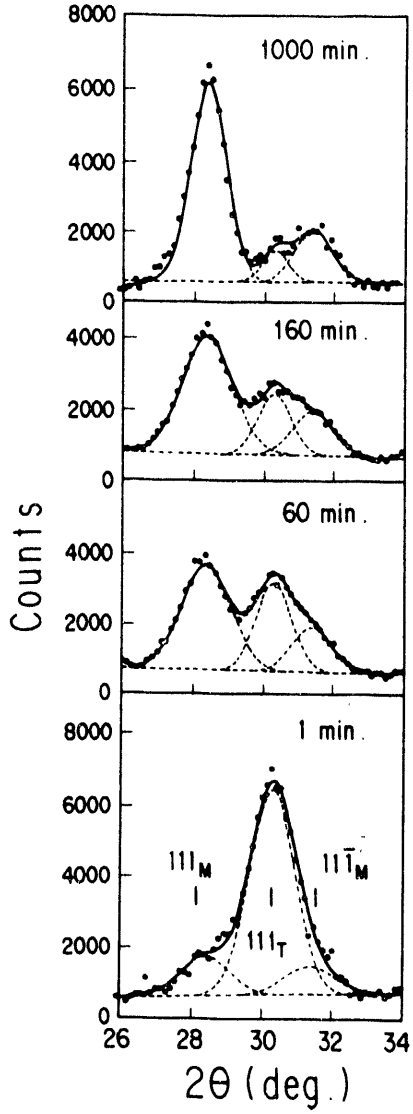


Fig. 3.11. Evolution in time of the diffraction pattern of $ZrO_2$ at 900°C, showing the transition from tetragonal to monoclinic.

---

1. Guest scientist from the Japan Atomic Energy Research Institute, Tokai, Japan.

## NEUTRON SCATTERING MEASUREMENT OF RESIDUAL STRESSES IN WELDS

*Steve Spooner, C. R. Hubbard,[1] S. A. David,[1] T. Dodson,[1] T. M. Holden,[2] J. H. Root,[2] J. Schroeder,[2] M. A. M. Bourke,[3] and J. A. Goldstone[3]*

The penetration of thermal neutrons can be used to advantage in the mapping of residual stress in metals joined by welding. The measurement of Bragg diffraction peaks using a high-resolution instrument permits the determination of *d*-spacing shifts which measure the macroscopic strains associated with residual stress. In the case of welding, the uneven thermal expansion produced during welding and, in some cases, solid state transformations during heating and cooling produce plastic deformation that leads to residual stress. In studies done at Chalk River, LANL, and ORNL, austenitic and ferritic steel welds have been studied with neutron diffraction methods. The distribution of residual stresses was mapped in a ferritic steel plate containing a multiple pass weld. The longitudinal stresses peak in the weld zone and tend toward small compressive stresses in the base metal. Figure 3.12 shows the mapping of residual stresses for each of the components. A less complete study of an austenitic steel plate indicates a quite different pattern of residual stress wherein the weld zone is in a state of almost isotropic compression and the heat-affected zone at the weld line is in a state of tension. The plastic deformation during welding which causes the residual stress is not well understood. The principal difference, however, is the austenite (FCC) to ferrite (BCC) transformation occurring in the ferritic steel during cooling. Finite element computations are at the stage where residual stresses can be calculated for welded plates, and it is hoped that this approach will lead to improved interpretation of residual stress measurements.

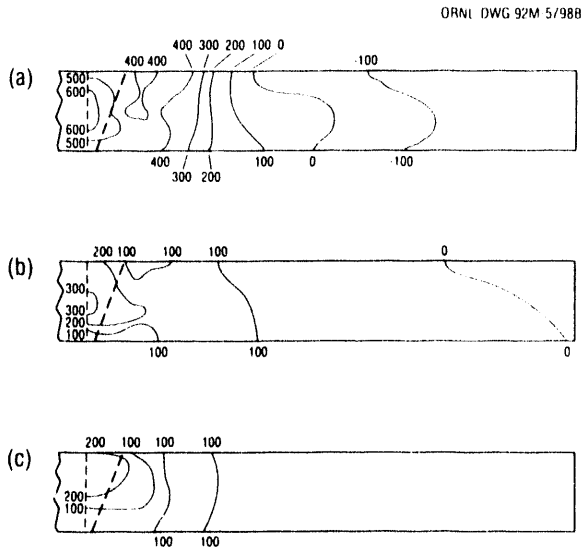


Fig. 3.12. The residual stresses in a 30-cm × 30-cm × 12-cm plate were determined in a section of the plate halfway along the weld line joining to two halves. The three orthogonal components of residual stress are given as (a) longitudinal (along the direction of the weld), (b) transverse (perpendicular to the weld line and in the plane of the plate) and (c) normal (perpendicular to the plane of the plate).

---

1. Metals and Ceramics Division, ORNL.
2. Chalk River Nuclear Laboratories, Chalk River, Canada.
3. Los Alamos National Laboratory, Los Alamos, N. Mex.

# INELASTIC NEUTRON SCATTERING

## SPIN WAVES IN $Mn_{90}Cu_{10}$

*J. A. Fernandez-Baca, M. E. Hagen,*[1]
*R. M. Nicklow, and Y. Tsunoda*[2]

The study of the magnetic excitations of the Mn-rich alloys should be a good test of the multiband calculations[3] of the spin dynamics of pure γ-Mn, which is a prototypical itinerant-electron antiferromagnet. These calculations predict spin waves with a very steep dispersion that at small wave vectors $q$ is linear in $q$. A spin wave damping, due to the decay into electron-hole pairs, that is also linear in $q$ is predicted as well. Because of the steep spin wave dispersion in these systems, neutron inelastic scattering measurements at high-energy transfers are required in order to resolve these excitations. A program to study the high-energy magnetic excitations of $Mn_{90}Cu_{10}$ and to complement the previous measurements of Nicklow and Tsunoda has been initiated.[4] In these measurements, which were performed using the HB-3 triple-axis spectrometer at the HFIR, Nicklow and Tsunoda observed resolved spin waves in $Mn_{90}Cu_{10}$ alloy at 25 and 30 meV at room temperature. Experiments have been performed at the hot-source based IN1 triple-axis spectrometer at the Institut Laue Langevin and at the HET chopper spectrometer at ISIS at the Rutherford Appleton Laboratory. Spin waves up to 68 meV at IN1[5] and up to 115 meV at HET have been observed. Six sets of IN1 data have been least-squares fitted simultaneously to the convolution of a model cross section with the full four-dimensional IN1 instrumental resolution. This analysis indicates that the spin waves in $Mn_{90}Cu_{10}$ are consistent with a linear dispersion relation with a stiffness constant of about 250 meV-Å and an energy gap of 7.5 meV. The spin wave damping is strong and is also consistent with a linear dependence in $q$. The analysis of the HET data is considerably more difficult and is still in progress.

---

1. Guest scientist from Keele University, Keele, United Kingdom.
2. Guest scientist from Osaka University, Osaka, Japan.
3. M. J. Gillan, *J. Phys. F* **3**, 1874 (1973).
4. R. M. Nicklow and Y. Tsunoda, *Bull. Am. Phys. Soc.* **32**, 415 (1987); unpublished.
5. J. A. Fernandez-Baca et al., *J. Magn. Magn. Mater.* **104–107**, 699 (1992).

## MAGNETIC EXCITATIONS IN THE TRIANGULAR ANTIFERROMAGNETIC $Mn_3Sn$

*P. Radhakrishna*[1] *and J. W. Cable*

The intermetallic compound $Mn_3Sn$ has a hexagonal crystal structure with lattice constants at room temperature of $a_0 = 5.665$ and $c_0 = 4.531$ Å. There are six Mn atoms per unit cell. Below $T_N = 420$ K, a triangular antiferromagnetic order develops in which nearest neighbor spins within the basal planes are oriented at 120°, while ferromagnetic alignment occurs for those spins along the c axis connected through an inversion center. Below 230 K, a helical magnetic phase occurs for

which the basal plane spin arrangement remains, but the spins rotate about the c axis with a period of about 10 $c_0$. Recently, Radhakrishna and Tomiyoshi[2] studied the magnetic excitations of this compound at temperatures above and below the helical phase transition. Their room temperature results show an anisotropy gap of about 4.1 meV and essentially linear dispersion in the {100} and {110} directions with the velocity in the {110} direction being about 35% higher than {100}. Because of low intensities, their low-temperature data were limited to energy transfers below 10 meV, and in this region, constant energy scans along $Q = (1, 0, \zeta)$ showed an unresolved three-peak structure with the outer peaks close to the modulation wave vector of the helical structure [$\tau \simeq (0, 0, \pm 0.1)$] and with essentially vertical dispersion. These measurements are extended to higher energy transfers to resolve the dynamic behavior of $Mn_3Sn$ better.

The results are summarized in Fig. 3.13 which gives the dispersion curves for both magnetic phases of $Mn_3Sn$. At $T$ = 295 K, the spin-wave energies can be written as $(\hbar\omega)^2 = \Delta^2 + A^2q^2$ with $\Delta$ = 4.3 meV, $A$ = 100 meV-Å for {100}, and $A$ = 135 meV-Å for {110}. These velocities are comparable to those found in other itinerant electron systems, such as MnCu and MnNi (~150 meV-Å). The anisotropy within the basal plane is unusual but probably arises from different interaction paths in these Kagomé-like hexagonal layers where some Mn atoms are replaced by nonmagnetic Sn atoms. Also unusual for an antiferromagnet is the

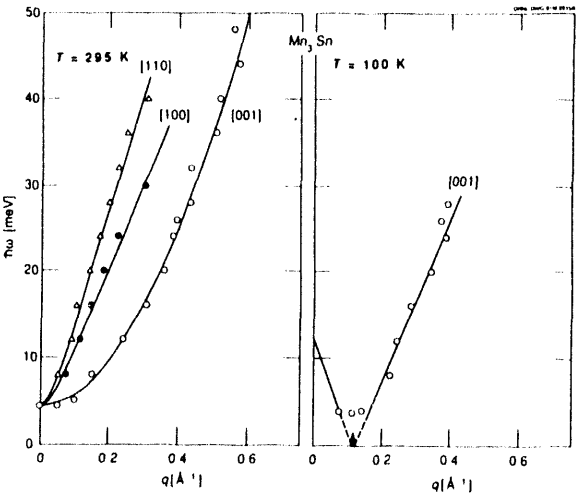


Fig. 3.13. Dispersion curves for the two magnetic phases of $Mn_3Sn$. The arrow in the right panel indicates the modulation wave vector of the helical phase.

quadratic dispersion along {10ζ} and {11ζ}, where the spin-wave energy can be described by $\hbar\omega = \Delta + 130\,q^2$ [meV]. This quadratic behavior results from the ferromagnetic coupling through the inversion center along the c axis.

The available results for the helical phase at $T$ = 100 K are shown in the right panel of Fig. 3.13. If the gap-like structure in the vicinity of the modulation wave vector is discounted, then the data are well represented by linear dispersion as shown in Fig. 3.13. This dramatic changeover from quadratic to linear dispersion is reminiscent of that observed in the ferromagnetic and helical phases of the rare-earth metals.

---

1. Guest scientist from the Jawaharlul Nehru Centre for Advanced Scientific Research, Bangalore, India.

2. P. Radhakrishna and S. Tomiyoshi, *J. Phys., Condens. Matter* **3**, 2523 (1991).

## MAGNONS IN FERROMAGNETIC TERBIUM UNDER HIGH PRESSURES

*S. Kawano,*[1] *J. A. Fernandez-Baca,*
and *R. M. Nicklow*

An experiment has been carried out in order to investigate the pressure dependence of the magnon dispersion relation of Tb in its ferromagnetic phase. Neutron inelastic scattering measurements have been performed along the crystal c axis at 90 K (well below the Curie temperature $T_c$ = 220 K) at ambient pressure, 4.3 kbar, and 15.2 kbar using a clamp-type high-pressure cell.[2] A pressure cell with a sapphire window was used for the ambient and 4.3-kbar measurements, and a cell with an alumina window was used for the 15.2-kbar measurements. The preliminary results of these measurements are shown in Fig. 3.14. The magnon dispersion curve at ambient pressure is in general agreement with the curve previously reported by Jensen et al.[3] The difference between the dispersion curves at ambient pressure and at 4.3 kbar is very small below $q$ = 0.5 Å, while above $q$ = 0.5, the dispersion shifts slightly toward higher energies. At 15.2 kbar, the hardening of the magnon spectrum is evident. Because of experimental difficulties derived from the high scattering background from the alumina in the pressure cell, it has not been possible to collect reliable data at small wave vectors at 15.2 kbar. However, due to the hardening of the spectrum with increasing pressure, it seems reasonable to expect that the energy gap will be enhanced at this pressure. Further measurements to complete the magnon dispersion relation at 15.2 kbar are in progress. These measurements will allow us to obtain information of the pressure dependence of the anisotropy and exchange interactions.

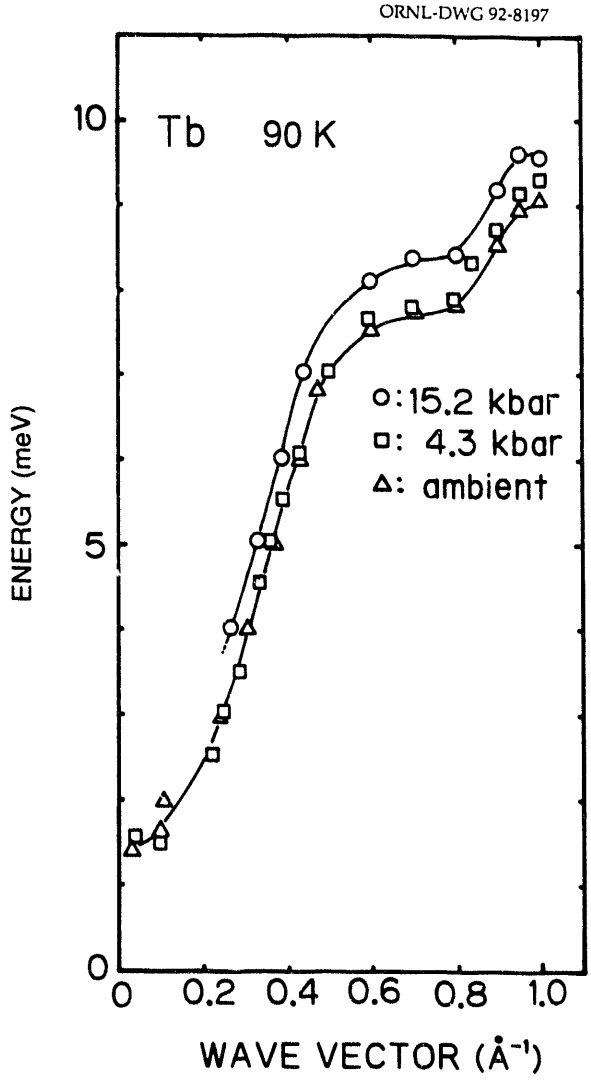


Fig. 3.14. Magnon dispersion relation for Tb along its c axis as a function of pressure. The solid lines are guides to the eye.

---

1. Guest scientist from Kyoto University, Osaka, Japan.
2. A. Onodera et al., *Jpn. J. Appl. Phys.* **26**, 152 (1987).
3. J. Jensen et al., *Phys. Rev. B* **12**, 303 (1975).

## DYNAMIC MAGNETIC CRITICAL PHENOMENA IN DYSPROSIUM

*M. Hagen*[1] *and H. R. Child*

The dynamic magnetic critical phenomenon at the paramagnetic-to-antiferromagnetic phase transition in dysprosium has been studied by inelastic neutron scattering. These measurements were carried out on an isotopic single crystal of $^{163}$Dy using the HB-3 triple-axis spectrometer at the HFIR. The transition in dysprosium is isomorphic with the transitions in holmium and terbium. The magnetic structure in the antiferromagnetic phase of these elements is a helix with the magnetic moments ferromagnetically aligned in the a-b plane but rotating in a direction along the c axis. The magnetic Bragg peaks, therefore, occur as satellites at positions $(0, 0, \pm \tau)$ about the nuclear Bragg peaks. In a previous study, Gaulin et al.[2] measured the critical exponents associated with the frequency-integrated magnetic critical scattering from dysprosium and holmium using neutron diffraction.

The inelastic measurements on dysprosium were performed at various temperatures between 181 and 190 K. At each temperature a series of scans were performed, along $(0, 0, 2 + q_c)$ and $(q_{ab}, q_{ab}, 2 + \tau)$ at $\omega = 0$, and inelastic scans at (0, 0, 2.24), (0.02, 0.02, 2.24), (0.08, 0.08, 2.24), (0, 0, 2.35), and (0, 0, 2.45). These spectra were fitted to the convolution integral of the four-dimensional spectrometer resolution function and the dynamic structure factor $S(q,\omega) = S^A(q,\omega) + S^F(q,\omega)$, the sum of a ferromagnetic and antiferromagnetic contribution. In these measurements, as in the diffraction measurements of Gaulin et al.,[2] both antiferromagnetic and ferromagnetic scattering was observed. The structure factor $S^A(q,\omega)$ is given by

$$S^A(q,\omega) = \frac{\chi^A}{1 + [(q_c - \tau)/\kappa_c^A)^2 + (q_{ab}/\kappa_{ab}^A)^2} \times \frac{\Gamma^A(q)}{\omega^2 + \Gamma^A(q)^2}$$

where $\Gamma^A(q) =$

$$\Gamma_0^A (1 + [(q_c - \tau)/\kappa_c^A]^2 + (q_{ab}/\kappa_{ab}^A)^2).$$

The structure factor $S^F(q,\omega)$ is given in the same form but with $\tau = 0$. The values of $\kappa_c^A$, $\kappa_{ab}^A$, $\chi^A$, and $\Gamma_0^A$ which resulted from these fits were themselves fitted to power law functions of the reduced temperature $t = (T-T_N)/T_N$ with $T_N = 180.5 \pm 0.1$ K. These power law fits led to the critical exponent results $\kappa_c^A = (0.369 \pm 0.020\text{Å}^{-1})\ \tau^{\upsilon_c}$, $\upsilon_c = 0.54 \pm 0.05$; $\kappa_{ab}^A = (0.385 \pm 0.033\text{Å}^{-1})\ \tau^{\upsilon_{ab}}$, $\upsilon_{ab} = 0.54 \pm 0.04$; $\chi^A = (47.9 \pm 1.5)\ \tau^{-\gamma}$, $\gamma = 1.05 \pm 0.05$, and $\Gamma_0^A = (0.43 \pm 0.03\ \text{THz})\ \tau^{\Delta}$, $\Delta = 0.93 \pm 0.03$. The critical amplitudes and exponents for $\kappa_c^A$, $\kappa_{ab}^A$, and $\chi^A$ are in good agreement with the values deduced from the diffraction measurements of Gaulin et al.

---

1. Guest scientist from Rutherford Appleton Laboratory, Chilton, Didcot, United Kingdom.

2. B. D. Gaulin, M. Hagen, and H. R. Child, *J. de Physique* **C8**, 327 (1988).

## A STUDY OF THE MAGNETIC CRITICAL SCATTERING FROM THE LONGITUDINALLY MODULATED ANTIFERROMAGNETS THULIUM AND ERBIUM[1]

*M. Hagen,*[2] *H. R. Child, J. A. Fernandez-Baca, and J. L. Zarestky*[3]

The temperature dependence of the magnetic critical scattering above $T_N$ and the staggered magnetization below $T_N$ have been measured in the longitudinally modulated antiferromagnets thulium and erbium using neutron diffraction. These measurements were carried out on the HB-1A and HB-2 spectrometers at the HFIR. The transitions, which occur at $T_N$ = 57.65 ± 0.10 K in thulium and at $T_N$ = 86.04 ± 0.20 K in erbium appear to be continuous second-order transitions. As longitudinally modulated antiferromagnets, thulium and erbium would be expected to belong to the $d$ = 3, $\nu$ = 2 universality class of the $d$ = 3 X-Y model. The value of $\nu$ is 2 for thulium and erbium because, although the number of spin degrees of freedom is only 1, the star of the ordering wave vector for the magnetic structure has two components.[4] An analysis of the critical scattering above $T_N$ has led to the exponents $\nu_c$ = 0.43 ± 0.02, $\nu_{ab}$ = 0.40 ± 0.02, and $\gamma$ = 0.90 ± 0.04 for thulium and $\nu_c$ = 0.41 ± 0.04 , $\nu_{ab}$ = 0.35 ± 0.05, and $\gamma$ = 0.73 ± 0.06 for erbium. These values are very different to the theoretical values for the $d$ = 3 X-Y model of $\nu$ = 0.65 and $\gamma$ = 1.3.[5] However, from the temperature dependence of the staggered magnetization, the exponents $\beta$ = 0.37 ± 0.03 for thulium and $\beta$ = 0.35 ± 0.03 for erbium have been determined, which are in good agreement with the theoretical value of $\beta$ = 0.35 for the $d$ = 3 X-Y model.[5] The difference between experiment and theory for the values of the exponents above $T_N$ is surprising. This is especially so because the experimentally observed exponents are smaller than the values for mean-field theory. This behavior can be explained if the value of the exchange interaction were to decrease with increasing temperature above $T_N$. Calculations have shown that shifting the $\nu$ exponents from the $d$ = 3 X-Y model values to those observed would require a reduction in the exchange of up to 15% at temperatures 10% above $T_N$.

---

1. Summary of paper to be published.
2. Guest scientist from Keele University, Keele, United Kingdom.
3. Guest scientist from Ames Laboratory, Iowa State University, Ames, Iowa.
4. D. Mukamel and S. Krinsky, *Phys. Rev. B* **13**, 5065 (1976).
5. See for example: *Magnetic Critical Scattering*, ed. by M. F. Collins, Oxford University Press, Oxford (1989).

## ARE THERE PRECURSOR EFFECTS ABOVE THE MARTENSITIC TRANSFORMATION IN A VIRGIN CRYSTAL OF Li METAL?

*H. G. Smith,* R. *Berliner,*[1] and *J. Trivisonno*[2]

There is no doubt that in many materials that undergo first-order martensitic phase transformations, there are often precursor effects above the transition. These precursors are sometimes in the form of phonon anomalies, diffuse scattering, and/or strong ultrasonic attenuation effects, to name a few.

In our extensive neutron scattering studies on the martensitic behavior of metallic lithium in both single-crystal and polycrystalline samples at atmospheric and modest pressures, effects that could be considered precursors or premartensitic phenomena—with negative results, contrary to reports by some investigators—have been looked at very carefully.[3] Clarification of these disagreements may be crucial for distinguishing between different theories of the mechanism for the transformation.

Some of the main points of contention are: (1) The short-wavelength low-lying phonons soften somewhat, contrary to quasiharmonic theory, but anharmonic phonon calculations predict this behavior for this branch in the alkali metals. Some materials show this behavior but clearly do not transform. Ultrasonic attenuation is a very sensitive tool in many systems, but Trivisonno's measurements[4] in Li show no evidence for attenuation until the onset of the transformation. Our initial phonon measurements[5] did not show even a slight dip in the $\Sigma_4$ branch at (1/3, -1/3, 0 ) as others have claimed.[3] (2) A temperature-dependent diffuse background in the bcc phase was observed, but this is attributed[6] in large part to the Debye-Waller factor in the large spin-dependent incoherent neutron scattering in Li, natural or isotopic $^7$Li, and is insufficient evidence for the presence and growth of embryos. (3) The sudden decrease in the (110) bcc intensity at the transition is corroborated by the sudden appearance of the 9R peak without a buildup in diffuse intensity at the appropriate $q$-vector.

The temperature-dependent behavior of the $\Sigma_4$ branch was investigated again recently under higher instrumental resolution with a virgin crystal of isotopic $^7$Li. The overall decrease in short-wavelength phonons with temperature was again confirmed with no apparent dip near (1/3, -1/3, 0). A very careful comparison was made of the bcc phonons at 200, 100, and 80 K. However, at 80 K it was concluded that the crystal had already transformed when the phonons were measured (the highest $T_c$ measured to date in our studies). Nevertheless, there were no discernible differences between the 100- and 80-K measurements.

The reduced phonon intensities reflected the reduced amount of the bcc phase (≈50%). If anything, the phonon widths at 80 K were equal to or less than at 100 K. An increase in widths would be expected if they somehow were associated with the transformation. Also, there was no change in the quasielastic line width between the two temperatures at (0.35, -0.35, 0)—perhaps a more sensitive measure of precursor effects. In studying diffuse scattering below the transition, caution must be used because there are 24 variants of 9R plus the remainder of the bcc crystal. The background may be very uneven.

Recent theoretical studies indicate that for pure materials undergoing first-order transitions, precursors are not required.[7]

---

1. University of Missouri, Columbia, Mo.
2. John Carroll University, Cleveland, Ohio.

3. W. Schwarz, O. Blaschko, and I. Gorgas, *Phys. Rev. B* **44**, 6785 (1991).

4. J. Trivisonno, A. R. Slotwinski, and M. P. Johnson, *J. de Physique* C5, 983 (1981).
5. H. G. Smith, *Phys. Rev. Lett.* 58, 1228 (1987).
6. C. M. McCarthy, C. W. Tompson, and S. A. Werner, *Phys. Rev. B* 22, 574 (1980).
7. J. Morris and R. Gooding, private communication.

## TEMPERATURE DEPENDENCE OF THE PHONON ENERGY IN LITHIUM OXIDE

*Y. Ishii,*[1] *R. M. Nicklow, and S. Katano*[1]

Lithium oxide ($Li_2O$) has the antifluorite structure with space group Fm3m. It is well known that lithium oxide is a superionic conductor because the lithium ion is very mobile above 500 K. This behavior affects the mechanical and electrical properties of $Li_2O$. To understand these properties of lithium oxide better, an inelastic neutron scattering measurement of some acoustic branches was carried out at 700 K. The temperature dependence of the phonon energy of the transverse acoustic branch ($\Sigma_3$) at the zone boundary was also measured.

The $^7Li_2O$ single crystal used in this experiment was grown from a sintered rod of $^7Li_2O$ by a floating-zone melting method with an infrared-light furnace. The specimen was annealed in high vacuum at 1300 K for 10 h to remove the residual stress induced by cutting and by the LiOH deposited on a surface.

Phonon energy measurements were carried out with the triple-axis neutron spectrometer installed at the HB-2 port of the HFIR. A pyrolytic graphite filter was used to eliminate $\lambda/2$ contamination. For all experiments, the final neutron energy was fixed at a value of 14.8 meV, and neutron energy loss was measured using the constant-$q$ method.

The phonon energies of the acoustic branches for wave vectors in the [111] and [001] directions measured at 700 K were slightly low compared with those phonon energies at room temperature. In Fig. 3.15 the phonon energy of the acoustic branch ($\Sigma_3$) at the zone boundary is shown as a function of temperature. Although this phonon has an energy of 30.6 meV at room temperature, it decreases to 25.1 meV at 700 K. In the harmonic model, phonon energies have no temperature dependence. This large temperature dependence apparently is caused by anharmonicity of the crystal potential of lithium oxide.

---

1. Guest scientist from the Japan Atomic Energy Research Institute, Tokai, Japan.

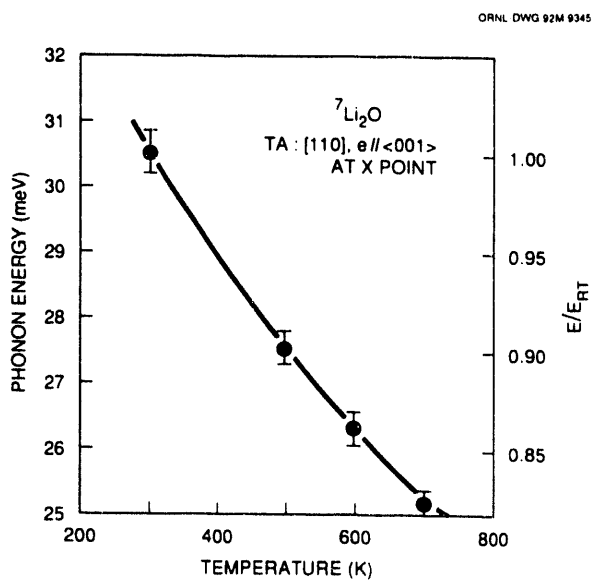


Fig. 3.15. Temperature dependence of the phonon energy of the acoustic branch $\Sigma_3$ at the zone boundary.

## LATTICE INSTABILITY IN $\beta_1$-AgZn[1]

*Y. Morii,[2] A. Nagawa,[3] Y. Matsuo,[3]*
*S. Funahashi,[2] H. R. Child,*
*and R. M. Nicklow*

The metastable $\beta_1$-AgZn (CsCl structure) is obtained by rapid quenching of the $\beta$ phase of the alloy (bcc structure) to room temperature. The $\beta_1$ phase is easily transformed to the $\zeta$ phase (hexagonal) at $T_c$ of about 390 K by heating. Having no martensitic transformation at lower temperature, the $\beta_1$-AgZn alloy has a stress-induced martensitic phase transition to the hexagonal close-packed structure at room temperature.

To study dynamical properties of the lattice which are related to these phase transitions, acoustic phonon dispersion relations along the main crystal axes of the alloy at room temperature were measured, and it was found that the $[\zeta\zeta 0]TA_1$ phonon branch has anomalously low energies at all values of its wave vector compared to the other phonon branches. An anomalous deformation in the curve at 331 K was observed. The anomaly grew with temperature until the phase transformation to the $\zeta$ phase. At 269 K, a clear dip in the dispersion curve is observed at the wave vector $\zeta \sim 1/3$. Associated with this phonon energy anomaly, or lattice instability, it was observed that along the [110] axis, diffuse scattering barely peaks at $\zeta = 1/3$. These observations suggest that a stacking sequence with a unit of 3 layers along the $[\zeta\zeta 0]$ direction is favorable. Expressing the phonon energy in terms of interlayer force constants, $\Phi_n$, where the layers are parallel to (110) planes, it was found that the next nearest neighbor force constant, $\Phi_2$, changes its sign from positive to negative as the temperature is raised and that $\Phi_4$ is still meaningful. It was also observed that the $[\zeta\zeta{-}2\zeta]TA$ phonon has anomalies such as relatively low energy and a temperature dependence at all wave vectors. Kitchingman[4] claimed that the $\beta_1$ to $\zeta$ phase transition takes place by an interchange of nearest neighbors which gives the disordered structure (same as that of the high-temperature $\beta$-phase structure) and then by a martensitic deformation of the disordered structure which leads to slip in $(11\bar{2})$ planes in the [111] direction. Therefore, it can be deduced that the instability in the $[\zeta\zeta{-}2\zeta]TA$ phonon and probably also in the $[\zeta\zeta 0]TA_1$ phonon would promote the structural transition from the $\beta_1$ phase in the alloy.

---

1. Summary of paper: *J. Phys. Soc. Jpn.* **60**, 4160 (1991).
2. Guest scientist from the Japan Atomic Energy Research Institute, Tokai, Japan.
3. Guest scientist from Nara Women's University, Nara, Japan.
4. W. J. Kitchingman, *Acta. Metall.* **10**, 799 (1962).

# 4. *Synthesis, Processing, and Characterization of Materials*

Research activities in the Solid State Division have traditionally been supported and advanced by a broad, internal program emphasizing the synthesis, processing, and characterization of advanced research materials. This internal activity encompasses the growth of large, high-quality single crystals, the development and synthesis of new types of glasses, the formation and characterization of nanophase textured ceramics, the growth of metal alloy single crystals and their application to the study of solidification phenomena, the development of new techniques for crystal growth and materials processing, and research on the synthesis and characterization of high-temperature superconductors. Since a number of unique or rare research materials result from this effort, a wide range of collaborative research is undertaken that involves university laboratories, other ORNL divisions, other national laboratories, and industrial research centers. The effort has enjoyed a successful history of applying materials synthesis and crystal growth techniques to the resolution of fundamental scientific issues as well as important energy-related problems.

This chapter is divided into the following four sections: *Solid Electrolytes and Thin-Film Batteries,* which reports on exciting research activities in the area of the development of new types of solid electrolytes and the application of these materials to the formation of microbatteries; *Perovskite-Structure Oxides,* which describes research activities dealing with an increasingly important class of ferroelectric materials for photorefractive, electro-optic, and thin-film substrate applications; *Optical Characterization of Impurities and Defects,* which reports on research in which optical techniques are used to determine both fundamental optical properties of materials as well as the properties of color centers and defects in crystals, and *Materials Properties,* which describes pioneering research in which alloy single crystals are applied to the study of solidification phenomena and research in which unique materials properties are applied to the development of new, highly stable analytical standards. Those aspects of the research dealing with high-$T_c$ superconductors are treated separately in Chapter 2 on high-temperature superconductivity.

# SOLID ELECTROLYTES AND THIN-FILM BATTERIES

## LITHIUM PHOSPHORUS OXYNITRIDE: A NEW AMORPHOUS THIN-FILM ELECTROLYTE[1]

*J. B. Bates, N. J. Dudney, G. R. Gruzalski, A. Choudhury,[2] R. A. Zuhr, and C. F. Luck*

Materials suitable as electrolytes in thin-film lithium batteries must have acceptable lithium-ion and low electronic conductivities and must be electrochemically stable in a lithium cell. While there are many materials that have acceptable electrical properties, few are chemically stable in contact with lithium, and fewer still are stable at the cell potentials of 2.5 to 4.5 V achievable in solid state cells. A new amorphous lithium-ion conducting electrolyte that satisfies all of the above requirements has been synthesized in thin-film form by rf magnetron sputtering of $Li_3PO_4$ in $N_2$. The composition and structure of the oxynitride films were investigated using a variety of ion and electron beam techniques and electron spectroscopies.

The results in Table 4.1 show that the ionic conductivity $\sigma$ increased and the activation energy $E_a$ decreased with increasing concentrations of $N_2$ in the process gas. The N content in the films deposited in pure $N_2$ was low, ranging from 3 to 6 at %. From the x-ray photoemission spectroscopy (XPS) measurements, there appear to be two major sites for N in the films:

(a) P = N - P (b) P - N(P)(P)

The ratio of N in structure (a) to that in structure (b) was determined to be about 4. The increase in the ionic conductivity of the amorphous films on incorporation of N is believed to be due at least partially to the formation of the cross-linked structure (b); it is estimated that about 30% of all the P in the films is bound in this structure. While the increase in conductivity is desirable, the major benefit gained on incorporation of N into the electrolyte is an increase in electrochemical stability. The discovery of this new electrolyte has allowed the

**Table 4.1. Comparison of the compositions, conductivities, and activation energies of amorphous lithium phosphate and phosphorus oxynitride electrolyte films deposited by rf magnetron sputtering of $Li_3PO_4$.**

| Process Gas | Film Composition | $\sigma$(25 C) $\times 10^8$ (S/cm) | $E_a$[(a)] (eV) |
|---|---|---|---|
| 3:2:0 | $Li_{2.7}PO_{3.9}$ | 7 | 0.68 |
| 13:0:1 | | 39 | 0.64 |
| 4:0:1 | | 84 | 0.56 |
| 0:0:1 | $Li_{3.1}PO_{3.8}N_{0.16}$ | 200 | 0.57 |
| " | $Li_{3.3}PO_{3.8}N_{0.22}$ | 240 | 0.56 |
| " | $Li_{2.9}PO_{3.3}N_{0.46}$ | 330 | 0.54 |

[(a)]Determined from a least-squares fit of $\sigma T = \sigma_o \exp(-E_a/kT)$ to conductivity data.

development of a 3.7-V rechargeable thin-film lithium battery described elsewhere in this report.[3]

---

1. Summary of paper to be published.
2. Metals and Ceramics Division, ORNL.
3. J. B. Bates et al., "Rechargeable Thin-Film Lithium Batteries," this report.

## RECHARGEABLE THIN-FILM LITHIUM BATTERIES[1]

*J. B. Bates, G. R. Gruzalski, N. J. Dudney, and C. F. Luck*

Research on the deposition and characterization of amorphous lithium electrolyte and vanadium oxide thin films is directed toward the development of a thin-film rechargeable lithium battery suitable for application as an integrated primary or standby power source for low-current electronic devices. The battery consists of a $V_2O_5$ cathode and a lithium anode separated by an amorphous lithium phosphorus oxynitride electrolyte.[2] Typically, the sputter-deposited cathode and electrolyte films are about 1 μm thick while the evaporated Li anode film is 5 μm thick (about ten times over capacity). Depending on the flow rate of the process gas (14% $O_2$ in Ar), two distinct types of $V_2O_5$ films were deposited by reactive sputtering of V: (1) rough crystalline films composed of micron-sized clusters or (2) smooth amorphous films. Cells fabricated with the crystalline or amorphous cathodes had open-circuit voltages of 3.6 to 3.7 V, but the rates of discharge and charge that cells with the crystalline cathodes could sustain without excessive polarization were significantly lower than those with amorphous cathodes, usually less than 10 μA/cm$^2$ and 1 μA/cm$^2$, respectively. Cells with the smooth amorphous cathodes, on the other hand, were discharged at rates of up to 100 μA/cm$^2$. A typical example of a charge-discharge cycle of a thin-film cell with a 1.2-cm$^2$ × ~1-μm-thick cathode is shown in Fig. 4.1. Between 3.6 and 1.5 V, the cell

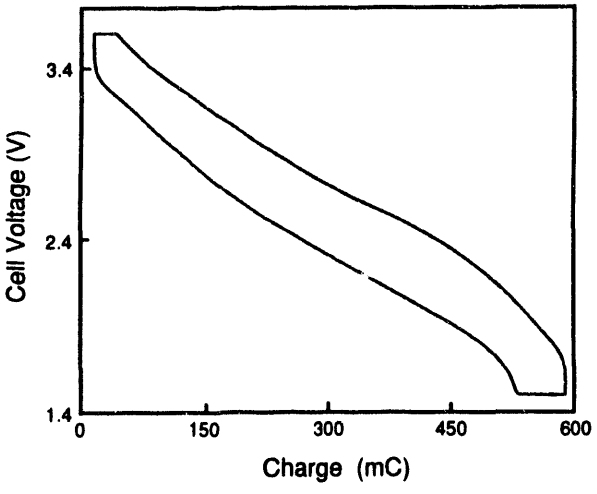


Fig. 4.1. A typical charge-discharge curve for a Li-$V_2O_5$ cell with discharge at 20 μA/cm$^2$ and charge at 5 μA/cm$^2$.

capacity is 575 mC, which corresponds to an insertion of about 2.5 moles of Li per mole of $V_2O_5$ into the cathode ($Li_{2.5}V_2O_5$) at 1.5 V. Including the mass of the anode, electrolyte, and cathode, the specific energy and the energy

density of the battery are about $10^6$ J/kg and $10^6$ J/l, respectively.

---

1. Summary of paper to be published.
2. J. B. Bates et al., "Lithium Phosphorus Oxynitride: A New Amorphous Thin-Film Electrolyte," this report.

## SPUTTERING OF LITHIUM COMPOUNDS FOR PREPARATION OF ELECTROLYTE THIN FILMS[1]

*N. J. Dudney, J. B. Bates, J. D. Robertson,[2] and C. F. Luck*

The rf sputtering of lithium compounds frequently results in lithium-deficient films compared to the initial target composition. RF magnetron sputtering of several lithium-phosphate and lithium-silicate compounds has been used to prepare lithium-electrolyte films for evaluation as a thin-film battery component. Lithium orthophosphate ($Li_3PO_4$) and lithium orthosilicate ($Li_4SiO_4$) behave very differently. Films grown by sputtering $Li_3PO_4$ in a process gas of argon or argon plus oxygen are nearly stoichiometric, Li/P~3, whereas films grown from $Li_4SiO_4$ are extremely lithium deficient having Li/Si compositions <1.3. The loss of lithium results from the decomposition and segregation of lithium away from the eroded area of the sputter target. The lithium transport appears to occur along the target's surface.

Sputtering of targets prepared as mixtures of $Li_4SiO_4$ and $Li_3PO_4$ suggests that the silicate phase acts as a wick for the transport of lithium away from the plasma. For targets with only 20% $Li_4SiO_4$ in $Li_3PO_4$, almost all of the lithium from both the phosphate and silicate phases is lost due to segregation rather than being sputtered. By replacing the lithium silicate phase with $SiO_2$, this lithium segregation is virtually eliminated. Lithium segregation for 20% $SiO_2$ + 80% $Li_3PO_4$ targets becomes apparent only at high rf power levels. The proportion of lithium being sputtered from the target can also be enhanced by using neon as the process gas, rather than argon, or by using a larger sputter source which increases the distance the lithium must migrate to the unsputtered surface of the target.

---

1. Summary of paper: *Solid State Ionics* (in press).
2. University of Kentucky, Lexington, Ky.

## EMISSION SPECTROSCOPY AS A PROBE OF THE RF SPUTTERING OF LITHIUM COMPOUNDS

*N. J. Dudney and J. B. Bates*

The emission spectrum of the plasma during rf magnetron sputtering of various lithium compounds was monitored using an optical fiber with a spherical lens positioned near the plasma and coupled to a monochromator and photodiode array detector.[1] Emission lines due to lithium, oxygen, and argon were identified between 650 and 800 nm. These lines were monitored to verify the stability of the sputtering process during the time required for film deposition. Attempts have also been made to use

the normalization process known as actinometry to determine the relative concentration of these species in the plasma and ultimately the lithium concentration in the sputter-deposited films.

The strong Ar line at 750 nm was determined to be relatively independent of the oxygen content in the process gas and was, therefore, chosen as the actinometer. The peak intensity of the 670.8-nm Li line was normalized by the intensity of this Ar line. The observed intensity ratio, $I_{Li}/I_{Ar}$, was found to be sensitive to the distance from the target surface and also to the presence or absence of the substrate holder in the plasma. To compare the intensity ratio with the lithium content of the deposited films, it is necessary to normalize the ratio by the observed deposition rate, $R$, of the film, $(I_{Li}/I_{Ar})/R$. For a fixed-fiber position and process-gas composition, the resulting lithium concentration in the deposited phosphosilicate films appears to be proportional to this quantity.

---

1. A. L .Wachs et al., *J. Vac. Sci. and Tech. A* **9**, 492 (1991).

## COMPOSITION ANALYSIS OF $Li_2O$-$P_2O_5$-$SiO_2$ ELECTROLYTE THIN FILMS

*N. J. Dudney, J. B. Bates, J. D. Robertson,[1] and R. A Zuhr*

Lithium phosphosilicate thin films were deposited by single- and dual-source rf magnetron sputtering. Several different analytical techniques were developed and evaluated to determine the composition and lateral homogeneity of the films as accurately as possible.

Energy-dispersive x-ray (EDX) spectrometry was used routinely to determine the relative Si and P compositions of selected spots (~1 mm) of the films. These results were compared with Rutherford backscattering spectrometry analysis of the same film areas. The agreement was quite good for the complete range of Si:P compositions. The lateral homogeneity of films deposited using various techniques was examined by EDX. Films sputter deposited from a single mixed phosphate plus silicate target at 20 mTorr were nearly homogeneous; at much lower process gas pressures, a large gradient in the Si:P composition was observed. Codeposition of films from two different sources led to inhomogeneous films unless the substrate was rotated during the film depositions.

The relative lithium content of the films was determined by proton-induced gamma-emission (PIGE) spectroscopy[2] and also by atomic emission spectrometry (AES). PIGE was the only nondestructive technique found to give accurate lithium concentrations. Both AES and PIGE techniques give average Li:P:Si film compositions for film areas 30–50 $mm^2$. For most films, the Li/P and Li/Si ratios determined by these techniques agreed well, within ~10%. The P/Si ratios were also consistent with EDX and RBS results. The analyses of the sputtered lithium phosphate films, however, were exceptional with larger discrepancies in the

measured Li/P ratios varying between 10 and 30% of the average value.

The films were examined for impurities by PIGE, EDX, and also infrared spectroscopy. Occasionally, a small F signal, corresponding to <1 at %, was observed by PIGE and confirmed by XPS. In addition, hydrogen and carbonate species have been detected by infrared absorption for several films. The majority of the films, however, were found to be free of any detectable concentrations of impurities.

---

1. University of Kentucky, Lexington, Ky.
2. J. D. Robertson et al., *Nucl. Instrum. and Methods in Phys. Res. Sect. B* **56/57**, 722 (1991).

## TIME-DOMAIN INVESTIGATION OF CIRCUITS CONTAINING CONSTANT PHASE ANGLE ELEMENTS

*G. R. Gruzalski*

Cells made up of thin-film amorphous $Li^+$ conductors sandwiched between blocking electrodes have been cycled between preset voltage limits. Typically, the cycling is done using constant-current densities <100 $\mu A/cm^2$, with the cells being held at the end of each charge or discharge cycle until the holding current (i.e., the current required to keep them at that voltage) drops below some preset value, which is often 5% of the charge or discharge current. The time dependence of the voltage response during charging or discharging and the time dependence of the holding currents suggest the existence of relaxation processes lasting for hours or even days.

The impedance of many of these cells has been determined[1] over the frequency range $10^{-2}$–$10^{+7}$ Hz. The impedance data show that the thin-film cells can be represented by equivalent circuits that include elements having an impedance of the so-called constant phase angle (CPA) form:

$$Z_{CPA} = \frac{1}{C(i\omega)^n}. \qquad (1)$$

Here, $C\omega^n$ is the magnitude of the complex admittance $(Z_{CPA})^{-1}$ and $\omega$ is the angular frequency; $C$ and $n$ are independent of $\omega$, and $0 < n < 1$. (For $n = 0$ or 1, the impedance becomes that of a resistor or capacitor, respectively.) To help gain some understanding of the cycling data, the time-dependent voltage response $v(t)$ was computed for several of the experimentally determined equivalent circuits subjected to various current configurations; emphasis was placed on determining precisely the initial transient response of one circuit combination which was present in all of the equivalent circuits (i.e., a CPA element in parallel with a resistor).

Two results emerge from this study. First, the voltage response $v(t)$ of a circuit consisting of a single CPA element in parallel with a resistor $R$ subjected to a constant current step may be written as follows:

$$v(t) = \frac{i_0}{C\Gamma(1+n)} \times t^n + O(t^{2n}), \qquad (2)$$

where $\Gamma$ is the gamma function. For small times $t$, $v(t)$ is independent of $R$ and is identical

to the voltage response of an isolated CPA element. Second, although an arbitrarily accurate (but somewhat complicated) approximation involving series expansions can be written down for $v(t)$, the following approximation is relatively simple and potentially useful:

$$v(t) = \frac{i_0}{C} \times \frac{t^n}{\left[1 + \frac{t^n}{RC}\right]} . \qquad (3)$$

Figure 4.2 compares this simple approximation with a more accurately computed result.

---

1. J. B. Bates et al., *Solid State Ionics* (in press).

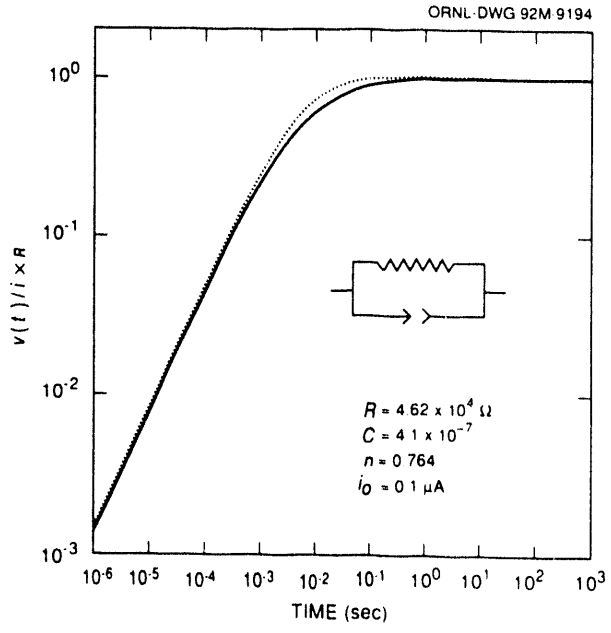


Fig. 4.2. A comparison of the approximation given by Eq. (3) (solid line) with a more-accurately computed result (dotted line). The symbol ->>- represents a CPA element.

# *PEROVSKITE STRUCTURE OXIDES*

## DIPOLE-GLASS BEHAVIOR OF LIGHTLY DOPED $KTa_{1-x}Nb_xO_3$[1]

*P. M. Gehring,[2] H. Chou,[2] S. M. Shapiro,[2] J. A. Hriljac,[2] D. H. Chen,[2] J. Toulouse,[3] D. Rytz,[4] and L. A. Boatner*

An enormous amount of scientific effort, both experimental and theoretical, has been devoted to the study of the behavior of isolated impurities in systems with soft phonon modes. One of the most interesting and controversial questions concerns the nature of the low-temperature phase in such systems in the dilute limit. The mixed perovskite systems $KTa_{1-x}Nb_xO_3$ (KTN) and $K_{1-x}Li_xTaO_3$ (KLT) have played major experimental roles in this area of research. In the context of KTN, do low levels of the dipolar impurity Nb induce a true structural-phase transition to a ferroelectric phase in $KTaO_3$, or does the addition of Nb produce instead a dipolar-glass phase with no change in structure?

It is widely accepted that concentrated KTN undergoes the same sequence of structural phase transitions as the pure niobate compound—but at progressively lower transition temperatures as the concentration of Nb is reduced. Measurements of the dielectric susceptibility as a function of temperature reveal these structural changes through the appearance of a peak at $T_c$ and form a basis for the current phase diagram. There is, however, considerable

debate about what happens at very low impurity levels.

A program of high-resolution x-ray diffraction experiments is being carried out to look for measurable changes in symmetry between 300 and 10 K in a series of single-crystal specimens of KTN in the limit $x \leq 0.157$. Such a program is of obvious fundamental importance in view of the fact that no diffraction data—x-ray or neutron—has been used to corroborate the currently accepted phase diagram of KTN, particularly in the dilute limit.

High-resolution x-ray diffraction measurements have been performed between 10 and 300 K on several single crystals of $KTa_{1-x}Nb_xO_3$ with $x \leq 0.157$. Contrary to the published phase diagram, no deviation from cubic symmetry is seen for $x \leq 0.060$. Instead, a low-temperature minimum in the cubic unit-cell volume is observed at a temperature $T_{min}$ which increases monotonically for $0.012 \leq x \leq 0.060$. Data for $x = 0.157$, however, are consistent with the previously established sequence of structural transitions from cubic to tetragonal to orthorhombic to rhombohedral symmetry. $T_{min}$ is associated with the onset of a dipolar-glass transition. In addition, a radial broadening of the linewidths is observed at $T_{min}$, indicating the presence of strain in the lattice. Powdering small pieces from these single crystals suppresses the unit-cell minimum and stabilizes the cubic phase down to 10 K, even for $x = 0.157$. From these measurements no deviation from cubic symmetry at any temperature for $0.012 \leq x \leq 0.060$ within our experimental uncertainty was observed. Instead, a striking minimum in the volume of the cubic unit cell is observed to occur at a characteristic temperature $T_{min}$ which scales with the impurity concentration.

---

1. Summary of paper: *Physical Review B* (in press).
2. Brookhaven National Laboratory, Upton, N.Y.
3. Lehigh University, Bethlehem, Pa.
4. Sandoz Produkte (Schweiz) AG, Basel, Switzerland.

## DIELECTRIC NONLINEARITY AND SPONTANEOUS POLARIZATION OF $KTa_{1-x}Nb_xO_3$[1]

*J. Toulouse,*[2] *X. M. Wang,*[2] *L. A. Knauss,*[2] *and L. A. Boatner*

Mixed ferroelectric systems can display properties that are very different from those of simple ferroelectrics. In particular, many systems are characterized by a diffuse phase transition (i.e., a phase transition taking place over a wide range of temperatures often called the Curie range). $KTa_{1-x}Nb_xO_3$ (KTN) is of particular interest in attempts to understand ferroelectric phase transitions in mixed systems; pure $KTaO_3$ remains cubic and paraelectric down to 0 K, while at the other end of the phase diagram, $KNbO_3$ exhibits a ferroelectric transition from a cubic to a tetragonal structure at 701 K. In between, this system forms solid solutions with $T_c$ varying continuously from 0 to 701 K.

In the present work, $KTa_{1-x}Nb_xO_3$ (KTN) in an intermediate-concentration range ($x = 15.7\%$) has been studied using dielectric-constant and spontaneous-polarization measurements. A large peak in the dielectric constant

($\varepsilon_{max} \simeq 70{,}000$) is observed at the temperature $T_c^*$. From room temperature down to $T_c^* + 20$ K, $\varepsilon$ obeys a Curie-Weiss law with $T_c \sim 142.3$ K. Below this temperature, $\varepsilon$ deviates from this law and $P$-$E$ hysteresis loops are observed. These results indicate that the phase transition exhibits a diffuse character which is related to the appearance of microscopic polarized regions or cells. The $\varepsilon$ peak at $T_c^*$ exhibits a cusp shape and becomes flattened upon application of low dc-bias fields. A corresponding dielectric loss peak is also observed, the position of which reveals the relaxational character of the transition. Through measurements of $\varepsilon(E,T)$ for different dc-bias fields, the dielectric nonlinearities in the transition range have been characterized; the first nonlinear coefficient $\varepsilon^{(2)}$, diverges in two distinct ranges, as $(T - T_c^*)^{-n}$, with $n \sim 9$ initially, and with $n \simeq 2$ closer to $T_c^*$. At intermediate concentrations, the present results indicate that the ferroelectric transition in KTN is not a classical second-order Landau transition but that it takes place in two steps: (1) the progressive appearance of polar cells around single or groups of few niobium ions and (2) the collective ordering of the individual electric dipoles modified by mutual strain interactions between the cells. Near and below $T_c^*$, the transition exhibits a relaxational character. Only for niobium concentrations above $x = \sim 40\%$ does the transition in KTN become a classical ferroelectric transition of the first order.

---

1. Summary of paper: *Phys. Rev. B* **43**, 8297 (1991).
2. Lehigh University, Bethlehem, Pa.

## DIELECTRIC AND RAMAN STUDY OF SHORT- AND LONG-RANGE ORDER IN KTN[1]

*P. DiAntonio,[2] X. M. Wang,[2] J. Toulouse,[2] and L. A. Boatner*

The mixed ferroelectric $KTaO_3$:Nb constitutes a particularly good system for the study of impurity-induced ferroelectricity. Pure $KTaO_3$ is an incipient ferroelectric that possesses a soft mode but does not undergo a phase transition. The addition of niobium induces significant changes in its properties and leads to a ferroelectric phase transition, and in the mixed ferroelectric $KTa_{1-x}Nb_xO_3$, the nature of this phase transition changes with the Nb concentration, $x$. In the present work, comparative dielectric and Raman results have been obtained for two significantly different Nb concentrations ($x = 15.7\%$ and $x = 1.2\%$).

A comparative study of the dielectric peak(s) and of two Raman lines associated with the first-order $TO_2$ and $TO_3$ phonon modes indicates that a ferroelectric transition occurs for Nb concentrations as low as 1.2%. At high Nb concentrations, two major transitions are observed, both marked by a dielectric peak and accompanied by the appearance of sharp $TO_2$ and $TO_3$ Raman lines, respectively. The first, higher transition is caused by interaction between polar clusters. At low Nb concentrations, the appearance of a sharp $TO_2$ line is not accompanied by a corresponding dielectric peak indicating intermediate but not long-range order. For all concentrations, the appearance of the $TO_3$ line coincides with a dielectric peak, marking a transition to a symmetry that must be lower than

tetragonal. These results indicate that the ferroelectric transition at intermediate concentrations is essentially due to the interactions between polar clusters.

---

1. Summary of paper: *Ferroelectrics* (in press).
2. Lehigh University, Bethlehem, Pa.

## SOFT MODE STUDIES IN $KTa_{1-x}Nb_xO_3$ USING TIME-RESOLVED THIRD-ORDER OPTICAL SUSCEPTIBILITY[1]

*P. Grenier,[2] D. Houde,[2] S. Jandl,[2] and L. A. Boatner*

The dynamical behavior associated with structural-phase transitions is a subject of long-standing interest in solid state science, and in particular, the simultaneous existence of quasi-elastic and phonon features in the dynamic response of such systems has been the subject of a number of theoretical and experimental investigations.[3–5] At the present time, the role played by interactions responsible for the so-called "central peak" phenomena and their associated contributions to the initiation of structural-phase transitions in a nominally pure system such as $KNbO_3$ is reasonably well-established. In the case of more complex solid-solution, mixed-crystal systems such as $KTa_{1-x}Nb_xO_3$ (KTN) however, the exact role played by the different constituent cations in influencing or determining the dynamics of the phase transition remains a subject of active investigation.

The relatively recent development of femtosecond optical lasers provided a powerful new technique for the study of the dynamics of displacive phase transitions which result in the formation of a ferroelectric phase. In particular, the method of impulsive, stimulated light scattering represents a general technique for following the time evolution of a dynamic system by employing an initial coherent excitation with pump pulses and a subsequent probing of the time evolution of the system by an additional time-delayed pulse. In the present work, the technique of stimulated light scattering is used to investigate the dynamics of the solid-solution system $KTa_{0.93}Nb_{0.07}O_3$ as a function of temperature in the temperature range below the phase transition. Determinations of the third-order optical susceptibility were employed to investigate the dynamical properties of the $A_1(TO)$ soft-phonon mode in $KTa_{0.93}Nb_{0.07}O_3$ as a function of temperature.

Results of the forward, nondegenerate, four-wave mixing investigation of the $A_11(TO)$ soft mode as a function of temperature in the range $10\ K < T < T_c$ show no indication of a coupling of the phonon to a relaxation mode, but evidence for coupling to some type of low-frequency excitations was obtained. Third-order optical susceptibility measurements as a function of the polariton wave vector and temperature are now being carried out. Coupled with infrared and Raman data, a better understanding of the critical dynamics in such systems should develop.

---

1. Summary of paper: *Physical Review B* (in press).
2. Université de Sherbrooke, Sherbrooke, Québec, Canada.
3. A. D. Bruce and R. A. Cowley, *Adv. Phys.* **29**, 1 (1980).

4. B. I. Halperin and C. M. Varma, *Phys. Rev. B* **14**, 4030 (1976).
5. S. M. Shapiro et al., *Phys. Rev. B* **6**, 4332 (1972).

## EFFECT OF NIOBIUM DOPING ON THE PROPERTIES OF PICOSECOND LASER-INDUCED TRANSIENT GRATINGS IN $KTa_{1-x}Nb_xO_3$[1]

*H. Liu,[2] R. C. Powell,[2] and L. A. Boatner*

The results of the observation of laser-induced transient gratings in $KTaO_3$ and $KTa_{1-x}Nb_xO_3$ (KTN) crystals produced by two-photon excitation without an external electric field were reported recently.[3] The origin of the optically induced change in the refractive index was attributed to the excitation of electrons from the valence band to the conduction band and subsequent trapping of the electrons at the $B^{5+}$ ions in $ABO_3$ perovskite crystals to create $B^{4+}$ ions in the excited state. The relaxation of the excited $B^{4+}$ ions to the ground state gives rise to the observed fluorescence. The results of fluorescence spectra and lifetime measurements demonstrate further that the gratings are due to the change in polarizability associated with the $B^{4+}$ ions in different electronic states. This change is related to the lattice relaxation caused by a change in the local electronic configuration of the $B^{4+}$ ions.

In the present work, a study of the properties of laser-induced transient gratings produced in $KTa_{1-x}Nb_xO_3$ crystals by picosecond-pulse, two-photon excitation was carried out by use of degenerate four-wave mixing (DFWM) techniques. The grating properties were found to depend on the Nb concentration. The diffraction efficiency of the gratings exhibited a maximum at an intermediate Nb concentration while the signal-decay rate increased uniformly with $x$. A lattice-relaxation model was developed to explain the experimental results that include the intrinsic lattice distortion due to the niobium ions in the normally cubic perovskite crystal and the strong electron-phonon interaction causing a lattice distortion around photoionized ions. The predictions of the theoretical model agree with the experimental data. The results of grating decay-rate measurements show that the excited states produced by two-photon laser excitation act as localized quasiparticles (excitons or polarons) having a hopping rate that increases with Nb concentration $x$. Strong electron-phonon coupling produces phonon-assisted, incoherent hopping migration.

The data indicate that the interaction causing the hopping is stronger for niobate ions than for tantalate ions, which in this model implies a stronger electron-phonon coupling for the former. This is consistent with the fluorescence lifetime observations that show a greater radiationless-decay rate for the niobate ions than for the tantalate ions.

The lattice-relaxation model developed to explain the results of DFWM measurements provides an enhanced understanding of the effects of Nb ions on the optical and structural properties of displacive-ferroelectric crystals (e.g., KTN). One important observation that is not yet understood fully involves the origin of the fast DFWM signal observed in $KNbO_3$ crys-

tals. The origin of this signal component is currently being investigated.

---

1. Summary of paper: *Phys. Rev. B* **44**, 2461 (1991).
2. Oklahoma State University, Stillwater, Okla.
3. H. Liu, R. C. Powell, and L. A. Boatner, *J. Appl. Phys.* **70**, 1 (1991).

## ORIGIN OF PICOSECOND-PULSE-INDUCED, DEGENERATE FOUR-WAVE MIXING SIGNALS IN $KTa_{1-x}Nb_xO_3$ CRYSTALS[1]

*H. Liu,[2] R. C. Powell,[2] and L. A. Boatner*

Measurements of the photorefractive effect in KTN have demonstrated the potential of this material for high-recording sensitivity in volume holographic applications. The photorefractive effect due to the linear electro-optic effect can be observed when the Nb content and temperature are such that the KTN system is in the ferroelectric phase. In the nonferroelectric cubic phase, photorefractive effects due to the quadratic electro-optic effect can also be observed and may be enhanced by applying an external electric field to the crystal. The goal of the present investigation was to determine what role Nb ions can play in changing the refractive index caused by laser excitation. The phenomena observed in this investigation are not associated directly with the structural-phase transitions or photorefractive effects of the materials. However, these phenomena are associated indirectly with these topics through the properties of the Nb ions which affect all the observed phenomena. For this purpose, a series of studies on the static and dynamic properties of laser-induced transient gratings in KTN have been carried out.

Transient gratings were produced in $KTa_{1-x}Nb_xO_3$ by picosecond-pulse, two-photon excitation using degenerate four-wave mixing techniques (DFWM). The excitation process was characterized through fluorescence studies, and the fluorescence was attributed to the transition between an excited state and the ground state of $B^{4+}$ ions that are produced in $ABO_3$ perovskite crystals. Strong electron-phonon coupling gives rise to the luminescence quenching. The observed DFWM signal was shown to be due predominantly to a phase grating caused by a change in the susceptibility associated with the formation of $Nb^{4+}$ or $Ta^{4+}$ ions in the peak region of the grating. The grating signal intensity was found to be dependent on the concentration of niobium ions and the crossing angle of the two laser-write beams.

This work has led to an initial observation of the formation of a transient grating in $KTa_{1-x}Nb_xO_3$ using a picosecond pulse DFWM without an external electric field applied to the crystal. The results reveal the mechanism of the grating formation and provide information about properties of the grating as a function of Nb concentration.

---

1. Summary of paper: *J. Appl. Phys.* **70**, 20 (1991).
2. Oklahoma State University, Stillwater, Okla.
3. L. A. Boatner, E. Kratzig, and R. Orlowski, *Ferroelectrics* **27**, 247 (1980).

## DIELECTRIC ACTIVE DEFECTS AND THERMAL CONDUCTIVITY OF UNDOPED $KTaO_3$[1]

*B. Daudin,[2] B. Salce,[2] J. L. Gravil,[2] and L. A. Boatner*

The cubic perovskite $KTaO_3$ is of fundamental interest because it represents one example of so-called "incipient" ferroelectricity. Due to the high polarizability of the lattice, which results in the existence of a soft transverse optic mode, $KTaO_3$ moves toward a phase transition with decreasing temperature, but in fact, it remains paraelectric down to the lowest temperatures near ~0 K. It has been shown that ferroelectric phase transitions can be induced in $KTaO_3$ by replacing Nb for Ta or Na/Li for K. In this case, the soft-mode energy goes to zero at a temperature $T_c$ depending on the concentration of the substituted ions. The true nature of the transition, however, remains somewhat controversial. Previous experiments have demonstrated that distorted microregions due to symmetry-breaking defects (SBD) exist in the paraelectric phase, even at high temperatures, both in undoped or Nb-doped $KTaO_3$. These microregions grow in size as the temperatures are lowered.

In an attempt to identify the SBD responsible for the presence of the distorted microregions, complex dielectric constant measurements have been performed on several undoped crystals, together with thermal-conductivity [$K(T)$] experiments. The real part of the dielectric constant ($\varepsilon'$) and the loss factor were also measured in the 4–100-K temperature range for various frequencies between 0.13 and 100 kHz.

A frequency-dependent dielectric-loss peak (observed at 44 K for 1 kHz) was found to be present in all samples. The correlation between the thermal conductivity at 6.5 K and the intensity of the dielectric-loss-factor peak strongly supports the assumption that below 20 K, $K(T)$ is governed by the interaction of acoustic phonons with both the transverse-optic soft mode and a dielectrically active entity—the nature of which is still unknown.[3]

---

1. Summary of paper: *Ferroelectrics* **106**, 69 (1990).
2. C.E.N.G., Grenoble, France.
3. B. Salce, A. M. de Goer, and L. A. Boatner, *J. Phys. Coll.* **42**, 424 (1981).

## STUDY OF FERROELECTRIC MICRODOMAINS DUE TO OXYGEN VACANCIES IN $KTaO_3$[1]

*P. Grenier,[2] M. Blouin,[2] and L. A. Boatner*

Ferroelectric microdomains, which extend over few unit cells in pure $KTaO_3$, have been thoroughly studied without a clear identification of their origin.[3–5] Recently, it has been conjectured that $Ta^{3+}$ ions in the vicinity of oxygen vacancies emit a strong luminescence (observed around 14550 $cm^{-1}$) that is associated with the formation of such ferroelectric microdomains. In the present work, this luminescence has been studied in both pure and reduced $KTaO_3$ and $KTaO_{0.94}Nb_{0.06}O_3$ in order to confirm the identity of the luminescent center and the nature of the microdomain that surrounds it.

A high-purity $KTaO_3$ crystal was cut in half, and one-half of the crystal was used as a reference while the other half was subjected to an anneal for 2 h in a hydrogen atmosphere at 1000 K thus creating oxygen vacancies. The annealed crystal remained colorless even though it had been reduced, and consequently, its carrier concentration was estimated to be $<10^{18}$ $cm^{-3}$. Two other crystals, a pure $KTaO_3$ and a $KTaO_{0.94}Nb_{0.06}O_3$ sample with $T_c \simeq 65$ K, were also investigated in this study. The red luminescence observed in both reduced "as grown" $KTaO_3$ and $KTaO_{0.94}Nb_{0.06}O_3$ single-crystal samples was studied as a function of temperature and applied magnetic field. These investigations of both pure and reduced $KTaO_3$ and $KTaO_{0.94}Nb_{0.06}O_3$ single crystals have established that the observed red luminescence in these materials is due to $Ta^{3+}$ ions in the vicinity of oxygen vacancies forming ferroelectric microdomains. The application of a magnetic field completes the energy-level scheme for these ions that are subjected successively to the crystal field, the spin-orbit interaction, and local symmetry distortions.

---

1. Summary of paper: *Physical Review B* (in press).
2. Université de Sherbrooke, Québec, Canada.
3. Y. Yacoby, *Phys. Rev. B* **31**, 275 (1978).
4. R. L. Prater, L. L. Chase, and L. A. Boatner, *Phys. Rev. B* **23**, 221 (1981).
5. B. Salce, A. M. de Goer, and L. A. Boatner, *J. Phys. Coll.* **42**, C6424 (1981).

## PROTONS AND OTHER DEFECTS IN Fe-DOPED $KTaO_3$[1]

*T. Scherban,[2] A. S. Nowick,[2]*
*L. A. Boatner, and M. M. Abraham*

Potassium tantalate ($KTaO_3$) represents an ideal perovskite host in which to study protons and other defects because it has a cubic structure and does not undergo a phase transition from its melting temperature (1356°C) to <1 K. The incorporation of protons into $KTaO_3$ crystals treated in $H_2O$ vapor was first demonstrated by Engstrom et al.[3] An interstitial proton combines with an adjacent oxygen ion to form an $OH^-$ center, thus giving rise to an absorption in the infrared. Potassium tantalate has also been shown to exhibit protonic conduction.

Studies of protons in perovskite oxides have shown that a key requirement for proton incorporation is that the material be acceptor doped. In a "dry" condition, oxygen vacancies ($V_{\ddot{o}}$) act to charge compensate the acceptors. However, when the material is treated in water vapor at high temperatures, protons may be introduced according to

$$H_2O(g) + V_{\ddot{o}} \rightarrow 2H_i + O_o^x, \qquad (1)$$

with the protons replacing the oxygen vacancies as charge compensators for the acceptor dopants. Since the interstitial proton associates strongly with an adjacent oxygen ion, $H_i$ and $(OH)_{\dot{o}}$ are equivalent.

Potassium tantalate is readily doped with transition-metal ions (e.g., $Cu^{2+}$, $Co^{2+}$, $Mn^{2+}$,

and $Fe^{3+}$) which substitute at the $Ta^{5+}$ site (thus, constituting acceptors), and the technique of electron paramagnetic resonance (EPR) spectroscopy can be used to monitor the local symmetry of the paramagnetic dopant ions. In combination with infrared (IR) spectroscopy to observe $OH^-$ absorption bands, the relationship between the various defects can be investigated. The $Fe^{3+}$ ion is unique in that a correlation has been shown to exist between proton incorporation and distribution of $Fe^{3+}$ ions in sites of two distinct symmetries.

In this study, a systematic investigation of Fe-doped $KTaO_3$ has been carried out using the techniques of IR, EPR, and electrical conductivity. By examining a large number of samples, both single-crystal (cut from various crystal boules and various parts of a particular crystal boule) and polycrystalline (the effects of dopant concentration) samples, as well as the crystalline nature of the host, were investigated. In addition, various thermal treatments in atmospheres of varying partial pressures of water vapor and oxygen ($P_{H_2O}$ and $P_{O_2}$, respectively) are given to the samples, and the changes which result in the defect structure and electrical conductivity were studied.

The results indicate that Fe-doped $KTaO_3$ treated in oxidizing atmospheres is an electronic (hole) conductor, as evidenced by the dependence of $\sigma$ on $P_{O_2}$ according to a $P_{O_2}{}^{1/4}$ power law at oxygen partial pressures greater than $10^{-12}$ atm. In support of this conclusion, the absence of an isotope effect (i.e., a difference in conductivities between samples treated in $H_2O$- and $D_2O$-saturated oxygen gas) indicates that the conduction mechanism is not protonic in this $P_{O_2}$ regime.

Upon oxidizing treatments, it is possible for Fe to change its oxidation state (from 3+ to 4+). The $Fe^{4+}$ ions may release holes to the valence band upon thermal activation. The observed activation energy of conduction, 0.84 eV, then represents the acceptor-ionization energy (i.e., the energy difference between the $Fe^{4+}$ acceptor level and the valence band).

---

1. Summary of paper: *Applied Physics A* (in press).
2. Columbia University, New York, N.Y.
3. H. Engstrom, J. B. Bates, and L. A. Boatner, *J. Chem. Phys.* **73**, 1073 (1980).

## STRAIN RELAXATION BY DOMAIN FORMATION IN EPITAXIAL FERROELECTRIC THIN FILMS[1]

*B. S. Kwak,[2] A. Erbil,[2] B. J. Wilkens,[3] J. D. Budai, M. F. Chisholm, and L. A. Boatner*

Equilibrium theories of epitaxy predict that below a certain critical thickness, lattice mismatch between a thick substrate and a thin film should be accommodated entirely by strain within the film.[4] Above this critical thickness, the strain of the film would be relieved partially by misfit dislocations. If the film undergoes a structural phase transition from a high-symmetry phase to a lower symmetry phase during cooling from the growth temperature, the bulk-epitaxial strain can be relieved by domain formation. The phenomenon is reminiscent of the formation of coherent alternating

twins in martensites. It is particularly important to understand such domain formation in ferroelectrics and high-$T_c$ superconductors, since it can have a profound influence on the physical properties of these materials.

A new theoretical analysis has been made for a specific epitaxial multidomain system (i.e., a $PbTiO_3$ thin film grown on $KTaO_3$) that compares the model predictions to the experimental measurements. A Landau Ginzburg Devonshire (LGD)-type free energy was used to evaluate the thin-film energy including the domain walls, and elasticity theory was employed to calculate the substrate-energy contribution close to the interface. Quantitative agreement between the theoretical predictions and experimental results was obtained for the relative domain abundances and spontaneous strains as a function of film thickness.

This new model should be applicable universally to all epitaxial ferroelectric and ferroelastic-oxide thin films. A more detailed explanation of this model in conjunction with experimental results will be presented in a subsequent report.

---

1. Summary of paper: *Physical Review Letters* (in press).
2. Georgia Institute of Technology, Atlanta, Ga.
3. Bell Communications Research, Red Bank, N.J.
4. C. A. Ball and J. H. van der Merwe, chap. 27 in *Dislocations in Solids*, ed. by F. R. N. Nabarro, North-Holland, Amsterdam, 1983.

## EFFECT OF ENVIRONMENT ON RADIATION-INDUCED OUTDIFFUSION OF NEUTRONS AND PROTONS FROM CRYSTALLINE $LiNbO_3$ AT LOW TEMPERATURES[1]

*R. Gonzalez,[2] E. Hodgson,[3] C. Ballesteros,[4] and Y. Chen*

Protons and deuterons normally form thermally stable configurations in oxides near room temperature and diffuse out of the crystals only at high temperatures. However, under electron irradiation protons and deuterons become highly unstable even at temperatures as low as 85 K[5] and even at these temperatures are quite mobile. Outdiffusion can be achieved efficiently in rutile ($TiO_2$) near room temperature by breaking the O-H (O-D) bond with the ionizing component of the electron irradiation and subsequently sweeping out the protons and deuterons along the c axis by means of an electric field.[6] A method of removing deuterons (protons) near room temperature without an applied electric field has been reported. These hydrogenic species can be extracted effectively from $LiNbO_3$ near room temperature by electron irradiation in vacuum. In contrast, this same effect is not observed when the irradiation is carried out in air.

Prior to electron irradiation, the samples were deuterated at 1273 K in flowing $D_2O$ vapor for 30 min. In Fig. 4,3 the logarithm of the $OD^-$ absorbance is plotted against the electron dose. The observed exponential decrease in the $OD^-$ absorption is consistent with a process involving a constant interaction

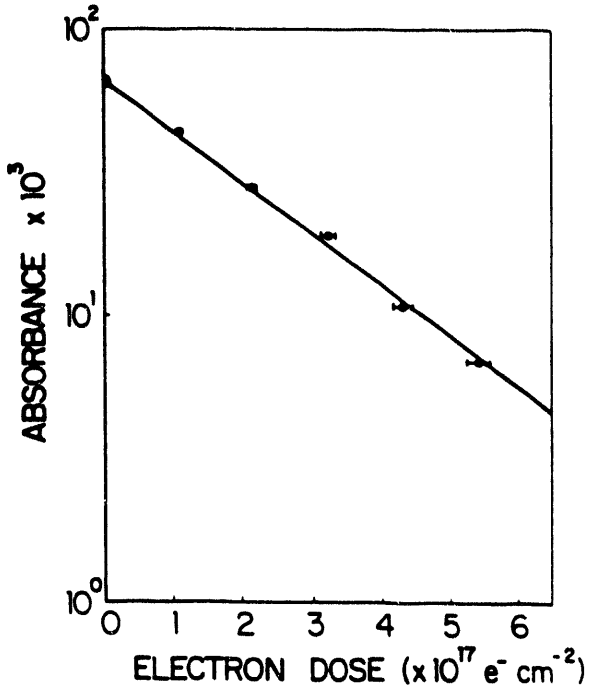


Fig. 4.3. Absorbance of the $OD^-$ ions at the 2570-$cm^{-2}$ band against electron dose at $T > 350$ K.

cross section. From the slope it is estimated that the effective cross section is ~$10^6$ b. This enormous magnitude indicates that the displacement of the deuterons is due to an ionization rather than an elastic-collision process.

The same experiments were performed by electron irradiating the deuterated samples in air. In contrast, these irradiations produced no significant change in the deuterium concentrations. These results demonstrate unambiguously the difference between electron irradiation in vacuum and in air. In the former, deuterons (protons) are removed, whereas in the latter the deuteron concentration remains unchanged. These results emphasize the important role played by the surrounding atmosphere.

---

1. Summary of paper: *Phys. Rev. Lett.* **67**, 2057 (1991).
2. Universidad Politécnica de Madrid, Madrid, Spain.
3. Centro de Investigaciones Energéticas, Medioambientales y Technológicas, Madrid, Spain.
4. Universidad Complutense, Madrid, Spain.
5. Y. Chen, M. M. Abraham, and H. T. Tohver, *Phys. Rev. Lett.* **37**, 1757 (1976).
6. Y. Chen, M. M. Abraham, and K. L. Tsang, *Phys. Rev. Lett.* **53**, 1077 (1984).

# *OPTICAL CHARACTERIZATION OF IMPURITIES AND DEFECTS*

## EFFECT OF THERMOCHEMICAL REDUCTION ON THE ELECTRICAL, OPTICAL ABSORPTION, AND POSITRON-ANNIHILATION CHARACTERISTICS OF ZnO CRYSTALS[1]

*R. M. de la Cruz,[2] R. Pareja,[2] R. Gonzalez,[2] L. A. Boatner, and Y. Chen*

The electrical properties, optical absorption characteristics, and positron-annihilation lifetimes have been determined for nominally pure ZnO single crystals that were thermochemically reduced (TCR) in Zn vapor in the temperature range 1100–1500 K. Electrical conductivity and Hall-effect measurements indicate that donors are produced as a result of the

TCR process. The concentration of donors, as determined from $(Re)^{-1}$ where $R$ is the Hall coefficient, was found to increase with the TCR temperature. The Hall mobility was determined to be in the range 110–130 $cm^2\ V^{-1}\ s^{-1}$.

Optical measurements show that the reduction results in an increase in the optical absorption near the two fundamental absorption edges. The optical-absorption spectra obtained for three ZnO samples are shown in Fig. 4.4. The spectrum labeled (a) in the figure was obtained using an as-grown single crystal with low electrical conductivity. After TCR at a temperature of 1273 K, the regime in which the optical absorption was low was significantly reduced, as shown in the spectrum labeled (b) and was confined to between 2.0 and 1.0 eV. Outside this range, the absorption became relatively intense. Following TCR of ZnO at the higher temperature of 1537 K, the absorption at the two sides of the spectrum became even more pronounced as illustrated in the curve labeled (c). The ZnO crystals became visibly brownish in color as a result of the reduction process. Positron-annihilation studies revealed that a well-defined positron state having a lifetime of 169 ± 2 ps exists in the reduced crystals, in contrast to the lifetime of 180 ± 3 ps characteristic of colorless, high-resistivity as-grown crystals. The lifetime of 169 ps is attributed to positron annihilation in the bulk material. It is concluded that defects produced by TCR of ZnO are not efficient positron traps, indicating that the defects either exist as interstitials or that they are positively charged.

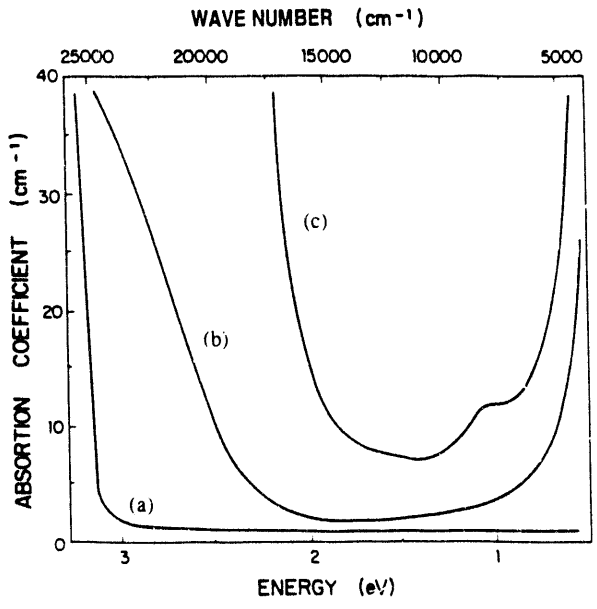


Fig. 4.4. Optical absorption spectra for three ZnO crystals: (a) virgin, (b) TCR at 1273 K, and (c) TCR at 1537 K.

---

1. Summary of paper: *Phys. Rev. B* **45**, 6581 (1992).
2. Universidad Complutense, Madrid, Spain.

## EFFECT OF SUBSTITUTIONAL HYDRIDE IONS ON THE CHARGE STATES OF OXYGEN VACANCIES IN THERMOCHEMICALLY REDUCED CaO AND MgO[1]

*Y. Chen, V. M. Orera,[2] R. Gonzalez,[3] R. T. Williams,[4] G. P. Williams[4] G. H. Rosenblatt,[4] and G. J. Pogatshnik[5]*

Wavelength-tunable laser action based on anion vacancies in alkali halides, lithium fluoride, and sapphire crystals has been demonstrated; alkali-halide tunable lasers are produced commercially. Continuous-wave laser

action based on the $F^+$ center (an oxygen vacancy with one electron) and the $F$ center (an oxygen vacancy with two electrons) in an electron-irradiated CaO crystal has been reported.[6] However, reproducibility of these results has not been successful.[7–9] Therefore, we undertook the present investigation to further examine the optical properties of the defects in order to shed some light on the discrepancy.

In the alkaline-earth oxides, anion vacancies are produced by thermochemical reduction (TCR) or bombardment with energetic particles. The former has several advantages over irradiation by energetic particles, including good thermal stability of the vacancies and high-quantum efficiency of the luminescence. However, there are also some limitations which may interfere with laser action in these materials. First, the anion vacancies in the oxides assume two charge states—the $F^+$ center and the $F$ center both are photoconvertible to some degree. Second, during TCR protons from $OH^-$ ions are trapped by the oxygen vacancies to form $H^-$ (hydride) ions. (The hydride ion is a proton with two electrons substituting for an $O^{2-}$ ion.) Therefore, in general, TCR produces $F$ centers and hydride ions, the relative distribution being determined primarily by the concentration of protons. Different methods to produce TCR CaO and MgO crystals with different hydride concentrations were used, and as a result, strongly contrasting optical characteristics appeared. Unless steps are taken to remove the protons, TCR of CaO and MgO crystals produces primarily $F$ centers and $H^-$ ions.

It is concluded that tunable lasers based on the intrinsic $F$ or the $F^+$ centers in CaO and MgO should not have been possible. First, excitation of the $F^+$ center in neutron- or electron-irradiated crystals causes holes to be released, and as a result, $V$-type centers are formed; these centers absorb over a broad wavelength spectrum (corresponding to a FWHM ~1.1 eV), encompassing the entire visible region. The magnitude of the absorption coefficient of the trapped-hole centers formed are of the order of a few $cm^{-1}$ and is estimated to be more than enough to negate any gain derivable from the $F^+$ centers. Second, the excited states of the $F$ center in both MgO and CaO are sufficiently close to the conduction band ($\approx$0.01 eV and $\approx$0.1 eV, respectively) that photoconversion is inevitable, as evidenced by the trapping of electrons by hydride ions. Third, recent time-resolved studies of luminescence spectra from $F$ and $F^+$ centers in MgO and CaO suggest that the $F^+$ first-excited state lies close to the conduction band edge.

---

1. Summary of paper: *Phys. Rev. B* **42**, 1410 (1990).
2. Universidad de Zaragoza, Zaragoza, Spain.
3. Universidad Politécnica de Madrid, Madrid, Spain.
4. Wake Forest University, Winston-Salem, N.C.
5. Southern Illinois University, Edwardsville, Ill.
6. B. Henderson, *Opt. Lett.* **6**, 437 (1981).
7. A. Müller, Diploma thesis, University of Hanover, Germany (1985).
8. K. German (private communication).
9. W. Gellerman (private communication).

## EXCITED-STATE ABSORPTION MEASUREMENTS OF $Sm^{2+}$ IN $CaF_2$, $SrF_2$, AND $SrCl_2$[1]

*J. K. Lawson,[2] H. W. H. Lee,[2] S. A. Payne,[2] and L. A. Boatner*

While the vast majority of rare-earth laser ions exploit the 4*f*-4*f* electronic transition, several lasers based on a 5*d*-4*f* transition exist. Divalent samarium in calcium fluoride (an early solid state laser system, discovered not long after ruby) is based on a 5*d*-4*f* transition. Similarly, cerium has exhibited gain on a 5*d*-4*f* transition in at least two hosts, and finally, neodymium in lanthanum trifluoride has shown gain on a high-lying 5*d*-4*f* transition. Since 5*d*-4*f* transitions are very different in nature from the familiar 4*f*-4*f* transitions, an entirely distinct class of laser systems is represented. However, the overall value of 5*d*-4*f* transitions as laser transitions has not yet been addressed adequately.

The major problem that is apparent from existing work on these systems, especially for the case of divalent rare-earth ions, is the presence of an extremely strong excited-state absorption (ESA) band.[3] In the present work, earlier measurements on $CaF_2$:$Sm^{2+}$ have been extended to include pump-probe measurements of $SrF_2$:$Sm^{2+}$ and $SrCl_2$:$Sm^{2+}$. Additionally, the electrostatic model developed by Pedrini, Rogemond, and McClure[4] for placing the energy levels of the impurity ion in the band gap of the host has been used in order to predict the onset of this type of ESA.

The strong ESA present in $Sm^{2+}$-doped materials can be explained as arising from a 5*d* → conduction-band transition. The unusual strength of this transition may be due to the mixing of the impurity and ligand orbitals which lead to intensity borrowing from valence band to conduction band transitions. This type of transition may limit the usefulness of 5*d*-4*f* transitions in all the divalent rare-earth ions and may be an issue in trivalent rare-earth ions as well. The electrostatic model allows trends in the onset of the ESA band for different hosts to be predicted. Since the depth of the impurity-ion energy levels from the conduction band is much more sensitive to the host than is the spacing between the impurity energy levels, it may be possible to select laser materials for other divalent rare-earth ions (e.g., $Eu^{2+}$) in which the ESA does not overlap the emission region.

---

1. Summary of paper: *OSA Proc. Adv. Solid State Lasers* **10**, 386 (1991).
2. Lawrence Livermore National Laboratory, Livermore, Calif.
3. S. A. Payne et al., *J. Chem. Phys.* **88**, 6751 (1988).
4. C. Pedrini, F. Rogemond, and D. S. McClure, *J. Appl. Phys.* **59**, 1196 (1986).

## POLARIZATION DEPENDENCE OF THE $^7F_0 \rightarrow {}^5D_0$ TWO-PHOTON TRANSITION IN $Sm^{2+}$ AND $Eu^{3+}$-DOPED MATERIALS[1]

*J. C. Gacon,[2] M. Bouazaoui,[2] B. Jacquier,[2] M. Kibler,[2] L. A. Boatner, and M. M. Abraham*

The origin of $J = 0 \rightarrow J = 0$ two-photon transitions of rare-earth ions in crystals remains a puzzling point of two-photon spectroscopy. In this regard, the spin-forbidden $^7F_0 \rightarrow {}^5D_0$ transition of $4f^6$ ions deserves special attention. Indeed, the standard second-order theory is expected to fail in this case since the second-rank

tensor $U^{(2)}$ cannot directly link pure $^7F_0$ and $^5D_0$ states. Nevertheless, a contribution of this spin-independent operator may arise from mixings via the spin-orbit and crystal-field interactions within the ground-configuration $4f^6$. However, the predominant contribution should arise, in this case, from the scalar term $W^{(11)0}$ appearing in the expansion of the second-order theory, when taking into account third-order corrections involving matrix elements of the spin-orbit interaction within the intermediate configuration $4f^5$-$5d$. Generally, these two contributions may be distinguished from each other by experimental methods since they lead separately to distinct polarization dependencies of the $^7F_0 \rightarrow {}^5D_0$ intensity. This $^7F_0 \rightarrow {}^5D_0$ two-photon transition of $Sm^{2+}$ and $Eu^{3+}$ ions in SrClF and $LuPO_4$ crystals, respectively, has been observed using a single linearly or circularly polarized infrared laser beam.

As expected, the $^7F_0 \rightarrow {}^5D_0$ transition appears as a single-sharp line centered at $\lambda = 1.381$ and 1.163 μm in the two-photon excitation spectra of the $Sm^{2+}$ and $Eu^{3+}$ compounds, respectively. Contrary to what is expected however, the intensity of this transition in both compounds cannot arise from the sole contribution of the so-called scalar term appearing in the Judd and Pooler model[3] describing $\Delta J = 0$ spin-forbidden, two-photon transitions within an $nl^N$ configuration. The experimental results are then shown to be reproduced correctly following a phenomenological approach in which an attempt has been made to fit the observed data with an expression in the form:

$$|M^7F_0 \rightarrow {}^5D_0|^2 = |\lambda\text{-}\mu(3\cos^2\theta\text{-}1)|^2, \qquad (1)$$

where $\lambda$ and $\mu$ are related to matrix elements of the $W^{(11)0}$ and $W^{(k_s k_l)2}$ tensors, respectively. The best fits are obtained for complex values of $\lambda$ and $\mu$ with $|\lambda/\mu| = 1.21$ and 1.33 for $Eu^{3+}$:$LuPO_4$ and $Sm^{2+}$:SrClF, respectively, to be compared with the value of (1.57) obtained for $Sm^{2+}$:BaClF.[4]

---

1. Summary of paper: *Eur. J. Solid State Inorg. Chem.* **28**, 113 (1991).
2. C.N.R.S., Villeurbanne, France.
3. B. R. Judd and D. R. Pooler, *J. Phys. C: Solid State Phys.* **15**, 591 (1982).
4. J. C. Gacon et al., *J. Lumin.* **45**, 162 (1990).

## PROPERTIES OF THE 800-NM LUMINESCENCE BAND IN NEUTRON-IRRADIATED MAGNESIUM OXIDE CRYSTALS[1]

*R. Gonzalez,[2] Y. Chen,*
*R. M. Sebek,[3] G. P. Williams, Jr.,[3]*
*R. T. Williams,[3] and W. Gellerman[4]*

Irradiation of undoped MgO single crystals by energetic neutrons (E > 0.1 MeV) produces several optically detectable defects, among which is an unidentified aggregate defect that absorbs at 573 nm (2.2 eV). The energy dependence of electron irradiation indicates that production of defects responsible for the 573-nm band has a relatively low threshold energy, compatible with two adjacent vacancies.[5] However, it is not a simple anion divacancy and is not paramagnetic.

Results are presented on the luminescence at 800 nm which occurs upon excitation of the

573-nm optical absorption band attributed to an aggregate defect in neutron-irradiated MgO crystals, both pure and doped. The study was undertaken to evaluate the suitability of this luminescence for a tunable laser. Absorption, luminescence, and excitation spectra were measured before and after isochronal annealing with goals of optimizing the luminescence intensity and stability of the responsible defect and reducing the background absorption in the crystal. The emission intensity is highest after annealing at ~550 K, independent of dose. A thermally induced absorption band at 565 nm, which emerges at ~550 K, does not contribute to the emission at 800 nm. Under low-intensity continuous excitation, the 573-nm absorption band is not susceptible to photoconversion. However, when pumped with high-intensity laser light, the band exhibits a decay which recovers within 0.5 s. Figure 4.5 shows the decay of the 800-nm luminescence following 3-ns pulsed excitation with 575-nm light. The initial response appeared rounded because of the 10-ns gate width at the detector. Thereafter, the decay is nearly a straight line on the semilog plot of Fig. 4.5, indicating a single exponential decay with $\tau = 15.5$ ns over the three decades plotted. There was no evidence of a long phosphorescence tail. The band shape remains essentially constant throughout the decay. Tests for laser action using pulsed and cw pump lasers were unsuccessful at 77 and 300 K.

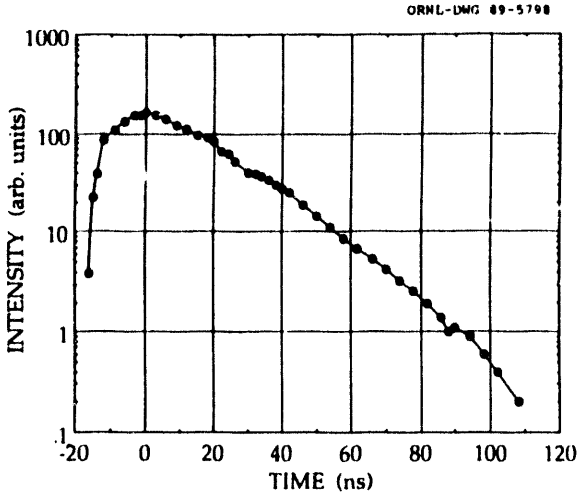


Fig. 4.5. Decay of the 800-nm luminescence following 3-ns pulsed excitation with 575-nm light at room temperature. The zero of time represents coincidence of the excitation pulse and the center of the 10-ns detector gate width.

---

1. Summary of paper: *Phys. Rev. B* **43**, 5228 (1991).
2. Universidad Politécnica de Madrid, Madrid, Spain.
3. Wake Forest University, Winston-Salem, N.C.
4. University of Utah, Salt Lake City, Utah
5. Y. Chen et al., *J. Phys. C* **3**, 2501 (1970).

## $[H^-Ca^+]^0$ DEFECT IN THERMOCHEMICALLY REDUCED CaO: A STATIC AND DYNAMICAL EPR STUDY[1]

*V. M. Orera,[2] M. L. Sanjuan,[2] and Y. Chen*

The role of hydrogen impurities in modifying the optical properties of thermochemically reduced (TCR) CaO has been the subject of extensive work in the past few years, and the following procedures are now well-established. First, the removal of hydrogen before TCR treatment results in a larger ratio of $F^+$ to $F$ concentrations. Second, the $F$-center phosphorescence has been linked unambiguously to the

presence of hydrogen impurities. Third, electrons released from the *F*-center excited states are trapped by hydrogen-related defects. Since the newly formed defects are metastable near room temperature, the electrons are released and move from trap to trap until recapture by some $F^+$ centers producing the delayed *F* luminescence.

Several hydrogen-related electron traps have been identified using electron paramagnetic resonance (EPR) and optical absorption techniques. In CaO, the defects produce two localized vibrational modes at 1048 and 1474 $cm^{-1}$ and an optical absorption band at ≈500 nm.[3] Assignment of the latter to a hydrogen-related defect has now been corroborated by observation of the local mode vibration of a deuterated species by the Raman technique.[4] In CaO, bleaching with *F* light below 77 K produces an EPR signal with $g \approx 2$ and hyperfine constant 28.5 MHz. This signal has also been associated with $H^{2-}$ defects, resulting from electrons trapped by existing $H^-$ ions. This defect, referred to as the $[H^-Ca^+]^0$ defect, acts as low-temperature traps for electrons released during the photoconversion of $F \rightarrow F^+$ centers. The defects are stable up to 80 K. Below 20 K the spectrum corresponds to the static situation, described by tetragonal symmetry with $g_\parallel = 2.0003(2)$ and $g_\perp = 1.9996(2)$, and $A_\parallel = 41.2 \pm 0.2$ MHz and $A_\perp = 21.4 \pm 0.2$ MHz. The nuclear Zeeman term and the hyperfine interaction are of similar strength, and the spectrum shows a strong "forbidden" lines pattern. Above 20 K electron hopping occurs among the six equivalent orientations. Using the line-shape method based on the stochastic Liouville equation, the evolution of the EPR spectrum with temperature has been studied. The motion is thermally activated with a small activation energy ≈0.0007 eV. A polaron-like behavior is proposed for the detect.

---

1. Summary of paper: *Phys. Rev. B* **42**, 7604 (1990).
2. Universidad de Zaragoza, Zaragoza, Spain.
3. V. M. Orera and Y. Chen, *Phys. Rev. B* **36**, 1244 (1987).
4. V. M. Orera, M. L. Sanjuán, and Y. Chen, unpublished.

## LUMINESCENCE OF $F^+$ CENTERS IN CaO CRYSTALS UNDER PULSED-LASER EXCITATION[1]

*J. L. Park,[2] Y. Chen, G. P. Williams, Jr.,[3] R. T. Williams,[3] and G. J. Pogatshnik[4]*

Luminescence of $F^+$ centers (oxygen vacancies each with one electron) has been investigated in thermochemically reduced (TCR), electron-irradiated, and neutron-irradiated CaO crystals. Time-dependent emission spectra following laser excitation into the $F^+$ absorption band at 351 nm were measured for the three types of crystals. In general, the $F^+$ emission will include the fluorescence of the $F^+$ center and phosphorescence due to ionization, trapping, and recombination effects.

Single crystals of CaO were grown at ORNL using the arc-fusion method. The selected crystals were clear and void-free. Vacancies were produced by TCR during crystal growth and via

knock-on damage by energetic neutrons or electrons. TCR CaO crystals invariably contained significant amounts of hydrogen from OH contamination of the starting material, unless steps were taken to extract hydrogen either from the melt or from the finished crystal. When protons are removed, $F^+$ centers become the predominant species. The decay of luminescence of $F^+$ centers in CaO was examined at a fixed wavelength of 415 nm following laser excitation at 351 nm. The sensitivity of the instrumentation for time-decay measurements at a single wavelength permits the luminescence to be followed over nine decades, from 20 ns up to 50 s (Fig. 4.6). The luminescence decay curves following 10-ns pulsed excitation of $F^+$ centers of TCR neutron-irradiated CaO crystals are shown in Fig. 4.6 at temperatures of 77 and 295 K. The experimental results do not show simple exponential decay curves of the luminescence. A fluorescence lifetime of ≤10 ns, the time-resolution limit of our instrumentation, was obtained. The $^2T_{1u} \rightarrow {}^2A_{1g}$ transition responsible for the $F^+$ luminescence should be strongly allowed. It is suggested that 10 ns is the intrinsic lifetime (i.e., the radiative lifetime of those $F^+$ centers that do not ionize in the excited state). The long decay can be explained by virtue of ionization from the $F^+$ excited state, charge trapping, and subsequent recombination to yield the $F^+$ phosphorescence.

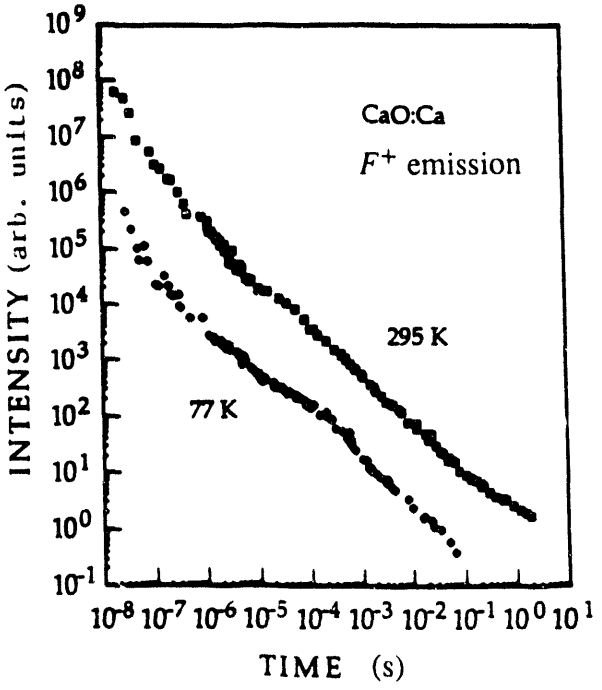


Fig. 4.6. Fluorescence decay curves at 295 and 77 K, following 351-nm excitation of the $F^+$ centers in a CaO:Ca crystal. The emission was monitored at 415 nm. The relative intensities at 295 and 77 K were not determined.

---

1. Summary of paper: *Phys. Rev. B* **43**, 11991 (1991).
2. North Carolina State University, Raleigh, N.C.
3. Wake Forest University, Winston-Salem, N.C.
4. Southern Illinois University, Edwardsville, Ill.

## OPTICAL PROPERTIES OF COLOR CENTERS IN CALCIUM-STABILIZED GADOLINIUM GALLIUM GARNETS[1]

*G. J. Pogatshnik,[2] L. S. Cain,[3] Y. Chen, and B. D. Evans[4]*

The optical absorption of defects in gadolinium gallium garnet crystals ($Gd_3Ga_5O_{12}$ or GGG) is of appreciable significance when considering these crystals as host materials for solid state lasers. Crystals of Czochralski-grown GGG were purchased from Allied

Corporation, Charlotte, N.C. Trace amounts of transition-metal and rare-earth impurities were also detected in the crystals. There was very little optical absorption throughout the visible region. In the near-uv region, a broad absorption band which extended from 400 nm to the band edge at approximately 230 nm (~5.4 eV) was observed. In addition, there was a series of sharp lines from the 4*f* states of $Gd^{3+}$ corresponding to the $^8S \rightarrow {}^6P, {}^6I$, and $^6D$ transitions at 310, 275, and 245 nm, respectively.

In the as-received GGG crystals, luminescence from $Cr^{3+}$ and $Fe^{3+}$ impurity ions in the near-infrared region was observed. The excitation wavelength was chosen to correspond to both the $Fe^{3+}$ charge-transfer band at 265 nm and the excitation of the chromium through the Gd → Cr energy transfer. The chromium emission spectrum exhibited a sharp 695-nm emission band characteristic of the $^2E \rightarrow {}^4A$ transition in a relatively high crystal field, along with the broad emission of the $^2T_1 \rightarrow {}^4A$ transition near 710 nm. The excitation spectrum of the *R*-line emission of $Cr^{3+}$ showed a strong Gd-to-Cr energy transfer, as illustrated in Fig. 4.7. The upper curve shows the room-temperature absorption spectrum of a 0.5-mm-thick GGG crystal. The lower spectrum is the excitation spectrum for the $Cr^{3+}$ emission at 695 nm. The excitation spectrum shows that there is evidence of significant energy transfer to the chromium from all the 4*f* levels of the $Gd^{3+}$ ions.

1. Summary of paper: *Phys. Rev. B* **43**, 1787 (1991).

2. Southern Illinois University, Edwardsville, Ill.
3. Davidson College, Davidson, N.C.
4. Boeing Electronics Company, Seattle, Wash.

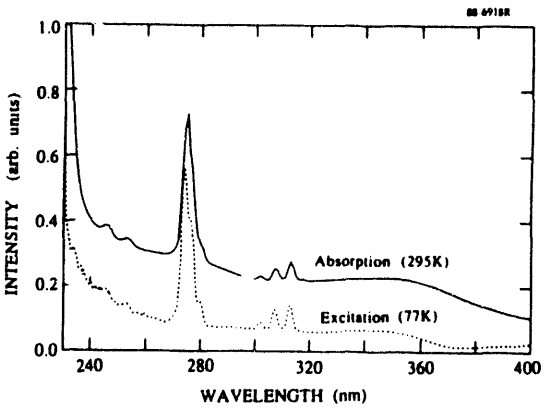


Fig. 4.7. Gadolinium-to-chromium energy transfer in GGG crystals. The top curve is the room-temperature absorption spectrum of a 0.5-mm-thick GGG crystal. The bottom curve is the excitation spectrum at 77 K of the $Cr^{3+}$ emission at 695 nm.

# *MATERIALS PROPERTIES*

## OPTICAL FUNCTIONS OF SILICON DETERMINED BY TWO-CHANNEL POLARIZATION MODULATION ELLIPSOMETRY[1]

*G. E. Jellison, Jr.*

Accurate values of the optical functions of silicon are essential for a number of applications in the semiconductor industry. The presently accepted values were determined using rotating analyzer ellipsometry,[2] which is particularly insensitive to small values of the extinction coefficient *k*; for Si, this occurs below the direct band gap (~3.4 eV). However, two-

channel polarization modulation ellipsometry (2-C PME) is well-suited for accurate measurements of small values of $k$.

Figure 4.8 shows the refractive index $n$ and $k$ of (100) silicon determined using 2-C PME. The raw ellipsometric data were corrected for the ~7.7-Å surface oxide, resulting in greatly increased accuracy in $k$. From this data, the dielectric function $\varepsilon$, absorption coefficient $\alpha$, and the normal-incidence reflectivity $R$ can be determined using

$$\varepsilon = \tilde{n}^2 = (n^2 k^2) + i2nk, \quad (1a)$$

$$\alpha = 4\pi k/\lambda, \quad (1b)$$

and

$$R = [(n-1)^2 + k^2] / [(n+1)^2 + k^2]. \quad (1c)$$

A comparison between this data set and that of Ref. 2 shows that the two data sets agree for photon energies greater than ~3.4 eV, but $k$ from the present data set is ~30–50% less than the $k$ from Ref. 2 for photon energies below ~3.1 eV. This improved accuracy has allowed workers to fit spectroscopic ellipsometry data better for a variety of samples, including polycrystalline Si and amorphous Si grown on oxidized Si[3].

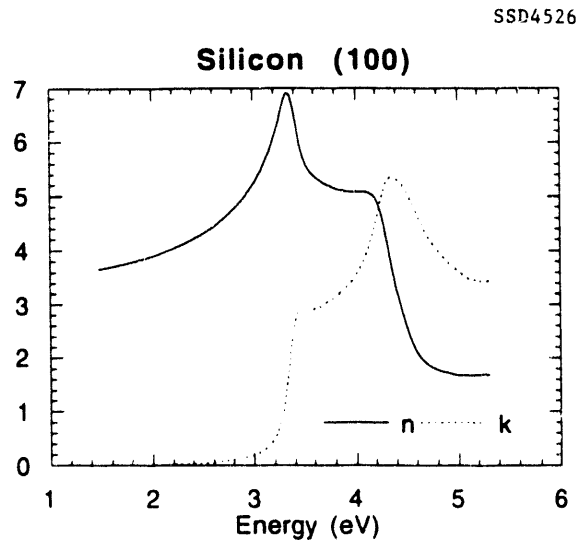


Fig. 4.8. The refractive index $n$ and extinction coefficient $k$ for silicon taken at room temperature.

---

1. Summary of paper: *Opt. Mater.* **1**, 41 (1992).
2. D. E. Aspnes and A. A. Studna, *Phys. Rev. B* **27**, 7466 (1983).
3. G. E. Jellison, Jr., "Spectroscopic Ellipsometry Studies of CVD-Grown Polycrystalline Amorphous Silicon," this report.

## SPECTROSCOPIC ELLIPSOMETRY STUDIES OF CVD-GROWN POLYCRYSTALLINE AND AMORPHOUS SILICON

*G. E. Jellison, Jr.*

Polycrystalline and amorphous silicon grown by chemical vapor deposition (CVD) on oxidized silicon are important starting materials for many integrated circuit applications, including RAM chips. One non-destructive diagnostic test used extensively on these materials is spectroscopic ellipsometry, since it is sensitive to the thickness and optical functions of the constituent layers. However, attempts to simulate the ellipsometry data using Bruggeman effective medium theory and known optical spectra have met with mixed success, since the Bruggeman model does not possess enough flexibility to allow for variations of the optical functions that are due to changes in growth conditions.

Recently, Forouhi and Bloomer[1] proposed a five-parameter formalism to represent the optical functions of amorphous Si. Using this formalism, spectroscopic ellipsometry data have been analyzed for samples of polycrystalline Si and amorphous Si grown on oxidized Si by CVD. The results of the fit are the thicknesses of a rough surface layer, the CVD-grown Si film, the $SiO_2$ film, and the parameters of the Forouhi and Bloomer model, which allow us to determine the optical functions of the CVD-grown film.

Figure 4.9 shows the comparison between the ellipsometric data and two different fits to the data. (The data are expressed in terms of complex $\rho = r_p/r_s$, where $r_p$ and $r_s$ are the Fresnel reflection coefficients for light polarized parallel and perpendicular to the plane of incidence, respectively.) Fit 1 parameterizes the optical functions of the outer CVD-grown layer using the formalism of Ref. 1, while fit 2 treats the CVD-grown layer as an effective medium consisting of "standard" amorphous Si and voids. Clearly, fit 1 is better, particularly in the long-wavelength range where interference effects become important.

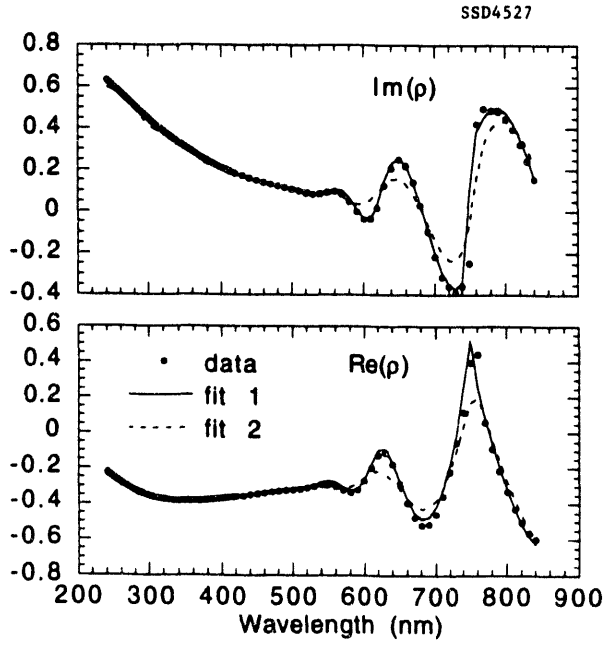


Fig. 4.9. Real and imaginary parts of $\rho$ for the sample *a*-Si plotted vs. wavelength.

---

1. A. R. Forouhi and I. Bloomer, *Phys. Rev. B* **34**, 7018 (1986).

## SAMPLE DEPOLARIZATION EFFECTS FROM THIN FILMS OF ZnS ON GaAs MEASURED BY SPECTROSCOPIC ELLIPSOMETRY[1]

*G. E. Jellison, Jr., and J. W. McCamy*[2]

For many years, ellipsometry measurements have been used to determine the thickness and optical constants of thin films. The older nulling ellipsometers and the newer spectroscopic rotating analyzer ellipsometers each measure two parameters to characterize the optical properties of the sample surface. If it is assumed that the sample itself does not depolarize the incident light, then these measurements can be used to determine the properties of the near-surface region of the sample. However, if the thin-film thickness varies over the incident probe beam, then the light becomes quasi-depolarized, and the normal ellipsometric methods to determine the optical functions and film thickness must be modified.

Recently, Jellison and Modine[3] designed and built a two-channel polarization modulation ellipsometer (2-C PME) that is capable of measuring all three of the associated ellipsometry

parameters $N$, $S$, and $C$. Generally, the quantity $\beta = (N^2+S^2+C^2)^{1/2} = 1$, if the sample surface does not depolarize the light. However, if the sample surface does depolarize the incident light beam, then $\beta < 1$, and the amount of depolarization is given by $1 - \beta$.

A series of ZnS films grown on GaAs were examined using 2-C PME and found to exhibit this depolarization effect. The ellipsometric data were analyzed using an air/rough layer/ZnS/GaAs model in which the rough layer was approximated as an effective medium of 50% voids and 50% ZnS, and the optical functions of the ZnS layer were approximated using the single-term Lorentz expression: $\tilde{n}^2 - 1 = A\lambda^2 / (\lambda^2 - \lambda^2_0 + i\Gamma\lambda)$. To simulate the distribution of ZnS film thickness, the reflectivity was calculated by convoluting over a square probability function: $p(d) = \frac{1}{2}\sigma_d$ for $|d - d_o| \leq \sigma_d$; $p(d) = 0$ otherwise. Very good fits to the raw $N$, $S$, and $C$ data were obtained, with a reduced $\chi^2 < 2$ for all samples examined. In addition, the calculated $\beta$ was compared with the experimentally determined $\beta$, also resulting in a very convincing fit and providing confidence that accurate optical constants can be derived in the presence of small film-thickness variations.

---

1. Summary of paper to be published.
2. Graduate student from The University of Tennessee, Knoxville, Tenn.
2. G. E. Jellison, Jr., and F. A. Modine, *Appl. Opt.* **29**, 959 (1990).

## PHYSICAL PROPERTY CHANGES IN ZIRCON AS A FUNCTION OF ALPHA-DECAY DAMAGE[1]

*B. C. Chakoumakos, R. C. Ewing,[2] G. R. Lumpkin,[3] T. Murakami,[4] W. C. Oliver,[5] and W. J. Weber[6]*

Based on density measurements, x-ray diffraction analysis, and high-resolution transmission electron microscopy (HRTEM) of a suite of natural zircon samples from Sri Lanka ($0.06 \times 10^{15}$–$6.8 \times 10^{15}$ $\alpha$-decay events/mg), three stages of damage accumulation may be delineated. Stage I ($<3 \times 10^{15}$ $\alpha$-decay events/mg) is characterized by sharp Bragg diffraction maxima with a minor contribution from the diffuse-scattering component. Electron diffraction patterns were sharp. Damage is dominated by the accumulation of isolated point defects, which cause unit-cell expansion and distortion that account for most of the decrease in density. These defects may anneal partially over geologic periods of time. Stage II ($3 \times 10^{15}$–$8 \times 10^{15}$ $\alpha$-decay events/mg) is characterized by significant decreases in the intensity of the Bragg diffraction maxima, which become asymmetric from increased contributions of the diffuse-scattering component. HRTEM indicated that the microstructure consists of distorted crystalline regions and amorphous "tracks" caused by $\alpha$-recoil nuclei. With increasing $\alpha$-decay dose, damaged crystalline regions are converted into aperiodic regions but with no further significant expansion of the

unit cell in the remaining crystalline regions. Stage III (>$8 \times 10^{15}$ α-decay events/mg) consists of material that is entirely aperiodic as far as can be determined by x-ray or electron diffraction. There was no evidence for the formation of $ZrO_2$ or $SiO_2$ final products during the last stage of metamictization. Based on modeled density changes, aperiodic regions continue to experience a change in structure as they are redamaged. During Stage II of the process, the modeled density of aperiodic regions changes from 4.5 g/cm$^3$ to 4.1 g/cm$^3$. Fission fragment damage does not contribute to the process of metamictization. The amorphization process is consistent with a model for the multiple overlap of displacement cascades, suggesting amorphization occurs as a result of defect accumulation rather than directly within a single displacement cascade.

For one of the natural single crystals of zircon, $ZrSiO_4$ from Sri Lanka, exhibiting zonation in U and Th contents, the hardness and elastic moduli have been determined as a function of α-decay dose using a mechanical properties microprobe. The zones vary in thickness from one to hundreds of micrometers and have uranium and thorium concentrations such that the α-decay dose varies between $2 \times 10^{15}$ and $8 \times 10^{16}$ α-decay events/mg (0.15 to 0.65 dpa). The transition from the crystalline to the aperiodic metamict state occurs over this dose range. For a traverse of 75 indent pairs across layers sampling a large portion of the crystalline-to-metamict transition ($3.7 \times 10^{15}$–$9.7 \times 10^{15}$ α-decay events/mg), both the hardness and elastic moduli decrease linearly with increasing α-decay dose. The radiation-induced softening follows a behavior similar to other radiation-induced changes (i.e., with the expansion of the unit-cell parameters, there is a decrease in density, birefringence, and hardness and bulk moduli).

---

1. Summary of papers: *Am. Mineral.* **76**, 1510 (1991); *Radiat. Eff. Defects in Solids* **118**, 393 (1991).
2. University of Mexico, Albuquerque, N. Mex.
3. Australian Nuclear Science & Technology Organization, New South Wales, Australia.
4. Japan Atomic Energy Research Institute, Tokai-Mura, Japan.
5. Metals and Ceramics Division, ORNL.
6. Pacific Northwest Laboratory, Richland, Wash.

## RARE-EARTH ELEMENT REFERENCE SAMPLES FOR ELECTRON MICROPROBE ANALYSIS[1]

*E. Jarosewich[2] and L. A. Boatner*

A knowledge of the rare-earth element concentration in rocks and minerals depends on numerous geochemical and petrological processes. While early analyses dealt primarily with the gross distribution of rare-earth (RE) elements in bulk samples, as new instrumentation became available, detailed analyses of individual mineral phases were undertaken. Although progress has been made in the development of programs for the theoretical reduction of analytical microprobe data, the most reliable results are still obtained by comparing

unknowns with standards of similar composition and, often, of similar crystalline structure. Since each sample contains only a single RE element, the lanthanide orthophosphates ($PO_4$) offer an excellent choice for microprobe calibration without the interference caused by the presence of other RE elements. The RE orthophosphates were synthesized previously at ORNL for various fundamental studies, and the details of the preparation and crystallographic and physical properties of these orthophosphates have been summarized.[3]

Since these samples appeared to be good candidates for standards, further characterization was undertaken to establish their homogeneity and stability. Three criteria must be met to qualify as acceptable microprobe reference samples. First, the samples should be homogeneous on a micron scale. Second, they must be stable under the electron beam. Third, they must be available in a sufficient quantity for bulk analyses and distribution. Ideally, independent analyses should be performed in establishing analytical standards, and in the present case, the RE orthophosphates were used as standards to check the known compositions of RE glasses.

For microprobe analyses of RE elements, the absence of interfering elements is of importance. To ascertain the degree of purity of the orthophosphates, all the samples were checked qualitatively with x-ray fluorescence by scanning Ka lines of each element and were also analyzed with the electron microprobe for interfering elements. No detectable interfering elements were found, and neutron activation analyses of seven samples showed only traces of other RE elements.

A total of 16 RE and related orthophosphates were synthesized and characterized for electron microprobe reference materials. These reference samples are homogeneous on a micron scale and are very stable under the electron beam. They are in reasonable supply and are available to researchers as standards for microprobe and other micro analyses.

---

1. Summary of paper: *Geostandards Newsletter* **15**, 397 (1991).
2. Smithsonian Institution, Washington, D.C.
3. L. A. Boatner and B. C. Sales, p. 495 in *Radioactive Waste Forms for the Future*, ed. by W. Lutze and R. C. Ewing, Elsevier Science Publishers, New York, 1988.

## THE APPLICATION OF SINGLE CRYSTALS TO ACHIEVE A QUANTITATIVE UNDERSTANDING OF WELD MICROSTRUCTURES[1]

*S. A. David,[2] J. M. Vitek,[2]*
*L. A. Boatner, and M. Rappaz[3]*

The fusion-zone microstructure has a crucial influence on both the hot-cracking behavior of weldments as well as the overall mechanical properties of welds. This microstructure is controlled by several factors. First, the weld-pool shape and dynamic nature of the weld pool affect the microstructural development. In recent years, considerable effort has been devoted to understanding the weld-pool dynamics and heat-source weld-pool interactions in

order to account for the development of the weld-bead shapes. A second factor that influences the development of the fusion-zone microstructure is the base-metal grain structure. In fusion welds, solidification initially occurs epitaxially at partially melted grains in the base metal, and crystallographic effects have a strong influence on the development of the overall microstructure. In particular, growth will take place along preferred crystallographic directions known as "easy growth" directions. In the present work, large single crystals of an Fe-15Ni-15Cr alloy have been utilized in order to increase our basic understanding of the factors that influence the development of weld microstructures. Oriented ternary-alloy single crystals were used to make electron beam (EB) welds along various principal directions lying in different principal crystallographic planes. By using oriented single crystals, it was possible to obtain crucial microstructural information that is ordinarily lost when welds are made on normal polycrystalline specimens.[4-6] This quantitative information regarding the microstructural properties of EB welds has provided valuable new insight into the fundamentals of the relationships between weld-pool shapes and weld microstructures.

A new three-dimensional geometrical analytical method has been developed in order to interpret the microstructural information resulting from welds made using oriented single crystals (Fig. 4.10). This analytical method establishes a direct correlation between the three-dimensional weld-pool shape and the dendritic

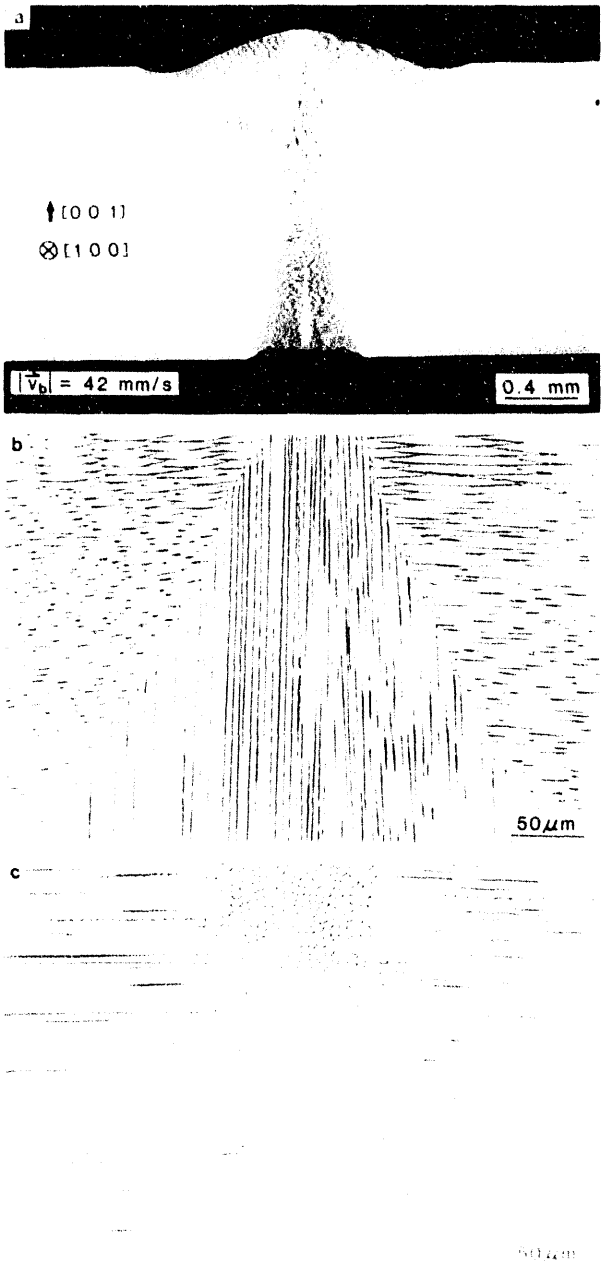


Fig. 4.10. Structure of a single-crystal weld made at 42 mm/s along a [100] direction on a (001) surface. (a) Transverse macroscopic view. (b) Higher magnification of (a), near the top of the weld, and (c) top view of microstructure.

microstructures that are observed in two-dimensional transverse micrographs and can be used to reconstruct the three-dimensional weld-

pool shape. The geometrical analysis and dendritic structures observed in single crystals can be extended to explain the observed microstructural features in bicrystal welds as well as in overlapping multipass welds. These results have significant practical applications in explaining microstructural features in weldments and in evaluating the weld-pool development.

---

1. Summary of paper: *Welding Journal* (in press).
2. Metals and Ceramics Division, ORNL.
3. Ecole Polytechnique Fedérale de Lausanne, Lausanne, Switzerland.
4. M. Rappaz et al., *Metall. Trans. A* **20A**, 1125 (1989).
5. M. Rappaz et al., *Metall. Trans. A* **21A**, 1767 (1990).
6. S. A. David et al., *Metall. Trans. A* **21A**, 1753 (1990).

## STUDY OF EPITAXIAL PLATINUM THIN FILMS GROWN BY METALLO-ORGANIC CHEMICAL VAPOR DEPOSITION (MOCVD)[1]

*B. S. Kwak,[2] P. N. First,[2] A. Erbil,[2] B. J. Wilkens,[3] J. D. Budai, M. F. Chisholm, and L. A. Boatner*

Heterostructures formed using various semiconducting materials have been investigated extensively during the past two decades because of a high level of interest in the development of device applications for such systems as well as for the opportunities they offer in studying fundamental issues in interface physics and the mechanisms of thin-film growth. Although heterostructures formed using materials other than semiconductors (e.g., metals, insulators, superconductors, and ferroelectrics) have not been investigated as extensively, the practical and fundamental potential of such systems is undoubtedly high—as demonstrated recently in the case of investigations of metal-semiconductor heterostructures. In the present work, the growth and properties of single-crystal oxide-metal heterostructures formed by MOCVD have been investigated.

Specifically, the MOCVD technique has been applied successfully to the growth of epitaxial platinum thin films on (100) surfaces of single-crystal potassium tantalate ($KTaO_3$) and strontium titanate ($SrTiO_3$).

Platinum was utilized as the metal component of the oxide-metal heterostructure since it exhibits little or no reaction with most oxide compounds. The MOCVD process employed in this work is unique in the sense that an oxidizing atmosphere is employed, thereby eliminating the incorporation of carbon in the thin film. Platinum thin films grown on $KTaO_3$ (100) at a rate of 70 nm/h showed strong RBS/channeling effects with a $\chi_{min}$ of 4%. In-plane $\phi$ and $\theta$-$2\theta$ scan x-ray diffraction analyses demonstrated the three-dimensional epitaxial alignment of the platinum film with the $KTaO_3$ substrate. Transmission electron micrographs viewed in cross section provided additional information regarding the nature of the epitaxial Pt-$KTaO_3$ interface. The room-temperature resistivity of a 60-nm-thick Pt film on $KTaO_3$ (100) was 12.0 $\mu\Omega$ cm. X-ray diffraction and pole-figure analyses showed that in the case of Pt films deposited on either fused quartz or Si(100) surfaces, the resulting films were polycrystalline and fully textured

with <111> orientations perpendicular to the substrate surfaces. While platinum thin films have previously been deposited by sputtering to form buffer layers for oxide superconductors and for ferroelectric $PbTiO_3$ films, the MOCVD method used here should be more suitable for the deposition of oxide-platinum hetero-structures since it overcomes many of the limitations that are inherent in vacuum deposition techniques that employ energetic particles. By eliminating such energetic particles, it should be possible to remove the associated damage effects and, thereby, gain additional insight into the intrinsic interfacial properties of heterostructures.

---

1. Summary of paper: *Journal of Applied Physics* (in press).
2. Georgia Institute of Technology, Atlanta, Ga.
3. Bell Communications Research, Red Bank, N.J.

# 5. *Ion Beam and Laser Processing*

Utilization of ion beams and lasers in basic research and materials synthesis and processing continues to offer exciting new opportunities in materials science. In this chapter, progress in ion beam processing, ion implantation and analysis, and laser and molecular beam processing of thin films is reported. This research is performed at the Surface Modification and Characterization Research Center (SMAC RC) and the pulsed-laser ablation and molecular-jet growth facilities.

Serving nearly 100 users each year, the SMAC RC continues to provide the scientific community with extensive capabilities for ion beam processing of the near-surface region of solids. Modification of the nonlinear optical properties of glasses, enhancement of the thermal stability of implanted waveguides, reduction in the bacterial adherence to surgical alloys, and assessment of the beneficial effects of implantation on pitting and corrosion in aqueous solutions containing chloride ions are examples of the variety of scientific projects which employ this facility. Fundamental studies concerned with characterizing and understanding the effects of both medium- and high-energy ion implantation on the growth of damage and its accumulation in elemental, compound, and alloy semiconductors continue to be emphasized. Buried amorphous layers have been formed in diamond by C ion implantation, and modification of the optical properties of $Al_2O_3$ have been achieved by high-energy Au ion implantation. Formation of multilayered structures involving $CoSi_2$ and the synthesis of $IrSi_3$ using high-energy implantation are among the new areas of research being pursued. Optimal conditions for electron cyclotron resonance plasma etching of polysilicon and plasma deposition of stoichiometric BN thin films have been determined, and thin C films have been grown on single-crystal Cu by ion implantation and laser annealing.

The Semiconductor Physics, Thin Films, and Photovoltaic Materials Program has introduced 10-ns resolution photography to study laser ablation plasma expansion into vacuum and gas atmospheres, and growth of carbon-free, epitaxial ZnS films on GaAs has been accomplished by the laser ablation process. In work on the development and characterization of molecular-jet thin-film deposition, monolayer growth control has been shown to be possible, and layer-by-layer synthesis of superlattices can be performed using this technique. The extensive work on thin-film superconductivity in this program is reported in Chapter 2.

# ION BEAM PROCESSING

## CROSS-SECTIONAL TRANSMISSION ELECTRON MICROSCOPY (TEM) OBSERVATION OF COPPER-IMPLANTED $SiO_2$ GLASS[1]

*H. Hosono,[2] H. Fukushima,[2] Y. Abe,[2] R. A. Weeks,[3] and R. A. Zuhr*

The use of ion implantation to modify significantly the surface and near-surface properties of glasses has been studied extensively over the past two decades. Of primary interest is the application of these techniques to the formation of optical waveguides by controlling the refractive index and introducing nonlinear optical properties. In this work, direct evidence for the formation of Cu colloids and the close relationship between colloid size and the implanted Cu concentration are reported.

Cross-sectional TEM photographs of $SiO_2$ glass implanted with $Cu^+$ at 160 keV to a dose of $6 \times 10^{16}$ $cm^{-2}$ showed numerous particles in the region from the implanted surface to a depth of >200 nm. Particle diameters were almost constant at a given depth, but varied in the range 2–8 nm with depth. Figure 5.1 shows the relationship between the distribution of diameters of these particles as a function of depth and the depth distribution of the implanted Cu concentrations. The concentration as a function of depth is bimodal in shape. It is evident from Fig. 5.1 that the distribution of particle diameters is close to the distribution of Cu concentrations.

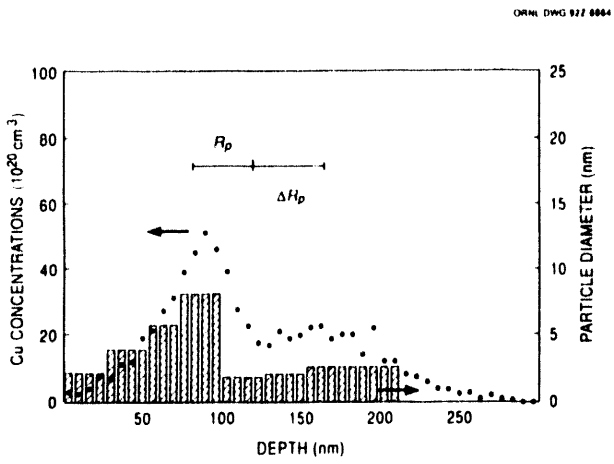


Fig. 5.1. Depth distributions of Cu concentration and Cu particle diameter in $SiO_2$ glass implanted to a dose of $6 \times 10^{16}$ $cm^{-2}$ at 160 keV. $Rp$ and $\Delta Rp$ denote mean range and straggling calculated using the TRIM code.

Buried triple layers of Cu colloids in $SiO_2$ glass were formed by sequential implantation. First, $Cu^+$ ions were implanted to a dose of $6 \times 10^{16}$ $cm^{-2}$ at 160 keV to form the dual layers shown in Fig. 5.1; then an additional dose of $2 \times 10^{16}$ ions $cm^{-2}$ at 35 keV was added. As expected, three layers of Cu colloids were formed. In this case the shape of the distribution of the diameters of the Cu colloids was also similar to that of the depth distribution of implanted Cu.

These data are the first direct evidence of the formation of copper particles in Cu-implanted $SiO_2$ glass, to our knowledge. As a first approximation, the diameter of the Cu colloids increases linearly with Cu concentra-

tion. Although further work will be needed to verify this, it is believed that this correlation will be useful in engineering colloid size by ion implantation.

---

1. Summary of paper to be published.
2. Nagoya Institute of Technology, Nagoya, Japan.
3. Vanderbilt University, Nashville, Tenn.

## PICOSECOND NONLINEAR OPTICAL RESPONSE OF COPPER CLUSTERS CREATED BY ION IMPLANTATION IN FUSED SILICA[1]

*R. H. Magruder[2] R. F. Haglund, Jr.,[2] L. Yang,[2] J. E. Wittig,[2] K. Becker,[2] and R. A. Zuhr*

Picosecond nonlinear optical materials are important for optical switching, sensing, and computing. Metallic nanoclusters embedded in a dielectric exhibit a nonresonant ultrafast nonlinear response at the bulk or surface plasmon frequency of the metal. In this work, both the linear and nonlinear responses of copper clusters formed by ion implantation into fused silica are reported.

High-purity fused silica disks were implanted with $Cu^+$ at 160 keV to a total dose of $\sim 12 \times 10^{16}$ ions $cm^{-2}$. The implantation parameters are listed in Table 5.1. The Cu concentrations (Table 5.1) and depth profiles of the implanted ions were determined by ion backscattering. Under plan-view TEM examination, all three samples exhibited spherical Cu particles of random crystallographic orientation embedded in the silica matrix.

The nonlinear index of refraction of the Cu-implanted silica was measured by the Z-scan technique.[3] Experimental values of the nonlinear index of refraction, $\gamma$, resulting from Z scans using a 100-ps pulse train from a frequency-doubled Nd:YAG laser with a peak irradiance $\sim 10^7$ W $cm^{-2}$ are shown in Table 5.1. Since the values for $\gamma$ are correlated generally with the total amount of implanted Cu, it is concluded that the refractive part of the optical nonlinearity is probably thermo-optic in character, but is influenced by the change in nanocluster size distribution introduced at higher ion beam current density. To test for an

**Table 5.1. Implantation parameters and $\gamma$ for three $SiO_2$ samples implanted with 160-keV $Cu^+$.**

| Sample | Nominal Dose (ions × $cm^{-2}$) | Number of Sides Implanted | RBS Measured Dose (ions × $cm^{-2}$) | Current Density ($\mu A \times cm^{-2}$) | $\gamma$ 100 ps, 532 nm ($cm^2 \times W^{-1}$) | $\gamma$ 5 ps, 583 nm ($cm^2 \times W^{-1}$) |
|---|---|---|---|---|---|---|
| 1 | $12 \times 10^{16}$ | 1 | $10 \times 10^{16}$ | 2.5 | $1.8 \times 10^{-7}$ | $1.8 \times 10^{-10}$ |
| 2 | $6 \times 10^{16}$ | 2 | $5.2 \times 10^{16}$ | 2.5 | $1.5 \times 10^{-7}$ | $1.1 \times 10^{-10}$ |
| 3 | $6 \times 10^{16}$ | 2 | $5.2 \times 10^{16}$ | 7.5 | $2.3 \times 10^{-7}$ | — |

ultrafast electronic nonlinearity, samples were irradiated with light from a 5-ps, cavity-dumped tunable dye laser. Results of Z-scan measurements with this laser at a wavelength of 583 nm are shown in the last column of Table 5.1. These values for $\gamma$ in Cu:silica are comparable to those measured for gold colloids in ruby-gold glass, which are believed to be due to an electronic Kerr nonlinearity arising primarily from intraband excitations of hot electrons.

---

1. Summary of paper to be published.
2. Vanderbilt University, Nashville, Tenn.
3. M. Sheik-Bahae et al., *IEEE J. Quantum Elect.* **26**, 760 (1990).

## ION-IMPLANTED OPTICAL WAVEGUIDES IN $KTaO_3$[1]

*J. Y. C. Wong,[2] L. Zhang,[2] G. Kakarantzas,[2] P. D. Townsend,[2] P. J. Chandler,[2] and L. A. Boatner*

Planar optical waveguides have been formed previously in a wide range of crystalline and glass insulators by using ion implantation. In principle, the approach has been to use light ions (e.g., helium) at high energy to form a damage layer where nuclear collisions occur at the end of the ion track. In the majority of the crystals examined so far, the damaged layer has a reduced refractive index; therefore, the layer between the surface and damage acts as an optical waveguide. For the more stable crystal structures, ionization and electronic excitation merely form color centers and isolated point defects. Consequently, annealing of the implanted crystals results in recovery of the point defects and loss of the color centers, but the heavily damaged structures at the nuclear-damage end of the ion track are more complex and are stable to higher temperatures. Detailed characterization of the refractive-index profiles and their thermal stability reveals considerable diversity in the detailed response of the various materials.

The present work was undertaken to attempt to form optical waveguides in $KTaO_3$—a material that has already been used in comparisons of ion implantation effects of crystalline oxides.[3,4]

Optical waveguides were formed by helium ion implantation in $KTaO_3$. The implantation forms a confinement barrier near the projected range of the ion by decreasing the refractive index as much as 16% for ion doses $4 \times 10^{16}$ ions/cm$^2$. This is the highest refractive index change yet reported for ion-implanted crystalline planar waveguides. Guiding modes (with moderately low loss) are produced without the need for annealing out of color centers. During annealing studies, the index change reduces during an anneal stage near 400°C, but waveguiding is maintained even after anneals to 900°C. Loss measurements indicate a planar-waveguide loss of <1 dB/cm after a 400°C anneal. Implanted $KTaO_3$ exhibits a similarity of index profiles to implanted $LiTaO_3$ and an exceptionally high index-change efficiency $\Delta n \sim 4\%$ for a dose of only $5 \times 10^{15}$ ions/cm$^2$. A stable amorphous phase is not formed, however,

in the highly disordered nuclear-collision region as the index modifications are reduced during the annealing process. Nevertheless, annealing results indicate that $KTaO_3$ waveguides have a remarkable thermal stability, and there is still a sufficient index change left, even at very high temperatures (900°C), for the waveguides to be effective.

---

1. Summary of paper: *J. Appl. Phys.* **71**, 49 (1992).
2. University of Sussex, Brighton, United Kingdom.
3. C. W. White et al., *Mater. Sci. Rep.* **4**, 41 (1989).
4. J. Rankin et al., *Nucl. Instrum. and Methods Phys. Res. Sect. B* **32**, 28 (1988).

## EFFECT OF OXYGEN IMPLANTATION ON THE THERMAL STABILITY OF Ti-IMPLANTED $LiNbO_3$

*D. B. Poker, D. G. Tonn,*[1] *and Uma B. Ramabadran*[2]

Implantation of Ti into $LiNbO_3$ has been shown to be an effective technique for the fabrication of optical waveguides. The technique offers advantages in the control of the Ti concentration profile as well as the maximum attainable concentration. However, the need to perform solid-phase epitaxy and thermal annealing following implantation can result in significant migration of the implanted Ti. The stability of the implanted Ti ($2.5 \times 10^{17}$ $cm^{-2}$, at 500°C) following high-temperature annealing (1000°C, 1–4 h) can be improved dramatically by an additional implant of oxygen before annealing. The improvement exhibits a threshold dependence upon the O/Ti ratio. Little effect is seen at ratios of 1.5 and below, while higher ratios produce significant improvement. With no oxygen implantation, the Ti migrates close to the surface during solid-phase epitaxy and gradually diffuses deeper during annealing, as seen in Fig. 5.2. In the sample implanted with an O/Ti ratio of 3, the Ti profile sharpens during annealing, producing a buried layer of high-Ti concentration, which is very stable against migration. Measurements were made of the loss of the transverse electric mode in planar waveguides fabricated with and without additional O implantation. The O-implanted guides exhibited two

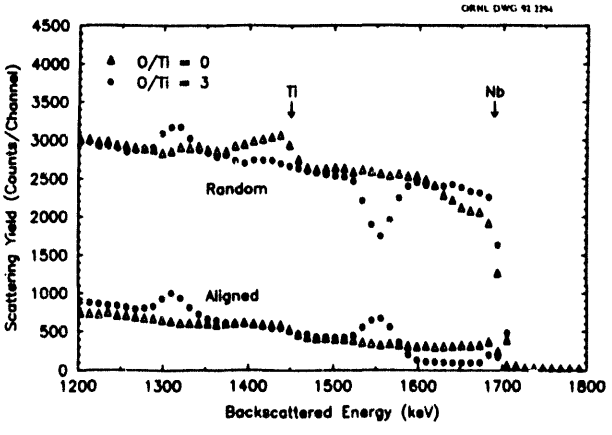


Fig. 5.2. Rutherford backscattering spectrum along random and aligned directions of $LiNbO_3$ implanted with Ti alone (open triangles) or Ti plus O (filled circles), after annealing. The peaks at 1300 and 1550 keV indicate a stabilized layer of enhanced Ti concentration below the surface on the sample implanted with an O/Ti ratio of 3. In the sample implanted with Ti alone, the peak at 1450 keV and the deficit at 1700 keV indicate that the implanted Ti has migrated to the surface during annealing.

modes, compared to a single mode for the guides implanted with Ti alone, though the O-implanted guides showed higher losses. The enhanced stability of the implanted Ti plus O suggests that this process could be used to produce single or even multiple buried waveguides, which previously has been impossible due to the high mobility of Ti implanted alone.

---

1. Oak Ridge Associated Universities faculty research participant from Baldwin-Wallace College, Berea, Ohio.
2. Wright Patterson Air Force Base, Dayton, Ohio.

## CHARGE INJECTION PROPERTIES OF IRIDIUM OXIDE FILMS PRODUCED ON Ti-6Al-4V ALLOY SUBSTRATES BY ION BEAM MIXING TECHNIQUES

*J. M. Williams, I-S. Lee,[1] and R. A. Buchanan[1]*

The charge injection capabilities of iridium oxide films, as produced on Ti-6Al-4V alloys by ion beam mixing techniques, have been investigated. Charge injection upon voltammetric cycling in electrolytes for this valence-change oxide is of interest for possible application in neural prosthetics.

Two surface preparations, a mechanical polish and a passivation treatment in concentrated $HNO_3$, were used for the alloy substrates. Iridium films of three thicknesses—6.6, 11.8, and 18.8 nm—were sputter deposited onto the substrates. Samples were ion mixed with appropriate doses and energies of Ti ions. Rutherford backscattering (RBS) analyses indicated that mixing results were as expected. Iridium inventory was ascertained at appropriate points during the tests by RBS analyses. Samples were repetitively cycled over a 1.4-V amplitude in a 0.1-M $H_2SO_4$ electrolyte at a scan rate of 100 mV/s.

For the samples that were not passivated at the start, about 300 cycles were required for the "activation" process (Fig. 5.3). This means that a small amount of oxygen is added in each cycle, in an irreversible reaction up until the film has three O atoms per Ir atom. Thereafter, the reversible charge injection is approximately constant at a level of about one electron/Ir atom, as long as the oxide coating stays on the substrate. A reduction in charge injection, such as occurred for the sample that was polished and ion mixed at 800 cycles, is caused by loss of Ir from the surface during the

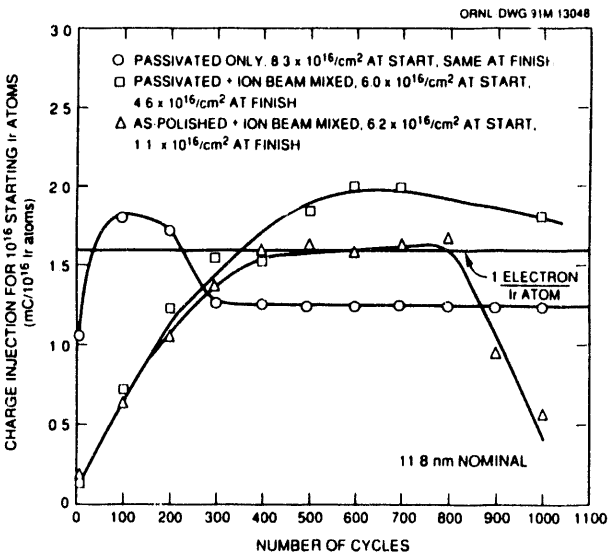


Fig. 5.3. Charge injection per $10^{16}$ starting Ir atoms vs. number of cycles for the set of samples of nominally 11.8-nm initial thickness. Results for the other thicknesses were similar.

cycling. This performance for the polished and ion-mixed samples was still much better than for samples that were polished only. For those samples (data not shown), adhesion was so poor that full activation could not be achieved.

Both the ion mixing and the prepassivation treatments greatly increased the stabilities of films under repeated cycling, in comparison with the mechanically polished surfaces. There was little difference in performance between samples that were passivated only and those that were passivated and ion beam mixed.

---

1. The University of Tennessee, Knoxville, Tenn.

## EFFECT OF NITROGEN ION IMPLANTATION IN ALUMINUM ON CORROSION PROPERTIES IN CHLORIDE MEDIA

*J. M. Williams, R. A. Buchanan,*[1] *and A. Gupta*[1]

Aluminum and aluminum alloys are susceptible to pitting-corrosion attack in aqueous solutions containing chloride ions (e.g., marine environments). A literature report[2] indicated that nitrogen ion implantation could prove beneficial in reducing this detrimental corrosion effect. This study was initiated to examine the possible benefits.

Commercially pure aluminum (AA1100) samples were implanted with 20-keV nitrogen ions to a fluence of $3.0 \times 10^{17}$ N atoms $cm^{-2}$. Electrochemical anodic polarization tests in de-aerated 1.0 wt. % NaCl solution indicated that the critical pitting potential of the aluminum was not changed by nitrogen ion implantation. However, these tests did indicate that the resistance to pit propagation was significantly improved by nitrogen implantation. Constant-potential tests were also performed in the de-aerated salt solution at an anodic potential 100 mV above the measured pitting potential for unimplanted and implanted samples. A potential of -340 mV (standard hydrogen electrode) was held for 30 min. The anodic charge transferred during this time (a direct measure of the amount of corrosion) was found to be 30–60 times less for the nitrogen-implanted aluminum than for the unimplanted aluminum.

Based on the above promising results, additional anodic-polarization and constant-potential tests were conducted in the same salt solution but in the aerated condition. The results were not encouraging. Both tests indicated somewhat detrimental effects due to nitrogen implantation.

Thus, when the salt solution was in the de-aerated condition, nitrogen implantation was beneficial; but when in the aerated condition, nitrogen implantation was somewhat detrimental. Since most practical chloride-containing solutions will be in the naturally aerated condition, the overall results indicate that nitrogen implantation of aluminum would not be an effective corrosion inhibition treatment. Implantation of certain metallic elements (e.g., Cr, Mo, W), which would allow

significant chemical modification of the normal $Al(OH)_3/Al_2O_3$ passive film, appears to be more a promising approach.

---

1. The University of Tennessee, Knoxville, Tenn.
2. S. Venkatraman et al., *Nucl. Instrum. and Methods Phys. Res. Sect. B* **19/20**, 241 (1987).

## THE EFFECT OF NITROGEN IMPLANTATION ON BACTERIAL ADHERENCE OF A SURGICAL Ti-6Al-4V ALLOY AS DETERMINED BY A NOVEL STAINING TECHNIQUE

*J. M. Williams, Beverly L. Giammara,*[1] *David J. Birch,*[1] *and Joanne J. Dobbins*[2]

The effect of nitrogen ion implantation into a surgical Ti-6Al-4V alloy on the growth of the bacterium, *Pseudomonas aeruginosa,* on the surface of the alloy was investigated. As part of the research, a new ruthenium tetroxide staining technique for quantifying the bacterial growth was developed. The program was motivated by the fact that colonization of component biomaterials by these infectious bacteria is a major issue related to the success of prostheses such as artificial hearts.

Calculated doses and energies for nitrogen ion implantation were chosen to produce added N atom fractions of 10, 20, 30, . . . at. % of the original atomic density of the alloy to a treated depth of about 150 nm. Samples were incubated for suitable times in a broth at 37°C containing the subject bacteria. Bacteria adhering to the surface were fixed and treated by the ruthenium tetroxide staining process. Retained bacteria were quantified by use of scanning electron microscopy, backscattered electron imaging, and energy dispersive microanalysis for the biologically incorporated Ru.

After a sharp drop for the nominal 10 at. % added nitrogen treatment, the retained bacteria then further decreased at a rate more or less inversely proportional to the added nitrogen dose (Fig. 5.4). An extrapolation to zero growth can be made for 63 at. % added nitrogen for the 12-h incubation time applicable for Fig. 5.4.

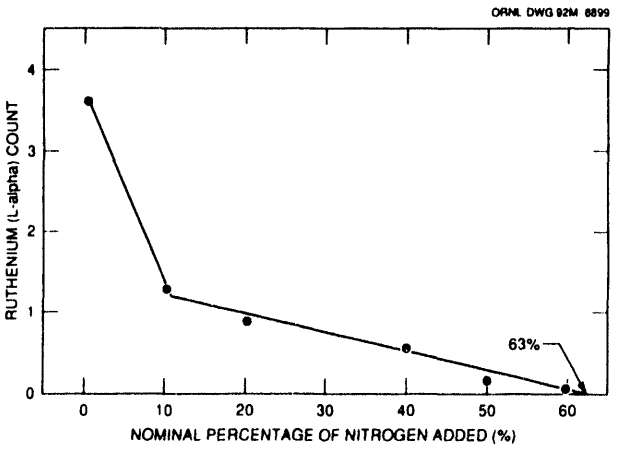


Fig. 5.4. Ruthenium L alpha count vs. implanted nitrogen dose for Ti-6Al-4V alloy samples. The Ru count is a measure of bacterial adherence.

Whether a near-zero adherence of bacteria could be experimentally obtained for somewhat larger N doses and for longer incubation times is not known. The relationship to implanted atomic species is also unknown. Nitrogen implantation is of practical use for wear inhibition in the orthopedic Ti alloy. As a highly biocompatible material, the alloy is already

among the most favorable materials in regard to the growth of bacteria. It is interesting that N implantation improves the alloy in this regard still further.

---

1. University of Louisville, Louisville, Ky.
2. Bellarmine College, Louisville, Ky.

## THE ROLE OF ELECTRONIC ENERGY LOSS IN THE ION BEAM AMORPHIZATION OF $Pb_2P_2O_7$[1]

*B. C. Sales, R. A. Zuhr, J. C. McCallum,[2] and L. A. Boatner*

The near-surface (0–200 nm) and end-of-range (EOR) (600–1000 nm) structural properties of ion-damaged $Pb_2P_2O_7$ have been determined using ion channeling and high-performance liquid chromatography. Single crystals of $Pb_2P_2O_7$ were implanted with 1-MeV $O^+$ ions at doses in the range $10^{11}$–$10^{16}$ ions/cm$^2$. Initiation of amorphization in the near-surface region, rather than at the EOR where most of the elastic nuclear collisions occur, reveals the importance of relatively weak electronic interactions (1500 eV/nm-ion) in producing or enhancing structural alterations leading to the amorphization of ion beam irradiated solids. The electronic interactions produced by the 1.0-MeV $O^+$ ions in the present experiments are about one order of magnitude smaller in energy than that generally thought necessary to produce displacive structural damage in insulating inorganic solids.

The chromatograms from the surface (0–200 nm) and EOR (600–1000 nm) regions are shown in Fig. 5.5 for $Pb_2P_2O_7$ crystals implanted with three different $O^+$ doses. For $O^+$ doses of $1 \times 10^{13}$ ions/cm$^2$ and lower, the chromatograms consist primarily of a $P_2$ peak that corresponds to the established structure of crystalline $Pb_2P_2O_7$. At $O^+$ doses near $5 \times 10^{13}$ $O^+$/cm$^2$, however, as shown in Fig. 5.5, there is an abrupt change in the chromatograms from the surface region. In addition to the $P_2$ anions, there are significant quantities of $P_1$, $P_3$, $P_4$, and $P_5$ phosphate chains, as well as smaller quanti-

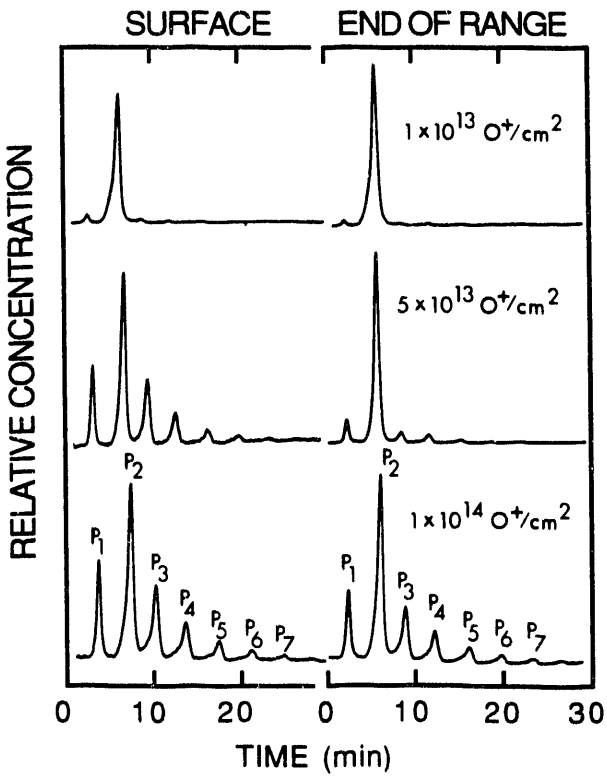


Fig. 5.5. Chromatograms indicating the distribution of phosphate chains of varying lengths in $Pb_2P_2O_7$ crystals implanted with 1.0-MeV $O^+$ ions at the doses indicated. For each ion implantation dose, the chromatograms from the surface (0–200 nm) region are shown on the left-hand side of the figure, while those for material in the EOR region are shown on the right-hand side.

ties of even longer $PO_4$ chains. This chromatogram is characteristic of amorphous $Pb_2P_2O_7$. For the same sample however, the chromatogram from the EOR region is indicative of a significantly lower amount of structural damage. This finding was verified using ion channeling techniques.

---

1. Summary of paper: *Physical Review B* (in press).
2. Royal Melbourne Institute of Technology, Melbourne, Victoria, Australia.

## ION BOMBARDMENT, ULTRASONIC, AND PULSED-LASER BEAM EFFECTS ON SMALL METALLIC CLUSTERS OF POTASSIUM IN MgO[1]

*J. Rankin,[2] P. Thevenard,[3] L. J. Romana,[4] L. A. Boatner, C. W. White, C. J. McHargue,[5] and L. L. Horton[6]*

The effects of high-density ionizing processes, elastic collisions, and shock waves on small metallic potassium precipitates in an MgO matrix were investigated. Toward this objective, MgO single crystals were implanted with $K^+$ ions and subsequently annealed to produce small clusters of potassium. The samples were then subjected to three distinct modifying treatments: ion beam bombardment with argon, ultrasonically induced cavitation bubbles, and pulsed-laser beam irradiation.

The formation of metallic clusters of implanted particles has been reported previously for MgO implanted with magnesium, iron, silver, gold, and alkali ions.[7–9] For MgO implanted with alkali ions, annealing at temperatures where the intrinsic defects ($F^+$ centers) created by elastic collisions are mobile is generally required to form alkali metal precipitates.

In the present work, small metallic precipitates of potassium were produced in ion-implanted layers ($5 \times 10^{16}$ $K^+$ ions $cm^{-2}$, 150 keV, 300 K) on {100} faces of single crystals of MgO by thermal annealing in air at 1000 K. The resulting potassium aggregates had a mean size of 7 nm as characterized by optical absorption measurements and analytical electron microscopy. The effects of three distinct treatments on these precipitates and the implanted layer as a whole were investigated. Ion bombardment with $Ar^{2+}$ ($1 \times 10^{16}$ ions $cm^{-2}$, 300 keV, 300 K) results in a dissolution of the metallic clusters and the production of $F^-$ and $V^-$ centers, as evidenced by the relative changes in the corresponding absorption bands. Rutherford backscattering spectroscopy indicates that this dissolution of precipitates does not result in any long-range redistribution of the potassium. Laser irradiation at a frequency near the absorption resonance of the potassium metal (1-μm wavelength) produces an exfoliation of the implanted layer. A similar effect occurs in ultrasonically treated samples where the entire implanted layer is removed after a 12-min. exposure to an energy flux of 120 W $cm^{-2}$.

The similarity of the results obtained from laser and ultrasonic treatments suggests that additional experiments are necessary to determine the role of localized heating in the exfoliation process.

Additionally, the influence of crystallographic orientation on the dissolution and exfo-

liation processes is being investigated for MgO crystals implanted on the {110} and {111} surfaces.

---

1. Summary of paper: *Surface and Coatings Technology* (in press).
2. Radcliffe College, Cambridge, Mass.
3. Université Claude Bernard, Lyon, France.
4. Oak Ridge Associated Universities postgraduate research participant. Present address: Université des Antilles et de La Guyane, Pourte a Pitre, French West Indies.
5. The University of Tennessee, Knoxville, Tenn.
6. Metals and Ceramics Division, ORNL.
7. P. Thevenard, *J. Phys. (Paris)* **37**, 526 (1976).
8. M. Treilleux et al., *Phys. Status Solidi a* **48**, 425 (1978).
9. M. Treilleux and G. Chassagne, *J. Phys. (Paris) Lett.* **40**, 161 (1979).

## ANNEALING OF Pb-IMPLANTED $SrTiO_3$ IN THE PRESENCE OF WATER VAPOR: A STUDY USING $D_2{}^{18}O$ LABELING[1]

*J. C. McCallum,[2] T. W. Simpson,[3] I. V. Mitchell,[3] J. Rankin,[4] and L. A. Boatner*

Water vapor is known to have a significant effect on the growth kinetics of ceramic oxides.[5] In previous studies of solid-phase-epitaxial (SPE) regrowth of Pb-implanted $SrTiO_3$, the addition of water vapor to the annealing ambient was found to enhance the recrystallization rate by an order-of-magnitude over the rate in dry nitrogen.[6,7] To gain a better understanding of the role of water vapor in altering the SPE growth kinetics in $SrTiO_3$, there are several processes that need to be investigated. First, it is important to identify the impurity species that is being transported from the annealing environment through the amorphous layer to the growth interface and to measure the diffusion kinetics of this process. Coupled with this, a study of the way in which the $H_2O$-related impurities are incorporated into the recrystallized lattice may provide insight into the nature of the atomic rearrangement processes at the growth interface that are responsible for the enhanced crystallization kinetics. Finally, the dissociation processes at the sample surface that provide an efficient path for $H_2O$-related impurities to enter the solid are of interest.

New measurements have been made of the regrowth behavior of Pb-implanted $SrTiO_3$ crystals in the presence of water vapor. Doubly labeled water vapor, $D_2{}^{18}O$, at greater than 95% enrichment in each isotope has been added to the annealing ambient, and depth profiles of D and $^{18}O$ have been obtained from the regrown crystals using secondary ion mass spectrometry (SIMS). The D and $^{18}O$ content has also been measured by nuclear reaction analysis using the reactions $D(^3He,p)^4He$ and $^{18}O(p,\alpha)^{15}N$. The crystals were regrown in a conventional furnace under a controlled gas ambient, and time-resolved optical reflectivity (TRR) was used to monitor the regrowth rate dynamically. An enhancement of the solid-phase-epitaxial regrowth rate is observed where water vapor is added to the annealing ambient. This rate increase is accompanied by incorporation of *D* throughout the regrown layer. $^{18}O$ is incorporated into the lattice but does not appear to penetrate deep enough to influence the regrowth rate.

Overall, a comparison of the SIMS data with TRR measurements of the growth velocity as a function of depth indicates that during annealing in wet ambients, hydrogen enters the implanted layer and diffuses throughout the amorphous region on a time scale which is short compared with the recrystallization rate. The hydrogen is then able to catalyze the amorphous-to-crystalline transformation at the growth interface. The SIMS data also suggest that the hydrogen remains trapped in the recrystallized material. At this stage, the nature of the hydrogen trapping sites is not known.

---

1. Summary of paper: *Materials Research Society Symposium Proceedings* (in press).
2. Royal Melbourne Institute of Technology, Melbourne, Australia.
3. University of Western Ontario, Ontario, Canada.
4. Mary Ingraham Bunting Institute, Cambridge, Mass.
5. J. Rankin et al., p. 207 in *Selected Topics in Electronic Materials*, ed. by B. R. Appleton, W. L. Brown, D. K. Biegelsen, and J. A. Knapp, Materials Research Society, Pittsburgh, Pa., 1988.
6. J. C. McCallum et al., *Nucl. Instrum. and Methods Phys. Res. Sect. B* **46**, 98 (1990).
7. J. Rankin, J. C. McCallum and L. A. Boatner, *J. Mater. Res.* **7**, 717 (1992).

## MULTIPLE ION IMPLANTATION EFFECTS ON HARDNESS AND FATIGUE PROPERTIES OF Fe-13Cr-15Ni ALLOYS[1]

*G. R. Rao,[2] E. H. Lee,[3] L. A. Boatner, B. A. Chin,[4] and L. K. Mansur[3]*

Ion implantation of metals has been shown previously to be an effective technique for improving fatigue properties. Implanting the metal surface with energetic ions delays and suppresses the formation of slip bands (the preferred initiation site for fatigue cracks) at the surface, thereby increasing overall fatigue life.[5,6] An earlier study showed that simultaneous dual implantations of four Fe-13Cr-15Ni model alloys with boron and nitrogen increased the hardness and improved fatigue life to a greater extent than did single implantation with either ion species.[7] These results indicated that multiple ion implantations could be an effective technique for improving fatigue properties significantly.

In the present study, the hardness and fatigue properties of complex engineering Fe-13Cr-15Ni alloys, based on the composition Fe-13Cr-15Ni-2Mo-2Mn-0.2Ti-0.8Si-0.06C, implanted simultaneously with boron and nitrogen have been investigated. Previous studies have shown that the hardness of these alloys increased, but the fatigue life decreased after a dual implantation.[8] This decrease was attributed to a shift to grain-boundary cracking from slip-band crack formation. To explore this hypothesis further, single-crystal specimens of an Fe-15Cr-15Ni alloy were implanted with boron and nitrogen ions and tested for fatigue life. The single-crystal results have been compared with the results obtained using polycrystalline specimens, and possible mechanisms of fatigue-crack initiation in ion-implanted metals were examined.

Eight complex alloys based on the composition Fe-13Cr-15Ni-2Mo-2Mn-0.2Ti-0.8Si-0.06C were simultaneously implanted with 400-keV

boron and 550-keV nitrogen and investigated for microhardness changes and bending fatigue life. The dual implantations were found to decrease the fatigue life of all eight alloys although the implantation increased near-surface hardness. This result was in contrast to the significant improvements found in the fatigue life of four B,N implanted simple Fe-13Cr-15Ni alloys. It was determined that the implantation suppressed surface slip-band formation (the usual crack initiation site), but in the complex alloys, this suppression promoted a shift to grain-boundary cracking. A similar phenomenon was also observed when the simple Fe-13Cr-15Ni alloys were implanted simultaneously with boron, nitrogen, and carbon, wherein fatigue life decreased; and again, grain-boundary cracks were observed. To test the hypothesis that ion implantation made the overall surface more fatigue-resistant but led to a shift to grain-boundary cracking, single-crystal specimens of the ternary alloy Fe-15Cr-15Ni were implanted with boron and nitrogen ions. The fatigue life decreased for the single-crystal specimens as well, due to the concentration of applied stress along fewer slip bands as compared with the "control" single-crystal specimens where the applied stress was relieved by slip-band formation over the entire gauge region.

---

1. Summary of paper: *Journal of Nuclear Materials* (in press).
2. Guest scientist from Auburn University on assignment in the Metals and Ceramics Division, ORNL.
3. Metals and Ceramics Division, ORNL.
4. Auburn University, Auburn, Ala.

5. H. Bakhru et al., *Nucl. Instrum. and Methods* **182/183**, 959 (1981).
6. K. V. Jata and E. A. Starke, Jr., *J. Metals* **8**, 23 (1983).
7. E. H. Lee and L. K. Mansur, *J. Mater. Res.* **4**, 1371 (1989).
8. G. R. Rao, E. H. Lee, and B. A. Chin, *Surface and Coatings Technology* (in press).

## ELECTRON CYCLOTRON RESONANCE MICROWAVE PLASMA-ETCH SYSTEM OPTIMIZATION[1]

*L. A. Berry,[2] S. M. Gorbatkin, John Swyers,[3] and G. H. Henkel[2]*

Electron cyclotron resonance (ECR) microwave plasmas are well-suited for a variety of thin-film processing applications, including thin-film deposition and etching, because of their ability to deliver high-current densities (10s of mA $cm^{-2}$) at low ion energies (a few 10s of eV) over 150–250-mm diam. One such process is gate polysilicon etching for metal-oxide-semiconductor device production, where an ~0.5-μm layer of polysilicon is deposited on a much thinner layer of $SiO_2$ and must be etched to form the gate electrode. High-etch rate of the polysilicon, etch uniformity over 200–250-mm diam, minimal etching and damage to the underlying oxide, and the ability to etch submicron features clearly are among the requirements for a successful etch process.

In this joint program between ORNL and SEMATECH (a consortium of U.S. semiconductor equipment manufacturers), members of the Solid State and Fusion Energy divisions evaluated a variety of ECR configurations for

use in a gate polysilicon etch process. Figure 5.6 shows one of the five configurations tested. It consists of a two-coil mirror field ECR source coupled to a multipole, multicusp confinement system. Etch performance was evaluated on 150-mm-diam wafers, both patterned (0.5-μm feature size) and unpatterned, in chlorine plasmas.

The configuration shown in Fig. 5.6 produced undoped poly-Si etch rates >3000 Å/min, $Si/SiO_2$ etch selectivities >25, and etch uniformities as good as 1.3%, but not simultaneously. Other configurations produced improved etch rate (>4000 Å/min) and selectivity (>100), but at the expense of uniformity (typically 6–10%). Additional improvements in etch performance can be achieved by changes in chemistry (e.g., oxygen additions) or refinements in the magnetic-field configuration.

---

1. Summary of paper: *Journal of Vacuum Science and Technology A* (in press).
2. Fusion Energy Division, ORNL.
3. SEMATECH Corporation, Austin, Tex. Present address: Advanced Micro Devices, Austin, Tex.

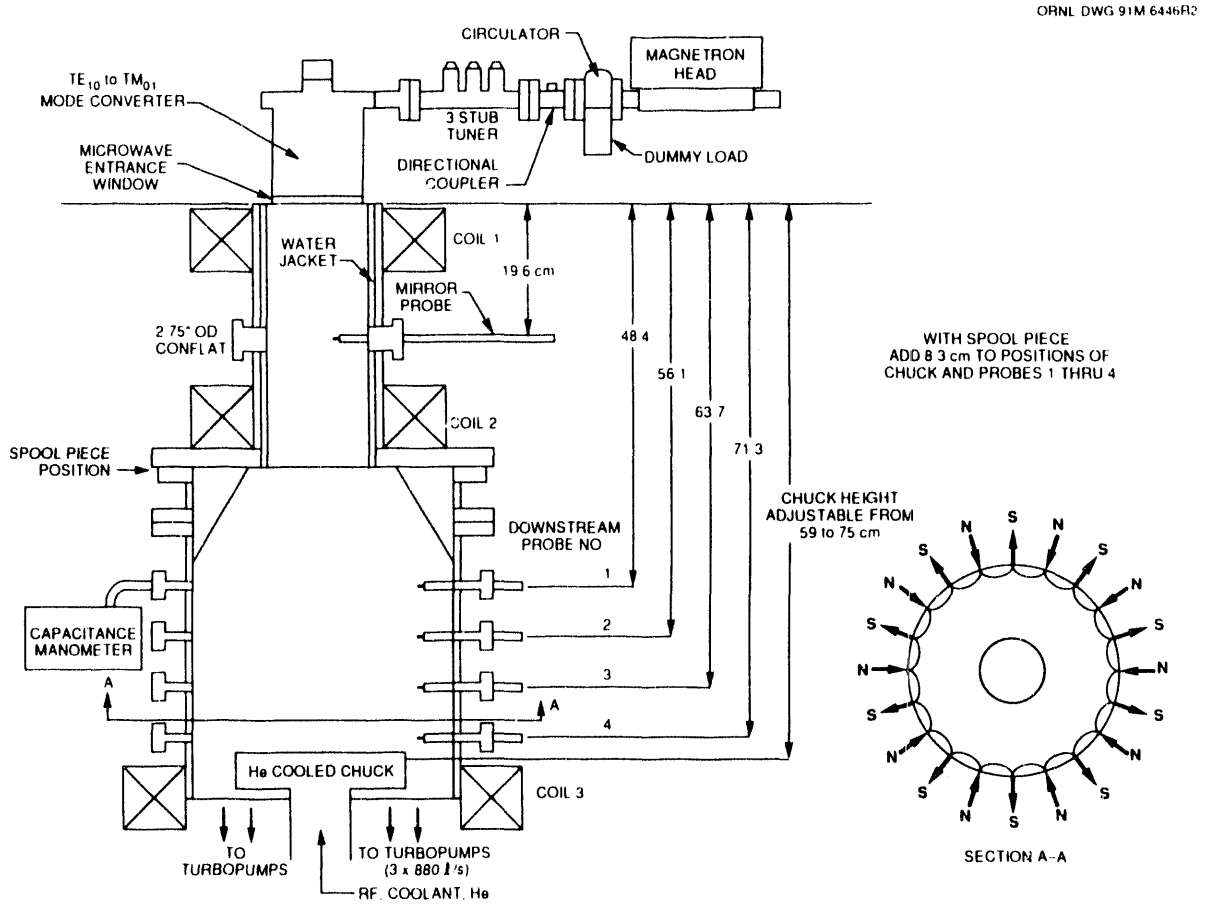


Fig. 5.6. Schematic diagram of ECR microwave etch system with multipole confinement.

## ELECTRON CYCLOTRON RESONANCE MICROWAVE PLASMA DEPOSITION OF BORON NITRIDE THIN FILMS

*S. M. Gorbatkin, Charles Barbour,*[1] *and T. Mayer*[1]

Electron cyclotron resonance microwave plasmas have been used for deposition of $B_xN_{1-x}$ thin films from borazine ($B_3N_3H_6$)-based plasmas. Boron nitride (BN) thin films have potential applications for electronic and optical device production, as well as tribological thin-film formation. Of special interest is the cubic-BN phase, which has a variety of properties second only to diamond and is superior to diamond for some applications (e.g., those requiring high-temperature oxidation resistance). The wurtzitic-BN phase is also of interest for tribological coatings.

Deposited films are being analyzed using a variety of techniques in collaboration with Sandia National Laboratories, including non-Rutherford-enhanced cross-section backscattering spectrometry, forward elastic recoil detection (ERD), and infrared absorption. Precise quantitative measurements of low-mass elements such as boron, nitrogen, and hydrogen are of special interest. All three elements can be detected using a 24-MeV $Si^{+5}$ analysis beam during ERD, with backscattering measurements used for additional determinations of B and N concentrations.

A wide range of stoichiometries are accessible even with pure borazine as the source gas, with the ratio of B/N ranging from 0.99 (stoichiometric BN) to 4.4. The hydrogen atomic fraction can vary ~1–20% and is typically 2–3% for stoichiometric BN films. No evidence of cubic-BN formation has been observed as measured by infrared absorption and transmission electron microscopy. Additional experiments are under way to evaluate proposed alternate mechanisms for cubic-BN phase stabilization and to characterize in more detail the structure of deposited films.

Future experiments will be directed toward understanding stoichiometry control, hydrogen incorporation, phase stabilization, and microstructure control, as well as evaluation of optical and mechanical properties, in more detail.

---

1. Sandia National Laboratories, Albuquerque, N. Mex.

## MEASUREMENT OF THE SATURATED D COVERAGE ON RECONSTRUCTED (100) Cu

*C. Walters,*[1] *D. B. Poker, D. M. Zehner, and E. W. Plummer*[2]

The Cu(100) surface undergoes reconstruction at low temperatures following exposure to atomic hydrogen. Several models, which result in different levels of hydrogen coverage for the saturated surface, have been proposed for the reconstruction. To differentiate between the various models, the d($^3$He, H) $^4$He nuclear reaction was used to measure the saturation coverage of atomic deuterium on a reconstructed (100) Cu surface. Four large-area detectors were mounted in front of the sample to yield a scattering solid angle of 1 sr, greatly increasing the sensitivity of the nuclear reaction analysis. A

40-μm Ni foil was placed between the detectors and the sample to absorb the low-energy-scattered $^3$He but to pass the high-energy H (13.5 MeV). A deuterated amorphous carbon film capable of withstanding the high temperatures involved in baking the UHV sample chamber was used as a calibration standard. The standard was fabricated, and the deuterium content was determined at the Max Planck Institute of Plasma Physics in Garching, Germany.

Following sputter cleaning and annealing at 775 K, the sample was cooled to 77 K and exposed to a flux of atomic deuterium produced by a hot W filament. Saturation coverage was determined using both thermal desorption spectroscopy and LEED, which was employed to confirm that the reconstruction was present over the entire crystal surface. Preliminary measurements indicate that the deuterium surface coverage saturates at approximately one monolayer.

---

1. Graduate student from the University of Pennsylvania, Philadelphia, Pa.
2. University of Pennsylvania, Philadelphia, Pa.

# *ION IMPLANTATION AND ANALYSIS*

## ION-INDUCED DAMAGE ACCUMULATION IN MeV-IMPLANTED SEMICONDUCTORS

*O. W. Holland and T. E. Haynes*

Damage accumulation in Si during MeV, self-ion irradiation at room temperature had been shown earlier to vary substantially along the path of the ion. A prominent feature of this damage profile is its stationary nature in the region shallower than the end-of-range of the ions. Damage initially increases with ion fluence in this region but quickly saturates at a low concentration even at fluences large enough to produce multiple displacements of all lattice atoms. Damage saturation and the flux dependence of the saturation level were modeled assuming homogeneous damage nucleation within the irradiated volume resulting from random interactions between mobile defects which survive quenching of the collision cascades.

The assumption of homogeneous nucleation has now been examined further by studying the temperature dependence of ion-induced damage in both elemental Si and Ge and in a variety of SiGe alloys. By fitting this dependence with the Morehead and Crowder[1] model, it was possible to determine a cutoff temperature for each substrate, $T_o$, beyond which only homogeneous nucleation of damage is possible. Below $T_o$, damage can form heterogeneously within the collision cascade via trapping of the primary point defects and their complexes during quenching. Results of high-energy, $Si^+$ ion irradiations of these materials demonstrated that damage growth in the near-surface region changed dramatically in the vicinity of $T_o$. This can be seen in Fig. 5.7, which shows ion channeling spectra from $Si_{0.5}Ge_{0.5}$ samples implanted at different fluences at a temperature near $T_o$ in part (a) and below in part (b). It is clear that damage in the near-surface region (at energies greater than 2.0 MeV) saturates in

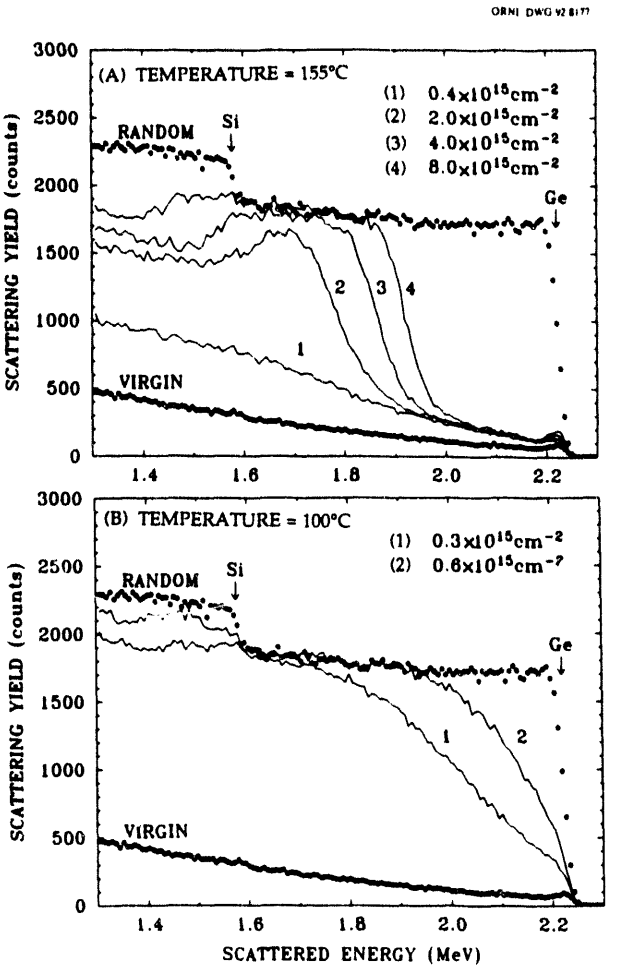


Fig. 5.7. Ion channeling spectra along <100> from $Si_{0.5}Ge_{0.5}$ samples implanted with various fluences of 1.5-MeV $Si^+$ ions at (a) 155°C and (b) 100°C. The cutoff or critical temperature as determined by fitting the temperature dependence of damage in this alloy with the Morehead and Crowder model was 160°C.

all samples implanted at $T_0$, while below this temperature, damage increases steadily with fluence. Similar results were observed in the different samples investigated. The correlation of damage saturation with $T_0$ clearly demonstrates the importance of the role of homogeneous nucleation to this growth phenomenon and validates its assumption in the proposed model.

---

1. F. F. Morehead, Jr., and B. L. Crowder, *Radiat. Eff.* **6**, 27 (1970).

## MECHANISMS OF DAMAGE GROWTH DURING ION IMPLANTATION OF UNSTRAINED Si-Ge ALLOYS[1]

*T. E. Haynes and O. W. Holland*

The mechanisms of damage growth during ion implantation of unstrained Si-Ge alloy epilayers have been investigated as a function of alloy composition. Thick, relaxed epitaxial $Si_{1-x}Ge_x$ layers having compositions of $x = 0.15$, 0.50, and 0.80 were implanted with $^{30}Si^+$ ions at energies between 70 and 100 keV, and the resulting damage profiles were measured by ion channeling. Figure 5.8 shows the peak damage levels produced by implantation of a dose of $1 \times 10^{14}$ Si $cm^{-2}$ at various temperatures. As the implantation temperature was increased through the range shown, the peak damage fraction in each of these alloys decreased from nearly 100% (fully amorphous) to approximately zero. Similar behavior was also observed at other doses and in elemental Si and Ge substrates. The temperature at which the damage yield approached zero increased with the Ge fraction of the alloy for $0 < x < 0.5$, but was independent of alloy composition for $0.5 < x < 1$. This temperature dependence was fit to a model in which the efficiency of the prompt, cascade-nucleated damage mechanism, which is dominant at low temperatures, is

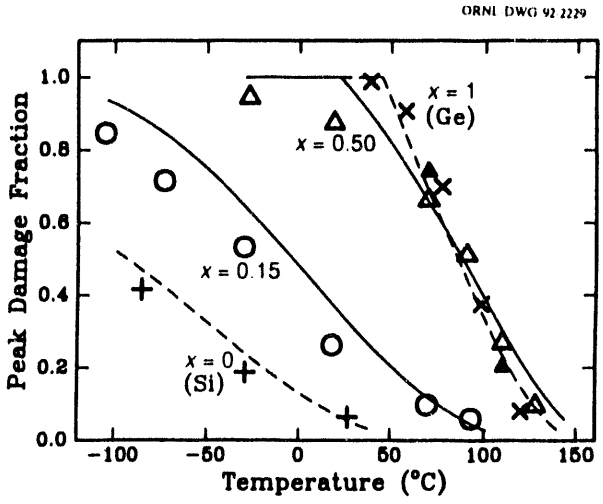


Fig. 5.8. The fraction of displaced atoms as measured by ion channeling at the peak of the damage profile is plotted as a function of implantation temperature for (+) Si, (o) $Si_{0.85}Ge_{0.15}$, (Δ) $Si_{0.5}Ge_{0.5}$, (▲) $Si_{0.2}Ge_{0.8}$, and (x) Ge, each implanted with $1 \times 10^{14}$ Si $cm^{-2}$. Dashed and solid curves are model fits for each substrate material.

assumed to be reduced by thermally activated out-diffusion of primary point defects from the cascade volume. In addition, within the temperature range where the damage efficiency decreased, but not at lower temperatures, the damage became strongly dependent upon dose rate, indicating the emergence of a second damage mechanism which involves the interaction of mobile defects. Therefore, such a dependence on temperature marks the transition between these two mechanisms of damage growth, and the increase of the transition temperature associated with increased Ge fraction for $x < 0.5$ implies that Ge reduces the mobilities of the primary defects. These results help to explain the reported phenomenon of preferential damage accumulation in the alloy layers of Si/SiGe heterostructures and provide a basis for comparison of damage growth in strained layers.

---

1. Summary of paper: *Applied Physics Letters* (in press).

## DEFECTS IN HIGH-ENERGY, SELF-ION-IMPLANTED Si PROBED BY POSITRON ANNIHILATION SPECTROSCOPY[1]

*O. W. Holland, Bent Nielsen,[2] T. C. Leung,[2] and K. G. Lynn[2]*

Vacancy-type defects produced by implantation of Si by 5.0-MeV self-ions at room temperature were studied over a range of ion doses from $10^{11}$ to $10^{15}$ $cm^{-2}$ using depth-resolved positron annihilation spectroscopy. The sensitivity of this probe was used to gain information on nucleation of open volume defects and their evolution during post-irradiation, thermal annealing. Depth profiling is accomplished by varying the energy of the positron beam so that the positron is trapped in the vicinity where it comes to rest by defects and annihilates with an electron. The emitted $\gamma$ quanta carry information about the site of annihilation which is extracted in various ways.

The defect concentration (divacancy) was observed to increase linearly with dose for low doses below ~$10^{12}$ $cm^{-2}$. Also, the concentration increased with depth until beyond the end-of-range of the ions where it decreases rapidly, indicating that the profile of these defects simply correlates with the energy of the ions

deposited in the lattice due to interactions with the atoms. These results were observed in both CZ-grown Si samples, which contain nominally 10 ppm of oxygen, and oxygen-free float-zone Si. Also, two main annealing stages were observed in both types of Si during in situ isochronal heating. Despite the differences in the oxygen content, these stages occurred at essentially the same temperatures in both samples. In the first stage (~200°C), a significant fraction of divacancies was observed to form larger vacancy clusters, although a complete removal of the divacancy at this temperature did not occur. These clusters were removed in the second stage (~675°C) after which the oxygen-free samples returned to their pre-irradiation state, whereas oxygen-defect complexes were formed in the CZ Si.

---

1. Summary of paper to be published.
2. Brookhaven National Laboratory, Upton, N.Y.

## RAMAN AND ION CHANNELING ANALYSIS OF DAMAGE IN ION-IMPLANTED GALLIUM ARSENIDE[1]

*T. E. Haynes, O. W. Holland, U. V. Desnica,[2] and J. Wagner[3]*

Raman scattering has been combined with ion channeling to investigate the damage microstructure in GaAs implanted with 100-keV Si at various doses and dose rates at room temperature. The development of different damage structures was monitored by comparing a Raman signal, which is specifically sensitive to amorphization in GaAs, to ion channeling measurements which can detect small-volume crystalline defects (e.g., dislocations and point-defect clusters) as well as amorphous regions. The correlation between the results from these two different types of measurements are illustrated in Fig. 5.9. The most significant implantation-induced change in the Raman scattering spectra was an increase in the intensities of three broad bands centered at 80, 180, and 250 $cm^{-1}$, which are attributed to amorphization. Thus, the ratio, $I(a)/I$ [longitudinal optical (LO)], of the scattering intensity at 250 $cm^{-1}$ to the intensity of the crystalline LO phonon peak at 292 $cm^{-1}$ was used as a measure of the amorphized fraction in

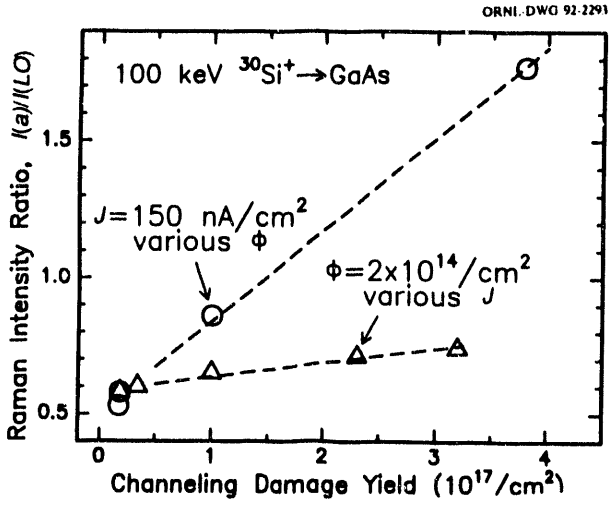


Fig. 5.9. The Raman scattering intensity ratio, $I(a)/I(LO)$, is plotted as a function of the total damage measured by ion channeling for two sets of Si-implanted GaAs: (o) various doses between 0.1 and $3 \times 10^{15}$ $cm^{-2}$ at a fixed dose rate of 0.15 μA $cm^{-2}$ and (Δ) a fixed dose of $2 \times 10^{14}$ $cm^{-2}$ with various dose rates between 0.15 and 12 μA $cm^{-2}$.

the implanted layer. There are clearly two distinct damage components, as indicated by the difference between the slopes of the two lines in Fig. 5.9. When the principal parameter was the implanted dose ($\phi$), the rate of growth of the amorphous fraction detected by Raman scattering was comparable to the growth rate of the damage measured by ion channeling. However, when the dose rate ($J$) was varied, Raman scattering showed a weaker sensitivity to the increase of damage than did ion channeling. These results demonstrate that the damage morphology in ion-implanted GaAs is dependent upon both dose and dose rate and, furthermore, that the dose-rate dependent damage component consists primarily of crystalline defects to which Raman scattering is less sensitive.

---

1. Summary of paper: *J. Appl. Phys.* 71, 2591 (1992).
2. Ruder Boskovic Institute, Zagreb, Croatia.
3. Fraunhofer-Institüt für Angewandte Festkorperphysik, Freiburg, Germany.

## EXTENDED DEFECT FORMATION IN ION-IMPLANTED AND ANNEALED GALLIUM ARSENIDE[1]

*M. J. Bollong,[2] K. S. Jones,[3] and T. E. Haynes*

Extended defects, primarily dislocation loops, are known to form during high-temperature annealing of gallium arsenide following ion implantation under certain conditions. At present, there is a lack of basic data on the mechanisms and conditions for formation of these defects, especially for implantation of heavy ions, even though their presence subsequently affects the diffusion profiles and electrical properties of the implanted dopants. Therefore, a study was initiated to characterize systematically the implantation conditions which lead to the formation of these extended defects, particularly at implant doses which are below the amorphization threshold (so-called type-I defects). Semi-insulating GaAs substrates were implanted with either $^{76}Ge$ or $^{75}As$ ions at 40, 110, and 160 keV and doses of 0.1, 0.2, 0.5, 1.0, and $2.0 \times 10^{14}$ $cm^{-2}$ in order to define the dose and energy windows for type-I defect formation. Implanted samples were characterized by ion channeling and transmission electron microscopy (TEM) prior to annealing and by TEM after capping and annealing at 800 and 900°C.

Two major observations have emerged from this study. First, the range of doses over which type-I defects formed was found to be dependent upon the ion energy. For instance, at an implant energy of 160 keV, the minimum dose of Ge for producing type-I defects was less than $0.1 \times 10^{14}$ $cm^{-2}$, while at the lower energies of 110 and 40 keV, this threshold dose increased to approximately $0.5 \times 10^{14}$ $cm^{-2}$. Such a dependence on energy had not been observed previously (e.g., for lighter ions) and suggests that the probability of forming type-I defects is sensitive to the initial depth distribution of the primary point defects. Efforts are under way to correlate these experimental results with Boltzmann transport calculations of the

primary interstitial and vacancy distributions. Secondly, the formation of type-I defects was shown to be dependent upon the ion species. Type-I defects were observed in samples implanted with $0.5 \times 10^{14}$ $cm^{-2}$ of Ge at ion energies of 110 and 40 keV, while none were found in samples implanted with As using the same dose and energies, in spite of the fact that the initial amount of damage was the same for both species. Thus, the annealing kinetics depend upon the chemical species that is implanted, such that Ge, as compared to As, promotes the formation and/or stabilization of type-I defects. Complementary experiments are planned with other ion species (e.g., $^{75}Se$) in order to clarify the mechanism underlying this chemical dependence.

---

1. Summary of paper: p. 785 in *Advanced III-V Compound Semiconductor Growth, Processing and Devices*, ed. by S. J. Pearton, D. K. Sadana, and J. M. Zavada, Materials Research Society, Pittsburgh, Pa., 1992.
2. SURA/ORNL Summer Cooperative Program student participant from the University of Florida, Gainesville, Fla.
3. University of Florida, Gainesville, Fla.

## FORMATION OF $CoSi_2$ IN SIMOX WAFERS BY HIGH-DOSE Co IMPLANTATION[1]

*T. P. Sjoreen, R. Jebasinski,[2] K. Schmidt,[2] S. Mantl,[2] H. Holzbrecher,[2] and W. Speier[2]*

Production of multilayered structures of $Si/CoSi_2/Si/SiO_2/Si$ has been accomplished by implanting high doses of Co into Si(100) SIMOX wafers at several energies between 100 and 200 keV, followed by rapid thermal annealing at 750°C for 30 s and 1150°C for 10 s. An excellent structure was formed in the sample implanted at 100 keV. At this energy, the as-implanted Co distribution remained entirely above the $SiO_2$ layer, and the influence of the amorphous $SiO_2$ layer on the $Si/CoSi_2/Si$ structure during annealing was negligible; the quality of the buried $CoSi_2$ layer, as observed by ion channeling and cross-sectional electron microscopy, was about the same as that observed in bulk Si wafers. However, as the implantation energy was increased and the implanted Co distribution moved closer to the $SiO_2$ layer, the crystallinity of the $CoSi_2$ layer degraded after annealing. At 100 keV, the ion channeling minimum yield in the $CoSi_2$ was 6%, but it increased to 24% at 180 keV. At 200 keV, a buried layer was not produced.

This degradation of layer crystallinity with energy and the failure to produce an epitaxial layer at 200 keV are attributed to the highly damaged condition in the as-implanted state of the Si between the peak of the Co distribution and the $SiO_2/Si$ interface. Ion channeling analysis of this Si region showed that the minimum yield was quite large, about 90% at 180 keV. At 200 keV, the minimum yield in this region reached 100% (i.e., the region became amorphous), which prevented the mesotaxial process from proceeding during the annealing cycle, although some coalescence was observed in the part of the Co distribution nearest the surface where the Si still remained crystalline in the as-implanted state. Further studies are under way to optimize the implan-

tation energy and dose necessary to produce an epitaxial $CoSi_2$ layer directly over the $SiO_2$ layer.

---

1. Summary of paper: *Mater. Sci. and Eng. B* **12**, 129 (1992).
2. Forschungszentrum, Jülich, Germany.

## SCHOTTKY BARRIER HEIGHTS OF ION BEAM SYNTHESIZED Si/$CoSi_2$ DIODES

*T. P. Sjoreen, A. Schüppen,*[1] *S. Mantl,*[1] *and L. Vescan*[1]

Schottky barrier heights ($\phi_B$) of Si/$CoSi_2$ diodes in both (111)- and (100)-oriented Si have been measured using current-voltage (IV), activation energy (AE), and capacitance-voltage (CV) techniques. Epitaxial $CoSi_2$/Si diodes were produced by implanting high doses of Co ions through either $SiO_2$ or metal/$SiO_2$ masks and subsequent annealing and processing. The implantations were carried out at energies of 100 and 200 keV with doses of $1\text{–}2 \times 10^{17}$ cm$^{-2}$. This was followed either by rapid thermal annealing at 750°C for 30 s and 1150°C for 10 s or by furnace annealing at 600°C for 1 h and 1000°C for 30 min. After annealing, the mask was removed by reactive ion or wet chemical etching, and the Si/$CoSi_2$/Si heterostructure was overgrown by low-pressure vapor phase epitaxy. Subsequent metallization and lithography were used to make diodes for both the bottom and top (mesa type) interfaces. The results of the IV and AE measurements were analyzed using conventional thermionic emission theory.

Analyses of the IV and AE data showed that the ideality factor ($n$) of the top diodes was in the range 1.01–2.0, while for the bottom diodes $n$ was consistently large with values 1.9–2.0. For the top diodes with $n < 1.2$, $\phi_B = 0.66 \pm 0.03$ and is independent of Si orientation. The CV measurements for these diodes also yielded $\phi_B$ values in agreement with the IV and AE measurements. This value of 0.66 is in excellent agreement with $\phi_B$ values reported in the literature. However, as might be expected, for diodes with $n > 1.2$ there was a large variation in the extracted $\phi_B$ values. The IV and AE measurements generally yielded values for $\phi_B$ in the range 0.77–0.83, while the CV measurements gave much higher values of 0.9–1.1. These results are not surprising, because it is generally agreed that large values of $n$ indicate that the diodes are either inhomogeneous or that there are other current transport mechanisms. Thus, the assumption of only thermionic emission in the analysis is no longer valid. Although it is not surprising that the electrical characteristics of the diodes can be quite different, as indicated by the large range in ideality factors (this can easily be attributed to processing problems), it is not understood at this time why all the bottom diodes have such large values of $n$. Recent high-resolution cross-sectional transmission electron microscopy investigations of Si/$CoSi_2$/Si structures made under conditions virtually identical to the diodes discussed here indicate that the lower interface has a more uniform (or homogeneous) structure than the top interface, which runs counter to the observed

ideality factors. Further experiments are needed to understand this problem.

---

1. Institut für Schicht- und Ionentechnik, KFA Jülich, Jülich, Germany.

## ION BEAM SYNTHESIS OF $IrSi_3$

*T. P. Sjoreen*

$IrSi_3$ is an interesting silicide because it has a very low Schottky barrier to *p*-type Si. For this reason, there is interest in using this material for IR sensors in CCD imaging arrays. Because $IrSi_3$ has a small lattice mismatch of -1.8% with (111)-oriented Si, there is a good possibility that an aligned layer of this material can be formed in Si(111) by ion implantation and annealing. Presently, experiments are under way to synthesize $IrSi_3$ by implanting 2-MeV Ir ions into (111) oriented Si with doses to $3.5 \times 10^{17}$ $cm^{-2}$ and annealing at temperatures in excess of 900°C. These temperatures are necessary to anneal the damaged substrate, to coalesce the Ir silicide precipitates into a single layer, and to ensure that the Ir silicides precipitated during implantation will be transformed to the $IrSi_3$ phase. Preliminary ion channeling analysis of a sample implanted with $2.5 \times 10^{17}$ Ir $cm^{-2}$ at a substrate temperature of 400°C and later annealed at 1000°C for 1/2 h showed some coalescence of the Ir silicide distribution but no epitaxial layer. Further annealing of the sample at the same temperature for 1/2 h and again for 1 h did not lead to additional coalescence, but it did improve the crystallinity near the surface. Analysis of the lattice damage in the as-implanted state indicated that the substrate temperature during implantation was too low. Further implantations are in progress at substrate temperatures of 450–600°C to increase the in situ annealing and improve crystallinity. This should lead to better coalescence during annealing and the formation of an epitaxial layer.

## ANALYSIS OF C FILMS FORMED ON SINGLE-CRYSTAL Cu BY ION IMPLANTATION AND LASER ANNEALING

*S. P. Withrow, D. M. Hembree, Jr.,*[1] *C. W. White, R. A. Zuhr, J. W. McCamy,*[2] *and S. J. Pennycook*

Polycrystalline diamond films can be grown on a variety of nondiamond materials using CVD techniques. However, such diamond is generally unsuitable for electronic and optoelectronic applications which require large single-crystal films with low-defect densities. Recently, a novel approach to synthesizing continuous diamond films heteroepitaxially on nondiamond substrates has been reported which involves laser annealing of C-implanted Cu substrates.[3] While the mechanism for diamond formation is not known, presumably it involves the segregation of C during the short time the Cu remains molten, followed by the formation of diamond during rapid cooling. This new technique has been utilized to form C films on single-crystal Cu using a wide range of laser processing conditions. Unfortunately, to date no successful growth of diamond has been observed.

Cu (100) and (110) samples were implanted in the near-surface region with carbon ions to a fluence of $1 \times 10^{18}$ cm$^{-2}$, equivalent to the number of C atoms in a diamond film with a thickness of 57 nm. Areas of several square millimeters in size were then pulsed-laser annealed in a flowing Ar ambient using a XeCl excimer laser at energy densities between 1.5 and 7.7 J cm$^{-2}$ and with 1–10 pulses.

The primary technique used for identifying the form of C present was Raman microprobe analysis. Different C morphologies have characteristic Raman-active modes that result in easily distinguishable peaks. Under most of the beam processing conditions used, carbon films of polycrystalline graphite and amorphous carbon regions were formed. In addition, a high-quality graphite film was observed after annealing at an energy of 6.4 J cm$^{-2}$. However, in no case has a Raman spectrum with a characteristic diamond signal been observed. Transmission electron microscopy on selected films etched from the surface corroborates these conclusions.

Rutherford backscattering was used to measure indirectly the C depth distribution by observing the "deficit" in backscattering from Cu as a result of the implanted C. In addition, the amount of C in the surface region was determined by taking advantage of the enhanced proton-C elastic backscattering cross-section at 1.73 MeV. It was found that laser annealing concentrates the implanted C into a film and moves it toward the sample surface. These effects are enhanced by increasing both the energy density and number of pulses. There is no loss of C, however, for annealing with single pulses at laser energies up to 7.6 J cm$^{-2}$ or with three pulses up to 6.5 J cm$^{-2}$.

---

1. Oak Ridge Y-12 Plant, Oak Ridge, Tenn.
2. Graduate student from The University of Tennessee, Knoxville, Tenn.
3. J. Narayan, V. P. Godbole, and C. W. White, *Science* **252**, 416 (1991).

## FORMATION OF BURIED AMORPHOUS LAYERS IN DIAMOND BY CARBON ION IMPLANTATION

*C. W. White, S. P. Withrow, R. A. Zuhr, L. Romana,[1] H. Naramoto,[2] and D. Hembree[3]*

Carbon ion implantation at liquid nitrogen temperature has been used to form buried damaged or amorphous layers in single-crystal (100) diamond in order to study the annealing behavior. Figure 5.10 shows ion channeling results obtained on a crystal implanted by C (300 keV, $5 \times 10^{15}$ cm$^{-2}$). In the as-implanted state, the aligned yield reaches a random value in the depth range from ~2000 to 3200 Å. Thermal annealing at 900 or 1100°C greatly reduces the displacement damage in the near-surface region, but a totally disordered region remains in the depth range 2250–3100 Å. In this state, the implanted region appears black. Surprisingly, however, Raman measurements made in the implanted region after annealing show almost no Raman scattering characteristic of graphite or amorphous carbon. In addition, the intensity of the 1332-cm$^{-1}$ Raman line char-

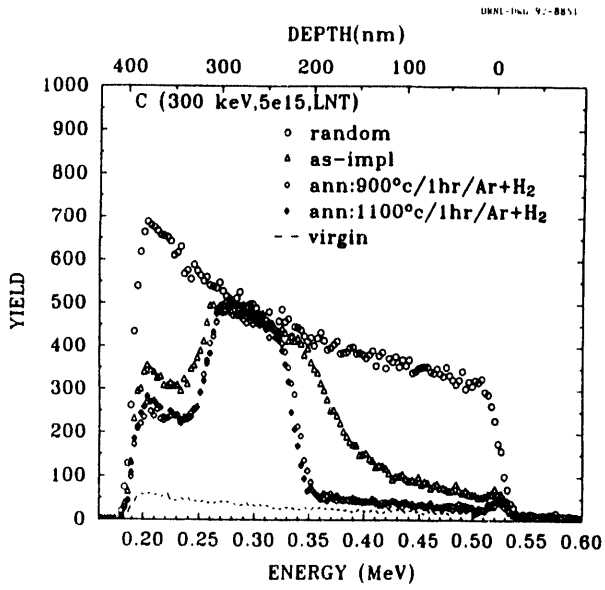


Fig. 5.10. RBS ion channeling results in (100) diamond after carbon implantation and thermal annealing.

acteristic of diamond is much weaker than in the unimplanted region. Further work is in progress to characterize the nature of the buried disordered region.

---

1. Oak Ridge Associated Universities postgraduate research participant.
2. Japan Atomic Energy Research Institute, Tokai, Japan.
3. Y-12 Plant, Oak Ridge, Tenn.

## NUCLEATION AND GROWTH O F DIAMOND ON CARBON-IMPLANTED SINGLE-CRYSTAL COPPER[1]

*T. P. Ong,[2] Fulin Xiong,[2]*
*R. P. H. Chang,[2] and C. W. White*

The nucleation and growth of diamond crystals on single-crystal copper surfaces have been studied by the use of microwave plasma-enhanced chemical vapor deposition (MPECVD) at 800°C. Prior to diamond growth, the single-crystal copper surface was modified by the implantation of C (60 or 75 keV) to a dose of $10^{18}$ $cm^{-2}$ with the copper crystal at an elevated temperature (~820°C). During the implantation of carbon ions into copper at elevated temperatures, the implanted carbon diffuses to the surface and forms a graphite film on the surface. The graphite film greatly enhances diamond crystallite nucleation compared with that which can be achieved on clean copper. Figure 5.11 is an optical micrograph showing preferential nucleation of diamond crystallites on a graphite dot (~250-μm diam) on a (111) Cu surface. For this experiment, an array of graphite dots was created on the Cu surface by implanting the crystal through a Ta shadow mask with 250-μm holes drilled in it. Following diamond growth by MPECVD, the density of diamond crystallites is much greater on the graphite dot [Fig. 5.11(a)] than on the surrounding unimplanted copper. The high-magnification photo [Fig. 5.11(b)] is taken in the center of the graphite dot and shows individual diamond crystallites which have nucleated preferentially on the edges of surface cracks in the graphite film. These cracks develop when the copper crystal is cooled to room temperature following carbon implantation because thermal expansion coefficients for graphite and copper are different. No evidence for epitaxial diamond deposition was observed. A model was proposed to account for enhanced diamond

ORNL PHOTO 2828-92

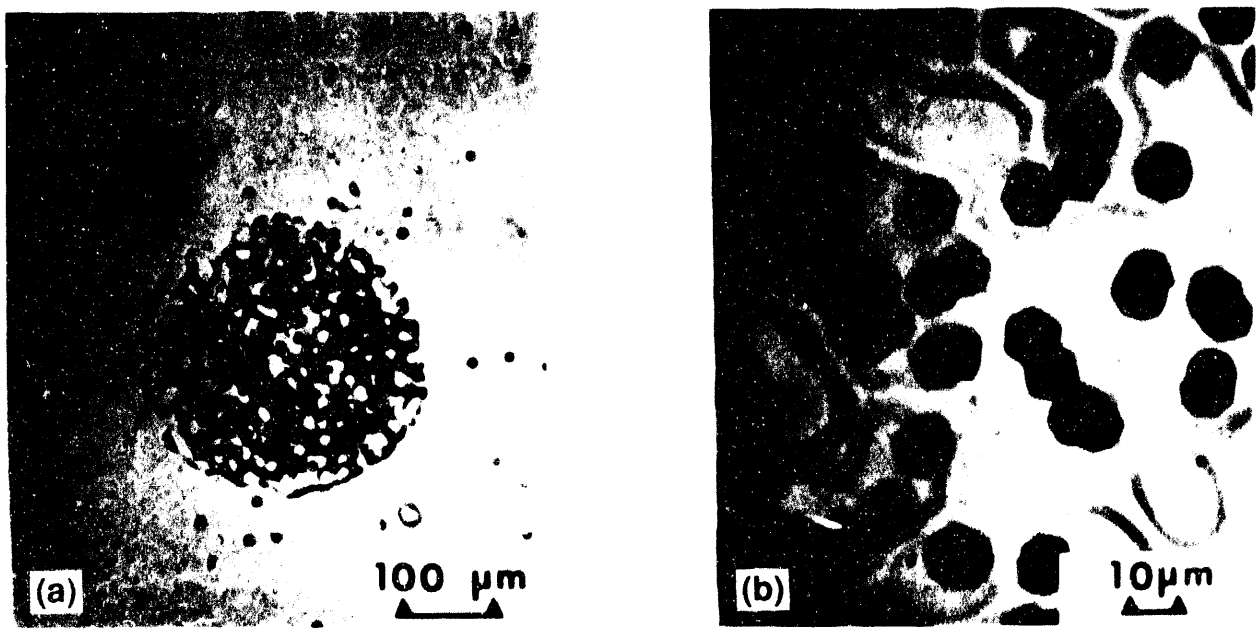


Fig. 5.11. Optical micrographs at (a) low and (b) high magnifications showing preferential nucleation of diamond crystallites on graphite islands grown on Cu(111) surfaces by carbon implantation through a shadow mask.

crystallite nucleation on these graphite surfaces.

---

1. Summary of paper to be published.
2. Northwestern University, Evanston, Ill.

## CONDUCTION IN ION-IMPLANTED SINGLE-CRYSTAL DIAMOND[1]

*J. D. Hunn,[2] N. R. Parikh,[2] M. L. Swanson,[2] and R. A. Zuhr*

Single-crystal type-IIa diamonds have been implanted with sodium and lithium, which are expected to be interstitial donors with energy levels of 0.3 and 0.1 eV, respectively. Temperature-dependent resistance measurements on these samples showed the creation of semiconducting layers with well-defined activation energies. Particular emphasis was applied to the implantation of sodium at different temperatures and doses; combined implantation energies of 55, 80, and 120 keV were used to provide a uniformly doped layer. Activation energies of 0.40–0.45 eV were observed in these implanted layers, indicating incomplete activation of the implanted species and residual lattice damage caused by the implantation process. A sample implanted to a concentration of $5 \times 10^{19}$ $Na^+$ $cm^{-3}$ at 550°C exhibited a single activation energy of 0.415 eV over the temperature range 25–500°C. Thermal annealing above 850°C was found to remove implantation damage as measured by optical absorption and Rutherford backscattering and

channeling. However, accompanying increases in the resistance of the implanted layer and the activation energy were observed. Implantation of carbon or neon was used to introduce equivalent damage densities, while not introducing electrically active species. Both the activation energies and the electrical resistances for these implants were generally higher than those produced by implantation with sodium (or boron). It was concluded that the electrical properties of the Na-implanted samples were at least partly due to electrically active Na but that residual implantation damage was still significant.

---

1. Summary of paper to be published.
2. University of North Carolina, Chapel Hill, N.C.

## MODIFICATION OF THE OPTICAL PROPERTIES OF $Al_2O_3$ BY ION IMPLANTATION[1]

*C. W. White, D. K. Thomas, D. K. Hensley, R. A. Zuhr, J. C. McCallum,[2] A. Pogary,[2] R. F. Haglund,[3] R. H. Magruder,[3] and L. Yang[3]*

Ion implantation is ideally suited as a technique to induce significant changes in the near-surface properties of materials. It has been observed that the implantation of Au into (0001)-oriented $Al_2O_3$ followed by thermal annealing to 1100°C for 1 h causes dramatic changes in the optical properties of $Al_2O_3$. This is demonstrated by the gray scale results in Fig. 5.12, which show the color of $Al_2O_3$ samples in the as-implanted state and after annealing for three doses of Au (at 2.75-MeV energy). In the as-implanted state, the

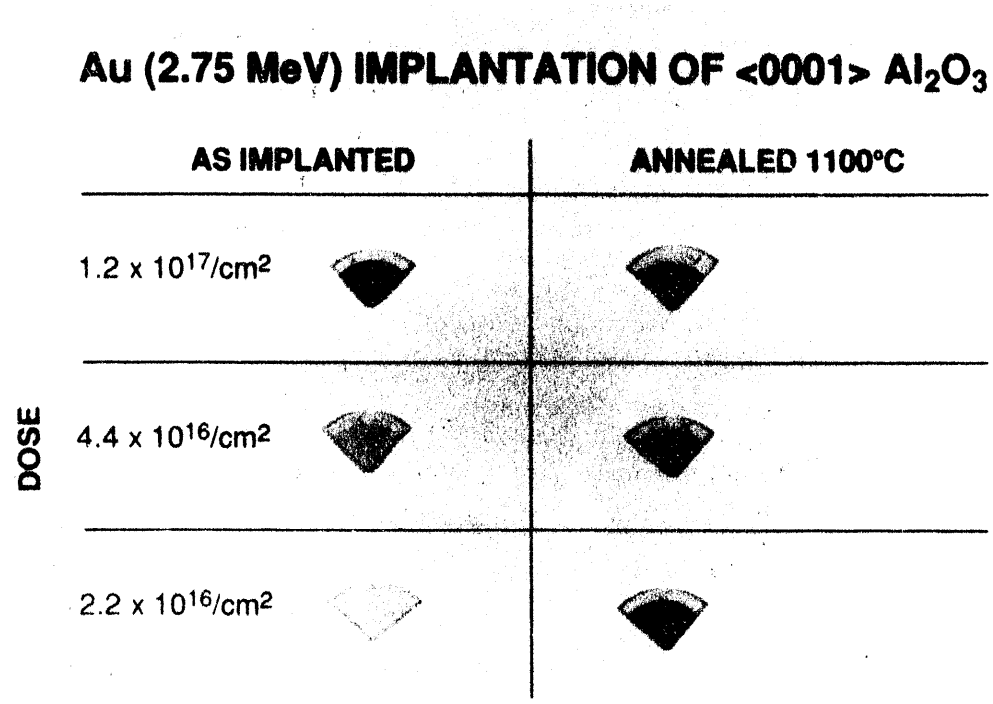


Fig. 5.12. Color changes produced in $Al_2O_3$ by Au implantation and thermal annealing.

implanted region is light gray. Thermal annealing causes the implanted material to become dark gray, and the optical density depends on the dose.

Optical absorption measurements show that thermal annealing causes the development of an intense absorption band at ~2.25 eV in the implanted material. Electron microscopy shows that a high density of small Au precipitates (colloidal particles) are formed by implantation followed by thermal annealing. The darker color and the 2.25-eV absorption band are attributed to the surface plasmon resonance absorption of colloidal Au particles embedded in the $Al_2O_3$ matrix, similar to results of others[4] for the implantation of Au into glass. The colloidal Au particles in $Al_2O_3$ exhibit strong nonlinear optical properties. Initial measurements (by degenerate four-wave mixing experiments) show that the third-order susceptibility for Au colloids in $Al_2O_3$ is ~$1.5 \times 10^{-8}$ esu, a value comparable to that for Au colloids in bulk glass.

---

1. Summary of paper to be published.
2. Oak Ridge Associated Universities postgraduate research participant. Present address: Royal Melbourne Institute of Technology, Melbourne, Australia.
3. Vanderbilt University, Nashville, Tenn.
4. G. W. Arnold, *J. Appl. Phys.* **46**, 4466 (1975).

# *LASER AND MOLECULAR BEAM PROCESSING OF THIN FILMS*

## FAST INTENSIFIED CCD PHOTOGRAPHY OF LASER ABLATION PLUME PROPAGATION IN VACUUM AND AMBIENT OXYGEN[1]

*D. B. Geohegan*

Fast photography of laser ablation plasma expansion into vacuum and background gases was performed with a gated, intensified CCD-array camera system. The sensitivity of the camera system provided stop-action imaging (~10-ns exposures) of plume emission under conditions commonly employed for pulsed-laser deposition: several centimeters from the target in vacuum or low background pressures, extending to hundreds of microseconds following the ablating laser pulse.

Hydrodynamical aspects of the initial stages of expansion, the formation of shock structures due to collisions with the background gas, and the thermalization of the laser plasma were investigated from two-dimensional digitized images of the visible plume emission. As shown in Figs. 5.13(b)–5.13(e), in vacuum the plasma emission begins on the surface of the pellet and then separates into two components. An essentially stationary component occupies a region out to $d \cong 1$ mm from the target surface and emits intensely for

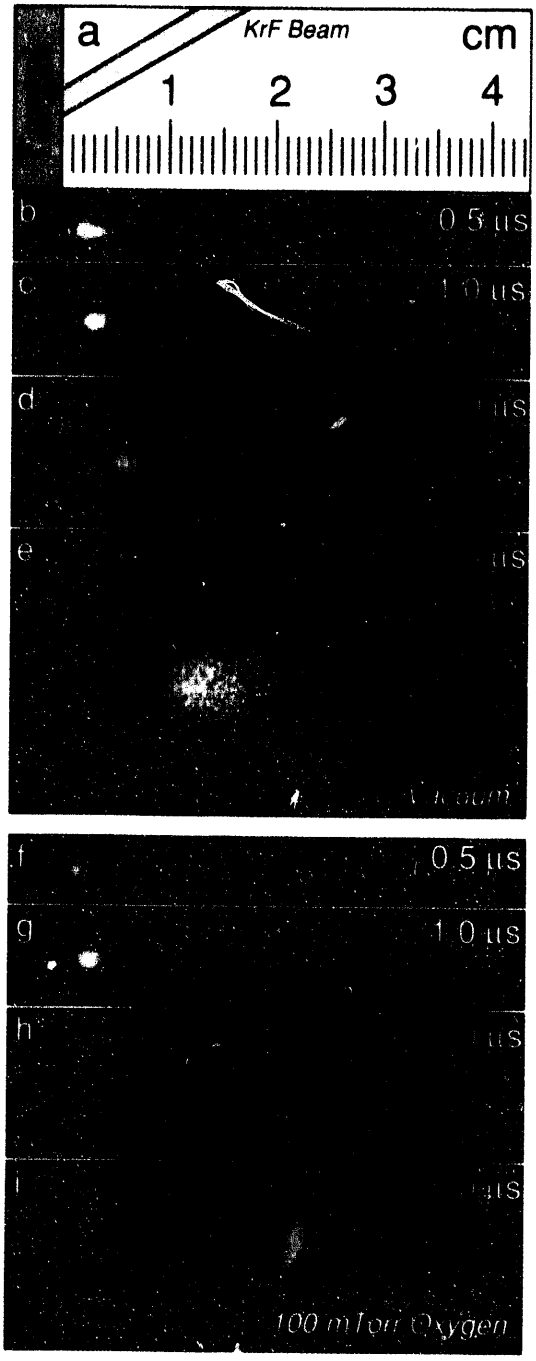


Fig. 5.13. Intensified CCD photographs of the visible plasma emission (exposure times 20 ns) following 1.0 $J$-cm$^{-2}$ KrF/YBCO ablation into [(b)–(e)] $1 \times 10^{-6}$ Torr vacuum and [(f)–(i)] 100-mTorr oxygen at the indicated delay times after arrival of the laser pulse. The 0.2-cm × 0.2-cm 248-nm laser pulse irradiated the YBCO target at an angle of 30° as shown in (a).

$\Delta t \leq 2.0$ μs. A second component expands nearly one dimensionally for the first 0.5 μs and then expands freely in a highly forward-directed pattern with a constant leading edge velocity of $v_{le} = 1.0$ cm-μs$^{-1}$.

The initial expansion into 100-mTorr oxygen [Figs. 5.13(f)–5.13(i)] is not distinguishable from the vacuum case for $\Delta t < 1.0$ μs, while the pressure of the plume material is greater than that of the ambient gas. At $\Delta t \geq 1.0$ μs, an expansion front becomes visible on the leading edge of the expanding plume as shown in Fig. 5.13(g). At later times, the plume coalesces into a stable shock front which displays marked slowing compared with the vacuum expansion. It was found that the position of the plume throughout the expansion was best fit by a drag model during the initial high-pressure period, while propagation after formation of the expansion front was adequately described by a blast-wave model.

---

1. Summary of paper: *Appl. Phys. Lett.* 60, 2732 (1992).

## GROWTH OF EPITAXIAL ZnS FILMS ON GaAs (001) AND (111) BY PULSED-LASER ABLATION[1]

*J. W. McCamy,[2] D. H. Lowndes, J. D. Budai, B. C. Chakoumakos, and R. A. Zuhr*

Although pulsed-laser ablation (PLA) has been used widely to grow epitaxial high-temperature superconductor films, its application to epitaxial compound semiconductor materials still is largely unexplored. PLA has

several potential advantages for semiconductor film growth, including the use of solid carbon-free sources; the ability to grade compositionally an epitaxial layer; the growth of smooth films; and the stoichiometric (congruent) transport of material from the ablation target to the substrate surface, when laser beam conditions are correctly adjusted. Zinc sulfide (ZnS) is a potentially attractive thin-film optoelectronic material because of its wide direct band gap ($E_g$ = 3.7 eV), which suggests such diverse applications as blue LEDs, laser diodes, optical waveguides, and index-matching windows for solar cells. Recently pulsed-KrF (248-nm) laser ablation of a polycrystalline ZnS target was used to grow high-quality, carbon-free, epitaxial ZnS thin films on GaAs (001) and (111) surfaces at growth temperatures $T_g$ = 150–450°C.

Growth was carried out in vacuum or in an inert, low-pressure atmosphere of ultrahigh purity (99.9999+%) helium. Most films were grown to a final thickness ~275 nm, and the ZnS film-growth rate was measured in situ from interference oscillations in the intensity of a HeNe (633-nm) laser beam reflected from the upper and lower surfaces of the growing film. It was found that the ZnS growth rate was the same on GaAs(001) and GaP(001) for all $T_g$, but the growth-rate ratio GR(111)/GR(001) for GaAs substrates was temperature-dependent, decreasing from 1.0 for $T_g$~ 250°C to 0.85 for $T_g$ = 450°C.

The crystal structure and epitaxial orientation of the films were characterized by Cu Kα x-ray diffraction (XRD). For ZnS grown on GaAs(001), analysis using a four-circle XRD goniometer showed that the ZnS(001) and GaAs(001) were aligned to within <0.2° and that the in-plane ZnS and GaAs (100) and (010) directions were also aligned [i.e., the ZnS film was fully epitaxial on GaAs(001)]. Similar results were obtained on GaAs(111).

The rocking curve line profiles for the ZnS(004) Kα1 and ZnS(111) Kα1 peaks were found to consist of two superimposed peaks, one narrow and one much broader, for each orientation. The narrow peak originates from regions of coherent addition of diffracted amplitudes, indicating that a region of near-perfect crystalline material exists. Rutherford backscattering channeling of films grown on GaAs (001) revealed the location of this material. The minimum yield, $\chi_{min}$, from the surface region was much less than that from material near the film-substrate interface. This is consistent with most of the strain and defects being located near the interface, with the uppermost region of the film much more nearly perfect.

High-resolution cross-section transmission electron microscopy analysis showed that stacking faults are the predominant defect in PLA-grown ZnS films, in agreement with earlier studies of MOCVD-grown epitaxial ZnS on GaAs and with the very low (5.4 mJ/cm$^2$) stacking fault energy of ZnS.[3] An upper bound on the density of the stacking faults was estimated to be ~$6 \times 10^{10}$ cm/cm$^3$, which is comparable to the best films grown by MOCVD.[3] Because stacking faults occur in ZnS on the {111}

planes, differences observed in our rocking curve profiles for the (00$\ell$) and ($\ell\ell\ell$) orientations also are consistent, with stacking faults being the predominant defect in PLA-grown ZnS films.

---

1. Summary of paper to be published.
2. Graduate student from The University of Tennessee, Knoxville, Tenn.
3. Y. M. Tairov and V. F. Tsvetkov, p. 2 in *Growth and Defect Structures*, Springer-Verlag, New York, 1984.

## IN SITU OBSERVATION OF SURFACE-REACTION-LIMITED GERMANIUM EPITAXIAL GROWTH PROCESSES BY TRANSIENT OPTICAL REFLECTOMETRY[1]

*J. W. Sharp[2] and Djula Eres*

Optical surface reflectometry was used to monitor the active layer during the epitaxial growth of Ge from pulsed-molecular jets of digermane ($Ge_2H_6$) molecules diluted in helium. The pulsed modulation of the digermane flux facilitates the separation and independent investigation of the elementary reaction steps, primarily digermane chemisorption followed by hydrogen evolution from the chemisorbed layer in this case. (The identity of the desorbing species has not been determined experimentally, but molecular hydrogen is the pre-eminent candidate.) Saturation of the surface via digermane chemisorption causes the sample reflectivity to decrease by ~0.5%. This observation is in agreement with model calculations provided that the chemisorption occurs at sites that are more optically absorbing than bulk Ge. This suggests that digermane is chemisorbed predominantly at nonhydrogenated sites.

For (100) surfaces of Si and Ge, both the chemisorption and hydrogen desorption processes were found to be first order. Digermane chemisorption is not thermally activated, while the hydrogen desorption rate is strongly temperature dependent. The measured hydrogen desorption rates were nominally a factor of 3 lower for Si substrates than for Ge substrates. This is believed to be due to the prolonged presence of Si at the growth front as has been observed during MBE Ge/Si heteroepitaxy.[3]

For Ge(100) substrates and the temperature ranges 410–480°C and 480–570°C, desorption activation energies of 2.25 ± 0.1 eV and 1.62 ± 0.1 eV were determined, respectively; the corresponding pre-exponential factors were $4.9 \times 10^{16} \pm 0.7$/s and $3.5 \times 10^{12} \pm 0.6$/s. The lower activation energy is in agreement with the expected value for desorption of the monohydride phase.[4] The increase in activation energy for the lower temperature range is believed to be caused by the presence of oxygen contamination at lower substrate temperatures.

---

1. Summary of paper to be published.
2. Graduate student from The University of Tennessee, Knoxville, Tenn.
3. Y. Kataoka, H. Ueba, and C. Tatsuyama, *J. Appl. Phys.* **63**, 749 (1988).
4. L. Surnev and M. Tikhov, *Surf. Sci.* **138**, 40 (1984).

## DIGITAL EPITAXY OF GROUP-IV SEMICONDUCTORS BY SURFACE-LIMITED PROCESSES[1]

*Djula Eres and J. W. Sharp*[2]

Thin-film growth of germanium in submonolayer increments was demonstrated using pulsed-molecular jets of digermane molecules. At low substrate temperatures, chemisorption of digermane terminates at monolayer thickness because hydrogen desorption is too slow to regenerate the active sites during the duration of the source-gas pulse. If the unreacted portion of the digermane pulse is rapidly pumped away, the subsequently regenerated sites will remain active until the next source-gas pulse arrives. The changes in the surface hydrogen coverage produced by digermane pulses are directly related to germanium thin-film growth per pulse.

Monitoring the oscillations in hydrogen coverage was accomplished in real time by a surface-sensitive optical reflectometry technique. For a particular substrate, the film thickness per pulse of source gas was found to depend on the substrate temperature, the delay time between source-gas pulses, and the chamber pump-out time. For a particular material, the thickness per pulse also depends on the crystallographic orientation of the substrate.

This new ability to control thin-film growth at the monolayer level is significant for development of a layer-by-layer growth technique for group-IV semiconductors, similar to atomic layer epitaxy for III–V and II–VI compounds. Of particular importance is the extension of this approach to the use of two or more different pulsed sources. Superlattices consisting of alternating layers of different materials, or multicomponent alloys, can be grown by adjusting the overlap between two consecutive pulses of different source gases. An additional advantage of this approach is that real-time monitoring of the hydrogen coverage can be utilized in combination with pulsed delivery as a feedback loop for precise control of the relationship between successive gas pulses.

---

1. Summary of paper: *Applied Physics Letters* (in press).
2. Graduate student from The University of Tennessee, Knoxville, Tenn.

## MODELING THE KINETICS OF SURFACE-LIMITED THIN-FILM GROWTH FROM HYDRIDIC SOURCE GASES

*Djula Eres*

The surface-limited thin-film growth reactions of silicon and germanium from hydridic source gases was simulated by a kinetic model. The model consists of two opposing first-order elementary reaction steps. The first elementary step was assigned to chemisorption of hydridic source gas molecules. The second elementary step represents desorption of molecular hydrogen from the growth surface. The hydrogen occupies active sites and limits chemisorption to a monolayer coverage. The essence of the model is that it treats film growth in terms of depletion of the active film growth sites by chemisorption and regeneration of these active sites by hydrogen desorption. Continuous film growth is characterized by a

steady-state hydrogen coverage that results from the dynamic equilibrium between chemisorption and desorption. The model explains the non-Arrhenius temperature dependence of the film-growth rates, the linear vs. nonlinear pressure dependence of the growth rates, and the temperature and pressure dependences of the transition region between the sub-linear regions in the growth curves.

Agreement between modeling results and experimental data suggests the following mechanistic model for surface-limited thin-film growth. Thin-film growth is initiated by a rapid chemisorption process that is temperature independent. At low substrate temperatures, the growth surface rapidly saturates with hydrogenated fragments because the hydrogen desorption process, through which new sites are generated, has a large activation energy (1.73 eV). Consequently, at low substrate temperatures the hydrogen desorption process is the rate-limiting step. At higher substrate temperatures, where the hydrogen desorption reaction becomes faster than chemisorption, the source gas supply rate becomes the rate-limiting step.

The model has been used to extract the kinetic parameters of the elementary reaction steps in silicon growth from silane and disilane, and in germanium growth from germane and digermane, using published temperature-dependent growth rates and hydrogen-coverage data.

## MOLECULAR BEAM APPARATUS FOR THIN-FILM GROWTH STUDIES

*Djula Eres*

Construction of a molecular beam apparatus for studies of semiconductor thin-film growth from gaseous source molecules was completed. The apparatus consists of three stages that are housed in differentially pumped chambers.

The molecular beam is generated in the first stage by a high-pressure supersonic expansion. The beam-generation stage is designed such that both pulsed and continuous molecular beams can be generated. The beams are spatially defined by a skimmer in the generation chamber and by an aperture in the chopper (second) chamber. The chopper is used in time-of-flight measurements of the molecular velocity distributions. The apparatus is designed such that the chopper stage can be removed in order to increase the molecular flux at the substrate for thin-film growth applications.

The main (third) chamber is equipped with a hemispherical electron energy analyzer to be used with an x-ray source for x-ray photoelectron spectroscopy measurements and with an electron gun for Auger electron spectroscopy measurements. A reflection high-energy electron diffraction (RHEED) system is used for in situ monitoring of the surface structure. The composition of the background gas in the chamber is monitored by a residual gas analyzer.

Samples are introduced through an entry-lock chamber in order to preserve the integrity of the vacuum in the main chamber. The sample manipulator in the main chamber has azimuthal and polar rotations and three linear degrees of freedom.

A schematic drawing of the molecular beam apparatus is shown in Fig. 5.14. The apparatus will be used to grow group-IV semiconductor thin films and to investigate associated growth phenomena.

SSD4541

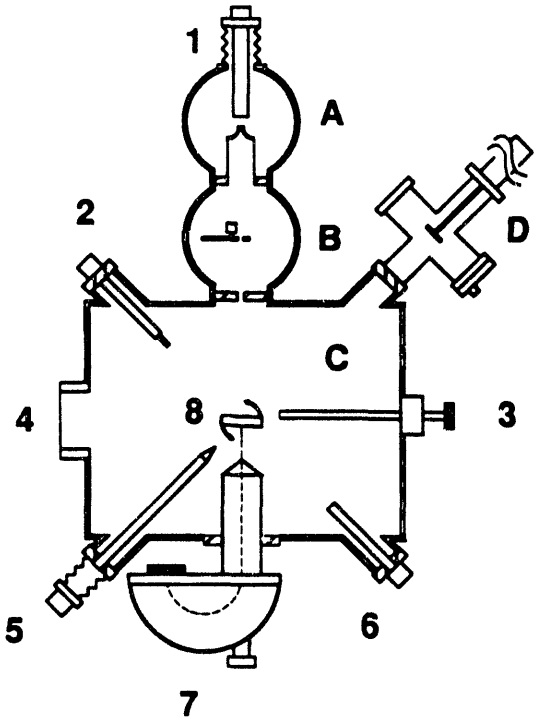


Fig. 5.14. Schematic diagram of the molecular beam apparatus showing: (A) beam generation chamber, (B) chopper chamber, (C) main chamber, and (D) entry lock chamber. Also shown are the (1) pulsed molecular beam valve, (2) residual gas analyzer, (3) RHEED gun, (4) RHEED screen, (5) x-ray source, (6) electron gun, (7) electron energy analyzer, and (8) sample stage.

## ENHANCED ADHESION OF COPPER FILMS ON SAPPHIRE SUBSTRATES BY PULSED-LASER PROCESSING: EXPERIMENTS AND MODEL CALCULATIONS[1]

*M. J. Godbole,[2] A. J. Pedraza,[2] Douglas H. Lowndes, and J. R. Thompson, Jr.[3]*

Previously it has been shown[4] that the adhesion of thin copper films to sapphire substrates can be enhanced at least threefold by using sputter deposition followed by excimer laser irradiation. A computer program to simulate heat flow during laser melting has now been used to relate the effects of interfacial thermal resistance and varying laser-energy density $E_\ell$ to the morphological and structural changes that occur during the pulsed-laser bonding and adhesion-enhancement process in these materials. The computer model allows for melting of the metallic film and/or the substrate and also indicates when film vaporization begins. Experimentally, copper films of 80-nm thickness were sputter deposited on sapphire substrates and laser irradiated with $0.2 \leq E_\ell \leq 3.5$ J/cm$^2$. The changes in film morphology and thickness as a function of $E_\ell$ were analyzed using energy dispersive x-ray spectroscopy.

Four regimes were established as a function of $E_\ell$. For $E_\ell < 0.3$ J/cm$^2$, the metal film partially detaches from the substrate due to thermal stresses in the solid state, while for energy densities above that critical value, larger portions of the film remain attached to the substrate and adhesion enhancement occurs. In the intermediate-energy density range, 0.5 J/cm$^2$ <

$E_\ell < 1.3$ J/cm$^2$, film evaporation begins, and for $E_\ell > 1.3$ J/cm$^2$, a laser-generated plasma forms that shields the sample from the incoming radiation. This shielding leads to a decrease in the specific removal rate of copper, and it is in this last regime that an intermediate compound can form at the substrate surface.

---

1. Summary of paper to be published.
2. Postgraduate fellow from The University of Tennessee, Knoxville, Tenn.
3. Adjunct research and development participant from The University of Tennessee, Knoxville, Tenn.
4. A. J. Pedraza et al., *J. Mater. Sci.* **24,** 15 (1989); *J. Vac. Sci. and Technol. A* **6,** 1763 (1988).

# 6. *Structure of Solids and Surfaces*

This chapter focuses on experimental studies of the structural properties of solids and surfaces. The techniques utilized include electron diffraction, electron microscopy, conventional and synchrotron x-ray diffraction, and surface spectroscopies; work on superconductivity in these programs is reported in Chapter 2.

Determining the arrangement of atoms within the surface region, the changes which occur with variation in temperature and the influence of adsorbates on surface structures continue to be emphasized in the Surface Physics Program. Both electron diffraction and scanning tunneling microscopy have been used to characterize large-scale periodic faceting on transition-metal carbide surfaces. A new high-temperature reconstruction for the Pt(111) surface and a shear displacement of the top layer of K(110) at 20 K, reminiscent of a bulk martensitic phase transition, have been observed. An enhanced mass density in the top layer of Cu(110), following adsorption of N, and the bonding of graphite monolayers to TaC have been determined using synchrotron radiation. Oxidation of K and selective quenching of negative ion resonances in chemisorbed oxygen have been studied.

The Electron Microscopy Program has continued the development of Z-contrast scanning electron microscopy, and the application of this microscopy to SiGe alloys has led to an observation of new types of growth-induced chemical ordering during molecular beam epitaxial deposition. These studies are complemented by experimental and computational investigations of the detailed structure of dislocations in semiconductors and by work initiated on the development of electron energy loss spectroscopy and energy dispersive x-ray analysis on a column-by-column basis.

Synchrotron x-ray diffraction investigations have utilized resonant nuclear scattering to demonstrate coherent and incoherent quasielastic scattering capabilities and 10-neV energy resolution x-ray scattering spectroscopy. Conventional x-ray studies of thin-film photonic materials, semiconductors, and high-temperature superconductors have provided epitaxy and lattice structural information for investigations of advanced film-growth techniques, in collaboration with academic and industrial institutions as well as within the Solid State Division. The X-Ray Diffraction Program is also playing an active role in a collaborative beam line proposal for the Advanced Photon Source.

# SURFACE PHYSICS

## NEW SURFACE RECONSTRUCTIONS ON TaC(110), (310), AND (210) STUDIED BY HIGH-RESOLUTION LEED

*J.-K. Zuo,[1] D. M. Zehner, and J. F. Wendelken*

Surface reconstructions are interesting for understanding the driving forces, for providing a rich testing ground for two-dimensional statistical models of collective phenomena, and for utilization as templates for epitaxial growth. Therefore, the reconstructed TaC(110), (310), and (210) surfaces have been investigated using a high-resolution low-energy electron diffractometer (HRLEED). For TaC(110), numerous extra reflections between integral-order beams in the LEED pattern are observed only along the [1$\bar{1}$0] direction and move back and forth between integral-order reflections with change in electron energy. From results of a detailed model calculation, it is possible to simulate the diffraction behavior and thus to propose that the surface consists of periodic (100) facets propagating along the [1$\bar{1}$0] direction like a ridge-and-valley grating with a complete absence of (110) terraces, as shown in Fig. 6.1(a). The average period of the grating structure is 6 row spacings, involving 15 missing rows. In the model, a distribution of inter-ridge spacing and ridge height of the grating is included also. For the TaC(310), three cycles of single-split-single peak alternation for LEED beams between two particular electron energies have been observed. If the surface were ideally truncated where each unit consists of a (100)

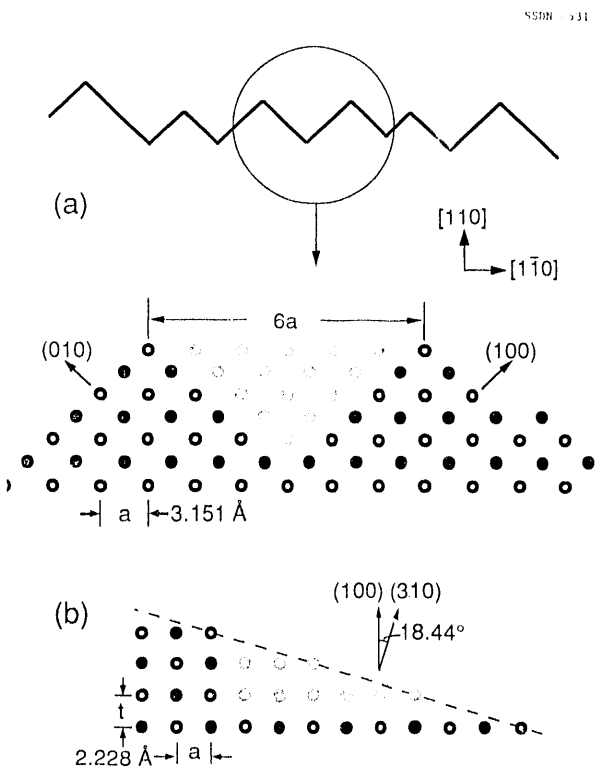


Fig. 6.1. (a) Side view of the alternating (100) and (010) faceting running along the [1$\bar{1}$0] direction for the TaC(110) surface. (b) Side view of the terrace-width and step-height tripling reconstruction for TaC(310) surface. In both cases, the ideally truncated surfaces will include the shaded circles.

terrace, three row spacings wide, and a single-height step, only one cycle of alternation should be observed instead of three.[2] Also, the separation of the split peak, which is a measure of average (100) terrace width, is 1/9 of the separation between integral-order reflections instead of 1/3 for an ideally truncated surface. These data clearly indicate that both the (100) terrace width and step height on the (310) surface are on average tripled [Fig. 6.1(b)], which is equivalent to nine missing rows. A similar reconstruction is also

observed for the TaC(210) surface, except now there are considerable quadruple-height steps coexisting with triple-height steps, and the average (100) terrace width is ~7 row spacings. These new surface structures, involving large mass transport, have not been observed previously.

---

1. Oak Ridge Associated Universities postgraduate research participant.
2. M. Henzler, in *Electron Spectroscopy for Surface Analysis*, ed. by H. Ibach, Vol. 4, Springer-Verlag, Berlin, 1977.

## A DIRECT OBSERVATION OF PERIODIC (100) FACETING ON THE TaC(110) SURFACE BY SCANNING TUNNELING MICROSCOPY

*J.-K. Zuo,*[1] *D. M. Zehner, J. F. Wendelken, and R. J. Warmack*[2]

The TaC(110) surface has been studied by high-resolution low-energy electron diffraction (HRLEED).[3] In that study, using results from a detailed model calculation, it was proposed that the surface consists of alternating (100) and (010) facets propagating along the [1$\bar{1}$0] direction like a ridge-and-valley grating, where (110) terraces are completely missing. The average ridge spacing of the grating is determined to be six lattice spacings (i.e., ~19 Å) in the [1$\bar{1}$0] direction. Also, a distribution of the ridge spacings and heights was proposed.

In order to confirm the proposed structure, an ultrahigh vacuum scanning tunneling microscopy (UHV-STM) investigation was conducted. After modification of an existing STM, structural images from the TaC(110) surface were successfully obtained. Shown in Fig. 6.2(a) is a 700 × 700 Å$^2$ height-mode STM image. A ridge-and-valley grating structure which propagates along the [1$\bar{1}$0] direction can be clearly discerned. Also, this image reveals defects in this structure which result in a corrugation on a larger length scale with

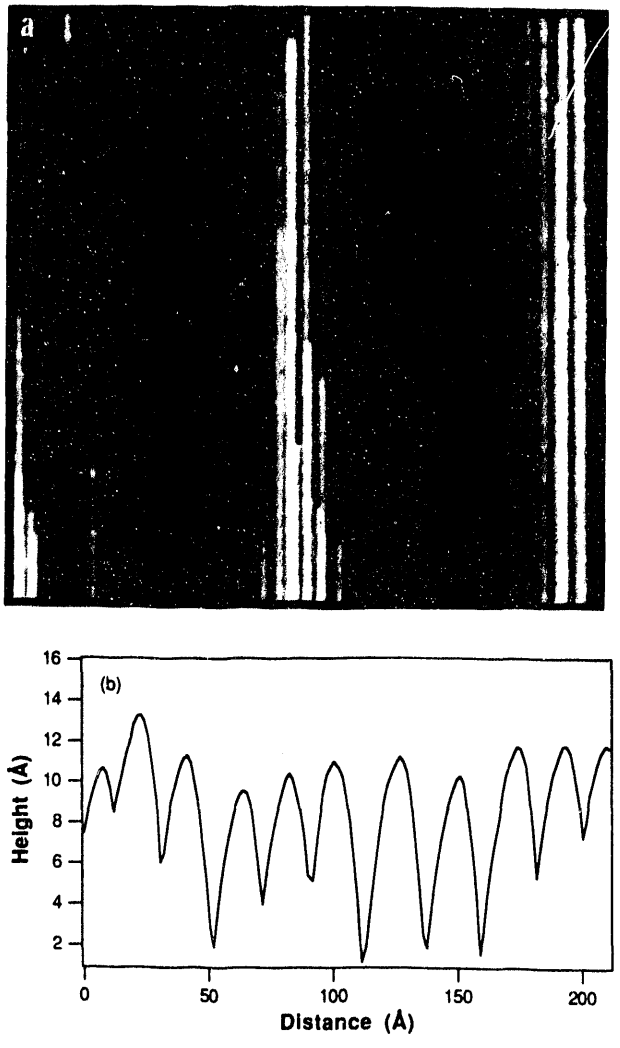


Fig. 6.2. (a) 700 × 700 Å$^2$ height-mode STM image from the TaC(110) surface where bias voltage $V_b$ = 100 mV and tunneling current $I_T$ = 1 nA and (b) line-cut profile for showing the cross section of a local structure.

amplitudes of ≤10 Å. To see the local grating structure, a line-cut profile is plotted in Fig. 6.2(b). As can be seen, the grating is not strictly regular but varies in ridge spacing and height. From a histogram of the ridge spacings, determined from several large area images, it was found that the distribution is indeed peaked at ~19.5 Å, in excellent agreement with our LEED results. The height varies from 2 to 12 Å. Furthermore, slope angles of the valley walls are determined to be 40–45°. This indicates that the valley walls are formed by either the (100) or (010) facets which make an angle of 45° with the (110) plane as determined from LEED data. In addition, it was also found that long-range order along the unreconstructed [001] direction is dependent on the annealing treatment and difficult to detect in the LEED observations.

---

1. Oak Ridge Associated Universities postgraduate research participant.
2. Health and Safety Research Division, ORNL.
3. J.-K. Zuo, D. M. Zehner, and J. F. Wendelken, "New Surface Reconstructions on TaC(110), (310), and (210) Studied by High-Resolution LEED," this report.

## ORIENTATIONAL EPITAXY OF THE HEXAGONALLY RECONSTRUCTED Pt(001) SURFACE[1]

*Doon Gibbs,[2] G. Grübel,[2] D. M. Zehner, D. L. Abernathy,[3] and S. G. J. Mochrie[4]*

An important aspect of the growth of one crystal upon another involves their relative orientation. Specifically, how are the high-symmetry directions of the ad-lattice and of the substrate lattice aligned? The present understanding of this question has been guided by the calculations of Novaco and McTague,[4] who explicitly considered incommensurate monolayers of rare gases adsorbed on a rigid, basal-plane substrate of graphite. These calculations showed that, even though there is no translational registry at the interface, there may exist a preferred orientation. This is called orientational epitaxy. These calculations also revealed that the high-symmetry directions of an incommensurate overlayer may be rotated away from the high-symmetry directions of the substrate and that the rotation angle is determined by the incommensurability of the overlayer.

X-ray scattering has been used to investigate the rotational behavior exhibited by the clean (001) surface of Pt between 300 and 1820 K. Between $T$ = 1685 and 1820 K, the surface reconstructs to form a buckled, hexagonal monolayer on top of the bulk planes of square symmetry lying immediately below. The top layer is incommensurate in both directions within the surface plane. In this phase, a hexagonal high-symmetry direction is aligned with the cubic (1,1,0) direction. As the temperature is reduced below $T$ = 1685 K, there is a structural transformation in which domains of the hexagonal overlayer rotate continuously to angles ±0.9° away from the bulk (1,1,0) direction as shown in Fig. 6.3. Remarkably, the rotational transformation exhibits mean-field behavior. At 1580 K, there is a second, discontinuous

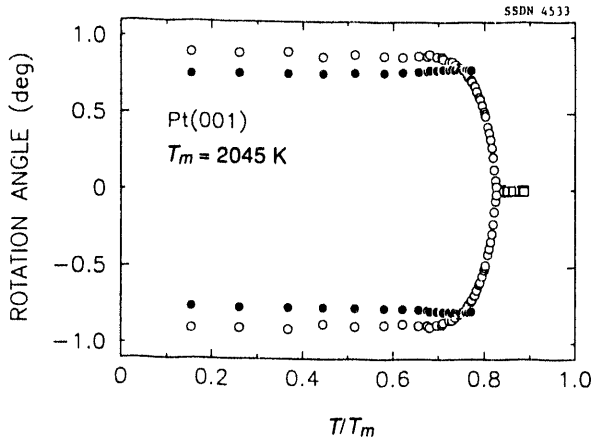


Fig. 6.3. The temperature dependence of the rotation angles of the hexagonal reconstruction for the Pt(001) surface. The temperature is expressed as a fraction of the bulk melting temperature.

transformation, leading to coexistence among domains of a slightly different rotation angle. Throughout the aligned and rotated hexagonal phases, the incommensurability varies only weakly, but in such a way that the area per atom remains approximately constant.

---

1. Summary of papers: *Phys. Rev. Lett.* **67**, 3117 (1991); *Phys Rev. B* **45**, 9272 (1992).
2. Brookhaven National Laboratory, Upton, N.Y.
3. Massachusetts Institute of Technology, Cambridge, Mass.
4. A. D. Novaco and J. P. McTague, *Phys. Rev. Lett.* **38**, 1286 (1977.

## RECONSTRUCTION OF THE Pt(111) SURFACE[1]

*A. R. Sandy,*[2] *S. G. J. Mochrie,*[2] *D. M. Zehner, G. Grübel,*[3] *K. G. Huang,*[3] and *Doon Gibbs*[3]

A simple idea underlies our understanding of the reconstruction of many metal surfaces. Compared with bulk atoms, surface atoms have fewer nearest neighbors. As a result, the surface energy may be reduced for an arrangement which leads to closer packing within the top layer. At the same time, such a reconstruction produces a misfit between the surface layer and those layers below it, which increases the surface energy. The balance of these effects determines the surface structure.

Using x-ray scattering, it was found that Pt(111) is unreconstructed for temperatures <0.65 of the bulk-melting temperature ($T_m$ = 2045), consistent with earlier work. However, our x-ray measurements reveal that above 0.65 $T_m$ the surface undergoes a continuous commensurate-incommensurate transformation into a structure which is isotropically compressed relative to the (111) planes of the bulk. The reconstructed surface layer is composed of ideal stacking regions and faulted stacking regions. Separating these commensurate sublattices are discommensurations (incorporating extra surface atoms). A similar structure has been observed at temperatures above 0.65 $T_m$ for Au(111).[4] Because the arrangement of discommensurations on Pt(111) is translationally disordered, the reconstructed phase is called a discommensuration fluid. Near the transformation, the discommensurations appear to be orientationally disordered as well, resulting in a continuous ring of diffraction surrounding the bulk truncation rods. However, with increasing temperature, the mean separation between discommensurations decreases, and sixfold orientational ordering of the discommensurations develops, as shown in Fig. 6.4.

---

1. Summary of paper: *Phys. Rev. Lett.* **68**, 2192 (1992).

2. Massachusetts Institute of Technology, Cambridge, Mass.
3. Brookhaven National Laboratory, Upton, N.Y.
4. K. G. Huang et al., *Phys. Rev. Lett.* **65**, 3313 (1990).

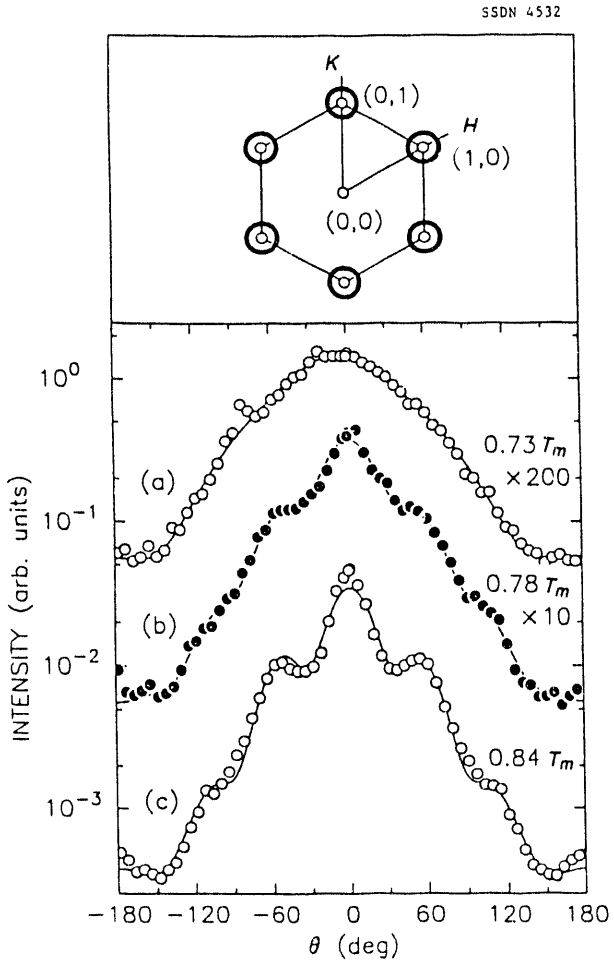


Fig. 6.4. "Ring scans" at (a) 0.73 $T_m$, (b) 0.78 $T_m$, and (c) 0.84 $T_m$. Solid lines are fits. The top panel illustrates the diffraction pattern above 0.65 $T_m$.

## X-RAY SCATTERING DETERMINATION OF THE Cu(110) (2×3)-N STRUCTURE[1]

*A. P. Baddorf, Geir Helgesen,[2] Doon Gibbs,[2] A. R. Sandy,[3] C. You,[3] and S. G. J. Mochrie[3]*

Nitrogen adsorption on Cu(110) results in a chemically inert surface structure involving considerable rearrangement of the copper atoms. The periodicity of the new structure is doubled in the [1$\bar{1}$0] direction and tripled along [001] to form a (2 × 3) reconstruction. Two divergent structural models have been proposed with one claiming the addition[4] and the other the removal[5] of one [1$\bar{1}$0] row of copper from the surface for every three rows on the unreconstructed clean surface. The Cu(110)-(2 × 3)N structure has been examined with a relatively new approach by measuring absolute x-ray reflectivities both to determine the surface structure and to evaluate the technique.

X rays generated at the BNL National Synchrotron Light Source were scattered from the sample surface located in an ultrahigh vacuum chamber. Reflected intensities were measured for eight distinct diffraction beams corresponding to in-plane wave vectors of the reconstructed overlayer. Reflectivities ranged from near 1 at bulk Bragg conditions to $10^{-9}$ at points in between.

The structure was determined by comparing experimental reflectivities with the results of calculations for various structural models. Comparison quickly revealed that the Cu density in the top layer was increased over that of

the clean surface, supporting an additional row model. Detailed calculations support a model which is shown in Fig. 6.5, where [1$\bar{1}$0] rows of

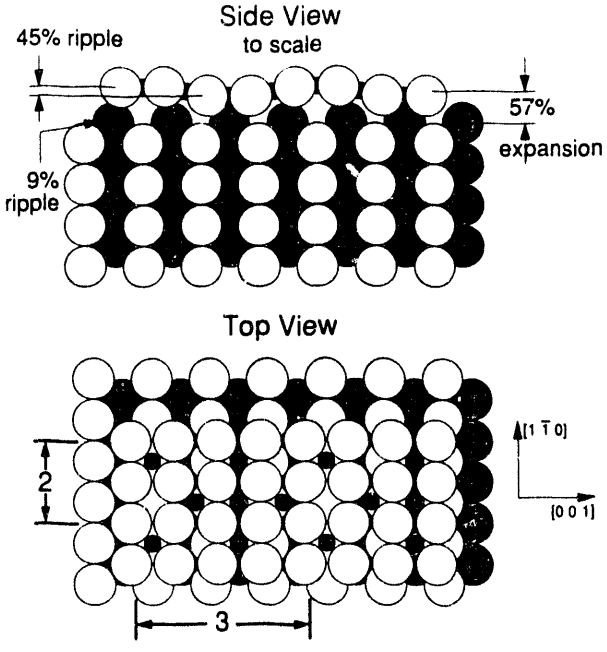


Fig. 6.5. Side and top views of the Cu(110)-(2×3)N structure. Large circles represent Cu atoms, small black circles represent N atoms.

copper are added to increase the Cu density in the top layer to 4/3 (its clean value), and which includes a large buckling in the top layer. It is believed that the resulting valleys were incorrectly interpreted as a missing row in some previous studies.[5]

---

1. Summary of paper to be published.
2. Brookhaven National Laboratory, Upton, N.Y.
3. Massachusetts Institute of Technology, Cambridge, Mass.

4. M. J. Ashwin and D. P. Woodruff, *Surf. Sci.* **237**, 108 (1990).
5. H. Niehus et al., *Phys. Rev. B* **43**, 12619 (1991).

## COMPOSITION AND STRUCTURE OF CLEAN AND OXIDIZED $Mo_{0.75}Re_{0.25}$(001) ALLOY SURFACE

*S. H. Overbury*[1] *and D. M. Zehner*

In order to confirm results of a previous LEED I-V analysis, low energy $Li^+$ ion scattering and LEED were used to investigate the surface structure and first- and second-layer compositions of a $Mo_{0.75}Re_{0.25}$(001) random alloy surface. A clean surface was obtained by heating in oxygen after a standard sputter-annealing treatment. Analysis of shadowing and blocking features from the clean surface are completely consistent with termination of the bcc lattice on a (001) plane. Estimates of the vertical spacing between first and second layers are obtained from measured critical angles as a function of ion energy. From analysis of ion scattering intensities measured at a variety of incident angles and ion energies, it is found that this alloy surface exhibits strong component redistribution with first- and second-layer Mo concentrations which are larger and smaller, respectively, than the bulk average values. These results are completely consistent with those obtained in the LEED analysis and more recent investigations involving x-ray photoemission studies of core-level shifts following oxygen adsorption.

Since the outermost layer is terminated almost completely in Mo, the effect of oxygen

adsorption upon structure and composition was also explored. Adsorption of oxygen near room temperature yields a poorly ordered surface exhibiting an attenuated $p(1 \times 1)$ pattern and weak, diffuse superlattice diffraction features, even following high-temperature anneals. Oxygen causes a thermally activated decrease in the Re single-scattering intensity, interpreted as a loss of Re from the second layer. Adsorption of oxygen at elevated temperatures produces a surface characterized by a $p(2 \times 1)$ LEED pattern. Initial analysis by ion scattering indicates that oxygen adatoms are adsorbed in fourfold hollow sites for both the $p(2 \times 1)$ and poorly ordered surfaces. Evidence for a missing-row reconstruction, observed previously by ion scattering for the oxygen/W(001) system, has not been clearly observed.

---

1. Chemistry Division, ORNL.

## SHEAR DISPLACEMENT OF THE K(110) SURFACE[1]

*B. S. Itchkawitz,[2] A. P. Baddorf, H. L. Davis, and E. W. Plummer[2]*

Investigations of clean alkali metal surfaces are motivated by their utility as experimental touchstones for theoretical descriptions of metal physics. Detailed examinations of the structure of these surfaces have, in the past, been quite limited. This study, using low-energy electron diffraction intensities, provides a detailed, quantitative structural determination of the (110) surface of single-crystal potassium which has surmounted the experimental constraints of high reactivity and low Debye temperature.

In this study, single crystals of K were grown in ultrahigh vacuum by evaporation from a getter source onto a clean Ni(100) substrate. Steps on the substrate allowed growth of a single orientation of crystalline K with several thousand angstroms thickness. Samples were then cooled to 25 K to minimize atomic vibrations. Subsequently, intensities of 38 diffraction beams were measured for electron energies between 30 and 230 eV using a video data acquisition system.

The structure was determined by comparing experimental diffraction intensities with the results of dynamical electron diffraction calculations for various structural models. The best model involves a shear displacement of surface atoms parallel to the surface as shown in Fig. 6.6. The shear displacement found in the

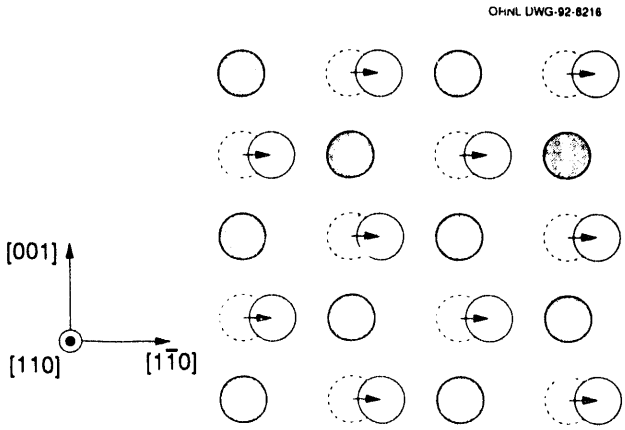


Fig. 6.6. Top view of K(110) structure. White circles represent surface atoms, gray circles represent second-layer atoms, and dashed lines indicate bulk-like structure.

top layer is 0.23 Å along the [1$\bar{1}$0] direction with little or no displacement in second and deeper layers. A small contraction (-0.7%) normal to the surface is also observed between the top two layers.

An analogy for this new surface phase can be made with the bulk martensitic phase transition observed in light alkali metals (Li, Na).[3] These transitions also involve a shear displacement along the [1$\bar{1}$0] direction. No bulk martensitic phase transition has been observed for K; however, a martensitic precursor at the surface has been considered. This study provides evidence of such a precursor.

---

1. Summary of paper: *Phys. Rev. Lett.* **68**, 2488 (1992).
2. University of Pennsylvania, Philadelphia, Pa.
3. P. C. Clapp, *Phys. Status Solidi b* **57**, 561 (1973).

## IDENTIFICATION OF OXYGEN SPECIES ON SINGLE-CRYSTAL K(110)[1]

*A. P. Baddorf and B. S. Itchkawitz*[2]

The interaction of oxygen with potassium has attracted attention in part due to the technological importance of potassium oxides as low work-function materials and their relevance to heterogeneous catalysis. This interaction also provides a unique environment to examine oxygen in a variety of states—monoxide, peroxide, superoxide, and even ozonide. Peroxides and superoxides are important in the oxidation process, in general, and may play a critical role in high-$T_c$ superconductors. However, the oxygen-potassium interaction has been examined previously only in photoemission studies from polycrystalline films.[3] No two studies offered the same interpretations but differed in the number, identification, or order of appearance of the oxygen species with coverage.

This study took a new approach, which involved combining vibrational spectroscopy using high-resolution electron energy loss spectroscopy, x-ray photoemission spectroscopy, and low-energy electron diffraction. Vibrational spectroscopy is well-suited for identification of species and provides a needed new perspective on the oxygen-potassium system. In addition, having discovered a process for growing single crystals of potassium with (110) surfaces, it was possible to observe the formation of ordered surface structures following oxygen adsorption.

In contrast with the interpretations of previous studies, the vibrational results show no molecular oxygen species. Two atomic species are observed after 5-L exposures at 88 K. The first to appear has a vibrational energy of 30 meV and an O 1*s* core-level binding energy at 532 eV. These values indicate chemisorbed atomic oxygen, with formal charge state $O^-$ bound in a multiply coordinated surface site. The second species is associated with an intense 41-meV vibration and a 529-eV O 1*s* core level. This can be identified as $K_2O$, with charge state $O^{2-}$. No long-range order is observed, perhaps due to the coexistence of these species.

Annealing the crystal to 240 K transfers a large fraction of the chemisorbed oxygen to subsurface sites. X-ray irradiation has a similar effect, in what appears to be a direct photochemical process that is not reproduced by electron bombardment. This photon-induced transformation of surface oxygen to subsurface oxygen has not been taken into account in previous photoemission experiments.

Even with considerable atomic oxygen on and below the surface, potassium remains reactive. However, no evidence of a peroxide or superoxide molecular species was observed for exposures up to 100 L.

---

1. Summary of paper: *Surf. Sci.* **264**, 73 (1991).
2. Guest scientist from the University of Pennsylvania, Philadelphia, Pa.
3. S. L. Qiu et al., *Phys. Rev. B* **41**, 7467 (1990); and references therein.

## SELECTIVE QUENCHING OF NEGATIVE ION RESONANCES IN CHEMISORBED OXYGEN ON Pt(111)

*L. Siller,*[1] *J. F. Wendelken, and R. E. Palmer*[2]

An outstanding issue in the study of the negative ion resonances which may be observed in HREELS is the degree to which the fundamental characteristics (i.e., energy, lifetime, symmetry, and decay channels) of the molecular resonance state are perturbed by chemisorption.[3] To address this issue, the HREELS cross sections of molecularly chemisorbed $O_2$ on Pt(111) were investigated and compared with a study of physisorbed $O_2$ on Pt(111).[4] This system is of particular interest because the physisorbed molecule ($T < 40$ K) appears to be a precursor to the chemisorbed species ($T > 40$ K), which itself is a precursor to dissociative adsorption of chemisorbed O atoms.

Two resonances were observed at 7.5 and 4.5 eV in the case of physisorbed $O_2$ on Pt(111) and assigned to the $^4\Sigma_u$ and $^2\Pi_u$ states, respectively. These resonances can be correlated with the $\sigma^*$ and $\pi^*$ resonant states observed in a recent near-edge x-ray adsorption fine structure (NEXAFS) study of the system,[5] since the same valence orbitals are populated in each case. In the case of chemisorbed molecular $O_2$, the $^4\Sigma_u$ resonance (shown in Fig. 6.7), is found to be shifted down in energy by 4 eV compared with the physisorbed molecule to 3.5 eV. A corresponding energy shift was observed in the

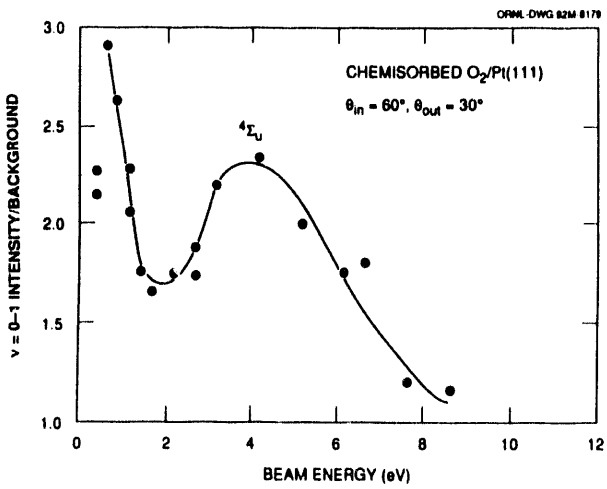


Fig. 6.7. Beam-energy dependence of $\upsilon$ = 0–1 vibration intensity for chemisorbed $O_2$ on Pt(111) showing the $^4\Sigma_u$ resonance at 3.5 eV and a low-energy, unidentified resonance.

NEXAFS study for the $\sigma^*$ resonance. This resonance displays the same angular scattering symmetry in the HREELS experiment, most importantly a node for emission normal to the surface, as was observed in the case of the physisorbed molecule. The $\pi^*$ resonance is even more dramatically perturbed and appears to be quenched selectively as a consequence of chemisorption. The intensity rise near the low-energy threshold shown in Fig. 6.7 indicates a second resonance which is not yet identified.

---

1. Graduate student from University of Cambridge, Cambridge, United Kingdom.
2. University of Cambridge, Cambridge, United Kingdom.
3. R. E. Palmer and P. J. Rous, *Review of Modern Physics* (in press).
4. J. F. Wendelken, L. Siller, and R. E. Palmer, "Observation of Negative Ion Resonances for Physisorbed Oxygen on Pt(111)," this report.
5. W. Wurth et al., *Phys. Rev. Lett.* **65**, 2426 (1990).

## OBSERVATION OF NEGATIVE ION RESONANCES FOR PHYSISORBED OXYGEN ON Pt(111)

*J. F. Wendelken, L. Siller,[1] and R. E. Palmer[2]*

Using high-resolution electron energy loss spectroscopy (HREELS), the negative ion resonance excitations of molecular oxygen physisorbed in a monolayer on Pt(111) have been studied. Two resonances have been observed in the vibrational excitation of the physisorbed molecule over the range $3 < E_i < 13$ eV, as shown in Fig. 6.8. Each resonance shows a distinct angular profile with maximum intensities observed in off-specular directions.

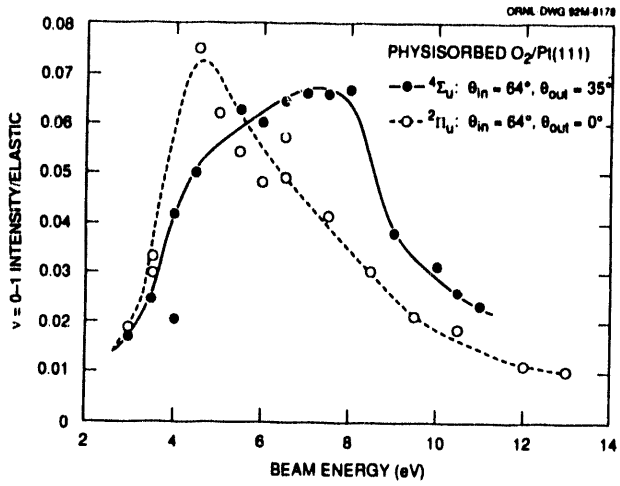


Fig. 6.8. Beam-energy dependence of $\upsilon$ = 0–1 vibration intensity for two scattering geometries which show the $^4\Sigma_u$ and $^2\Pi_u$ resonances for physisorbed oxygen on Pt(111).

From a comparison of the energy and angular dependences to previous results for molecular oxygen adsorbed on graphite,[3,4] the $^4\Sigma_u$ shape resonance at 7.5 ± 0.5 eV and the $^2\Pi_u$ shape resonance at 4.5 ± 0.5 eV have been observed. Electrons emitted from a resonant state reflect the symmetry of the electron orbitals associated with the resonance, and the $^4\Sigma_u$ resonance has an emission node perpendicular to the molecular axis, while the $^2\Pi_u$ resonance emits electrons in this direction. The physisorbed oxygen molecule is known to lie parallel to the surface, and no intensity in the vibrational loss peak with a beam energy of 7.5 eV at an emission angle perpendicular to the surface is observed, while intensity is observed at 4.5 eV at this angle. Preferred emission directions are also preferred excitation directions, and hence, the resonances for molecules which are aligned by adsorption may be excited selectively.

While the geometry of the physisorbed molecule is the same on both platinum and graphite (i.e., parallel to the surface), the energies of both resonances are shifted downward for platinum as compared to the graphite values of 8.5 and 6.5 eV for the $^4\Sigma_u$ and $^2\Pi_u$ resonances, respectively. These shifts are primarily the result of image potential and multiple scattering effects. The $^4\Sigma_u$ energy shift can be explained readily with a simple dielectric theory to be primarily the result of the differing image potentials, but a complete explanation for both resonances will require a detailed multiple scattering calculation.

---

1. Graduate student from University of Cambridge, Cambridge, United Kingdom.
2. University of Cambridge, Cambridge, United Kingdom.
3. E. T. Jensen, R. E. Palmer, and P. J. Rous, *Phys. Rev. Lett.* **65**, 1301 (1990).
4. R. E. Palmer et al., *Phys. Rev. Lett.* **60**, 329 (1988).

## ANGLE-RESOLVED PHOTOEMISSION FROM A MONOLAYER OF GRAPHITE ON THE TaC(111) SURFACE[1]

*B. S. Itchkawitz,[2] P. F. Lyman,[2] G. W. Ownby, and D. M. Zehner*

Recent studies[4,5] comparing the phonon structure of a graphite overlayer on transition-metal carbide surfaces to that of bulk graphite have sought to attribute the deviations between the overlayer and bulk modes to electron transfer from the substrate into the antibonding $\pi^*$-band of the graphite overlayer. Using angle-resolved photoemission and synchrotron radiation, the validity of the rigid-band model has been examined to describe this charge transfer for a graphite monolayer on the TaC(111) surface.

Angle-resolved photoemission of the valence bands in normal emission showed that at $\bar{\Gamma}$ the graphite $\sigma_1$ band energy is -23.0 eV and the $\pi_1$ band energy is -10.3. A linearized augmented-plane-wave calculation of the band structure of an isolated graphite monolayer predicts these energies to be -19.3 and -7.6 eV, respectively.[6] Both the $\sigma_1$ and the $\pi_1$ bands disperse toward $E_F$ with increasing $k_{||}$. In the off-normal spectra, a dip in the density of states was observed at 3.4 eV below $E_F$, even as the $\pi_1$ band dispersed across this region. This low density of states corresponds to the meeting of the bonding $\pi$ and antibonding $\pi^*$-bands at $\bar{K}$, which in bulk graphite occurs at $E_F$.

The experimental and theoretical band energies are compared in Table 6.1. For the graphite monolayer on TaC(111), the rigid-band model would ascribe these energy differences to charge transfer from the

**Table 6.1. Comparison of the experimental electronic band energies of a monolayer of graphite on TaC(111) with the theoretical electronic band energies[5] for an isolated graphite monolayer.**

| | Theory BE (eV) | Experiment BE (eV) | Δ BE(eV) |
|---|---|---|---|
| $\pi$-$\pi^*(\bar{K})$ | 0 | 3.4 | 3.4 |
| $\sigma_1(\bar{\Gamma})$ | 19.2 | 23.0 | 3.8 |
| $\pi_1(\bar{\Gamma})$ | 7.5 | 10.3 | 2.8 |

substrate, which partially fills the antibonding $\pi^*$-band, thereby raising $E_F$ and increasing the binding energy of all the valence bands equally. However, the observed nonuniform energy shifts do not conform to a rigid shift of the bands. Therefore, hybridization between the electronic bands of TaC and the graphite monolayer is not negligible and must be included in descriptions of the electronic band structure of the graphite overlayer.

---

1. Summary of paper to be published.
2. University of Pennsylvania, Philadelphia, Pa.
3. Oak Ridge Associated Universities postgraduate research participant.
4. T. Aizawa et al., *Phys. Rev. Lett.* **64**, 768 (1990).
5. T. Aizawa et al., *Phys. Rev. B* **42**, 11469 (1990).
6. M. Posternak et al., *Phys. Rev. Lett.* **50**, 761 (1983).

## SURFACE ELECTRONIC STRUCTURE AND OFF-SITE AUGER TRANSITIONS ON TaC(111) OBSERVED WITH AUGER-PHOTOELECTRON COINCIDENCE SPECTROSCOPY[1]

*R. A. Bartynski,[2] S. Yang,[2] L. Hulbert,[3] C.-C. Kao,[3] M. Weinert,[3] and D. M. Zehner*

Core-level binding energy shifts have been used widely to characterize the properties of solid surfaces. Physical attributes ranging from chemical state and geometric structure to electronic relaxation energies and screening effects have been inferred from the magnitude and sign of surface core-level shifts. However, most surface properties are governed by the local valence-band configuration. The ability to study valence levels of the first atomic layer of a solid would greatly enhance the fundamental understanding of these properties. This has been accomplished using Auger-photoelectron coincidence spectroscopy (APECS).

By demanding coincidence between emission from the Ta $N_7VV$ Auger transition and the surface-shifted Ta $4f_{7/2}$ core level of TaC(111), the contribution to the Auger spectrum originating from the first atomic layer was isolated and found to be significantly different from the bulk spectrum as shown in Fig. 6.9. The line shape of the coincidence surface Auger spectrum was

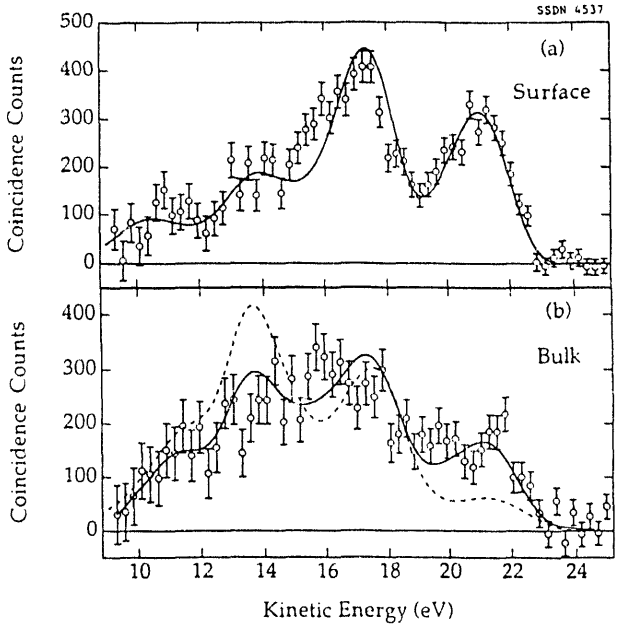


Fig. 6.9. Primary (a) surface and (b) bulk $N_7VV$ Auger spectra. The solid curve in (a) is the SCDOS from the first Ta layer. The dashed curve in (b) is a weighted sum of the SCDOS from second and deeper layers. The solid curve in (b) is the average of the experimental surface Auger spectrum and the SCDOS from second and deeper layers.

well-described by a self-convolution of the valence-band density of states (SCDOS) from the surface layer of a TaC(111) slab calculation. These results indicate that correlation effects are small for this surface and that APECS may be used to monitor atoms at solid surfaces as they are modified by either chemical or physical means. The Auger spectrum obtained in coincidence with the bulk (i.e., second and deeper layers) Ta $4f_{7/2}$ core level shows evidence of a novel off-site Auger transition whereby a core hole in the second Ta layer first hops to a surface Ta site before decaying. A fit to the data requires inclusion of a contribution from the first layer. This observation and similar results obtained earlier for Ta(100) indicate that such hole hopping is a general phenomenon and that off-site Auger transitions cannot *a priori* be dismissed as negligible for covalently bonded systems.

---

1. Summary of paper: *Phys. Rev. Lett.* **68**, 2247 (1992).
2. Rutgers University, Piscataway, N.J.
3. Brookhaven National Laboratory, Upton, N.Y.

# *ELECTRON MICROSCOPY*

## SUB-ANGSTROM MICROSCOPY THROUGH INCOHERENT IMAGING AND IMAGE RECONSTRUCTION[1]

*S. J. Pennycook, D. E. Jesson, A. G. Ferridge,[2] and M. J. Seddon[2]*

In Z-contrast scanning transmission electron microscopy (STEM), it is not necessary to recover the wave function at the crystal exit face nor to determine the projected crystal potential. Therefore, both the phase problem of electron diffraction and the problems of nonlinear imaging associated with conventional high-resolution electron microscopy are effectively by-passed, providing a new and attractive route to sub-Å microscopy.

Z-contrast images are given by a straightforward convolution of a sharp object function, with a comparatively broad probe, which is an ideal situation in which to apply the maximum entropy method to restore the lost high-spatial frequency information. Figure 6.10(a) shows a small region of a Si⟨110⟩ image obtained with a VG Microscope HB501UX. The 2.2-Å resolution is insufficient to resolve the Si dumbbells, although images of individual dumbbells are elongated along the [001] direction, as expected. However, Fig. 6.10(b) shows a maximum entropy reconstruction of the image performed with the Cambridge MemSys 5 software of S. G. Gull and J. Skilling.[3] The reconstruction has resolved the dumbbells (though with some rotation due to sample tilt) giving an average separa-

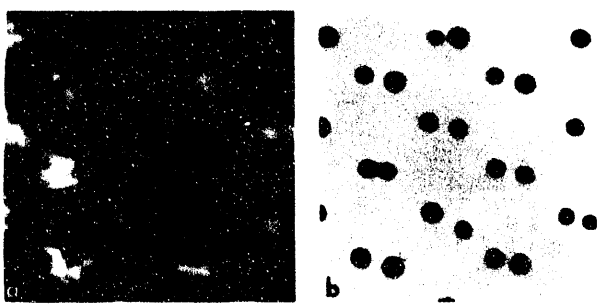


Fig. 6.10. (a) Z-contrast image of Si⟨110⟩ and (b) maximum entropy reconstruction resolving the two atomic columns of the dumbbells.

tion of 1.33 ± 0.20 Å for the two columns of a dumbbell, remarkably close to the true value of 1.36 Å and almost a factor of 2 below the original image resolution.

It is believed that the maximum entropy method will provide a similar enhancement to the ~1.2-Å resolution images that are predicted for the 300-keV Z-contrast STEM (on order), since the width of the object function would still be almost an order of magnitude below the theoretical minimum probe size. This would allow sub-Å information to be extracted from Z-contrast images in a simple and robust manner.

---

1. Summary of paper to be published.
2. The Wellcome Research Laboratories, Beckenham, Kent, United Kingdom.
3. S. F. Gull and J. Skilling, *IEEE Proc.* **131F**, 646 (1984).

## DIRECT IMAGING OF THE ORDERED PHASE IN $Si_xGe_{1-x}$ ALLOYS BY Z-CONTRAST SCANNING TRANSMISSION ELECTRON MICROSCOPY[1]

*D. E. Jesson, S. J. Pennycook, J.-M. Baribeau,[2] and D. C. Houghton[2]*

Since bulk diffusion at typical molecular beam epitaxy growth temperatures (~400°C) is negligible, lateral segregation occurring at the surfaces during growth is essentially frozen into the bulk. The as-grown microstructure, therefore, acts as a fingerprint for surface atomistic processes, and cross sectional Z-contrast images provide a unique way of accessing these processes experimentally.

A typical image of a $Si_{0.6}Ge_{0.4}$ alloy is shown in Fig. 6.11(a). The brighter spots consist of Ge-rich dumbbell columns [Fig. 6.11(b)], and the less bright spots consist of Si-rich dumbbell columns. Clearly, the alloy is not random but consists of alternating Si-rich, Ge-rich (111) planes. These observations can be explained by continuing the lateral segregation model[1] for successive layers of growth. Assuming that the subsurface strain set up by the compositional ordering begins to influence the phase of the

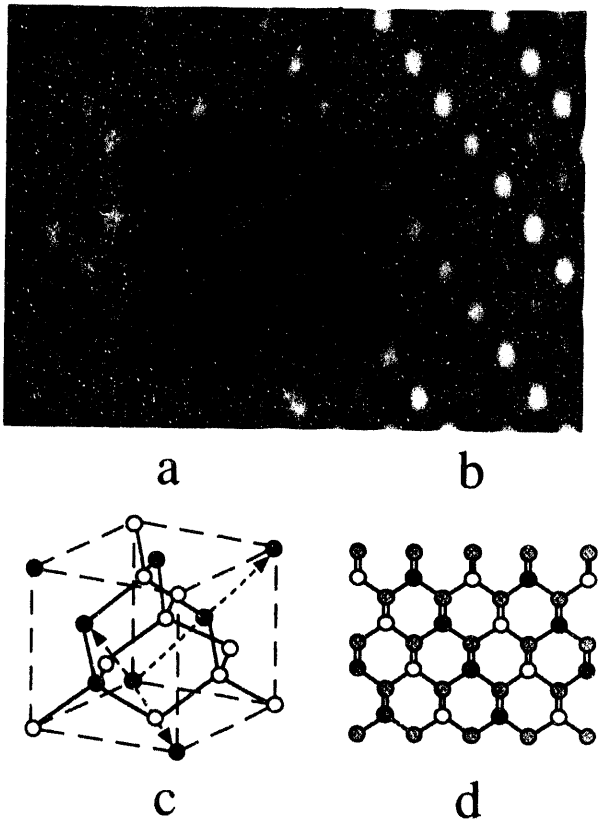


Fig. 6.11. Experimental (a) and simulated (b) images showing the [110] projection (d) of a new ordered phase (c). The dashed arrows define the primitive unit cell of the new ordered phase.

surface dimerization during the initial stages of island nucleation, the model generates new long-range-ordered structures shown in Figs. 6.11(c) and 6.11(d). Image simulation of the [110] projection of the structure [Fig. 6.11(b)] produces excellent agreement with experiment [Fig. 6.11(a)]. It is important to realize that this structure represents a significant departure from current preconceptions of the ordered phase in these alloys. The structure is monoclinic (space group Bm) and is ordered along two sets of (111) planes, which may have important implications for the electro-optical properties of $Si_xGe_{1-x}$ alloys. More fundamentally, the observation of this structure by Z-contrast imaging lends strong credence to the lateral segregation model and provides important insight into semiconductor growth.

---

1. Summary of paper: *Phys. Rev. Lett.* **68**, 2062 (1992).
2. National Research Council of Canada, Ottawa, Canada.

## STEP-DRIVEN LATERAL SEGREGATION DURING MOLECULAR BEAM EPITAXIAL GROWTH OF $Si_xGe_{1-x}$ ALLOYS[1]

*D. E. Jesson, S. J. Pennycook, J.-M. Baribeau,[2] and D. C. Houghton[2]*

Despite the obvious scientific and technological importance of $Si_xGe_{1-x}$ alloys, little is known about the fundamental atomistic processes which occur at step edges during molecular beam epitaxy (MBE) growth. In particular, it is not known how these processes influence the atomic-scale structure of as-grown material.

It is well-known that under conditions of high supersaturation, Si homoepitaxy proceeds via the propagation of type $S_B$ steps[3] associated with monolayer height islands.[4] However, the island edge consists of both high-energy and low-energy $S_B$ steps as shown in Fig. 6.12. The high-energy step has energetically costly dangling bonds, whereas the edge atoms of the low-energy step are rebonded. Both steps would like Ge atoms to occupy the shaded binding sites at the step edges (since Ge has a lower surface energy than Si) so that both

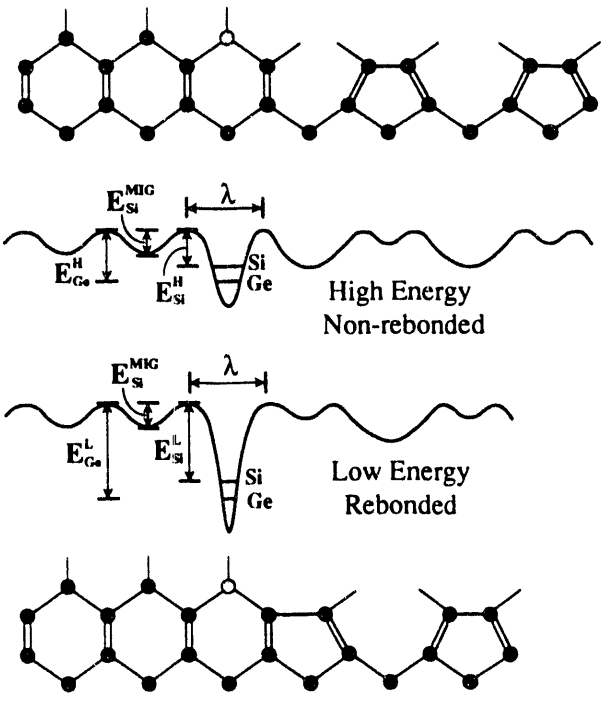


Fig. 6.12. [110] projection of high-energy non-rebonded and low-energy rebonded type $S_B$ steps with accompanying energy level schematics.

steps will compete for available Ge in the reservoir of mobile atoms surrounding the island. A simple rate equation analysis of island growth[1] enables us to calculate the Si composition of the low-energy and high-energy $S_B$ steps as a function of temperature. No ordering was found at low- or high-growth temperatures due to the respective atom trapping or equilibrium segregation behavior at the step edges. However, at intermediate temperatures, the two steps behave very differently. The low-energy step acts as an effective atom trap whereas the high-energy step moves toward its equilibrium segregation value and becomes Ge rich. Therefore, the model predicts growth-induced compositional ordering within an island as a result of nonequilibrium growth. This is the first suggestion that atomic-scale microsegregation can occur laterally at nonequivalent steps during MBE growth and represents a new physical explanation for compositional ordering in semiconductor systems.

1. Summary of paper: *Phys. Rev. Lett.* **68**, 2062 (1992).
2. National Research Council of Canada, Ottawa, Canada.
3. D. J. Chadi, *Phys. Rev. Lett.* **59**, 1691 (1987).
4. R. J. Hamers, U. K. Köhler, and J. E. Denuth, *J. Vac. Sci. and Technol. A* **8**, 195 (1990).

## ATOMIC STRUCTURE OF INTERFACIAL MISFIT DISLOCATIONS[1]

*M. F. Chisholm, M. Mostoller, T. Kaplan, and M. Karimi*[2]

The atomic structure of perfect dislocation cores in the $Si_xGe_{1-x}$/Si (001) interface has been investigated experimentally with high-resolution Z-contrast imaging and simulated theoretically with molecular dynamics calculations. This information is of great significance for the formation of dislocations, dislocation mobility, and the role of dislocations as point-defect sources and sinks, which are all highly dependent on the core structure. In Ge-rich films on Si that are constrained by a capping oxide to grow layer by layer, it was observed that perfect dislocation cores have nearly non-existent dissociation widths and reside entirely in the Ge-rich film. The observed atomic structure and interfacial offset of the cores are being compared with structures calculated by dynamical simulations using empirical many-body potentials in order to test the range of applicability of published Si/Ge potentials and to provide input for new potentials.[3]

It is known that the energetics of nontetrahedral bonded structures in Si and Ge are often poorly predicted by classical potentials. Therefore, our initial simulation efforts have centered on perfect edge dislocations in model single crystals and in model Si/Ge bicrystals because this defect has been predicted to produce no dangling bonds and to maintain fourfold coor-

dination[4] (Figure 6.13). The strain energy associated with this defect was fit to the predictions of elasticity theory to obtain an estimate of the dislocation core radius and core energy parameter. The values obtained were in very good agreement with those deduced from the observations of dislocation nucleation in $Si_xGe_{1-x}$ films on Si.

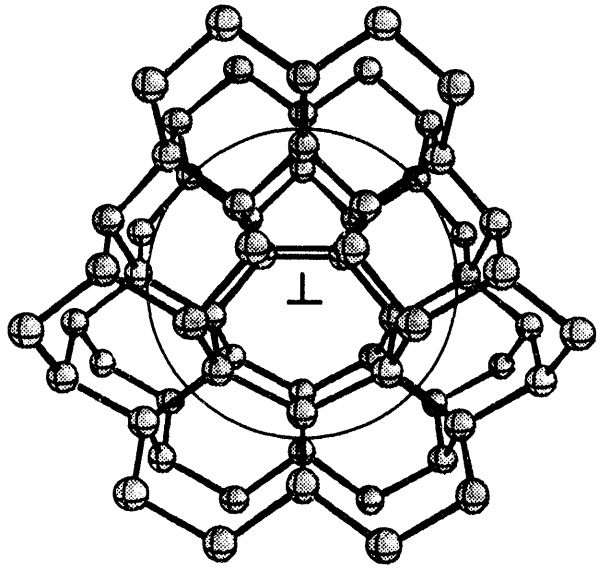

Fig. 6.13. Edge dislocation ($b = a/2$ [1 $\bar{1}$0]) core viewed along the [110] direction as calculated using the Stillinger-Weber Si potential.[5] The circled rings of five and seven atoms seen in the core are expected to be a common defect feature in diamond cubic material surfaces and grain boundaries.

In order for this or any potential to be used with confidence, it is necessary to combine calculations with detailed experimental observations. Using this synergistic approach, it has been found that the Stillinger-Weber potentials[5] must be modified in order to reproduce the observed dislocation offset at Ge/Si interfaces. The parameters of the new model will be adjusted to provide a better fit to the elastic constants and, more generally, the lattice dynamics of Si and Ge.

---

1. Summary of paper to be published.
2. Oak Ridge Associated Universities faculty research participant from Alabama A&M University, Normal, Ala.
3. M. Mostoller et al., "Simulations of $(a/2)$[110] Edge Dislocations in Si, Ge, and Ge-Si Films," this report.
4. J. Hornstra, *J. Phys. Chem. Solids* **5**, 129 (1958).
5. F. H. Stillinger and T. A. Weber, *Phys Rev. B* **31**, 5262 (1985).

## SURFACE NUCLEATION OF PARTIAL DISLOCATIONS IN HIGHLY STRAINED SiGe FILMS ON Si(001)[1]

*M. F. Chisholm and S. J. Pennycook*

Using the implantation and oxidation technique,[2] it has been possible to extend layer growth of Ge-rich films on Si to a thickness 3 to 6 times greater than that previously obtained. Additionally, misfit accommodation is seen clearly to be initiated by the nucleation of Shockley partial dislocations at the film/oxide interface, just as predicted by Hirth 30 years ago.[3] Strain relaxation is observed to be delayed to the limit which is set by spontaneous slip. That is, the formation of misfit dislocations (as surface nucleated half-loops) occurs at the critical shear stress of the material. There is no indication that the dislocations are catalyzed by obvious stress concentrators or produced by the reaction of other dislocations. Figure 6.14 is the

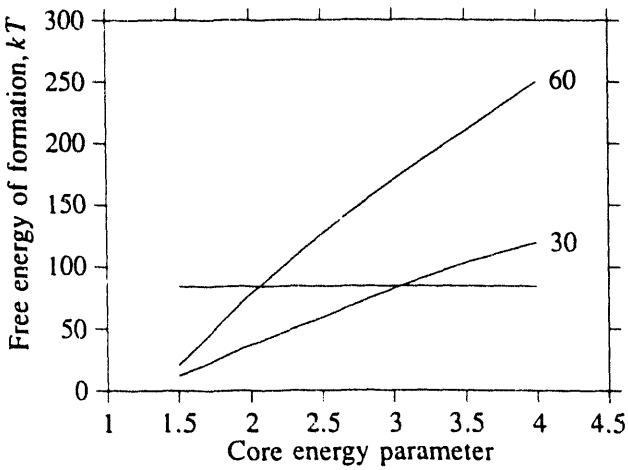


Fig. 6.14. Calculated barrier to dislocation formation as a function of the core-energy parameter for the two most likely surface nucleated half-loops. The horizontal line is the upper limit of a barrier to formation consistent with an appreciable nucleation rate.

calculated barrier of formation for the 30° Shockley partial dislocation and for the 60°-type perfect dislocation as a function of the core-energy parameter. For an appreciable nucleation rate per unit volume, the barrier must be <85 $k_BT$. Since it is observed that strain relief is initiated by the formation of the partial dislocations, the core energy parameter should have a value between 2 and 3. This is considerably larger than the values deduced by others in lower misfit SiGe films grown by more conventional techniques. However, because the implantation and oxidation growth technique provides access to a regime of film thickness and strain where uncertainties in the dislocation generation mechanism and the film strain state are significantly reduced, it is believed that the half-loops which have been observed in the low misfit films are the result of heterogeneous nucleation or dislocation multiplication mechanisms. One important implication of these results is that if the heterogeneous dislocation nucleation sites can be eliminated, highly strained dislocation-free SiGe films would be stable at conventional processing and operating temperatures with respect to the spontaneous formation of dislocations. This would allow significant advances in heterojunction physics and device technology due to the observed beneficial role of strain in modifying optical and electronic properties of semiconductors.[4]

---

1. Summary of paper to be published.
2. O. W. Holland et al., *Appl. Phys. Lett.* **51**, 520 (1987).
3. J. P. Hirth, p. 218 in *The Relation between the Structure and Mechanical Properties of Metals* H.M.S.O., London, 1963 .
4. T. P. Pearsall, *Thin Solid Films* **184**, 451 (1990).

## DIRECT ATOMIC IMAGING OF INTERFACES[1]

*S. J. Pennycook and D. E. Jesson*

The incident electron probe in the scanning transmission electron microscope (STEM) consists of a converging spherical wave, which necessitates a coherent angular integration of fast-electron Bloch states to describe the electron wave function inside a crystal. However, since only tightly bound nondispersive s-type Bloch states contribute to the Z-contrast image, accurate image simulation can be achieved with states calculated for axial illumination. In addi-

tion, the thickness integration needed to simulate the image can be performed analytically.

A particular advantage of the Z-contrast approach over phase-contrast imaging is that the object function depends only on the intensity of the *s* states, not their eigenvalues. Therefore, these images are relatively insensitive to small overlaps of the tails of the potentials from neighboring strings, so proximity effects are avoided and direct imaging is achieved.

In complex situations, then, accurate simulations can be based on *s* states calculated for simple model unit cells, one for each type of string present. For instance, in the case of the $(YBa_2Cu_3O_{7-x})_m(PrBa_2Cu_3O_{7-x})_n$ superlattices, it was found that convergence of a full 241 beam calculation for the complete unit cell could be achieved with a 3-Å spacing of strings using only 45 beams. The ratio of integrated intensities along Y strings compared to Pr strings is shown in Fig 6.15, with and without absorption.

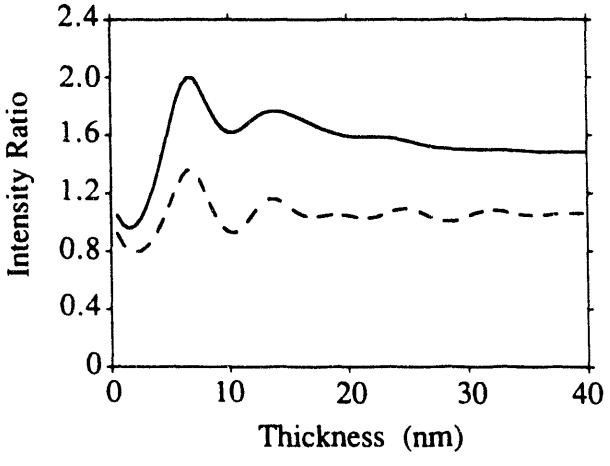


Fig. 6.15. Ratio of integrated intensities in Y to Pr as a function of thickness using full dynamical calculations with model unit cells, with absorption (solid line) and without absorption (dashed line).

The experimental results on this material are intermediate between these two extremes, indicating that conventional absorption models[2] need to be modified to describe accurately the thickness dependence of Z-contrast images from heavy strings.

---

1. Summary of paper: *Acta Metallurgica* (in press).
2. D. M. Bird and Q. A. King, *Acta Crystallogr. A* **24**, 390 (1968).

## THE DEPENDENCE OF Z-CONTRAST IMAGES ON CRYSTAL TILT AND MICROSCOPE MISALIGNMENTS[1]

*D. E. Jesson and S. J. Pennycook*

One of the major limitations of conventional phase-contrast microscopy is the sensitivity of the image to small crystal tilts and/or misalignments.[2] This can give rise to confusing and sometimes misleading information when studying crystal projections and interfaces. Incoherent Z-contrast imaging overcomes many of the limitations associated with coherent imaging methods, including no confusing contrast reversals with specimen thickness or objective lens defocus.[3] Therefore, an outstanding question remains as to what extent does Z-contrast imaging also overcome the tilt and misalignment problems associated with phase-contrast imaging.

Figure 6.16 shows a montage of Z-contrast images obtained from Si⟨110⟩. Each image (A–F) corresponds to a specific crystal tilt as shown on the accompanying large-angle channeling pattern. Image A was obtained with the

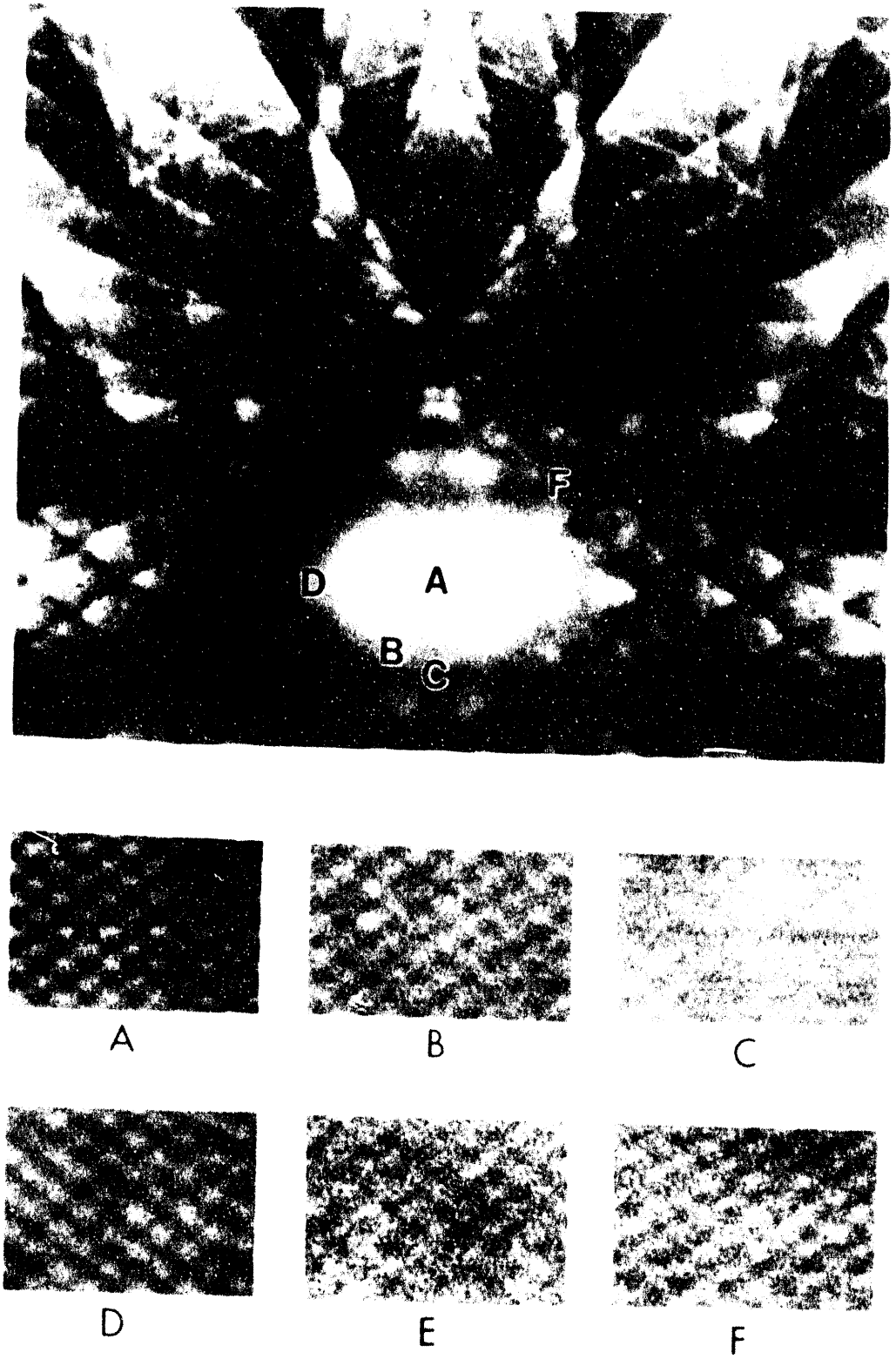


Fig. 6.16. Montage of Z-contrast images obtained from Si⟨110⟩. Images A–F correspond to a specific crystal tilt as shown on the accompanying large-angle channeling pattern. Point G on this image defines the center of a displaced objective aperture where the image became swamped by the background.

beam perfectly along the [110] zone axis and corresponds to point A on the channeling pattern. The distance A–C corresponds to 12 mrad.

Remarkably, the image remains constant over the entire tilt range. The major effect of tilt is a decrease in the peak to background resulting from a change in the effective probe at the surface with a smaller proportion of s-states being excited. However, unlike phase contrast, no confusing artifacts are present in the image. Similarly, Z-contrast images are insensitive to misalignments, point G corresponding to the center of a displaced objective aperture where the image became swamped by the background.

These results demonstrate that under standard operating conditions, crystal tilts and misalignments will not hinder the study of materials by Z-contrast imaging.

---

1. Summary of paper to be published.
2. D. J. Smith et al., *Ultramicroscopy* **11**, 263 (1983).
3. S. J. Pennycook and D. E. Jesson, *Phys. Rev. Lett.* **64**, 938 (1990).

## COLUMN-BY-COLUMN ENERGY DISPERSIVE X-RAY ANALYSIS

*N. D. Browning*[1] *and S. J. Pennycook*

While the Z-contrast[2] imaging technique can give a good representation of the structure of a material, a spectroscopic compositional analysis is not possible. As was shown elsewhere in this report,[3] local band structure and light element composition can be determined by electron energy loss spectroscopy (EELS). However, for elements with a mass number $Z > 10$, it is difficult to find a suitable absorption edge in the range where the EELS signal is localized at the probe ($\Delta E > 200$ eV) and is within the detection range of the spectrum recording system (<1000 eV). This range can be addressed by x-ray fluorescence, because for energy dispersive x-ray (EDX) analysis, the range of the detector is 0–20 keV, making it possible to find characteristic peaks for most elements. In addition, the signal is highly localized at the atom site making a column-by-column compositional analysis possible.

The x-ray detector in the scanning transmission electron microscope (STEM) is situated in the pole-piece of the objective lens. The conventional formation of the convergent probe by an objective aperture generates X rays by electron collisions with the aperture blade which swamp the signal from the specimen. However, by inserting a "virtual objective aperture" at an optically equivalent position to the objective aperture, but sufficiently far away enough to avoid contribution to the detected x-ray signal, this is eliminated. Forming the optimum probe with this configuration requires a retuning of the microscope lenses, but it has been shown that the 2.2-Å Z-contrast spatial resolution can be retained.

Column-by-column EDX will be important for the study of compositional changes at interfaces and defects (e.g., grain boundary segregation). Additionally, with the virtual objective aperture configuration, both EELS and x-ray

signals can be recorded simultaneously from individual atomic columns, using Z-contrast imaging to position the probe. Column-by-column imaging and analysis represent a long-awaited link between high-resolution electron microscopy and analytical electron microscopy.

---

1. Oak Ridge Associated Universities postgraduate research participant.
2. S. J. Pennycook and D. E. Jesson, *Phys. Rev. Lett.* **64**, 938 (1990).
3. N. D. Browning and S. J. Pennycook, "Column-By-Column Electron Energy Loss Spectroscopy," this report.

## COLUMN-BY-COLUMN ELECTRON ENERGY LOSS SPECTROSCOPY

*N. D. Browning[1] and S. J. Pennycook*

Electron energy loss spectroscopy (EELS) is a well-established and very sensitive technique for the microanalysis of materials. The energy lost by a transmitted electron beam is characteristic of the chemical composition and electronic structure of the specimen. Collection of such information from individual atomic columns in materials is being attempted by combining EELS with Z-contrast imaging. A major concern, however, is the range over which a fast electron can cause a particular excitation event, which is described classically by the impact parameter, $b$. A root mean-square impact parameter can be defined as[2]

$$b_{RMS} = \frac{\hbar v \theta_{max}}{\Delta E\left[(\theta^2_{max}+\theta^2_E)ln\left(1+\frac{\theta^2_{max}}{\theta^2_E}\right)\right]^2}$$

where $\Delta E$ is the energy loss, $v$ is the electron velocity, $\theta_{max}$ is the aperture limited cut-off angle, and $\theta_E = \Delta E/2E$ ($E$ is the incident beam energy). In a scanning transmission electron microscope (STEM), the experimental spatial resolution limit is given by adding the probe size (~2.2 Å for the VG HB501UX STEM) and the impact parameter in quadrature. Figure 6.17 shows the spatial resolution of the energy-loss signal as a function of collection angle for various energy losses. For energy losses above ~300 eV and a collection angle of 30 mrad, the spatial resolution of the energy-loss signal is comparable to the resolution obtainable by Z-contrast imaging.[3] Because the Z-contrast technique

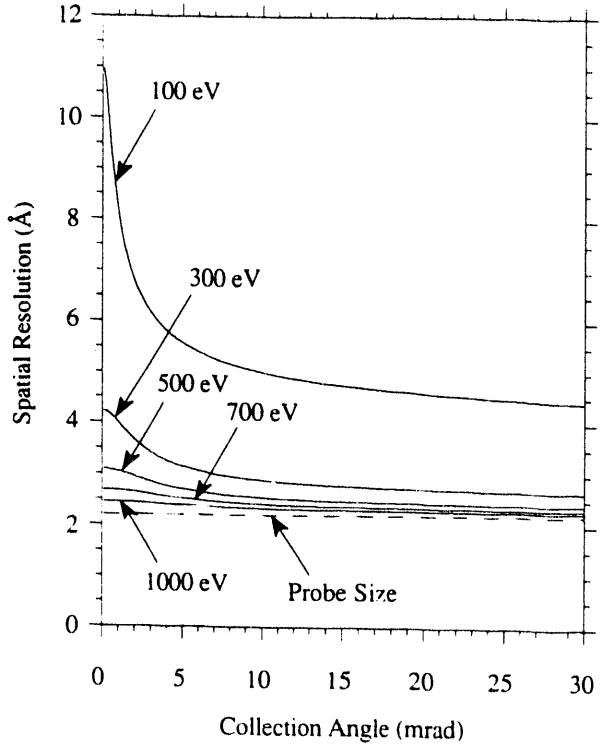


Fig. 6.17. The effective probe size as a function of collection angle for a series of energy losses.

requires the same operating conditions as needed to perform EELS, it can be used to position the electron probe on a particular atom column.

These two complementary techniques will be of particular importance in studying the high-temperature superconductor $YBa_2Cu_3O_{7-\delta}$, where the Z-contrast technique can determine accurately the positions of the heavy metal elements, but not the important oxygen atoms. The oxygen K-edge spectrum can be used to quantify the oxygen concentration to <1% and provide information on the local band structure.[4] Therefore, by using Z contrast and EELS together, grain boundaries and other defects in $YBa_2Cu_3O_{7-\delta}$ can be investigated with regard both to composition and to band structure.

---

1. Oak Ridge Associated Universities postgraduate research participant.
2. S. J. Pennycook, *Contemp. Phys.* **23**, 371 (1982).
3. S. J. Pennycook and D. E. Jesson, *Phys. Rev. Lett.* **64**, 938 (1990).
4. N. D. Browning, J. Yuan, and L. M. Brown, *Supercond. Sci. Technol.* **4**, S346 (1990).

## NEW APPROACHES TO PRECISION TRANSMISSION ELECTRON MICROSCOPE (TEM) SPECIMEN PREPARATION

*J. T. Luck and M. F. Chisholm*

The goal of specimen preparation for the TEM is to produce quickly and consistently an electron transparent specimen with no mechanical artifacts. The major problem in preparing cross-section samples is the differential ion milling of the glue, the film, and the substrate. Often, either the film or substrate will mill away completely before the other is electron transparent. A new approach involving mechanically thinning to <1 μm is being developed to minimize the ion milling time required. With this process, it should be possible to thin a TEM plan view or cross section to <1 μm, sometimes to as thin as 500 Å, in less than 8 h.

This method uses a tripod polisher equipped with three micrometers that allows the specimen to be tilted parallel to the plane of polish defined by the polishing wheel. This particular method of sample preparation produces a uniformly thin specimen. Using an L-shaped attachment and only two of the micrometers, a wedge-shaped specimen is produced that is thinnest at the edge of interest and gradually increases in thickness. Both approaches eliminate the need for ion milling.

For each of the above techniques, it has been found that the polishing wheel must be polished to a mirror finish and covered by a flat glass plate to prevent damage to the specimen caused by bumps under the polishing cloth. The polishing media are silicon carbide or diamond lapping films and SYTON HT-50, GLANZOX, or INSEC chemical polishes, depending on the sample material. It was found that the grit size must be reduced gradually from 60 to 0.5 μm (removing at each step at least 3 times the grit diameter used previously) to remove material damaged by the previous size grit. At no time is any pressure applied to the polisher.

It is possible to polish mechanically Si directly to electron transparency (<0.5 μm) using this method, and as the method is perfected,

final sample thicknesses consistently <1 μm will be obtained. As a result, the ion milling time will be reduced greatly, which in turn will significantly improve our ability to prepare difficult sample materials (e.g., the oxide superconductors).

## MOLECULAR BEAM EPITAXY (MBE) SYSTEM TO STUDY GROWTH MECHANISMS OF SiGe ALLOYS AND MULTILAYERS

*E. Takasuka,*[1] *D. E. Jesson, J. F. Wendelken, T. C. Estes, and S. J. Pennycook*

A research-scale MBE unit has been constructed specifically to study atomic-scale growth processes in the Si-Ge system. Since bulk diffusion is negligible at typical growth supersaturations, the atomic processes occurring at the surface during growth are frozen into the as-grown microstructure and are accessible directly by cross-sectional Z-contrast imaging. By growing specially tailored specimens in this unique way, growth kinetics (using monolayer Ge markers), microsegregation, and the metastable routes involved in two-dimensional to three-dimensional growth, as well as dopant segregation mechanisms and the atomistic role of surfactants, may be studied. Using amorphous capping layers, it may also be possible to study atomic-scale island growth through plan-view imaging in the 300-kV scanning transmission electron microscope. This would be similar to scanning tunneling microscopy but with the exciting prospect of distinguishing Si and Ge atoms.

The system has a small growth chamber for research-scale MBE with two e-beam sources and an effusion cell. To obtain atomic-scale growth control of alloys and multilayers, each e-beam source is provided with an electron impact emission spectroscopy rate controller. The sample holder has the capacity to heat a 1-in.-diam substrate to 1000°C with a pyrolytic boron nitride heater, which provides the least contamination with good temperature uniformity. The vacuum is on the order of $10^{-10}$ Torr, and a load-lock system provides for sample transfer.

In situ growth observation can be performed using reflection high-energy electron diffraction (RHEED). Figure 6.18(a) shows a RHEED pattern of a (2 × 1) Si(100) reconstructed sur-

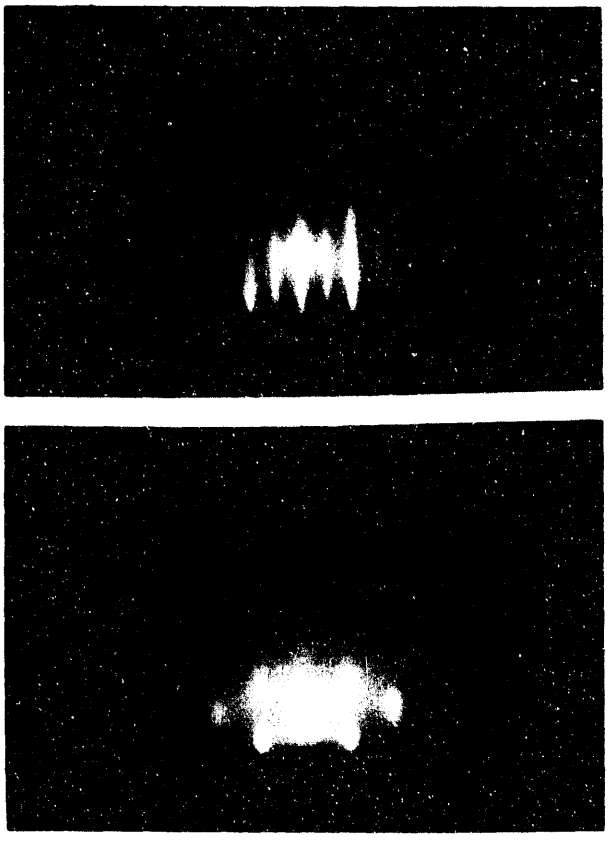

Fig. 6.18. RHEED pattern of (a) smooth (2 × 1) Si(100) reconstructed surface and (b) subsequent three-dimensional growth of Ge.

face. This clean and smooth surface was obtained by 800°C annealing in a $10^{-9}$-Torr vacuum followed by Si buffer layer growth. Figure 6.18(b) shows a RHEED pattern of a Ge surface layer grown on Si(100) at 600°C. The spotty pattern reveals the expected three-dimensional island growth of Ge on Si.

---

1. Guest Scientist from Sumitomo Metal Industries, Ltd., Amagasaki, Japan.

## DIRECT IMAGING OF GaAs/Si HETERO-INTERFACES[1]

*E. Takasuka,[2] S. J. Pennycook, M. F. Chisholm, K. Asai,[3] and K. Fujita[3]*

The excellent properties of compound semiconductor materials (e.g., high mobilities and direct band gaps) prompt a wide range of research on the fabrication of high-speed devices and electro-optic devices. For example, compound semiconductor growth on Si (e.g., GaAs/Si) is of major interest in attempts to integrate the desirable properties of compound semiconductors with the mature technology of Si.[4] However, differences in lattice constant and thermal expansion between epitaxial layer and substrate lead to many interfacial defects which are of major concern for device properties. Direct imaging by Z-contrast scanning transmission electron microscopy (STEM) has been used to probe the interface and the origin of the defects to gain some insight on ways to suppress defect generation.

Figure 6.19(a) shows a Z-contrast image of the interface of GaAs/Si. The GaAs layers were grown by molecular beam epitaxy (MBE) at a temperature of 650°C and a growth rate of 100 Å/min. The substrate surface roughness and the atomic-scale location of stacking faults in the epitaxial layer are easily identified through the image contrast, which depends on atomic number. In situ reflection high-energy electron diffraction (RHEED) observations have not been able to indicate such surface roughness. The higher magnification image [Fig. 6.19(b)] shows that the stacking faults originate mainly on surface steps and occasionally from an irregularity on the surface. This irregularity may be precipitated surface con-

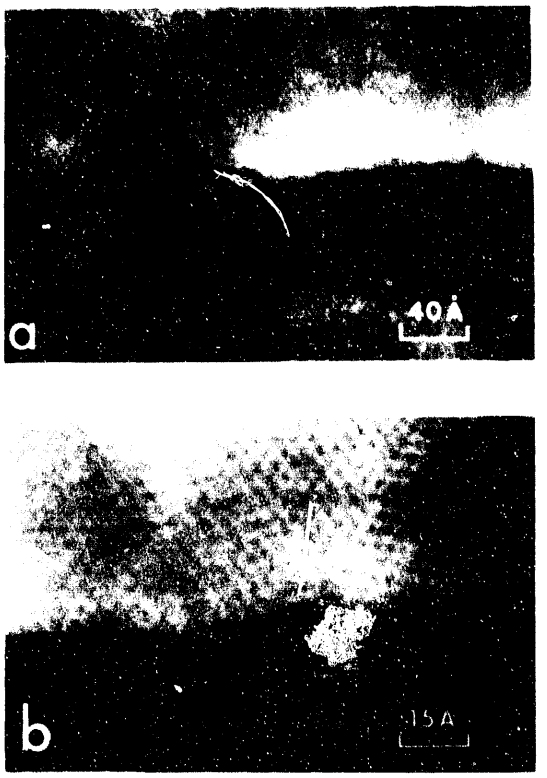


Fig. 6.19. Z-contrast image of GaAs/Si interfaces showing (a) surface roughness and grown-in stacking fault and (b) stacking fault originating from a surface irregularity.

tamination (e.g., SiC), and further investigation by a spectroscopic technique such as electron energy loss spectrometry (EELS) will be needed. By RHEED observations, the growth is shown to be three dimensional. The surface step, or the irregularity, which is shown in Figs. 6.19(a) and 6.19(b) is a likely coalescence site for the islands. The fine-scale roughness could be a trigger for the grown-in defects present in the epitaxial layer.

The atomic-scale compositional sensitivity of Z-contrast STEM and its ability to distinguish interface roughness from interdiffusion are proving very useful in understanding and controlling process-induced defects in epitaxial semiconductor materials.

---

1. Summary of paper to be published.
2. Guest Scientist from Sumitomo Metal Industries, Ltd., Amagasaka, Japan.
3. Sumitomo Metal Industries, Ltd., Amagasaka, Japan.
4. S. F. Fang et al., *J. Appl. Phys.* **68**, R31 (1990).

# *X-RAY DIFFRACTION*

## RESONANT NUCLEAR BRAGG SCATTERING FROM A MOSAIC $^{57}Fe_2O_3$ CRYSTAL[1]

*J. Z. Tischler, B. C. Larson, G. E. Ice,[2] and P. Zschack[2]*

As part of the development of ultrahigh resolution x-ray spectroscopy, the intensity and time structure of resonant nuclear Bragg scattering from mosaic $^{57}Fe_2O_3$ were investigated. Using sagittally focused synchrotron X rays and an epitaxial $^{57}Fe_2O_3$ crystal with ~20-arcsec mosaic width, resonant beams of 165 photons/s were obtained on the F-2 wiggler beam line at the Cornell High-Energy Synchrotron Source (CHESS), and 25 photons/s were measured using the X-14 bending magnet beam line at the BNL National Synchrotron Light Source (NSLS). While these resonant beams are low compared with the ~$10^5$ photons/s anticipated from undulators on the Advanced Photon Source, they demonstrate that sufficient intensity is available for developing resonant scattering techniques and for performing selected scattering experiments on existing synchrotron bending magnet and wiggler beam lines.

The time spectrum of the resonant photons (delayed relative to the incident synchrotron x-ray pulses) was measured using the resonant nuclear (777) reflection of the $^{57}Fe_2O_3$ crystal. The results showed the speedup (superradiance) of the emission of resonant photons for mosaic crystals to be considerably smaller than the speedup for diffraction from a perfect crystal at the exact Bragg angle. The decreased speedup for a mosaic crystal is understood as a reduction in collective effects and low reflectivity associated with diffraction more than a few seconds off the exact Bragg angle. The results were found to be in overall agreement with the theoretically predicted[3] $I(t) \sim (t/\tau)^{-1}\exp(-t/\tau)$ time dependence of the scattering ($\tau$ = 141 ns is the mean life of an isolated Mössbauer nucleus). For short times compared with $\tau$, the emission rate for mosaic crystals is significantly greater

than the ~exp(-$t/\tau$) rate for a single nucleus and a correspondingly wide energy width can be expected; however, for $t >> \tau$, the exponential dominates the fall-off rate, and the energy width of the photons approaches that of an isolated Mössbauer state. This result is important for the development of ultrahigh resolution x-ray spectroscopy because it indicates that energy resolution in the neV range is possible even in the presence of large (~1-μeV) hyperfine splitting.

---

1. Summary of paper to be published.
2. Metals and Ceramics Division, ORNL.
3. Yu. Kagan, A. M. Afanase'v and V. G. Kohn, *J. Phys.* C **12**, 615 (1979).

## DEVELOPMENT OF neV X-RAY SPECTROSCOPY USING RESONANT NUCLEAR BRAGG REFLECTIONS AND RESONANT FILTERS

*J. Z. Tischler, B. C. Larson. E. E. Alp,[1] and Q. Shen[2]*

Application of the neV scale energy resolution of resonant nuclear Bragg monochromators to spectroscopic investigations of condensed matter requires an analyzer with similar energy resolution. Because the energy spectrum of an antiferromagnetic $^{57}Fe_2O_3$ resonant monochromator consists of four lines (of which the two strongest are 800 neV apart), this can be accomplished through the use of an $^{57}Fe_2O_3$ resonant filter, which has absorption lines matching the emission of the monochromator. An $^{57}Fe_2O_3$ powdered filter was used to make a Doppler velocity analysis of the energy resolution available using nuclear Bragg monochromators.

Using the F-2 wiggler line at CHESS, time-resolved Doppler velocity measurements were made of the transmission of resonant photons from an $^{57}Fe_2O_3$ monochromator through a 9.6-mg/cm$^2$-enriched $^{57}Fe_2O_3$ filter. Figure 6.20 shows the velocity spectrum of the transmission for four delay times (after the arrival of the synchrotron pulses). The presence of only single dips indicates that the absorption lines of the filter match the emission lines of the resonant monochromator; at higher velocities, dips from neighboring lines would occur, of course. From the widths of the dips, it was observed that the energy distribution of the monochromated beam becomes more narrow at longer delay

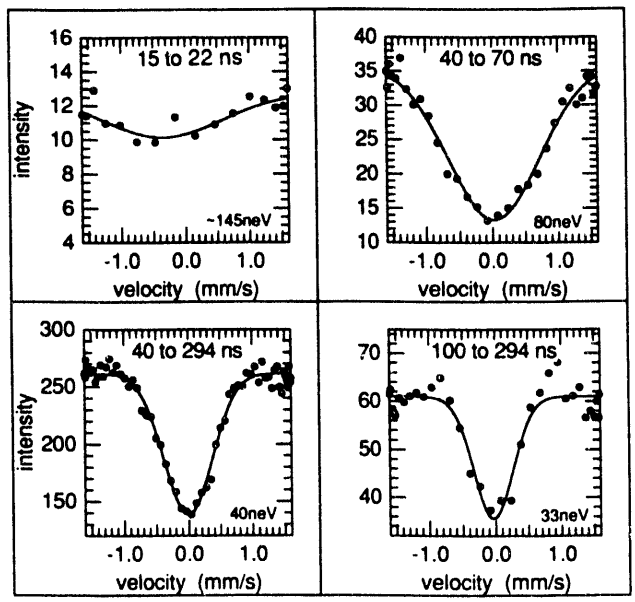


Fig. 6.20. Doppler shift resonant absorption spectra of the monochromatic beam for selected time intervals; the energy widths are given in neV.

times, as expected for emission from resonant states. For instance, the energy width for the velocity spectrum collected from 40 to 70 ns is more than twice that from 100 to 294 ns. All the widths are much less than the 800-neV splitting in the $^{57}Fe_2O_3$ and are in the range of the minimum width, $2\Gamma$, achievable using a radioactive Mössbauer source (10 neV = $2\Gamma$). With thinner filters and longer delay times, energy widths approaching $2\Gamma$ should be obtainable using the present technique; however, the reduced intensity at longer times will be a limiting factor.

---

1. Argonne National Laboratory, Argonne, Ill.

2. CHESS, Cornell University, Ithaca, N.Y.

## DEMONSTRATION OF neV SCATTERING SPECTROSCOPY USING THE PHASE TRANSITION IN $BaTiO_3$

*J. Z. Tischler, B. C. Larson, L. A. Boatner, E. E. Alp,[1] T. Mooney,[1] and Q. Shen[2]*

As a demonstration of neV x-ray spectroscopy using synchrotron radiation, measurements of the scattering properties of $BaTiO_3$ near its ferroelectric phase transition, $T_c$ = 119°C, have been made. Conventional Mössbauer measurements[3] show disagreement about the existence of quasielastic broadening of the Bragg scattering at 20–30° above $T_c$. In this work, the sharp collimation of a $^{57}Fe_2O_3$ resonant monochromator was used to study the (002) Bragg reflection from $BaTiO_3$, where the outgoing beam was analyzed with a $^{57}Fe_2O_3$ filter on a Doppler velocity drive and a timing x-ray detector.[4]

Figure 6.21(a) shows the time spectrum of the resonant photon beam after scattering from the (002) Bragg reflection at temperatures of 30, 120, and 150°C. These data were obtained using undulator radiation from a dedicated run at CHESS where resonant beams of ~1500 photons/s were provided. For coherent radiation, the time spectrum is the Fourier transform

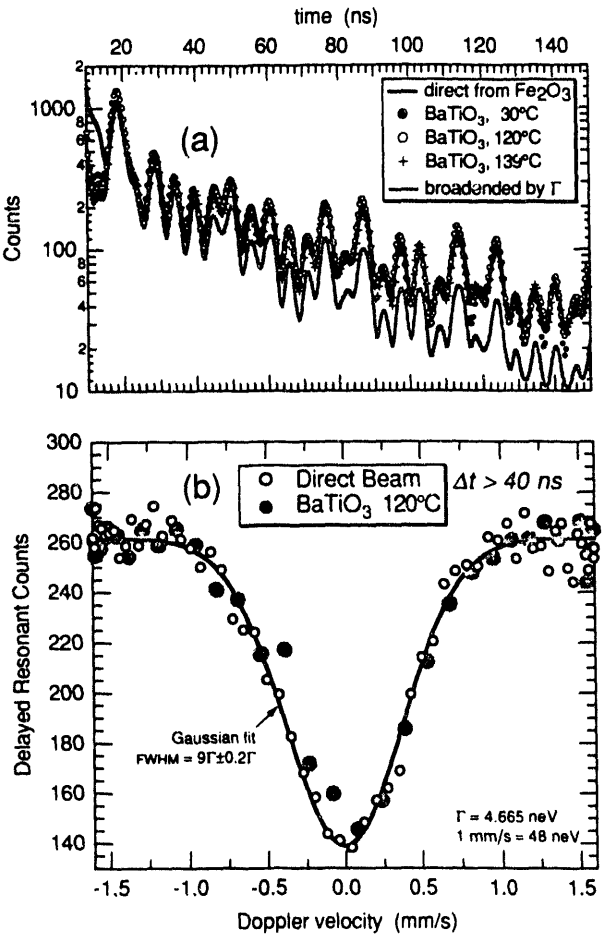


Fig. 6.21. (a) Time spectrum of resonant photons after reflecting from $BaTiO_3$; (b) Doppler velocity measurements of the energy widths before and after reflecting from $BaTiO_3$.

of the energy spectrum; therefore, coherent energy broadening will steepen the time spectrum. Since the three curves in Fig. 6.21(a) are essentially coincident, there is no evidence for coherent quasielastic scattering; coherent broadening of only ~5 neV would have yielded the much steeper gray curve. Incoherent quasielastic scattering would not change the time spectrum of the resonant beam, but it can be detected by measuring the energy width of the scattered photons using a resonant filter and a Doppler velocity drive. Figure 6.21(b) shows velocity spectra of the incident and diffracted beams made at 120°C with an incident beam of ~150 photons/s from wiggler radiation at CHESS. The width of the scattered beam is seen to be the same as that of the incident beam. Although additional measurements are needed, these initial results demonstrate the technique and show that no significant coherent or incoherent quasielastic broadening is present in the Bragg reflection at the temperatures measured.

---

1. Argonne National Laboratory, Argonne, Ill.
2. CHESS, Cornell University, Ithaca, N.Y.
3. V. N. Gavrilov, E. V. Zolotoyabko, and E. M. Iolin, *Phys. Rev. Lett.* 75A, 429 (1980); C. N. W. Darlington and D. A. O'Connor, *Phys. Status Solidi a* 96, 389 (1986).
4. J. Z. Tischler et al., "Development of neV X-Ray Spectroscopy Using Resonant Nuclear Bragg Reflections and Resonant Filters," this report.

## EPITAXIAL GROWTH AND DOMAIN FORMATION IN MOCVD $PbTiO_3$ EPITAXIAL FERROELECTRIC THIN FILMS[1]

*B. S. Kwak,[2] A. Erbil,[2] J. D. Budai, M. F. Chisholm, L. A. Boatner, K. Zhang,[2] and B. J. Wilkens[3]*

Ferroelectric lead titanate thin films have been grown successfully on $SrTiO_3$, MgO, and $KTaO_3$ (001) substrates using the metallo-organic chemical vapor deposition (MOCVD) technique. The films were characterized structurally using x-ray diffraction, electron microscopy, and Rutherford backscattering. In each case, the tetragonal films were found to consist of three-dimensional epitaxial domains oriented with either the a-axis (a⊥ domains) or the c-axis (c⊥ domains) aligned near the substrate [001] normal. It was found that domain formation is controlled both by substrate-film interactions (e.g., lattice matching and differential thermal contraction) and by strains induced by the cubic-to-tetragonal structural phase transition, which occurs during cooling from the growth temperature.

Films on $SrTiO_3$ substrates, where the in-plane lattice match is excellent, consisted of predominantly c⊥ domains with a single in-plane orientation. This alignment of the spontaneous polarization c-axis enhances the ferroelectric properties required for applications in thin-film electronics or optoelectronics devices. In contrast, films grown on MgO substrates with a greater lattice mismatch contained both a⊥ and c⊥ domains, each exhibiting several in-

plane epitaxial orientations. The observed alignments were found to be in agreement with near-coincident site lattice models of the $PbTiO_3$-MgO interface.

Films grown on $KTaO_3$ substrates were found to consist of periodic arrays of a⊥ and c⊥ domains; in this case, with the in-plane film and substrate axes approximately aligned. X-ray diffraction was used to measure both the relative domain volumes and the spontaneous strains as a function of film thickness. A theoretical analysis was carried out combining a Landau-Ginzburg-Devonshire film free-energy (including domain walls) and elastic-energy contributions from the substrate; excellent quantitative agreement between theoretical predictions and experimental results was obtained.

---

1. Summary of papers to be published.
2. Georgia Institute of Technology, Atlanta, Ga.
3. Bell Communications Research, Red Bank, N.J.

## STRUCTURAL EVOLUTION OF THE AMORPHOUS PHASES PRODUCED BY HEATING CRYSTALLINE $MgHPO_4 \cdot 3H_2O$[1]

*B. C. Sales, B. C. Chakoumakos, L. A. Boatner, and J. O. Ramey*

Synthetic crystals of the mineral newberyite ($MgHPO_4 \cdot 3H_2O$) were grown from an aqueous solution containing $Mg(NO_3)_2 \cdot 6H_2O$, $H_3PO_4$, and urea. The slow thermal decomposition of urea (at 60°C) was used to increase the solution pH which resulted in nucleation and growth of relatively large, optically clear newberyite crystals ($5 \times 5 \times 5$ $mm^3$). The mineral newberyite is currently found in bat guano, urinary stones, and animal calculi. In the ancient ocean before the development of life, newberyite was probably the dominant phosphate mineral and, hence, may have played a role in the evolution of life on the planet. The present interest in newberyite, however, is related to an unusual crystalline-to-amorphous transition that occurs during heating. This transition is investigated using high-performance liquid chromatography (HPLC), x-ray diffraction (XRD), differential scanning calorimetry (DSC), and thermogravimetric analysis. The dehydration of newberyite results in amorphous XRD patterns that remain essentially unchanged over the interval between 150 and 600°C. In contrast, over the same temperature interval, the HPLC results (Fig. 6.22) show a dramatic evolution in the distribution of chains of corner-linked $PO_4$ tetrahedra resulting in the formation of chains up to 13 $PO_4$ tetrahedra in length. Above 600°C, crystalline $Mg_2P_2O_7$ is formed. At each annealing temperature the distribution of phosphate anions is in agreement with theory. During the crystalline-to-amorphous transition, the original crystal shape is preserved even though the crystals lose up to 36% of their original weight. High-pressure DSC experiments with newberyite resulted in the formation of a unique crystalline phosphate phase that contained equal amounts of orthophosphate and pyrophosphate anions.

---

1. Summary of paper: *Journal of Materials Research* (in press).

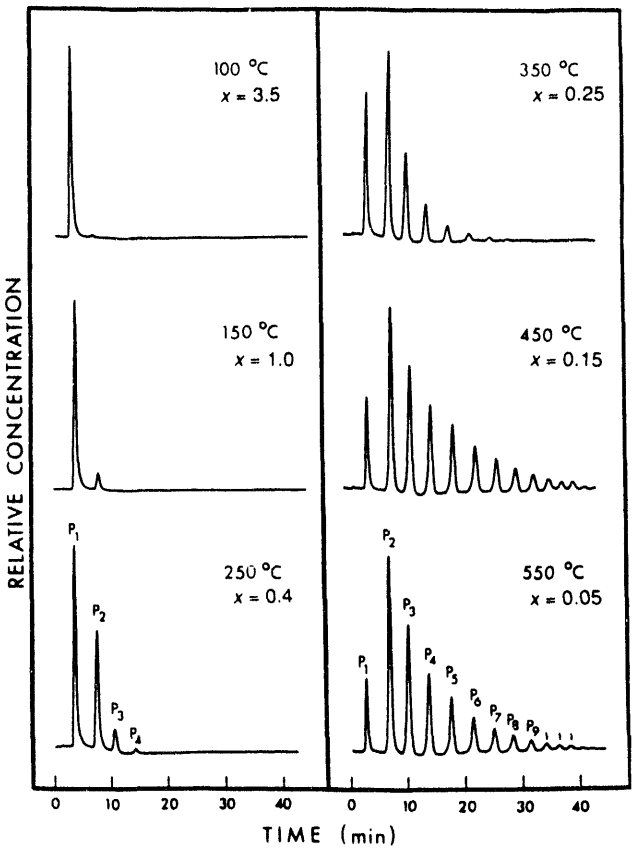


Fig. 6.22. Chromatograms from samples of $MgHPO_4 \cdot 3H_2O$ heated in flowing oxygen for one hour at the indicated temperatures. The position and area under each peak in the chromatogram indicate the identity and quantity of a particular phosphate anion designated by $P_1$, $P_2$, ... $P_n$. A phosphate anion labeled $P_n$ means that the anion consists of $n$ corner-linked $PO_4$ tetrahedra. The water content, $x$, of the samples as determined from weight loss measurements is also shown.

## SINGLE CRYSTAL ANALYSIS OF MIXED (Ln/T)$PO_4$) ORTHOPHOSPHATES[1]

*D. F. Mullica,[2] E. L. Sappenfield,[2] and L. A. Boatner*

New results have been obtained in the course of a continuing systematic investigation of the morphological and structural properties of mixed solid-solution orthophosphates. Structural data have now been refined for several mixed-lanthanide orthophosphates with varying relative rare-earth compositions. These results provide a basis for future solid state chemical investigations dealing with the process of the structural integration and association of diverse cations, α-active transuranic isotopes, and fission productions into the lattices of mixed $Ln/LnPO_4$ systems. Additionally, from the practical point of view, unresolved problems related to radioactive waste disposal are impacted by the results of solid state structural studies of the type presented here. Such results, in fact, address directly the question of the practicality of using monazite-type and/or zircon-type structural analogues as primary host lattices for actinide-waste disposal. Investigations of mixed-lanthanide orthophosphates are possible because solid solutions of these compounds can be synthesized over a wide range of mixed rare-earth compositions [i.e., $(Ln_{1-x}^{(A)}/Ln_x^{(B)})PO_4$]. This capability suggests that within certain limitations, it should be possible to adjust the local crystal-field strength at the Ln-site. This type of structural regulation may allow the magnetic, optical, and other properties of dopant ions in mixed-phosphate systems to be controlled.

The structural investigations of the mixed lanthanide orthophosphates 1:1 $(Gd/Tb)PO_4$, 3:1 $(Gd/Tb)PO_4$, and 9:1 $(Lu/Tb)PO_4$ were carried out by the use of three-dimensional single-crystal x-ray diffractometry. Each mixed orthophosphate compound crystallized in the

tetragonal space group $I4_1/amd$ ($D_{4h}^{19}$, No. 141) ($Z = 4$) with lattice constants of $a$ = 6.9449(9), 6.9647(7), and 6.8003(8) and $c$ = 6.0680(18), 6.0900(6), and 5.9638(6) for 1:1 (Gd/Tb)$PO_4$, 3:1 (Gd/Tb)$PO_4$, and 9:1 (Lu/Tb)$PO_4$, respectively. The final least-squares full-matrix refinements, based on 313, 310, and 283 unique reflections, yielded $R$-values equal to 0.023, 0.017, and 0.030, respectively. The lanthanide ions are eight coordinated to oxygen atoms, and the resulting polyhedra are best described as two orthogonal interpenetrating tetrahedra, bis-bisphenoidal ($D_{2d}$) geometry (Fig. 6.23). Each

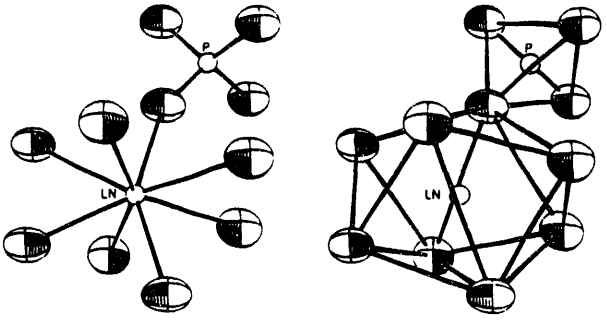


Fig. 6.23. A projected view of the eight-coordinated mixed (Ln/Tb)$PO_4$ system. (a) The two interpenetrating tetrahedral (bisphenoidal) sets, which are horizontal and perpendicular to the viewer, are quite distinctive. (b) A distorted triangulated dodecahedron (bis-bisphenoid, $D_{2d}$) is formed by connecting the oxygen vertices. The four-coordinated phosphate group displays a distorted tetrahedral geometry.

orthogonal tetrahedron has distinct Ln-O bond lengths. The $PO_4$ groups in each compound form distorted tetrahedra. The important bond distances and angles, crystal data, and parameters have been determined for the various mixed orthophosphates.

---

1. Summary of paper: *Journal of Solid State Chemistry* (in press).
2. Baylor University, Waco, Tex. 76798.

## CONCEPTUAL DESIGN REPORT FOR PROPOSED BEAM LINES AT THE ADVANCED PHOTON SOURCE[1]

*B. C. Larson and J. Z. Tischler*

Conceptual design work is in progress on a proposed beam line at the Advanced Photon Source (APS). This proposal is a collaborative access team (CAT) effort by the Solid State and the Metals and Ceramics divisions of ORNL, the University of Illinois at Urbana–Champaign (UIUC), and Allied-Signal, Inc., (AS) to instrument a sector composed of an undulator insertion device (ID) beam line and a bending magnet (BM) beam line at the APS. The instrumentation will include a high-resolution diffraction station and a surface/interface diffraction station on the high-brightness undulator ID line and an absorption spectroscopy station and a diffuse scattering and general diffraction station on the BM line, as shown in Fig. 6.24.

The CAT affiliation with UIUC and AS will provide direct access to the high flux, high collimation, small beam size, and time-structure features of the 7-GeV source presently under construction at Argonne National Laboratory. At an energy of 8 keV the sagittally and vertically focused ID line will provide ~20 times higher flux, 40 times higher collimation, and a

beam size one-third that of the sagittally focused X-14 beam line that is operated by ORNL and UIUC at the National Synchrotron Light Source (NSLS). The more conventional BM line will have collimation similar to X-14, but with ~5 times the flux at 8 keV and less than one-half the beam size. Both the ID and BM lines will provide another order of magnitude (relative) increase in flux for energies >20 keV because of the more rapid falloff with energy of the 2.5-GeV NSLS. The higher collimation and reduced beam size will be particularly important for surface scattering, high-resolution diffuse scattering, polarized beam magnetic x-ray scattering, and meV- and neV-range energy resolution x-ray scattering. The APS time-structure (120-ps pulse width and 177-ns pulse spacing) will provide for nanosecond resolution diffraction measurements, which are not available using the 19-ns pulse spacing of the NSLS, and the combination of time-structure, high collimation, and high flux will provide neV resolution resonant x-ray beams with 100–1000 times the power available using existing wiggler synchrotron sources.

---

1. Summary of *Conceptual Design Report for the UNI-CAT Beam Line Proposal* (submitted to APS Beam Line Proposal Review Committee).

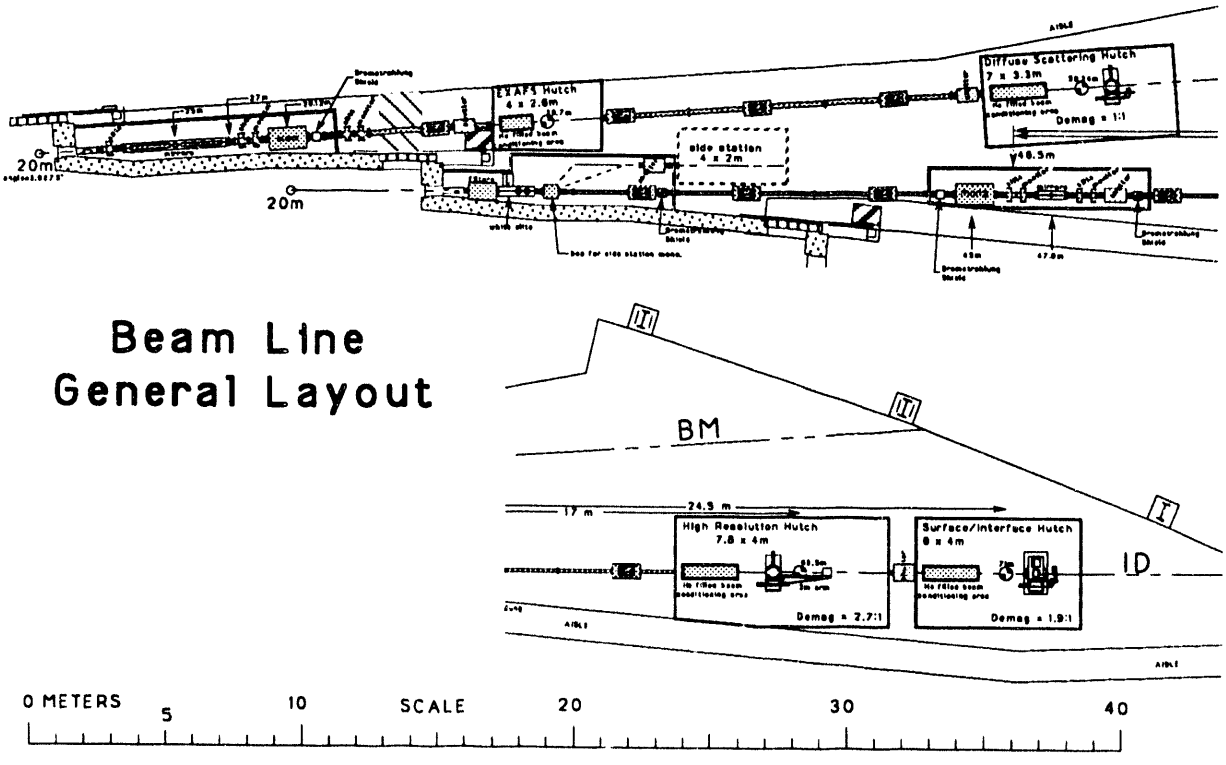


Fig. 6.24. Conceptual design plan view of the undulator ID and BM beam lines proposed for the APS.

# *Publications and Papers*

## *(October 1, 1990–March 31, 1992)*

## *JOURNAL ARTICLES*


M. M. Abraham and C. E. Bamberger, "Electron Paramagnetic Resonance Spectroscopic Determination of $Ti^{3+}$ in Several Titanium Phosphate Compounds," *J. Am. Ceram. Soc.* **74**, 2299 (1991).

M. M. Abraham, B. Bleaney, R. W. Hill, M. J. M. Leask, R. C. C. Ward, and M. R. Wells, "Thermal and Magnetic Properties of Barium Holmium Fluoride, $BaHo_2F_8$," *Proc. R. Soc. Lond. A* **435**, 159 (1991).

M. M. Abraham, J. M. Baker, B. Bleaney, A. A. Jenkins, P. M. Martineau, and J. Z. Pfeffer, "Magnetic Resonance of Lanthanide Ions as Magnetic Probes in the Antiferromagnetic Phase of Dysprosium Phosphate," *Proc. R. Soc. Lond. A* **435**, 605 (1991).

B. K. Annis, J. S. Lin, E. M. Scherr, and A. G. MacDiarmid, "Evidence for the Development of a One-Dimensional Array of Crystallites in Stretched Polyaniline and the Effect of $Cl^-$ Doping," *Macromol.* **25**, 429 (1992).

A. P. Baddorf and D. M. Zehner, "Chemisorption of Nitrogen on Cu(110): Coverage and Site Determination," *Surf. Sci.* **238**, 255 (1990).

A. P. Baddorf and E. W. Plummer, "Enhanced Surface Anharmonicity Observed in Vibrations on Cu(110)," *Phys. Rev. Lett.* **66**, 2770 (1991).

A. P. Baddorf and J. F. Wendelken, "High Coverages of Oxygen on Cu(110) Investigated with XPS, LEED, and HREELS," *Surf. Sci.* **256**, 264 (1991).

A. P. Baddorf and E. W. Plummer, "Surface Anharmonicity: Temperature Dependence of Phonon Energies on Cu(110)," *J. Electron Spectrosc. and Relat. Phenom.* **54/55**, 541 (1990).

A. P. Baddorf and B. S. Itchkawitz, "Identification of Oxygen Species on Single-Crystal K(110), *Surf. Sci.* **264**, 73 (1991).

I. M. Baker, E. M. Schulson, J. R. Michael, and S. J. Pennycook, "The Effects of Both Deviation from Stoichiometry and Boron on Grain Boundaries in $Ni_3Al$," *Philos. Mag. B* **62**, 659 (1990).

John H. Barrett, O. S. Oen, and O. W. Holland, "Further Aspects of Enhanced Ion Scattering Near 180°," *Phys. Rev. B* **43**, 2471 (1991).

J. M. Bass, J. A. Blackman, and J. F. Cooke, "The Role of the Exchange Matrix in the Itinerant-Electron Theory of Ferromagnetism," *J. Phys., Condens. Matter* **4**, L275 (1992).

J. B. Bates, J. C. Wang, and Y. T. Chu, "Interface and Bulk Relaxation in Solid Ionic Conductors," *J. Non-Cryst. Solids* **131–133**, 1046 (1991).

K. Becker, L. Yang, R. F. Haglund, Jr., R. H. Magruder, R. A. Weeks, and R. A. Zuhr, "Laser-Induced Fluorescence and Nonlinear Optical Properties of Ion-Implanted Fused Silica," *Nucl. Instrum. and Methods Phys. Res. Sect. B* **59/60**, 1304 (1991).

P. C. Becker, G. M. Williams, N. M. Edelstein, J. A. Koningstein, L. A. Boatner, and M. M. Abraham, "Observation of Novel Electron-Phonon Coupling Effects in $YbPO_4$," *Phys. Rev. B* **45**, 5027 (1992).

L. A. Berry and S. M. Gorbatkin, "Electron Cyclotron Resonance Microwave Ion Sources for Thin-Film Processing," *Nucl. Instrum. and Methods Phys. Res. Sect. B* **56/57**, 1133 (1991).

M. M. Bialkowski, G. S. Hurst, J. E. Parks, D. H. Lowndes, and G. E. Jellison, Jr., "Charge Emission from Silicon and Germanium Surfaces Irradiated with KrF Excimer Laser Pulses," *J. Appl. Phys.* **68**, 4795 (1990).

J. A. Blackman, K. N. Trohidou, and J. F. Cooke, "High-Energy Spin Waves in Cubic and HCP Transition Metals," *J. Magn. Magn. Mater.* **104–107**, 721 (1992).

B. Blum, E. W. Plummer, H. L. Davis, and D. M. Zehner, "Bismuth-Induced Structures on Copper (100)," *J. Vac. Sci. and Technol. A* **9**, 1703 (1991).

J. D. Budai, M. F. Chisholm, R. Feenstra, D. H. Lowndes, D. P. Norton, L. A. Boatner, and D. K. Christen, "Preferred Alignment of Twin Boundaries in $YBa_2Cu_3O_x$ Thin Films and $YBa_2Cu_3O_x/PrBa_2Cu_3O_x$ Superlattices on $SrTiO_3$," *Appl. Phys. Lett.* **58**, 2174 (1991).

G. S. Canright and A. G. Rojo, "Two Phases of the Anyon Gas and Broken $T$ Symmetry: Some Exact Results," *Int. J. Mod. Phys. B* **5**, 1553 (1991).

G. S. Canright, "Numerical Studies of Fractional Statistics," *Int. J. Mod. Phys. B* **5**, 2791 (1991).

G. S. Canright and A. G. Rojo, "Some Consequences of $PT$ Symmetry for Optical Rotation Experiments," *Phys. Rev. Lett.* **68**, 1601 (1992).

E. Caponetti, E. M. D'Aguanno, R. Triolo, and S. Spooner, "Kinetics of Particle Growth and Particle Composition of a Commercial Al-Li Alloy by Means of Small-Angle Scattering," *Philos. Mag. B* **63**, 1201 (1991).

B. C. Chakoumakos, B. C. Sales, and L. A. Boatner, "Alpha-Decay-Induced Condensation of Phosphate Anions in a Mineral," *Am. Mineral.* **75**, 1447 (1990).

B. C. Chakoumakos, W. C. Oliver, G. R. Lumpkin, and R. C. Ewing, "Hardness and Elastic Modulus of Zircon as a Function of Heavy-Particle Irradiation Dose: I. In Situ α-Decay Event Damage," *Radiat. Eff. Defects Solids* **118**, 393 (1991).

B. C. Chakoumakos, G. A. Lager, and J. A. Fernandez-Baca, "Refinement of the Structures of $Sr_3Al_2O_6$ and the Hydrogarnet $Sr_3Al_2(O_4D_4)_3$ by Rietveld Analysis of Neutron Powder Diffraction Data," *Acta Crystallogr. Sect. C* **48**, 414 1992).

S. L. Chang, S. H. Chen, R. L. Rill, and J. S. Lin, "Measurements of Monovalent and Divalent Counterion Distributions Around Persistence Length DNA Fragments in Solution," *J. Phys. Chem.* **94**, 8025 (1990).

S. L. Chang, S. H. Chen, R. L. Rill, and J. S. Lin, "Measurement and Interpretation of Counterion Distribution Around Cylindrical Polyelectrolytes," *Prog. Colloid and Polym. Sci.* **84**, 409 (1991).

Y. Chen, M. M. Abraham, and D. F. Pedraza, "Radiation Damage in $Al_2O_3$ Crystals Implanted with 3.8-MeV $Fe^{2+}$ Ions," *Nucl. Instrum. and Methods Phys. Res. Sect. B* **59/60**, 1163 (1991).

S-W. Cheong, G. Aeppli, T. E. Mason, H. Mook, S. M. Hayden, P. C. Canfield, Z. Fisk, K. N. Clausen, and J. L. Martinez, "The Incommensurate Magnetic Fluctuations in $La_{2-x}Sr_xCuO_4$," *Phys. Rev. Lett.* **67**, 1791 (1991).

M. F. Chisholm and S. J. Pennycook, "Structural Origin of Reduced Critical Currents at $YBa_2Cu_3O_{7-\delta}$ Grain Boundaries," *Nature* **351**, 47 (1991).

D. K. Christen and R. Feenstra, "Effects of Thermal Processing and Oxygen Composition on Flux Pinning in High-$J_c$ Epitaxial $YBa_2Cu_3O_{7-x}$ Thin Films," *Physica C* **185–189**, 2225 (1991).

L. Civale, M. W. McElfresh, A. D. Marwick, F. Holtzberg, C. Feild, J. R. Thompson, and D. K. Christen, "Scaling of the Hysteric Magnetic Behavior in $YBa_2Cu_3O_7$ Single Crystals," *Phys. Rev. B* **43**, 13732 (1991).

L. Civale, A. D. Marwick, T. K. Worthington, L. Krusin-Elbaum, F. Holtzberg, M. A. Kirk, J. R. Thompson, Y. Sun, and J. R. Clem, "Vortex Confinement by Columnar Defects in $YBa_2Cu_3O_7$ Crystals: Enhanced Pinning at High Fields and Temperatures," *Phys. Rev. Lett.* **67**, 648 (1991).

F. Claro and G. D. Mahan, "Comment on 'Local-Field Distribution in Random Dielectric Media,'" *Phys. Rev. Lett.* **66**, 1644 (1991).

D. Comedi, R. Kalish, and J. H. Barrett, "A Method for the Determination of Atomic Displacements in Compound Crystals by Means of RBS-PIXE-Channeling Experiments," *Nucl. Instrum. and Methods Phys. Res. Sect. B* **63**, 451 (1992).

B. Daudin, B. Salce, J. L. Gravil, and L. A. Boatner, "Dielectric Active Defects and Thermal Conductivity of Undoped $KTaO_3$," *Ferroelectrics* **106**, 69 (1990).

S. A. David and L. A. Boatner, "Single Crystals for Welding Research," *ORNL Review* **24**, 32, (1991).

S. A. David, J. M. Vitek, M. Rappaz, and L. A. Boatner, "Microstructure of Stainless Steel Single-Crystal Electron Beam Welds," *Metall. Trans. A* **21**, 1753 (1990).

U. V. Desnica, J. Wagner, T. E. Haynes, and O. W. Holland, "Raman and Ion Channeling Analysis of Damage in Ion-Implanted GaAs: Dependence on Ion Dose and Dose Rate," *J. Appl. Phys.* **71**, 2591 (1992).

W. S. Dubner, J. M. Schultz, and G. D. Wignall, "Estimation of Incoherent Backgrounds in SANS Studies of Polymers," *J. Appl. Crystallogr.* **23**, 469 (1990).

R. Feenstra, T. B. Lindemer, J. D. Budai, and M. D. Galloway, "Effect of Oxygen Pressure on the Synthesis of $YBa_2Cu_3O_{7-x}$ Thin Films by Postdeposition Annealing," *J. Appl. Phys.* **69**, 6569 (1991).

J. A. Fernandez-Baca, R. M. Nicklow, Z. Tun, and J. J. Rhyne, "Neutron Scattering Study of the Magnetic Excitations of Thulium Metal," *Phys. Rev. B* **43**, 3188 (1991).

J. A. Fernandez-Baca, M. E. Hagen, R. M. Nicklow, Y. Tsunoda, and S. M. Hayden, "Magnetic Excitations in the Itinerant Antiferromagnet $Mn_{90}Cu_{10}$," *J. Magn. Magn. Mater.* **104–107**, 699 (1992).

R. S. Fishman and G. Vignale, "Breakdown of Spin-Wave Approximation for a Heisenberg Ferromagnet," *Phys. Rev. B* **44**, 658 (1991).

R. S. Fishman and S. H. Liu, "Coupling Between Longitudinal and Transverse Fluctuations in a Heisenberg Ferromagnet," *J. Phys., Condens. Matter* **3**, 8313 (1991).

R. S. Fishman and S. H. Liu, "Nonlinear Dynamics of a Heisenberg Ferromagnet," *Phys. Rev. B* **45**, 5414 (1992).

R. S. Fishman and S. H. Liu, "Onset of Long-Range Order in a Paramagnet," *Phys. Rev. B* **45**, 5406 (1992).

K. Flensberg, and M. Jonson, "Quantum Fluctuations and Charging Effects in Small Tunnel Junctions," *Phys. Rev. B* **43**, 7586 (1991).

K. Flensberg and H. O. Frota, "Charging Effects in Tunnel Junctions: A Four Level Study," *Solid State Commun.* **77**, 917 (1991).

K. Flensberg, S. M. Girvin, M. Jonson, D. R. Penn, and M. D. Stiles, "Coulomb Blockade in Single Tunnel Junctions: Quantum Mechanical Effects of the Electromagnetic Environment," *Z. Phys. B* **85**, 395 (1991).

E. M. Forgan, D. McK. Paul, H. A. Mook, S. L. Lee, R. Cubitt, J. S. Abell, F. Gencer, and P. Timmins, "Neutron Diffraction from the Flux-Line Lattice," *Physica C* **185**, 247 (1991).

H. O. Frota and G. D. Mahan, "Screened Anderson Model," *Phys. Rev. B* **43**, 10755 (1991).

H. O. Frota, "Charge Susceptibility of Spin-Degenerate Anderson Model," *Phys. Rev. B* **44**, 8433 (1991).

H. O. Frota and G. D. Mahan, "Band Tails and Bandwidths in Simple Metals," *Phys. Rev. B* **45**, 6243 (1992).

J. C. Gacon, M. Bouazaoui, B. Jacquier, M. Kibler, L. A. Boatner, and M. M. Abraham, "Polarization Dependence of the $^7F_0 \rightarrow {}^5D_0$ Two-Photon Transition in $Sm^{2+}$- and $Eu^{3+}$-Doped Materials," *Eur. J. Solid State Inorg. Chem.* **28**, 113 (1991).

M. D. Gehlsen, J. H. Rosedale, F. S. Bates, G. D. Wignall, L. Hansen, and K. Almdal, "Molecular Weight Scaling in Critical Polymer Mixtures," *Phys. Rev. Lett.* **68**, 2452 (1992).

D. B. Geohegan, "Laser Ablation Processing," *J. Mater. Educ.* **12**, 383 (1990).

D. Gibbs, G. Grübel, D. M. Zehner, D. L. Abernathy, and S. G. J. Mochrie, "Orientational Epitaxy of the Hexagonally Reconstructed Pt(001) Surface," *Phys. Rev. Lett.* **67**, 3117 (1991).

L. I. Glazman and M. Jonson, "Breakdown of Conductance Quantization and Mesoscopic Fluctuations in the Quasi-Ballistic Regime," *Phys. Rev. B* **44**, 3810 (1991).

A. Golanski, W. H. Christie, M. D. Galloway, J. L. Park, S. J. Pennycook, D. B. Poker, J. L. Moore, H. E. Harmon, and C. W. White, "Ion Beam Induced Diffusion and Crystallization in High-Dose Er-Implanted Si," *Nucl. Instrum. and Methods Phys. Res. Sect. B* **59/60**, 444 (1991).

A. Golanski, J. L. Park, S. J. Pennycook, and C. W. White, "Low-Temperature Mesotaxy of Ion Beam Synthesized $ErSi_2$," *J. Appl. Phys.* **70**, 1853 (1991).

A. Golanski and C. W. White, "Radiation-Induced Effects in Ion Beam Synthesis of Erbium Silicide," *Nucl. Instrum. and Methods Phys. Res. Sect. B* **63**, 384 (1992).

A. Golanski, A. Grob, J. J. Grob, O. W. Holland, S. J. Pennycook, and C. W. White, "Dynamics of Lattice Damage Accumulation for MeV Ions in Silicon," *Nucl. Instrum. and Methods Phys. Res. Sect. B* **62**, 365 (1992).

R. Gonzalez, Y. Chen, R. M. Sebek, G. P. Williams, R. T. Williams, and W. Gellerman, "Properties of the 800-nm Luminescence Band in Neutron-Irradiated Magnesium Oxide Crystals," *Phys. Rev. B* **43**, 5228 (1991).

R. Gonzalez, E. R. Hodgson, C. Ballesteros, and Y. Chen, "Effect of Environment on Radiation-Induced Removal of Deuterons and Protons in Crystalline $LiNbO_3$ at Low Temperatures," *Phys. Rev. Lett.* **67**, 2057 (1991).

S. M. Gorbatkin, R. A. Zuhr, J. Roth, and H. Naramoto, "Damage Formation and Substitutionality in $^{75}As^{2+}$-Implanted Diamond," *J. Appl. Phys.* **70**, 2986 (1991).

G. R. Gruzalski, S.-C. Lui, and D. M. Zehner, "Work-Function Changes Accompanying Changes in Composition of (100) Surfaces of $HfC_x$ and $TaC_x$," *Surf. Sci.* **239**, L517 (1990).

S. M. Gulwadi, M. V. Rao, D. S. Simons, O. W. Holland, Won-Pyo Hong, Catherine Caneau, and Harry B. Dietrich, "Range Statistics and Rutherford Backscattering Studies of Fe-Implanted $In_{0.53}Ga_{0.47}As$," *J. Appl. Phys.* **69**, 162 (1991).

S. M. Gulwadi, R. K. Nadella, O. W. Holland, and M. V. Rao, "Rutherford Backscattering Studies on High-Energy Si-Implanted InP," *J. Electron. Mater.* **20**, 615 (1991).

R. F. Haglund, Jr., H. C. Mogul, R. A. Weeks, and R. A. Zuhr, "Changes in the Refractive Index of Fused Silica Due to Implantation of Transition-Metal Ions," *J. Non-Cryst. Solids* **130**, 326 (1991).

S. M. Hayden, G. Aeppli, H. A. Mook, S.-W. Cheong, and Z. Fisk, "Spin Dynamics in the Two-Dimensional Antiferromagnet $La_2CuO_4$," *Phys. Rev. B* **42**, 10220 (1990).

S. M. Hayden, G. Aeppli, H. Mook, D. Rytz, M. F. Hundley, and Z. Fisk, "Magnetic Fluctuations in $La_{1.95}Ba_{0.05}CuO_4$," *Phys. Rev. Lett.* **66**, 821 (1991).

T. E. Haynes and O. W. Holland, "Dose Rate Effects on Damage Accumulation in $Si^+$-Implanted Gallium Arsenide," *Appl. Phys. Lett.* **58**, 62 (1991).

T. E. Haynes and O. W. Holland, "Dose Rate Effects on Damage Formation in Ion-Implanted Gallium Arsenide," *Nucl. Instrum. and Methods Phys. Res. Sect. B* **59/60**, 1028 (1991).

T. E. Haynes and O. W. Holland, "Comparative Study of Implantation-Induced Damage in GaAs and Ge: Temperature and Flux Dependence," *Appl. Phys. Lett.* **59**, 452 (1991).

J. B. Hayter, "Advanced Neutron Source—The User's Perspective," *Trans. Am. Nucl. Soc.* **62**, 139 (1990).

J. B. Hayter, "SANS Studies of Ferrofluids," *Neutron News* **1**, 22 (1990).

J. B. Hayter, "Determination of Structures in Ferrofluids by Small-Angle Scattering," *J. Chem. Soc. Faraday Trans.* **87**, 403 (1991).

J. B. Hayter and C. D. West, "Status of the Advanced Neutron Source Project," *Neutron News* **3**, 16 (1992).

W. O. Hofer, "Ion-Induced Electron Emission from Solids," *Scanning Microsc. Supp.* **4**, 265 (1990).

O. W. Holland and C. W. White, "Ion-Induced Damage and Amorphization in Si," *Nucl. Instrum. and Methods Phys. Res. Sect. B* **59/60**, 353 (1991).

H. Hosono, R. A. Weeks, H. Imagawa, and R. A. Zuhr, "Formation of Oxygen-Deficient Type Structural Defects and State of Ions in $SiO_2$ Glasses Implanted with Transition-Metal Ions," *J. Non-Cryst. Solids* **120**, 250 (1990).

J. J. Hoyt and S. Spooner, "The Surface Energy of Metastable $Al_3Li$ Precipitates from Coarsening Kinetics," *Acta Metall. Mater.* **39**, 686 (1991).

K. G. Huang, Doon Gibbs, D. M. Zehner, A. R. Sandy, and S. G. J. Mochrie, "Phase Behavior of the Au(111) Surface: Discommensurations and Kinks," *Phys. Rev. Lett.* **65**, 3313 (1990).

S. L. Hulbert, C. C. Kao, R. F. Garrett, R. A. Bartynski, S. Yang, M. Weinert, E. Jensen, and D. M. Zehner, "A Comparison of the Surface Electronic Structure of Ta(100) and TaC(111) Using Auger-Photoelectron Coincidence Spectroscopy," *J. Vac. Sci. and Technol. A* **9**, 1919 (1991).

B. S. Itchkawitz, A. P. Baddorf, H. L. Davis, and E. W. Plummer, "Shear Displacement of the K(110) Surface," *Phys. Rev. Lett.* **68**, 2488 (1992).

S. Jandl, M. Banville, P. Dufour, S. Coulombe, and L. A. Boatner, "Infrared Study of Oxygen Vacancies in $KTaO_3$," *Phys. Rev. B* **43**, 7555 (1991).

E. Jarosewich and L. A. Boatner, "Rare-Earth Element Reference Samples for Electron Microprobe Analysis," *Geostandards Newsletter* **15**, 397 (1991).

G. E. Jellison, Jr., and B. C. Sales, "The Determination of the Optical Functions of Transparent Glasses Using Spectroscopic Ellipsometry," *Appl. Opt.* **30**, 4310 (1991).

G. E. Jellison, Jr., "Use of the Biased Estimator in the Interpretation of Spectroscopic Ellipsometry Data," *Appl. Opt.* **30**, 3354 (1991).

G. E. Jellison, Jr., "Optical Functions of Silicon Determined by Two-Channel Polarization Modulation Ellipsometry," *J. Opt. Mater.* **1**, 41 (1992).

G. E. Jellison, Jr., "Examination of Thin $SiO_2$ Films on Si Using Spectroscopic Polarization Modulation Ellipsometry," *J. Appl. Phys.* **69**, 7627 (1991).

G. E. Jellison, Jr., "Two Channel Spectroscopic Polarization Modulation Ellipsometry: A New Technique for the Analysis of Thin $SiO_2$ Films," *Thin Solid Films* **206**, 294 (1991).

D. E. Jesson, S. J. Pennycook, and J.-M. Baribeau, "Direct Imaging of Interfacial Ordering in Ultrathin $(Si_mGe_n)_p$ Superlattices," *Phys. Rev. Lett.* **66**, 750 (1991).

D. E. Jesson and S. J. Pennycook, "High-Resolution Z-Contrast Imaging of Semiconductor Interfaces," *Mater. Res. Soc. Bull.* **16**, 34 (1991).

D. E. Jesson and S. J. Pennycook, "Intuitive Imaging of Semiconductor Interfaces Using Z-Contrast STEM," *Scanning* **13**, 65 (1991).

D. E. Jesson, S. J. Pennycook, J.-M. Baribeau, and D. C. Houghton, "Step-Driven Lateral Segregation and Long-Range Ordering During $Si_xGe_{1-x}$ Epitaxial Growth," *Phys. Rev. Lett.* **68**, 2062 (1992).

E. C. Jones, D. K. Christen, C. E. Klabunde, J. R. Thompson, D. P. Norton, R. Feenstra, D. H. Lowndes, and J. D. Budai, "Flux Creep in the Josephson Mixed State of Granular-Oriented $YBa_2Cu_3O_{7-x}$ Thin Films," *Appl. Phys. Lett.* **59**, 3183 (1991).

M. Jonson and G. D. Mahan, "Electron-Phonon Contribution to the Thermopower of Metals," *Phys. Rev. B* **42**, 9350 (1990).

N. H. Karam, A. Mastrovito, V. Haven, K. Ismail, S. J. Pennycook, and H. I. Smith, "Patterning and Overgrowth of Nanostructure Quantum Well Wire Arrays by LP-MOVPE," *J. Cryst. Growth* **107**, 591 (1991).

M. Karimi and M. Mostoller, "Embedded-Atom-Method Study of (110) Surface Relaxation and Bulk Vibrations in Pb," *Phys. Rev. B* **45**, 6289 (1992).

H. R. Khan, J. R. Thompson, and J. G. Ossandon, "Magnetization and Critical Current Density Related to Microstructure in $YBa_2Cu_3O_{\sim 7}$-Ag Composites," *Supercond. Sci. and Technol.* **4**, 133 (1991).

R. A. Klemm and S. H. Liu, "Interlayer Pairing and c-Axis Versus ab-Plane Gap Anisotropy in High-$T_c$ Superconductors," *Physica C* **176**, 189 (1991).

R. A. Klemm and S. H. Liu, "Intralayer-Versus-Interlayer Pairing in the Copper Oxide Superconductors," *Phys. Rev. B* **44**, 7526 (1991).

R. A. Klemm and S. H. Liu, "Crossover from Real Space to Intraband Pairing in the Copper Oxide Superconductors," *Physica C* **191**, 383 (1992).

G. H. Kwei, A. C. Lawson, and Mark Mostoller, "Vibrational Properties and Atomic Debye Temperatures for $La_2CuO_4$ from Neutron Powder Diffraction," *Physica C* **175**, 135 (1991).

I.-S. Lee, R. A. Buchanan, and J. M. Williams, "Charge-Injection Densities of Iridium and Iridium-Ion-Implanted Ti-6Al-4V With Relevancy to Neural Stimulation," *J. Biomed. Mater. Res.* **25**, 1039 (1991).

Y. D. Lee, P. J. Phillips, and J. S. Lin, "The Influence of Crystallinity Distribution on Small-Angle X-Ray Scattering from Semicrystalline Polymers," *J. Polym. Sci.* **29**, 1235 (1991).

H. Liu, R. C. Powell, and L. A. Boatner, "Effect of Niobium Doping on the Properties of Picosecond Laser-Induced Transient Gratings in $KTa_{1-x}Nb_xO_3$," *Phys. Rev. B* **44**, 2461 (1991).

H. Liu, R. C. Powell, and L. A. Boatner, "Origin of Picosecond Pulse-Induced, Degenerate Four-Wave Mixing Signals in $KTa_{1-x}Nb_xO_3$ Crystals," *J. Appl. Phys.* **70**, 20 (1991).

S. H. Liu and R. A. Klemm, "Interlayer Pairing: A Possible New Type of Superconductivity in Layered Materials," *Chinese J. Phys.* **29**, 157 (1991).

S. H. Liu and R. A. Klemm, "Intralayer Versus Interlayer Pairing in the Copper Oxide Superconductors: The Three- and Four-Layer Problems," *Phys. Rev. B* **45**, 415 (1992).

R. H. Magruder III, R. A. Weeks, R. A. Zuhr, and G. Wichard, "Optical Absorption of Cu-Implanted Silica," *J. Non-Cryst. Solids* **129**, 46 (1991).

R. H. Magruder III, R. A. Zuhr, and R. A. Weeks, "Dose Rate Dependence of the Optical Absorption of Cu-Implanted Silica," *Nucl. Instrum. and Methods Phys. Res. Sect. B* **59/60**, 1308 (1991).

G. D. Mahan, "Polarons in the Layered Electron Gas," *Phys. Rev. B* **43**, 2934 (1991).

G. D. Mahan and L. E. Oliveira, "Quasi-Fermi-Levels in Quantum-Well Photoluminescence," *Phys. Rev. B* **44**, 3150 (1991).

G. D. Mahan, "Piezoelectricity in Insulators," *Int. J. Mod. Phys. B* **5**, 2531 (1991).

G. D. Mahan, "Benedick's Effect: Nonlocal Electron Transport in Metals," *Phys. Rev. B* **43**, 3945 (1991).

G. D. Mahan, "Inhomogeneous Thermoelectrics," *J. Appl. Phys.* **70**, 4551 (1991).

T. E. Mason, G. Aeppli, and H. A. Mook, "Magnetic Dynamics of Superconducting $La_{1.86}Sr_{0.14}CuO_4$," *Phys. Rev. Lett.* **68**, 1414 (1992).

C. J. McHargue, P. S. Sklad, C. W. White, G. C. Farlow, A. Perez, and G. Marest, "Microstructural and Chemical Effects in $Al_2O_3$ Implanted with Iron at Room Temperature and Annealed in Oxidizing or Reducing Atmospheres," *J. Mater. Res.* **6**, 2145 (1991).

C. J. McHargue, P. S. Sklad, C. W. White, J. C. McCallum, A. Perez, and G. Marest, "Microstructural and Chemical Effects in $Al_2O_3$ Implanted with Iron at 77 K and Annealed in Oxidizing or Redu·ng Atmospheres," *J. Mater. Res.* **6**, 2160 (1991).

F. W. Meyer, S. H. Overbury, C. C. Havener, P. A. Zeijlmans van Emmichoven, and D. M. Zehner, "Evidence for Above-Surface and Subsurface Neutralization During Interactions of Highly Charged Ions with a Metal Target," *Phys. Rev. Lett.* **67**, 723 (1991).

F. W. Meyer, S. H. Overbury, C. C. Havener, P. A. Zeijlmans van Emmichoven, J. Burgdörfer, and D. M. Zehner, "Electron Emission During Interactions of Multicharged N and Ar Ions with Au(110) and Cu(001) Surfaces," *Phys. Rev. A* **44**, 7214 (1991).

H. A. Mook, M. Mostoller, J. A. Harvey, N. W. Hill, B. C. Chakoumakos, and B. C. Sales, "Observation of Phonon Softening at the Superconducting Transition in $Bi_2Sr_2CaCu_2O_8$," *Phys. Rev. Lett.* **65**, 2712 (1990).

R. M. Moon and R. M. Nicklow, "Neutron Scattering of Lanthanide Materials," *J. Magn. Magn. Mater.* **100**, 139 (1991).

Y. Morii, A. Nagasawa, Y. Matsuo, S. Funahashi, H. R. Child, and R. M. Nicklow, "Lattice Instability in $\beta_1$-AgZn," *J. Phys. Soc. Jpn.* **60**, 4160 (1991).

T. Motooka and O. W. Holland, "Amorphization Processes in Self-Ion-Implanted Si: Dose Dependence," *Appl. Phys. Lett.* **58**, 2360 (1991).

T. Murakami, B. C. Chakoumakos, R. C. Ewing, and G. R. Lumpkin, "Alpha-Decay Event Damage in Zircon," *Am. Mineralogist* **76**, 1510 (1991).

A. Nagasawa, K. Kita, Y. Morii, K. Fuchizaki, S. Katano, S. Funahashi, and H. R. Child, "ω-Like Diffraction Anomaly in the Premartenistic $\beta_1$ Phase of $AuCuZn_2$ Alloy," *Mater. Trans. JIM* **32**, 1011 (1991).

J. Narayan, V. P. Godbole, and C. W. White, "Laser Method for Synthesis and Processing of Continuous Single-Crystal Diamond Thin Films on Nondiamond Substrates," *Science* **252**, 416 (1991).

R. M. Nicklow, "Oak Ridge High Flux Isotope Reactor," *Neutron News* **2**, 7 (1991).

D. P. Norton, D. H. Lowndes, B. C. Sales, J. D. Budai, B. C. Chakoumakos, and H. R. Kerchner, "Superconductivity and Hole Doping in $Pr_{0.5}Ca_{0.5}Ba_2Cu_3O_{7-\delta}$ Thin Films," *Phys. Rev. Lett.* **66**, 1537 (1991).

D. P. Norton, D. H. Lowndes, S. J. Pennycook, and J. D. Budai, "Depression and Broadening of the Superconducting Transition in Superlattices Based on $YBa_2Cu_3O_{7-\delta}$: Influence of the Barrier Layers," *Phys. Rev. Lett.* **67**, 1358 (1991).

D. P. Norton, D. H. Lowndes, W.-Y. Zheng, S. Zhu, and R. J. Warmack, "Scanning Tunneling Microscopy of Pulsed-Laser-Deposited $YBa_2Cu_3O_{7-\delta}$ Epitaxial Thin Films: Surface Microstructure and Growth Mechanisms," *Phys. Rev. B* **44**, 9760 (1991).

B. M. Ocko, Doon Gibbs, K. G. Huang, D. M. Zehner, and S. G. J. Mochrie, "Structure and Phases of the Au(001) Surface: Absolute X-Ray Reflectivity," *Phys. Rev. B* **44**, 6429 (1991).

V. M. Orera, R. I. Merino, Y. Chen, R. Cases, and P. J. Alonso, "Intrinsic Electron and Hole Defects in Stabilized Zirconia Single Crystals," *Phys. Rev. B* **42**, 9782 (1990).

S. H. Overbury, F. W. Meyer, and M. T. Robinson, "Computer Simulations of Relaxation Processes in Scattering of Multicharged Ions from Metal Surfaces," *Nucl. Instrum. and Methods Phys. Res. Sect. B* **67**, 126 (1992).

T. F. Page, C. J. McHargue, and C. W. White, "SEM Electron Channeling Patterns as a Technique for the Characterization of Ion Implantation Damage," *J. Microsc.* **163**, 245 (1991).

J. L. Park, Y. Chen, G. P. Williams, Jr., R. T. Williams, and G. J. Pogatshnik, "Luminescence of $F^+$ Centers in CaO Crystals Under Pulsed-Laser Excitation," *Phys. Rev. B* **43**, 11991 (1991).

D. McK. Paul, E. M. Forgan, H. A. Mook, R. Cubitt, S. L. Lee, M. L. Norton, H-Y Tang, and P. Timmins, "Anomalous Neutron Scattering from the Flux-Line Lattice in $K_{0.6}Ba_{0.4}BiO_3$," *Physica C* **185**, 1837 (1991).

S. J. Pennycook and D. E. Jesson, "High-Resolution Z-Contrast Imaging of Crystals," *Ultramicroscopy* **37**, 14 (1991).

S. J. Pennycook, "Imaging in Materials Science," *Mater. Res. Soc. Bull.* **16**, 19 (1991).

S. J. Pennycook, "Z-Contrast Electron Microscopy," *Materials and Processing Report* **6**, 1 (1991).

S. J. Pennycook, M. F. Chisholm, D. E. Jesson, D. P. Norton, D. H. Lowndes, R. Feenstra, H. R. Kerchner, and J. O. Thomson, "Interdiffusion, Growth Mechanisms, and Critical Currents in $YBa_2Cu_3O_{7-x}/PrBa_2Cu_3O_{7-x}$ Superlattices," *Phys. Rev. Lett.* **67**, 765 (1991).

S. J. Pennycook, "Atomic Scale Imaging of Materials Chemistry by Z-Contrast Scanning Transmission Electron Microscopy," *Anal. Chem.* **64**, 263A (1992).

S. J. Pennycook, "Compositional Imaging with Large-Angle Electron Scattering," *EMSA Bulletin* **22**, 51 (1992).

T. G. Perring, A. T. Boothroyd, D. McK. Paul, A. D. Taylor, R. Osborn, R. J. Newport, J. A. Blackman, and H. A. Mook, "High-Energy Spin Waves in BCC Iron," *J. Appl. Phys.* **69**, 6219 (1991).

Sune Pettersson, "Solving the Phonon Boltzmann Equation with the Variational Method," *Phys. Rev. B* **43**, 9238 (1991).

G. J. Pogatshnik, L. S. Cain, B. D. Evans, and Y. Chen, "Optical Properties of Color Centers in Gadolinium Gallium Garnets," *Phys. Rev. B* **43**, 1787 (1991).

P. Radhakrishna and J. W. Cable, "Magnetic Excitations in the Triangular Antiferromagnet $Mn_3Sn$," *J. Magn. Magn. Mater.* **104–107**, 1065 (1992).

S. Raman, J. A. Fernandez-Baca, R. M. Moon, and J. E. Lynn, "Thermal Neutron Scattering Length and Capture by $^{46}Ca$," *Phys. Rev. C* **44**, 518 (1991).

J. Rankin, J. C. McCallum, and L. A. Boatner, "The Effect of Annealing Environments on the Epitaxial Recrystallization of Ion-Beam-Amorphized $SrTiO_3$," *J. Mater. Res.* **7**, 717 (1992).

M. V. Rao, R. K. Nadella, and O. W. Holland, "Elevated Temperature 3-MeV Si and 150-keV Ge Implants in InP:Fe," *J. Appl. Phys.* **71**, 126 (1992).

M. Rappaz, S. A. David, J. M. Vitek, and L. A. Boatner, "Analysis of Solidification Microstructures in Fe-Ni-Cr Single-Crystal Welds," *Metall. Trans. A* **21** 1767 (1990).

M. Rasolt, T. Edis, and Z. Tesanovic, "Kosterlitz-Thouless Transition and Charge Redistribution in the Superconductivity of YBCO/PBCO Superlattices," *Phys. Rev. Lett.* **66**, 2927 (1991).

J. D. Robertson, J. B. Bates, N. J. Dudney, and R. A. Zuhr, "Ion Beam Analysis of Lithium-Ion Conducting Amorphous Electrolyte Films," *Nucl. Instrum. and Methods Phys. Res. Sect. B* **56/57**, 722 (1991).

M. T. Robinson, "Computer Simulation Studies of High-Energy Collision Cascades," *Nucl. Instrum. and Methods Phys. Res. Sect. B* **67**, 396 (1992).

A. G. Rojo and G. S. Canright, "Ordering of Chirality for Many Planes of Anyons," *Phys. Rev. Lett.* **66**, 949 (1991).

A. G. Rojo and A. J. Leggett, "Sign of the Coupling Between *T*-Violating Ground States In Second-Order Perturbation Theory," *Phys. Rev. Lett.* **67**, 3614 (1991).

A. G. Rojo and G. S. Canright, "Antiferromagnetic Ordering of Symmetry Breaking in Multiple Planes," *Int. J. Mod. Phys. B* **5**, 1565 (1991).

A. G. Rojo and G. D. Mahan, "Current Drag from the van der Waals Interaction," *Phys. Rev. Lett.* **68**, 2074 (1992).

T. M. Rosseel, J. P. Young, C. R. Vane, R. A. Zuhr, and R. S. Peterson, "High-Resolution Heavy-Ion-Induced X-Ray Satellite Emission Study of Implanted Sulfur as a Probe of Co-Implanted Oxygen in an Oxide Substrate," *Nucl. Instrum. and Methods Phys. Res. Sect. B.* **56/57**, 41 (1991).

Björn G. R. Rudberg and M. Jonson, "Tunneling in a Self-Consistent Dynamic Image Potential," *Phys. Rev. B* **43**, 9358 (1991).

B. C. Sales and L. A. Boatner, "Differing Structures of Amorphous Solids," *ORNL Review* **23**, 19, (1991).

B. C. Sales, J. O. Ramey, J. C. McCallum, and L. A. Boatner, "Structural Differences Between the Glass State and Ion-Beam-Amorphized States of Lead Pyrophosphate," *J. Non-Cryst. Solids* **126**, 179 (1991).

B. C. Sales and B. C. Chakoumakos, "Hole Filling and Hole Creation in the Superconducting Compounds $Bi_2Sr_{2-x}RE_xCuO_{6+y}$, RE = La, Pr, Nd, and Sm," *Phys. Rev. B* **43**, 12994 (1991).

A. R. Sandy, S. G. J. Mochrie, D. M. Zehner, K. G. Huang, and Doon Gibbs, "Structure and Phases of the Au(111) Surface: X-Ray Scattering Measurements," *Phys. Rev. B* **43**, 4667 (1991).

E. Y. Sheu, S. H. Chen, B. L. Carvalho, J. S. Lin, and M. Capel, "Interpretation of Small-Angle X-Ray Scattering Intensity Distribution from Fluctuating Lamellae in a Ternary System: Sodium Octyl Sulfate-Water-Decanol," *Langmuir* **7**, 1895 (1991).

R. Siegele, J. Roth, B. M. U. Scherzer, and S. P. Withrow, "Trapping of D in SiC and Damage Due to Implantation," *J. Nucl. Mater.* **176/177**, 1010 (1990).

T. P. Sjoreen, R. Jebasinski, K. Schmidt, S. Mantl, H. Holzbrecher, and W. Speier, "Formation of $CoSi_2$ in SIMOX Wafers by High-Dose Co Implantation," *Mater. Sci. and Eng.* **B12**, 129 (1992).

P. S. Sklad, L. Romana, C. J. McHargue, C. W. White, and J. C. McCallum, "The Effect of Post-Implantation Annealing on the Microstructure of $Al_2O_3$ Implanted with Iron at -185°C," *Nucl. Instrum. and Methods Phys. Res. Sect. B* **59/60**, 1187 (1991).

H. G. Smith, R. Berliner, J. D. Jorgensen, and J. Trivisonno, "Pressure Effects on the Martensitic Transformation in Metallic Sodium," *Phys. Rev. B* **43**, 4524 (1991).

C. Tangari, R. Ullman, J. S. King, and G. D. Wignall, "Small-Angle Neutron Scattering from Bimodal Melts of Polystyrene," *Macromol.***23**, 5266 (1990).

Z. Tesanovic, Mark Rasolt, and Lei Xing, "Superconductivity in a Very High Magnetic Field," *Phys. Rev. B* **43**, 288 (1991).

Z. Tesanovic, Mark Rasolt, and Lei Xing, "Reply to 'Comments on *Phys. Rev. Lett.* **63**, 2425 (1989) by K. Scharnberg, C. T. Rieck, and M. R. Norman,'" *Phys. Rev. Lett.* **66**, 841 (1991).

J. R. Thompson, Y. R. Sun, and F. H. Holtzberg, "Long-Term Nonlogarithmic Magnetic Relaxation in Single-Crystal $YBa_2Cu_3O_7$ Superconductor," *Phys. Rev. B* **44**, 458 (1991).

J. R. Thompson, Y. R. Sun, A. P. Malozemoff, D. K. Christen, J. G. Ossandon, H. R. Kerchner, A. Marwick, and F. Holtzberg, "Reduced Flux Motion Via Creep Annealing in High-$J_c$ Single-Crystal $YBa_2Cu_3O_7$," *Appl. Phys. Lett.* **59**, 2612 (1991).

J. Z. Tischler and B. C. Larson, "Resonant Nuclear Bragg Diffraction from Epitaxial $^{57}Fe_2O_3$ on Natural $Fe_2O_3$," *J. Appl. Phys.* **70**, 7532 (1991).

L. M. Toth, J. S. Lin, and L. K. Felker, "Small-Angle X-Ray Scattering from Zirconium (IV) Hydrous Tetramers," *J. Phys. Chem.* **95**, 3106 (1991).

J. Toulouse, X. M. Wang, L. A. Knauss, and L. A. Boatner, "Dielectric Nonlinearity and Spontaneous Polarization of KTN in the Diffuse Transition Range," *Phys. Rev. B* **43**, 8297 (1991).

K. N. Trohidou, J. A. Blackman, and J. F. Cooke, "Calculation of the High-Energy Spin-Wave Spectrum of HCP Cobalt," *Phys. Rev. Lett.* **67**, 2561 (1991).

C. E. Vallet and C. W. White, "Application of Ion Implantation to Electrochemical Studies," *Nucl. Instrum. and Methods Phys. Res. Sect. B* **59/60**, 855 (1991).

G. Vignale, P. Skudlarski, and M. Rasolt, "Current-Density-Functional Theory of the Surface Properties of Electron-Hole Droplets in a Strong Magnetic Field," *Phys. Rev. B* **45**, 8494 (1992).

A. L. Wachs, J. B. Bates, N. J. Dudney, and C. F. Luck, "Plasma Diagnostic Studies of the Influence of Process Variables upon the Atomic and Molecular Species Ejected from $(1\text{-}x)Li_4SiO_4{:}xLi_3PO_4$ Targets During RF Magnetron Sputtering," *J. Vac. Sci. and Technol. A* **9**, 492 (1991).

J. C. Wang and J. B. Bates, "Non-Debye Dielectric Response and Distribution of Activation Energies," *Solid State Ionics* **50**, 75 (1992).

X. M. Wang, J. Toulouse, and L. A. Boatner, "Longitudinal Elastic Behavior of the Mixed Ferroelectric KTN," *Ferroelectrics* **112**, 225 (1990).

G. D. Wignall, B. K. Annis, and R. Triolo, "X-Ray Scattering Studies of the Structure of Aqueous Hydroxy-Propyl cellulose Solutions," *J. Polym. Sci. Part B* **29**, 349 (1991).

G. D. Wignall and F. S. Bates, "Neutron Scattering in Materials Science: SANS Studies of Polymers," *Mater. Res. Soc. Bull.* **15**, 73 (1990).

G. D. Wignall, "Instrumental Resolution Effects in Small-Angle Scattering," *J. Appl. Cryst.* **24**, 479 (1991).

J. M. Williams, A. Gonzales, J. Quintana, I. S. Lee, R. A. Buchanan, F. C. Burns, R. J. Culbertson, M. Levy, and J. R. Treglio, "Ion Implantation for Corrosion Inhibition of Aluminum Alloys in Saline Media," *Nucl. Instrum. and Methods Phys. Res. Sect. B* **59/60**, 845 (1991).

R. F. Wood, "Spin Polarons, Hole Filling, and High-$T_c$ Superconductivity in $YBa_2Cu_3O_7$ and $PrBa_2Cu_3O_7$ Alloys and Layered Films," *Phys. Rev. Lett.* **66**, 829 (1991).

R. F. Wood and J. F. Cooke, "$d^9$ Spin-Polaron Theory of High-$T_c$ Superconductivity," *Phys. Rev. B* **45**, 5585 (1992).

W. Xia, S. N. Hsu, C. C. Han, S. A. Pappert, B. Zhu, C. Cozzolino, P. K. L. Yu, S. S. Lau, D. B. Poker, C. W. White, and S. A. Schwarz, "Ion Mixing of Semiconductor Superlattices," *Nucl. Instrum. and Methods Phys. Res. Sect. B* **59/60**, 491 (1991).

W. Xia, S. A. Pappert, B. Zhu, A. R. Clawson, P. K. L. Yu, S. S. Lau, D. B Poker, C. W. White, and S. A. Schwartz, "Ion Mixing of III-V Compound Semiconductor Layered Structures," *J. Appl. Phys.* **71**, 2602 (1992).

M. Yethiraj, R. A. Robinson, D. S. Sivia, J. W. Lynn, and H. A. Mook, "Neutron Scattering Study of the Magnon Energies and Intensities in Iron," *Phys. Rev. B* **43**, 2565 (1991).

D. M. Zehner, S. G. J. Mochrie, B. M. Ocko, and Doon Gibbs, "Structure and Phases of the Au(001) Surface: X-Ray Scattering Measurements," *J. Vac. Sci. and Technol. A* **9**, 1861 (1991).

P. A. Zeijlmans van Emmichoven, C. C. Havener, F. W. Meyer, and D. M. Zehner, "Electron Emission During Multicharged Ion-Surface Interactions," *Nucl. Instrum. and Methods Phys. Res. Sect. B* **56/57**, 136 (1991).

J. Zhang, N. C. Tien, E. W. Lin, H. H. Wieder, W. H. Ku, C. W. Tu, D. B. Poker, and S. N. G. Chu, "Molecular Beam Epitaxial Growth and Characterization of Pseudomorphic Modulation-Doped Field-Effect Transistors," *Thin Solid Films* **196**, 295 (1991).

Ji-Guang Zhang, Xiang-Xin Bi, E. McRae, P. C. Eklund, B. C. Sales, and Mark Mostoller, "Optical Studies of Single-Crystal $Nd_{2-x}Ce_xCuO_{4-\delta}$," *Phys. Rev. B* **43**, 5389 (1991).

R. A. Zuhr, T. E. Haynes, M. D. Galloway, S. Tanaka, A. Yamada, and I. Yamada, "Formation of Aluminum Films on Silicon by Ion Beam Deposition: A Comparison with Ionized Cluster Beam Deposition," *Nucl. Instrum. and Methods Phys. Res. Sect. B* **59/60**, 308 (1991).

J.-K. Zuo and J. F. Wendelken, "Substrate Temperature Effects on $(\sqrt{3}\times\sqrt{3})R30°$ Domain Growth of Ag on Si(111) Surface," *Appl. Surf. Sci.* **48/49**, 366 1991.

J.-K. Zuo and J. F. Wendelken, "Defect and Impurity Effects on the Initial Growth of Ag on Si(111)," *J. Vac. Sci. and Technol. A* **9**, 1539 (1991).

J.-K. Zuo and J. F. Wendelken, "Scaling of the $(\sqrt{3}\sqrt{3})30°$ Domain Size Distribution with Coverage for Ag/Si(111)," *Phys. Rev. Lett.* **66**, 2227 (1991).

# *BOOKS AND PROCEEDINGS*

D. L. Abernathy, D. Gibbs, G. Grübel, K. G. Huang, S. G. J. Mochrie, B. M. Ocko, A. R. Sandy, and D. M. Zehner, "X-Ray Reflectivity Studies of Au Surfaces," p. 37 in *Surface X-Ray and Neutron Scattering*, ed. by H. Zabel and I. K. Robinson, Springer-Verlag, Berlin, 1992.

Harry A. Atwater, Frances A. Houle, and Douglas H. Lowndes, eds., *Surface Chemistry and Beam-Solid Interactions*, Materials Research Society, Pittsburgh, Pennsylvania, 1991.

A. P. Baddorf and E. W. Plummer, "Surface Anharmonicity: Temperature Dependence of Phonon Energies on Cu(110)," p. 541 in *Vibrations at Surfaces 1990*, ed. by Yves Chabel and Fritz Hoffman, Elsevier Science Publishers, Amsterdam, 1990.

K. Becker, L. Yang, R. F. Haglund Jr., R. H. Magruder, R. A. Weeks, and R. A. Zuhr, "Laser-Induced Fluorescence and Nonlinear Optical Properties of Ion-Implanted Fused Silica," p. 1304 in *Ion Beam Modification of Materials '90*, ed. by S. P. Withrow and D. B. Poker, North-Holland, Amsterdam, 1991.

J. B. Bates, N. J. Dudney, B. C. Sales, J. D. Robertson, R. A. Zuhr, G. R. Gruzalski, and C. F. Luck, "Thin-Film Amorphous Electrolytes: The $Li_2O$-$SiO_2$-$P_2O_5$ System," p. 569 in *Solid State Ionics II*, ed. by Gholam-Abbas Nazri, Duward F. Shriver, Robert A. Huggins, and Minko Balkanski, Materials Research Society, Pittsburgh, Pennsylvania, 1991.

L. A. Boatner, T. F. Ciszek, and T. Surek, eds., *American Crystal Growth 1990, Proceedings of the Eighth American Conference on Crystal Growth*, North-Holland, Amsterdam, 1991.

J. S. Brodkin, W. Franzen, R. J. Culbertson, and J. M. Williams, "Characterization of Ion-Implanted Aluminum and Iron by Spectroscopic Ellipsometry," p. 289 in *Surface Chemistry and Beam-Solid Interactions*, ed. by Harry A. Atwater, Frances A. Houle, and Douglas H. Lowndes, Materials Research Society, Pittsburgh, Pennsylvania, 1991.

Y. Chen, M. M. Abraham, and D. F. Pedraza, "Radiation Damage in $Al_2O_3$ Crystals Implanted with 3.8-MeV $Fe^{2+}$ Ions," p. 1163 in *Ion Beam Modification of Materials '90*, ed. by S. P. Withrow and D. B. Poker, North-Holland, Amsterdam, 1991.

Y. Chen, V. M. Orera, and R. Gonzalez, "Prospects for Wavelength Tunable Lasers Based on Vacancy Defects in Alkaline-Earth Oxides," *Proceedings of the 5th International Laser Conference*, Irkutsk, USSR, 1990.

D. K. Christen, C. E. Klabunde, R. Feenstra, D. H. Lowndes, D. P. Norton, J. D. Budai, H. R. Kerchner, J. R. Thompson, S. Zhu, and A. D. Marwick, "Orientation-Dependent Critical Currents in $YBa_2Cu_3O_{7-x}$ Epitaxial Thin Films: Evidence for Intrinsic Flux Pinning?" p. 336 in *Superconductivity and Its Applications*, AIP Conference Proceedings 219, ed. by Yi-Han Kao, Philip Coppens, and Hoi-Sing Kwok, American Institute of Physics, New York, 1991.

L. Civale, M. W. McElfresh, A. D. Marwick, T. K. Worthington, A. P. Malozemoff, F. Holtzberg, C. Feild, J. R. Thompson, D. K. Christen, and M. A. Kirk, "Critical Currents in Proton-Irradiated $YBa_2Cu_3O_{7-\delta}$ Crystals," p. 25 in *Progress in High-Temperature Superconductivity*, Vol. 31, ed. by J. L. Heiras, L. E. Sansores, and A. A. Valladares, World Scientific Publishing Co., Singapore, 1991.

N. J. Dudney, J. B. Bates, J. D. Robertson, and C. F. Luck, "Sputter Deposition of Lithium Silicate–Lithium Phosphate Amorphous Electrolytes," p. 579 in *Solid State Ionics II*, ed. by Gholam-Abbas Nazri, Duward F. Shriver, Robert A. Huggins, and Minko Balkanski, Materials Research Society, Pittsburgh, Pennsylvania, 1991.

L. J. Effler, J. F. Fellers, and J. S. Lin, "Small-Angle X-Ray Scattering Behavior of Microporous Fibers Used in Composite Structures," p. 179 in *Composite Applications—The Role of Matrix, Fiber, and Interface*, ed. by T. L. Vigo and B. J. Kinzig, VCH Publishers, Inc., New York, 1992.

D. Eres, "High-Speed Epitaxy Using Supersonic Molecular Jets," p. 11 in *Surface Chemistry and Beam-Solid Interactions*, ed. by Harry A. Atwater, Frances A. Houle, and Douglas H. Lowndes, Materials Research Society, Pittsburgh, Pennsylvania, 1991.

D. B. Geohegan, "In Situ Laser Ablation Plasma Diagnostics in the Film-Growth Regime—Effects of Ambient Background Gases," p. 557 in *Surface Chemistry and Beam-Solid Interactions*, ed. by Harry A. Atwater, Frances A. Houle, and Douglas H. Lowndes, Materials Research Society, Pittsburgh, Pennsylvania, 1991.

A. Golanski, W. H. Christie, M. D. Galloway, J. L. Park, S. J. Pennycook, D. B. Poker, J. L. Moore, H. E. Harmon, and C. W. White, "Ion Beam Induced Diffusion and Crystallization in High-Dose Er-Implanted Si," p. 444 in *Ion Beam Modification of Materials '90*, ed. by S. P. Withrow and D. B. Poker, North-Holland, Amsterdam, 1991.

A. Golanski, R. Feenstra, M. D. Galloway, J. L. Park, S. J. Pennycook, H. E. Harmon, and C. W. White, "Ion Beam Synthesis of Buried Single-Crystal Erbium Silicide," p. 319 in *Surface Chemistry and Beam-Solid Interactions*, ed. by Harry A. Atwater, Frances A. Houle, and Douglas H. Lowndes, Materials Research Society, Pittsburgh, Pennsylvania, 1991.

T. E. Haynes and O. W. Holland, "Dose Rate Effects on Damage Formation in Ion-Implanted Gallium Arsenide," p. 1028 in *Ion Beam Modification of Materials '90*, ed. by S. P. Withrow and D. B. Poker, North-Holland, Amsterdam, 1991.

J. B. Hayter, "The Advanced Neutron Source," p. 27 in *Neutron Scattering for Materials Science*, ed. by S. M. Shapiro, S. C. Moss, and J. D. Jorgensen, Materials Research Society, Pittsburgh, Pennsylvania, 1990.

J. B. Hayter, "Status of the Advanced Neutron Source," p. 75 in *Proceedings of the XI International Conference on Advanced Neutron Sources*, KEK, Tsukuba, Japan, 1990.

J. B. Hayter, "Optical Neutron Polarizers," p. 890 in *Proceedings of the XI International Conference on Advanced Neutron Sources*, KEK, Tsukuba, Japan, 1990.

O. W. Holland and C. W. White, "Ion-Induced Damage and Amorphization in Si," p. 353 in *Ion Beam Modification of Materials '90*, ed. by S. P. Withrow and D. B. Poker, North-Holland, Amsterdam, 1991.

J. A. Horton, C. T. Liu, and S. J. Pennycook, "Grain Boundary Structure as a Function of Aluminum Level in $Ni_3Al$," p. 417 in *High-Temperature Ordered Intermetallic Alloys*, ed. by Lyman Johnson and J. O. Stiegler, Materials Research Society, Pittsburgh, Pennsylvania, 1991.

D. E. Jesson and S. J. Pennycook, "Structural and Compositional Mapping at Si-Ge Interfaces Using Z-Contrast STEM," p. 800 in *Proceedings of the 49th Annual Meeting of the Electron Microscopy Society of America*, ed. by G. W. Bailey, San Francisco Press, Inc., San Francisco, California, 1991.

D. E. Jesson, S. J. Pennycook, and J.-M. Baribeau, "Direct Imaging of Ordering in Si-Ge Alloys, Ultrathin Superlattices, and Buried Ge Layers," p. 141 in *Si Molecular Beam Epitaxy*, ed. by J. C. Bean, E. H. C. Parker, S. S. Iyer, Y. Shiraki, E. Kasper, and K. L. Wang, Materials Research Society, Pittsburgh, Pennsylvania, 1991.

K. S. Jones, M. Bollong, T. E. Haynes, M. D. Deal, E. L. Allen, and H. G. Robinson, "Ion Implantation Related Defects in GaAs," p. 785 in *Advanced III-V Compound Semiconductor Growth, Processing, and Devices*, ed. by S. J. Pearton, D. K. Sadana, and J. M. Zavada, Materials Research Society, Pittsburgh, Pennsylvania, 1992.

M. Jonson, "Tunneling Times in Quantum Mechanical Tunneling," p. 193 in *Quantum Transport in Semiconductors*, ed. by D. Ferry and C. Jacoboni, Plenum Publishing Company, New York, 1991.

H. R. Kerchner, J. O. Thomson, and R. Feenstra, "AC Susceptibility of Superconductive Thin Films," p. 997 in *Advances in Cryogenic Engineering—Materials*, Vol. 38, ed. by F. R. Pickett and R. P. Reed, Plenum Publishing Company, New York, 1992.

R. A. Klemm and S. H. Liu, "Interlayer Pairing and c-Axis Versus ab-Plane Gap Anisotropy in High-$T_c$ Superconductors," p. 609 in *High-Temperature Superconductivity*, ed. by J. Ashkenazi and G. Vizzoli, Plenum Publishing Company, New York, 1991.

B. C. Larson and J. Z. Tischler, "Time-Resolved Techniques: An Overview," p. 90 in *Advanced X-Ray/EUV Radiation Sources and Applications*, ed. by James P. Knauer and Gopal K. Shenoy, Society of Photo-Optical Instrumentation Engineers, Bellingham, Washington, 1990.

B. C. Larson and J. Z. Tischler, "Time-Resolved Techniques: An Overview," p. 275 in *Current Overviews in Optical Science and Engineering II, SPIE Advent Technology Series*, Vol. 2, ed. by Richard Feinberg, Society of Photo-Optical Instrumentation Engineers, Bellingham, Washington, 1991.

J. K. Lawson, H. W. H. Lee, S. A. Payne, and L. A. Boatner, "Excited-State Absorption Measurements of $Sm^{2+}$ in $CaF_2$, $SrF_2$, and $SrCl_2$," p. 386 in *OSA Proceedings on Advanced Solid-State Lasers*, Vol. 10, ed. by George Dubé and Lloyd Chase, Optical Society of America, Washington, D.C., 1991.

S. H. Liu, Theodore Kaplan, and L. J. Gray, "Deterministic Sand Pile—Route to Chaos in Large Systems," p. 33 in *Proceedings of the Twelfth Annual International Conference of the IEEE Engineering in Medicine and Biology Society*, ed. by Peder C. Pedersen and Banu Onaral, IEEE, New York, 1990.

S. H. Liu, "Theory of Bulk and Interface Constant Phase Elements in Electrode-Electrolyte Systems," p. 327 in *Condensed Matter Physics Aspects of Electrochemistry*, ed. by M. P. Tosi and A. A. Kornyshev, World Scientific Publishing Company PTE Ltd., Singapore, 1991.

D. H. Lowndes, D. P. Norton, J. D. Budai, D. K. Christen, C. E. Klabunde, R. J. Warmack, and S. J. Pennycook, "Growth and Transport Properties of Y-Ba-Cu-O/Pr-Ba-Cu-O Superlattices," p. 150 in *Progress in High-Temperature Superconducting Transitors and Other Devices*, Vol. 1394, Society of Photo-Optical Instrumentation Engineers, Bellingham, Washington, 1990.

R. H. Magruder III, R. A. Zuhr, and R. A. Weeks, "Dose Rate Dependence of the Optical Absorption of Cu-Implanted Silica," p. 1308 in *Ion Beam Modification of Materials '90*, ed. by S. P. Withrow and D. B. Poker, North-Holland, Amsterdam, 1991.

G. D. Mahan, "Theory of Photoemission," p. 25 in *Photoemission and Absorption Spectroscopy of Solids and Interfaces with Synchrotron Radiation*, ed. by M. Campagna and R. Rosei, North-Holland, Amsterdam, 1990.

G. D. Mahan, *Many-Particle Physics*, 2nd Ed., Plenum Publishing Corporation, New York, 1990.

G. D. Mahan, "Short-Range Polarization in Insulators," p. 325 in *Solid State Sciences*, ed. by R. Catlow and R. W. Grimes, World Scientific Publishing Company PTE Ltd., Singapore, 1991.

G. D. Mahan, "Quantum Boltzman Equation for Linear Transport," p. 101 in *Quantum Theory of Transport*, ed. by D. Ferry and C. Jacoboni, Plenum Publishing Company, New York, 1992.

D. N. Mashburn and D. B. Geohegan, "$Y_2Ba_2Cu_3O_{7-x}$ Laser-Ablation Plume Dynamics Measurements by Nanosecond Response Ion Probe: Comparison with Optical Measurements," p. 181 in *SPIE Proceedings*, Vol. 1187, ed. by T. Venkatesan, Society of Photo-Optical Instrumentation Engineers, Bellingham, Washington, 1989.

C. J. McHargue, A. Perez, and J. C. McCallum, "The Chemical State of Iron Ions Implanted Into Silicon Carbide," p. 1362 in *Ion Beam Modification of Materials '90*, ed. by S. P. Withrow and D. B. Poker, North-Holland, Amsterdam, 1991.

S. G. J. Mochrie, D. Gibbs, and D. M. Zehner, "X-Ray and Neutron Scattering Studies of the Structure and Phase Behavior of Surfaces and Interfaces," p. 35 in *Physics News in 1990*, ed. by Phillip F. Schewe, American Institute of Physics, New York, 1991.

H. A. Mook, G. Aeppli, S. M. Hayden, Z. Fisk, and D. Rytz, "Neutron Scattering Measurements of the Magnetic Excitations of High-Temperature Superconducting Materials," p. 21 in *Dynamics of Magnetic Fluctuations in High-Temperature Superconductors*, ed. by G. Reiter, Peter Horsch, and Gregory C. Psaltakis, Plenum Publishing Company, New York, 1991.

D. P. Norton, D. H. Lowndes, D. K. Christen, E. C. Jones, J. D. Budai, T. D. Ketcham, D. St. Julien, K. W. Lay, and J. E. Tkaczyk, "$Y_2Ba_2Cu_3O_{7-x}$ Thin-Film Growth on Single-Crystal and Polycrystalline Yttria-Stabilized Zirconia," p. 157 in *Science and Technology of Thin-Film Superconductors II*, ed. by R. D. McConnell and Rommel Noufi, Plenum Publishing Company, New York, 1990.

D. P. Norton, D. H. Lowndes, X. Zheng, R. J. Warmack, S. J. Pennycook, and J. D. Budai, "Superconducting Transport Properties and Surface Microstructure for $YBa_2Cu_3O_{7-\delta}$-Based Superlattices Grown by Pulsed-Laser Deposition" p. 311 in *Laser Ablation: Mechanisms and Applications*, ed. by J. C. Miller and R. F. Haglund, Jr., Springer-Verlag, New York, 1991.

S. J. Pennycook, D. E. Jesson, and M. F. Chisholm, "Atomic Scale Imaging of the Structure and Chemistry of Semiconductor Interfaces," p. 182 in *Nanostructures and Microstructure Correlation with Physical Properties of Semiconductors*, SPIE Proceedings Vol. 1284, Society of Photo-Optical Instrumentation Engineers, Bellingham, Washington, 1990.

S. J. Pennycook and D. E. Jesson, "Compositional Mapping Using Large-Angle Electron Scattering," p. 10 in *Proceedings of the 49th Annual Meeting of the Electron Microscopy Society of America*, ed. by G. W. Bailey, San Francisco Press, Inc., San Francisco, 1991.

S. J. Pennycook, D. E. Jesson, and M. F. Chisholm, "High-Resolution Z-Contrast Imaging of Superlattices and Heterostructures," p. 27 in *Microscopy of Semiconducting Materials*, Institute of Physics Conference Series No. 117: Section I, Institute of Physics, London, 1991.

Sune Pettersson, "On the Choice of Trial Function in Theoretical Calculations of the Thermal Conductivity," p. 415 in *Proceedings of the 21st International Conference on Thermal Conductivity*, Plenum Publishing Company, New York, 1990.

R. A. Phaneuf, F. W. Meyer, D. C. Gregory, C. C. Havenor, P. A. Zeijlmans van Emmichoven, S. H. Overbury, D. M. Zehner, G. H. Dunn, J. S. Thompson, E. K. Wahlin, and A. C. H. Smith, "Low-Energy Collisions of Multiply Charged Ions with Electrons, Atoms, and Surfaces," p. 403 in *Atomic and Molecular Physics*, ed. by C. Cisneros, I. Alvarez, and T. J. Morgan, World Science Publishers, Singapore, 1992.

S. Raman and J. B. Hayter, "The Advanced Neutron Source," p. 923 in *Proceedings of the Seventh International Conbference on Capture Gamma-Ray Spectroscopy and Related Topics*, Volume 238, American Institute of Physics, New York, 1991.

S. T. Sekula, "Static and Dynamic Magnetization Properties of $YBa_2Cu_3O_2$ Thin Films," p. 276 in *Proceedings of European Conference on High-$T_c$ Thin Films and Single Crystals, Progress in High-Temperature Superconductivity*, Vol. 24, ed. by W. Gorzkowski, M. Gutowski, A. Reich, and H. Szymczak, World Scientific Publishing Company PTE Ltd., Singapore, 1991.

P. S. Sklad, L. Romana, C. J. McHargue, C. W. White, and J. C. McCallum, "The Effect of Post-Implantation Annealing on the Microstructure of $Al_2O_3$ Implanted with Iron at -185°C," p. 1187 in *Ion Beam Modification of Materials '90*, ed. by S. P. Withrow and D. B. Poker, North-Holland, Amsterdam, 1991.

C. E. Vallet and C. W. White, "Application of Ion Implantation to Electrochemical Studies," p. 855 in *Ion Beam Modification of Materials '90*, ed. by S. P. Withrow and D. B. Poker, North-Holland, Amsterdam, 1991.

G. Vignale, Mark Rasolt, and D. J. W. Geldart, "Magnetic Fields and Density Functional Theory," p. 235 in *Advances in Quantum Chemistry, Vol. 21, Density Functional Theory of Many-Fermion Systems*, ed. by Samuel B. Trickey, Academic Press, New York, 1990.

G. D. Wignall, "Neutron Scattering from Amorphous Polymers and Networks," p. 207 in *Elastomeric Polymer Networks*, Eugene Guth Memorial Volume, ed. by J. E. Mark, Prentice Hall, New York, 1991.

J. M. Williams, A. Gonzales, J. Quintana, R. A. Buchanan, I.-S. Lee, F. C. Burns, R. J. Culbertson, M. Levy, and J. R. Treglio, "Ion Implantation for Corrosion Inhibition of Aluminum Alloys in Saline Media," p. 845 in *Ion Beam Modification of Materials '90*, ed. by S. P. Withrow and D. B. Poker, North-Holland, Amsterdam, 1991.

S. P. Withrow and D. B. Poker, eds., *Ion Beam Modification of Materials '90*, North-Holland, Amsterdam, 1991.

W. Xia, S. N. Hsu, C. C. Han, S. A. Pappert, B. Zhu, C. Cozzolino, P. K. L. Yu, S. S. Lau, D. B. Poker, C. W. White, and S. A. Schwarz, "Ion Mixing of Semiconductor Superlattices," p. 491 in *Ion Beam Modification of Materials '90*, ed. by S. P. Withrow and D. B. Poker, North-Holland, Amsterdam, 1991.

R. A. Zuhr, T. E. Haynes, M. D. Galloway, S. Tanaka, A. Yamada, and I. Yamada, "Formation of Aluminum Films on Silicon by Ion Beam Deposition: A Comparison with Ionized Cluster Beam Deposition," p. 308 in *Ion Beam Modification of Materials '90*, ed. by S. P. Withrow and D. B. Poker, North-Holland, Amsterdam, 1991.

## *REPORTS ISSUED*

Y. Chen and F. W. Wiffen, *DOE Task Force Meeting on Electrical Breakdown of Insulating Ceramics in a High Radiation Field*, Oak Ridge National Laboratory, CONF-9105176 (August 1991).

J. A. Fernandez-Baca, R. M. Nicklow, M. Hagen, and Y. Tsunoda, "A Study of the Magnetic Excitations in the Itinerant Antiferromagnet $Mn_{90}Cu_{10}$," p. 94 in *ILL Experimental Reports and Theory College Activities*, Institut Laue Langevin, Grenoble, France (1990).

D. Gibbs, G. Grübel, D. M. Zehner, D. L. Abernathy, and S. G. J. Mochrie, "Structure and Phases of Pt(001) Surface," p. 317 in *National Synchrotron Light Source Annual Report 1990*, Brookhaven National Laboratory, BNL-52272, (April 1991).

G. Grübel, K. G. Huang, Doon Gibbs, D. M. Zehner, A. R. Sandy, and S. G. J. Mochrie, "High-Temperature Reconstruction of Pt(111)," p. 318 in *National Synchrotron Light Source Annual Report 1990*, Brookhaven National Laboratory, BNL-52272 (April 1991).

G. R. Gruzalski, D. M. Zehner, S.-C. Lui, and D. Heskett, "Work-Function Variations Accompanying Changes in the Composition of $HfC_x$ and $TaC_x$," p. 143 in *National Synchrotron Light Source Annual Report 1990*, Brookhaven National Laboratory, BNL-52272 (April 1991).

B. C. Larson and C. J. Sparks, *DOE/DMS Workshop on Future Synchrotron VUV and X-Ray Beam Lines*, Oak Ridge National Laboratory, CONF-9110340 (March 1992).

S.-C. Lui, G. R. Gruzalski, D. M. Zehner, and D. Heskett, "Surface Core Level Shifts for Hf(0001)," p. 143 in *National Synchrotron Light Source Annual Report 1990,* Brookhaven National Laboratory, BNL-52272 (April 1991).

S. G. J. Mochrie, D. M. Zehner, B. M. Ocko, and L. D. Gibbs, "Phases and Transitions of the Au(001) Surface," p. 307 in *National Synchrotron Light Source Annual Report 1990,* Brookhaven National Laboratory, BNL-52272 (April 1991).

A. R. Sandy, S. G. J. Mochrie, K. G. Huang, L. D. Gibbs, B. M. Ocko, and D. M. Zehner, "X-Ray Surface Diffraction Study of the Au(111) Surface," p. 309 in *National Synchrotron Light Source Annual Report 1990,* Brookhaven National Laboratory, BNL-52272 (April 1991).

A. R. Sandy, S. G. J. Mochrie, K. G. Huang, L. D. Gibbs, and D. M. Zehner, "X-Ray Reflectivity Study of the Relaxation of the Au(110) Surface," p. 308 in *National Synchrotron Light Source Annual Report 1990,* Brookhaven National Laboratory, BNL-52272 (April 1991).

A. R. Sandy, S. G. J. Mochrie, K. G. Huang, G. Grübel, L. D. Gibbs, and D. M. Zehner, "The Pt(111) Surface—X-Ray Reflectivity," p. 308 in *National Synchrotron Light Source Annual Report 1990,* Brookhaven National Laboratory, BNL-52272 (April 1991).

## *PATENTS GRANTED*

Yok Chen, *Method for Enhancement of Useful Luminescence from Vacancy Defects in Refractory Oxides for Tunable Lasers,* U.S. Patent No. 4,9963,755 (October 16, 1990).

Chin-Chi Tsai, Steven M. Gorbatkin, and Lee A. Berry, *Plasma Generating Apparatus for Large Area Plasma Processing,* U.S. Patent No. 5,032,202 (July 16, 1991).

## *THESES*

J. G. Ossandon, "Magnetization Studies of the Effects of Oxygen Deficiency $\delta$ on the Superconductive Properties of Aligned $YBa_2Cu_3O_{7-\delta}$ Materials," Ph.D. Thesis, The University of Tennessee, Knoxville, Tennessee, 1991.

## *PAPERS PRESENTED AT TECHNICAL MEETINGS*

**DOE-BES Information Meeting, Argonne, Illinois, October 1–2, 1990:**

H. L. Davis, "Layer-By-Layer Constituent Segregation in Surfaces of Substitutionally Random Binary Alloys" (invited paper)

Douglas H. Lowndes, David P. Norton, J. D. Budai, D. K. Christen, and C. E. Klabunde, "Preparation and Properties of High-$T_c$ Superconductor Superlattices" (invited paper)

S. J. Pennycook, "Compositional Imaging of Interfaces in Semiconductors and Superconductors by Z-Contrast STEM" (invited paper)

**SPIE Conference on Progress in High-Temperature Superconducting Transistors, Santa Clara, California, October 4–5, 1990:**

D. H. Lowndes, David P. Norton, J. D. Budai, D. K. Christen, C. E. Klabunde, R. J. Warmack, and S. J. Pennycook, "Growth and Transport Properties of Y-Ba-Cu-O/Pr-Ba-Cu-O Superlattices" (invited paper)

**Thirty-Seventh Annual AVS Symposium and Topical Conferences, Toronto, Canada, October 8–12, 1990:**

Arthur P. Baddorf and E. W. Plummer, "Anharmonicity in Surface Phonons on Cu(110)"

B. Blum, E. W. Plummer, H. L. Davis, and D. M. Zehner, "Bi-Induced Overlayer Structures on Cu(001)"

H. L. Davis, D. M. Zehner, D. V. Gemunden, B. Dötsch, and K. Müller, "Layer-by-Layer Segregation and Deep Multilayer Relaxation in the Random Alloy Surface $Mo_{85}Re_{15}(100)$"

S. L. Hulbert, C. C. Kao, R. F. Garrett, M. Weinert, R. A. Bartynski, S. Yang, E. Jensen, and D. M. Zehner, "A Comparison of the Surface Electronic Structure of Ta(100) and TaC(111) by Auger Photoelectron Coincidence Spectroscopy"

A. L. Wachs, J. B. Bates, N. J. Dudney, R. A. Zuhr, C. F. Luck, and J. D. Robertson, "Plasma Diagnostic Studies of the Influence of Process Variables upon the Compositions of Electrolyte Films Deposited by RF Magnetron Sputtering"

D. M. Zehner, S.-C. Lui, G. R. Gruzalski, D. R. Heskett, and X. Shi, "Surface 4*f* Core-Level Shift in Hf(0001)"

J.-K. Zuo and J. F. Wendelken, "$(\sqrt{3}\times\sqrt{3})R30°$ Domain Growth of Ag on the Si(111) Surface"

**The Mining, Minerals, and Materials Society Fall Meeting, Detroit, Michigan, October 15–18, 1990:**

J. J. Hoyt, and S. Spooner, "The Study of Particle Coarsening by Small-Angle Scattering"

C. S. Pande, C. L. Vold, M. A. Imam, E. Dantsker, and S. Spooner, "Study of Early Stages of Precipitation Kinetics in HSLA (A710) Steel Using Small-Angle Neutron Scattering"

S. Spooner and S. A. David, "Investigation of Strain Distributions in a 1-in.-Thick Stainless Steel Plate Containing a Multiple-Pass Weld"

**Eleventh International Conference on Advanced Neutron Sources (ICANS-XI), Tsukuba, Japan, October 22–26, 1990:**

John B. Hayter, "Optical Neutron Polarizers" (invited paper)

John B. Hayter, "Status of the Advanced Neutron Source" (invited paper)

**Thirty-Fifth Annual Conference on Magnetism and Magnetic Materials, San Diego, California, October 29–November 1, 1990:**

J. W. Cable, B. Gillon, I. Mirebeau, G. Parette, and Y. Nakai, "Atomic and Magnetic Spatial Correlations in Fe-13.5% V" [*J. Appl. Phys.* **69**, 6150 (1991)]

S. M. Hayden, G. Aeppli, S.-W. Cheong, H. A. Mook, Z. Fisk, and D. Rytz, "Neutron Scattering Studies on Lanthanum Cuprates" [*J. Appl. Phys.* **69**, 4519 (1991)] (invited paper)

H. A. Mook, "Recent Neutron Studies of High-$T_c$ Materials" [*J. Appl. Phys.* **69**, 5391 (1991)] (invited paper)

T. G. Perring, A. T. Boothroyd, D. McK. Paul, A. D. Taylor, R. Osborn, R. J. Newport, J. A. Blackman, and H. A. Mook, "High-Energy Spin Waves in BCC Iron" [*J. Appl. Phys.* **69**, 6219 (1991)]

**Twelfth Annual International Conference of the IEEE/Engineering in Medicine and Biology Society (IEEE/EMBS), Philadelphia, Pennsylvania, November 1–4, 1990:**

S. H. Liu, Theodore Kaplan, and L. J. Gray, "Deterministic Sand Pile—Route to Chaos in Large Systems" (invited paper)

**Annual Meeting of the Optical Society of America, Boston, Massachusetts, November 4–9, 1990:**

G. E. Jellison, Jr., "The Use of the Biased Estimator in the Interpretation of Spectroscopic Ellipsometry Data"

G. E. Jellison, Jr., and B. C. Sales, "The Determination of the Optical Functions of Transparent Glasses Using Spectroscopic Ellipsometry"

**Eleventh International Conference on the Application of Accelerators in Research and Industry, Denton, Texas, November 5–8, 1990:**

L. A. Berry and S. M. Gorbatkin, "Characteristics of ECR Plasmas for Advanced Deposition and Etch Technology"

T. E. Haynes and O. W. Holland, "A Comparative Study of Damage Accumulation in GaAs, Ge, and Si During Ion Implantation" (invited paper)

P. A. Zeijlmans van Emmichoven, C. C. Havener, F. W. Meyer, and D. M. Zehner, "Electron Emission During Multicharged Ion-Surface Interactions" (invited paper)

**Emerging Trends in Ion Implant Technology, San Jose, California, November 7, 1990:**

R. A. Zuhr, "Direct Deposition of Epitaxial Thin Films from Mass-Analyzed Low-Energy Ion Beams"

**American Nuclear Society 1990 Winter Meeting, Washington, D.C., November 11–15, 1992:**

J. B. Hayter, "Advanced Neutron Source—The User's Perspective" (invited paper)

**Materials Research Society Fall Meeting, Boston, Massachusetts, November 26–December 1, 1990:**

J. B. Bates, N. J. Dudney, A. L. Wachs, G. R. Gruzalski, R. A. Zuhr, B. C. Sales, and J. D. Robertson, "Thin-Film Amorphous Electrolytes" (invited paper)

S. P. Bozeman, C. T. Kao, N. R. Parikh, L. E. McNeil, M. L. Swanson, and T. E. Haynes, "Electrical, Optical, and Lattice Location Studies of Defects Created by Dual Implantation in GaP"

J. S. Brodkin, W. Franzen, R. J. Culbertson, and J. M. Williams, "Characterization of Ion-Implanted Aluminum and Iron by Spectroscopic Ellipsometry"

B. C. Chakoumakos, J. A. Fernandez-Baca, B. C. Sales, and H. A. Mook, Jr., "Rietveld Analysis of $Bi_2Sr_{2-x}La_xCuO_{6+y}$ from Neutron Powder Diffraction Data"

M. F. Chisholm and S. J. Pennycook, "Structure of Grain Boundaries in $YBa_2Cu_3O_{7-\delta}$ Superconductors"

D. K. Christen, C. E. Klabunde, J. R. Thompson, H. R. Kerchner, D. P. Norton, D. H. Lowndes, R. Feenstra, and J. D. Budai, "Thermally Activated Flux Motion and Limitations on Critical Currents in Epitaxial Thin Films of $YBa_2Cu_3O_{7-x}$"

N. J. Dudney, J. B. Bates, A. L. Wachs, and C. F. Luck, "Sputter Deposition of Lithium Silicate-Lithium Phosphate Amorphous Electrolytes" (invited paper)

D. Eres, "Very High Speed Epitaxy Using Supersonic Molecular Jets" (invited paper)

R. Feenstra, D. K. Christen, J. D. Budai, M. D. Galloway, D. H. Lowndes, and D. P. Norton, "A New Method for Post-Annealing of $YBa_2Cu_3O_{7-x}$ Films at Temperatures Below 800°C"

D. B. Geohegan, "In Situ Laser Ablation Plasma Diagnostics in the Film-Growth Regime—Effects of Ambient Background Gases"

A. Golanski, R. Feenstra, M. D. Galloway, J. L. Park, S. J. Pennycook, J. M. Williams, and C. W. White, "Ion Beam Synthesis of Buried Single-Crystal Erbium Silicide"

J. A. Horton, C. T. Liu, and S. J. Pennycook, "Grain Boundary Structure as a Function of Aluminum Level in $Ni_3Al$"

T. E. Huber, P. W. Schmidt, C. A. Huber, and J. S. Lin, "SAXS Study of Selenium-Impregnated Porous Vycor Glass"

D. E. Jesson, S. J. Pennycook, and J.-M. Baribeau, "Direct Imaging of Interfacial Ordering in Ultrathin $Si_m(Ge_n)_p$ Superlattices Using Z-Contrast STEM"

H. R. Kerchner, J. O. Thomson, J. R. Thompson, J. Ossandon, D. P. Norton, and D. H. Lowndes, "Dynamic Magnetic Hysteresis of In Situ Grown $YBa_2Cu_3O_7/PrBa_2Cu_3O_7$ Superlattice Thin Films"

David P. Norton, Douglas H. Lowndes, J. D. Budai, D. K. Christen, R. Feenstra, and B. C. Sales, "In Situ Growth of $YBa_2Cu_3O_{7-x}/Pr_{0.7}Y_{0.3}BaCuO_{7-x}$ Superlattice Structures by Pulsed-Laser Ablation"

S. J. Pennycook, M. F. Chisholm, D. E. Jesson, D. P. Norton, and D. H. Lowndes, "Interface Structure and Interdiffusion in $YBa_2Cu_3O_{7-x}/PrBa_2Cu_3O_{7-x}$ Superlattices Studied by Z-Contrast STEM"

S. J. Pennycook, D. E. Jesson, and M. F. Chisholm, "Compositional Imaging of Semiconductor Interfaces by Z-Contrast STEM"

B. C. Sales and B. C. Chakoumakos, "Enhancement of $T_c$ with Rare-Earth Doping in $Bi_2Sr_{2-x}RE_xCuO_{6+y}$, RE = La, Pr, Nd, and Sm"

J. R. Thompson, Y. R. Sun, D. K. Christen, J. G. Ossandon, H. R. Kerchner, A. Marwick, and F. Holtzberg, "Reduced Flux Motion in High-$J_c$, Proton-Irradiated Single-Crystal $YBa_2Cu_3O_7$"

A. L. Wachs, J. B. Bates, N. J. Dudney, and C. F. Luck, "The Synthesis of Lithium Silicate-Lithium Phosphate Amorphous Electrolytes by RF Magnetron Sputtering: A Plasma Diagnostic Study"

**The University of Miami Workshop on Electronic Structure and Mechanisms for High Superconductivity, Miami, Florida, January 3–9, 1991:**

R. A. Klemm and S. H. Liu, "Interlayer Pairing and c-Axis Versus ab-Plane Gap Anisotropy"

D. H. Lowndes and D. P. Norton, "Kosterlitz-Thouless-Like Behavior over Extended Ranges of Temperature and Layer Thickness in Crystalline $YBa_2Cu_3O_{7-x}/PrBa_2Cu_3O_{7-x}$ Superlattices" (invited paper)

**Winter Meeting on Low-Temperature Physics, Cuernavaca, Mexico, January 13–16, 1991:**

L. Civale, M. W. McElfresh, A. D. Marwick, T. K. Worthington, A. P. Malozemoff, F. Holtzberg, C. Feild, J. R. Thompson, D. K. Christen, and M. A. Kirk, "Critical Currents in Proton-Irradiated $YBa_2Cu_3O_{7-\delta}$ Crystals" (invited paper)

**Conference on the Microphysics of Surfaces: Beam-Induced Processes, Santa Fe, New Mexico, February 11–13, 1991:**

R. A. Zuhr and T. E. Haynes, "Oriented Aluminum Films on Silicon by Direct Ion Beam Deposition" [*Technical Digest on The Microphysics of Surfaces: Beam-Induced Processes* **3**, 139 (1991)].

**TMS Annual Meeting, New Orleans, Louisiana, February 17–21, 1991:**

B. C. Sales, J. O. Ramey, J. C. McCallum, and L. A. Boatner, "Structural Differences Between the Glass State and Ion-Implanted Layers on Lead Pyrophosphate" (invited paper)

**WATTec '91—Eighteenth Annual Technical Conference and Exhibition, Knoxville, Tennessee, February 19–22, 1991:**

J. B. Hayter, "Applications of the Advanced Neutron Source Reactor"

R. M. Moon, "Experimental Studies Being Conducted at the High Flux Isotope Reactor—Part 2" (invited paper)

**Generalized Structure Analysis System (GSAS) Workshop, Los Alamos New Mexico, February 27–March 1, 1991:**

B. C. Chakoumakos, G. A. Lager, and J. A. Fernandez-Baca, "Crystal Structure Refinements of $Sr_2Al_2O_6$ and the Hydrogarnet $Sr_3Al_2(D_4O_4)_3$"

**Materials in Washington/Washington Materials Forum, Washington, D.C., February 28–March 1, 1991:**

S. M. Gorbatkin and L. A. Berry, "Poly-Si Etching Using Electron Cyclotron Resonance Microwave Plasma Sources" (invited paper)

**Third U.S.–Mexico Atomic and Molecular Physics Symposium, Cocoyoc, Mexico, March 13–16, 1991:**

R. A. Phaneuf, F. W. Meyer, D. C. Gregory, C. C. Havener, P. A. Zeijlmans van Emmichoven, S. H. Overbury, D. M. Zehner, G. H. Dunn, J. S. Thompson, E. K. Wahlin, and A. C. H. Smith, "Low-Energy Collisions of Multiply Charged Ions with Electrons, Atoms, and Surfaces" (invited paper)

**American Physical Society Meeting, Cincinnati, Ohio, March 18–22, 1991:**

A. P. Baddorf and B. S. Itchkawitz, "Adsorption on Single-Crystal K(110)" [*Bull. Am. Phys. Soc.* **36**, 854 (1991)]

R. Berliner, L. M. Johnstone, J. Trivisonno, and H. G. Smith, "The Martinsitic Phase Transformation in Lithium Magnesium Alloys" [*Bull. Am. Phys. Soc.* **36**, 479 (1991)]

B. Blum, E. W. Plummer, H. L. Davis, and D. M. Zehner, "LEED-IV Analysis of Clean Cu(100) and Cu(100)-*c*(2×2)Bi" [*Bull. Am. Phys. Soc.* **36**, 704 (1991)]

L. A. Boatner, R. E. Boekenhauer, J. Rankin, and D. L. Gilmore, "Ultrasonic Cavitation-Induced Fracture of MgO Single Crystals" [*Bull. Am. Phys. Soc.* **36**, 1035 (1991)]

J. D. Budai, R. T. Young, S. R. Ovshinsky, and B. S. Chao, "Epitaxial Orientations for YBaCuO Films on Silver Substrates" [*Bull. Am. Phys. Soc.* **36**, 475 (1991)]

Y. Chen, M. M. Abraham, D. F. Pedraza, G. J. Pogatshnik, and B. D. Evans, "Radiation Damage in Sapphire Implanted with 3.8-MeV $Fe^{2+}$ Ions" [*Bull. Am. Phys. Soc.* **36**, 944 (1991)]

D. K. Christen, R. Feenstra, C. E. Klabunde, D. P. Norton, and J. D. Budai, "Effects of Oxygen Composition on Critical Currents and Flux Pinning in Epitaxial $YBa_2Cu_3O_{7-x}$ Thin Films" [*Bull. Am. Phys. Soc.* **36**, 882 (1991)]

L. Civale, A. Marwick, T. K. Worthington, L. Krusin-Elbaum, A. P. Malozemoff, F. Holtzberg, C. A. Feild, J. R. Thompson, and M. A. Kirk, "Critical Current Enhancement by the Extended Vortex Confinement in YBaCuO Single Crystals" [*Bull. Am. Phys. Soc.* **36**, 669 (1991)]

J. F. Cooke, J. A. Blackman, and K. N. Trohidou, "Itinerant-Electron Theory of Magnetic Excitations in Ferromagnetic Iron and Cobalt" [*Bull. Am. Phys. Soc.* **36**, 642 (1991)]

H. L. Davis, D. M. Zehner, B. Dötsch, A. Wimmer, and K. Müller, "Layer-by-Layer Segregation and Deep Multilayer Relaxation in the $Mo_{75}Re_{25}(100)$ Surface" [*Bull. Am. Phys. Soc.* **36**, 705 (1991)]

P. DiAntonio, J. Toulouse, and L. A. Boatner, "Distortion-Induced First-Order Raman Lines at 200 and 279 $cm^{-1}$ in KTN and KLT" [*Bull. Am. Phys. Soc.* **36**, 1021 (1991)]

B. Dötsch, A. Wimmer, L. Hammer, K. Müller, H. L. Davis, and D. M. Zehner, "LEED and HREELS Investigations of the Hydrogen-Covered $Mo_{0.85}Re_{0.15}(100)$ Surface" [*Bull. Am. Phys. Soc.* **36**, 705 (1991)]

R. Feenstra, S. J. Pennycook, D. P. Norton, and J. D. Budai, "Localized Conversion of Epitaxial YBCO from c⊥ to a⊥ by Ion Implantation and Low Oxygen Pressure Annealing" [*Bull. Am. Phys. Soc.* **36**, 425 (1991)]

K. P. Gallagher, X. Zhang, J. P. Rung, and J. S. Lin, "Cocrystallization in Blends of Polybutylene Terephthalate and Poly(ester-ether) Segmented Block" [*Bull. Am. Phys. Soc.* **36**, 435 (1991)]

P. M. Gehring, H. Chou, S. M. Shapiro, J. Toulouse, D. Rytz, and L. A. Boatner, "High-Resolution X-Ray Scattering Study of the Dipolar Glass $K(Ta_xNb_{1-x})O_3$" [*Bull. Am. Phys. Soc.* **36**, 656 (1991)]

G. Grübel, Doon Gibbs, D. M. Zehner, D. L. Abernathy, and S. G. J. Mochrie, "Phase Behavior of Au and Pt(001) Surfaces" [*Bull. Am. Phys. Soc.* **36**, 457 (1991)]

T. E. Huber, P. W. Schmidt, J. S. Lin, and C. A. Huber, "SAXS Study of Selenium-Injected Porous Vycor Glass" [*Bull. Am. Phys. Soc.* **36**, 610 (1991)]

G. E. Jellison, Jr., "Examination of Thin $SiO_2$ Films on Si Using Spectroscopic Polarization Modulation Ellipsometry" [*Bull. Am. Phys. Soc.* **36**, 645 (1991)]

O. T. Jiang, T. Gustafsson, P. Haberle, and D. M. Zehner, "Surface Structures of Clean and Reconstructed Au(113)" [*Bull. Am. Phys. Soc.* **36**, 705 (1991)]

E. C. Jones, D. K. Christen, C. E. Klabunde, J. R. Thompson, D. P. Norton, R. Feenstra, D. H. Lowndes, and J. D. Budai, "Transport Critical Currents in Granular-Oriented $YBa_2Cu_3O_{7-x}$ Thin Films" [*Bull. Am. Phys. Soc.* **36**, 882 (1991)]

R. A. Klemm and S. H. Liu, "Intra- Versus Interlayer Pairing in Layered Superconductors: Role of the Magnetic Field" [*Bull. Am. Phys. Soc.* **36**, 420 (1991)]

B. C. Larson and J. Z. Tischler, "Mössbauer Resonant X-Ray Beams for High-Resolution X-Ray Spectroscopy" [*Bull. Am. Phys. Soc.* **36**, 625 (1991)]

S. H. Liu and R. A. Klemm, "Intra- Versus Interlayer Pairing in Layered Superconductors: Three- and Four-Layer Models" [*Bull. Am. Phys. Soc.* **36**, 771 (1991)]

D. H. Lowndes, "Copper Oxide Superconducting Superlattices" [*Bull. Am. Phys. Soc.* **36**, 367 (1991)] (invited paper)

H. A. Mook, "Phonons and Spin Fluctuations in High-$T_c$ Superconductors" [*Bull. Am. Phys. Soc.* **36**, 387 (1991)] (invited paper)

David P. Norton, "High-$T_c$ Superconductivity and Hole Filling in R-123 Superlattices and Thin Films" [*Bull. Am. Phys. Soc.* **36**, 731 (1991)] (invited paper)

J. G. Ossandon, J. R. Thompson, B. C. Sales, D. K. Christen, H. R. Kerchner, B. C. Chakoumakos, J. E. Tkaczyk, J. O. Thomson, and Y. R. Sun, "Influence of Oxygen Deficiency on the Reversible and Irreversible Superconducting Properties of Grain-Aligned $YBa_2Cu_3O_{7-x}$ Ceramics" [*Bull. Am. Phys. Soc.* **36**, 1030 (1991)]

W. M. Pramenko, R. C. Head, G. J. Pogatshnik, Y. Chen, and M. M. Abraham, "Comparative Thermoluminescence Studies of Neutron-Irradiated and Thermochemically Reduced CaO Crystals" [*Bull. Am. Phys. Soc.* **36**, 944 (1991)]

Mark Rasolt, Taner Edis, and Zlatko Tesanovic, "Kosterlitz-Thouless Transition and Charge Redistribution in the Superconductivity of YBCO-PBCO Superlattices" [*Bull. Am. Phys. Soc.* **36**, 732 (1991)]

A. R. Sandy, S. G. J. Mochrie, G. Grübel, K. G. Huang, Doon Gibbs, and D. M. Zehner, "High-Temperature Reconstruction of Pt(111)" [*Bull. Am. Phys. Soc.* **36**, 457 (1991)]

Paul W. Schmidt, David M. Nelson, Yanyan Tang, G. Walter, R. Kranold, and J. S. Lin, "Small-Angle X-Ray Scattering Studies of Some Porous Glasses and Precursor Materials from Which the Glasses Were Made" [*Bull. Am. Phys. Soc.* **36**, 610 (1991)]

E. Y. Sheu, M. M. De Tar, D. A. Storm, and J. S. Lin, "Small-Angle X-Ray Scattering Study for Droplet/Lamellae Phase Transition of AOT/Water/Decane Microemulsion" [*Bull. Am. Phys. Soc.* **36**, 1007 (1991)]

H. G. Smith, "Structure and Lattice Dynamics of the 9*R* Phase of Samarium" [*Bull. Am. Phys. Soc.* **36**, 918 (1991)]

Y. Sun, J. R. Thompson, F. Holtzberg, D. K. Christen, and J. G. Ossandon, "Relaxation of Magnetization in Single-Crystal, High-$J_c$ $YBa_2Cu_3O_7$ Superconductor" [*Bull. Am. Phys. Soc.* **36**, 369 (1991)]

J. R. Thompson, J. G. Ossandon, D. K. Christen, H. R. Kerchner, and H. A. Mook, "The Irreversibility Line and Upper Critical Field of Single-Crystal $La_{1.85}Sr_{0.15}CuO_{4-\delta}$" [*Bull. Am. Phys. Soc.* **36**, 618 (1991)]

J. Z. Tischler, B. C. Larson, and P. Zschack, "Effect of a Resonant Filter on the Time Structure of Mössbauer Resonant X-Ray Beams" [*Bull. Am. Phys. Soc.* **36**, 625 (1991)]

D. G. Tonn, D. B. Poker, R. E. Boekenhauer, and L. A. Boatner, "RBS Channeling Study of Ultrasonic Cavitation Damage on Single-Crystal MgO Surfaces" [*Bull. Am. Phys. Soc.* **36**, 1035 (1991)]

J. Toulouse, Henry Chou, S. Shapiro, B. Hennion, and L. A. Boatner, "Phase Transition and Acoustic-Optic Mode Interaction in $KTaO_3$:Nb" [*Bull. Am. Phys. Soc.* **36**, 762 (1991)]

X. M. Wang, L. A. Knauss, J. Toulouse, and L. A. Boatner, "Nonlinear Dielectric Behavior in the Mixed Ferroelectric $KTa_{1-x}Nb_xO_3$" [*Bull. Am. Phys. Soc.* **36**, 1023 (1991)]

S. Zhu, D. K. Christen, C. E. Klabunde, R. Feenstra, D. P. Norton, and D. H. Lowndes, "Aspects of Thermally Activated Flux Motion in $YBa_2Cu_3O_{7-x}$ Epitaxial Thin Films" [*Bull. Am. Phys. Soc.* **36**, 833 (1991)]

J.-K. Zuo and J. F. Wendelken, "Growth Kinetics of the Ag(111) Island to $(\sqrt{3}\times\sqrt{3})$R30°C Phase Transition for Ag/Si(111)" [*Bull. Am. Phys. Soc.* **36**, 407 (1991)]

**Gordon Conference on Superconductivity, Ventura, California, March 19–23, 1991:**

H. A. Mook, "Neutron Scattering Measurements on High-Temperature Superconductors" (invited paper)

**Seventh Oxford Conference on Microscopy of Semiconducting Materials, Oxford, United Kingdom, March 25–28, 1991:**

S. J. Pennycook, D. E. Jesson, and M. F. Chisholm, "High-Resolution Z-Contrast Imaging of Superlattices and Heterostructures" (invited paper)

**Oak Ridge Workshop on Laser Ablation Mechanisms and Applications, Oak Ridge, Tennessee, April 8–10, 1991:**

David B. Geohegan, "Spectroscopic and Ion Probe Characterization of Laser-Produced Plasmas Used for Thin-Film Growth" (invited paper)

David P. Norton, D. H. Lowndes, X. Zheng, R. J. Warmack, S. J. Pennycook, and J. D. Budai, "Superconducting Transport Properties and Surface Microstructure for $YBa_2Cu_3O_{7-\delta}$" (invited paper)

**Scanning '91, Atlantic City, New Jersey, April 8–12, 1991:**

D. E. Jesson and S. J. Pennycook, "Intuitive Imaging of Semiconductor Interfaces Using Z-Contrast STEM" (invited paper)

**Spring Meeting of the German Physical Society, Münster, Germany, April 8–12, 1991:**

B. Dötsch, A. Wimmer, L. Hammer, K. Müller, H. L. Davis, and D. M. Zehner, "LEED Investigation of the Molybdenum/Rhenium (100) Alloy"

**First North Alabama Student Materials Research Conference, Normal, Alabama, April 13, 1991:**

J. M. Williams, "Ion Implantation of Metals and Ceramics" (invited paper)

**Twenty-Second Annual Meeting of the American Physical Society, Division of Atomic, Molecular, and Optical Physics, Washington, D.C., April 22–24, 1991:**

P. A. Zeijlmans van Emmichoven, C. C. Havener, F. W. Meyer, and D. M. Zehner, "Computer Simulations of the Neutralization of Multicharged Ions Close to Metal Surfaces" [*Bull. Am. Phys. Soc.* **36**, 1371 (1991)]

F. W. Meyer, S. H. Overbury, C. C. Havener, P. A. Zeijlmans van Emmichoven, and D. M. Zehner, "Evidence for Above-Surface Neutralization During Interactions of Highly Charged Ions with a Metal Surface" [*Bull. Am. Phys. Soc.* **36**, 1371 (1991)]

**Twenty-Seventh Annual Symposium, New Mexico Chapter, American Vacuum Society, Albuquerque, New Mexico, April 22–26, 1991:**

John F. Wendelken and Jiang-Kai Zuo, "Surface Morphology and Thin-Film Growth Studies with High-Resolution LEED: Ag/Si(111)" (invited paper)

**International Conference on Metallurgical Coatings and Thin Films, San Diego, California, April 22–26, 1991:**

G. E. Jellison, Jr., "Two-Channel Spectroscopic Polarization Modulation Ellipsometry: A New Technique for the Analysis of Thin $SiO_2$ Films" (invited paper)

**Ninety-Third Annual Meeting and Exposition of the American Ceramic Society, Cincinnati, Ohio, April 28–May 2, 1991:**

J. B. Bates, N. J. Dudney, B. C. Sales, and C. F. Luck, "Electrical and Dielectric Properties of Amorphous $Li_2O$-$P_2O_5$ Thin Films"

L. A. Boatner, R. E. Boekenhauer, J. Rankin, and D. L. Gilmore, "Cavitation-Induced Fracture of MgO Ceramics and Single Crystals"

B. S. Kwak, A. Erbil, B. J. Wilkens, and L. A. Boatner, "MOCVD of Epitaxial Ferroelectric Titanate Thin Films"

B. C. Sales and B. C. Chakoumakos, "Hole Filling and Hole Creation in the Superconducting Compounds $Bi_2Sr_{2-x}RE_xCuO_{6+y}$, RE = La, Pr, Nd, and Sm"

**Materials Research Society Spring Meeting, Anaheim, California, April 29–May 4, 1991:**

M. F. Chisholm and S. J. Pennycook, "Atomic Structure of $YBa_2Cu_3O_{7-\delta}$ Grain Boundaries" (invited paper)

D. E. Jesson, S. J. Pennycook, and J.-M. Baribeau, "Direct Imaging of Ordering in Si-Ge Ultrathin Superlattices and Alloy Layers Using Z-Contrast STEM"

Mark V. Parish, B. C. Chakoumakos, and Viren M. Pathare, "Examination of the Crystal Growth Front Interfaces and Grain Boundaries During Melt Processing"

S. J. Pennycook, D. E. Jesson, and M. F. Chisholm, "Imaging of Metal Silicide/Si Interfaces and Interface Defects by Z-Contrast STEM"

**Scanning Microscopy International Meeting, Bethesda, Maryland, May 4–9, 1991:**

D. P. Norton, D. H. Lowndes, S. J. Pennycook, R. Feenstra, and R. J. Warmack, "Epitaxial Growth of Oxide Superconductor Thin Films and Superlattices" (invited paper)

**International Symposium on Mechanical Alloying, Kyoto, Japan, May 7–10, 1991:**

J. R. Thompson, C. Politis, and Y. C. Kim, "Properties of Materials with a Fine Length Scale: Mechanically Alloyed Metals and the High-Temperature Superconductor $YBa_2Cu_3O_7$" (invited paper)

**Conference on Ion Implantation of Medical Devices, Atlantic City, New Jersey, May 8, 1991:**

J. M. Williams, C. W. White, and C. J. McHargue, "Ion Implantation of Ceramic Materials" (invited paper)

**Physical Phenomena at High Magnetic Fields, Tallahassee, Florida, May 15–18, 1991:**

M. Rasolt, "Thermodynamic and Transport Properties of Superconductivity in the High Quantum Limit of an Applied Magnetic Field" (invited paper)

**Eleventh Annual TVC-AVS Symposium and Equipment Exhibition, Oak Ridge, Tennessee, May 15–18, 1991:**

N. J. Dudney, J. B. Bates, J. D. Robertson, R. A. Zuhr, A. L. Wachs, and C. F. Luck, "Magnetron Sputter Deposition of $Li_2O$-$SiO_2$-$P_2O_5$ Thin Films" (invited paper)

S. M. Gorbatkin and L. A. Berry, "Electron Cyclotron Resonance (ECR) Microwave Plasmas for Poly-Si Etching" (invited paper)

D. E. Jesson and S. J. Pennycook, "Direct Imaging of Ultrathin Si-Ge Superlattices Using Z-Contrast STEM" (invited paper)

D. P. Norton, "Pulsed-Laser Deposition of YBCO-Based Superconducting Superlattices" (invited paper)

J. Sharp, D. Eres, and D. Lowndes, "Germanium Thin-Film Growth Using a Pulsed Molecular Jet Source" (invited paper)

J.-K. Zuo and J. F. Wendelken, "High-Angular Resolution LEED Studies of Epitaxial Growth" (invited paper)

**Office of Naval Research Workshop on Magnetic Susceptibility of Superconductors and Other Spin Systems, Coolfont, West Virginia, May 20, 1991:**

J. R. Thompson, D. K. Christen, H. R. Kerchner, L. A. Boatner, B. C. Sales, B. Chakoumakos, R. Feenstra, H. Hsu, J. Brynestad, D. M. Kroeger, J. M. Williams, Y. Sun, Y. C. Kim, J. G. Ossandon, A. P. Malozemoff, L. Civale, A. D. Marwick, T. K. Worthington, and F. Holtzberg, "Studies of 'Non-Ideal' Superconductors Using DC Magnetic Methods" (invited paper)

**International Conference on Advanced Materials (ICAM) 91, Strasbourg, France, May 27–31, 1991:**

R. Feenstra, D. K. Christen, T. B. Lindemer, J. D. Budai, S. J. Pennycook, and M. D. Galloway, "Properties of Low-Temperature, Low-Oxygen Pressure Post-Annealed $YBa_2Cu_3O_{7-x}$ Films" (invited paper)

V. C. Matijasevic, R. H. Hammond, P. Rosenthal, K. Shinohara, A. F. Marshall, M. R. Beasley, and R. Feenstra, "Evidence for Cation Disorder in In Situ Grown YBaCuO Superconducting Films," (invited paper)

T. P. Sjoreen, R. Jebasinski, K. Schmidt, S. Mantl, H. Holzbrecher, and W. Speier, "Formation of $CoSi_2$ in SIMOX Wafers by High-Dose Cobalt Implantation"

**DOE Research Assistance Task Force Meeting on Electrical Breakdown of Insulating Ceramics in a High-Radiation Field, Vail, Colorado, May 28–June 6, 1991:**

L. A. Boatner, Y. Chen, and M. M. Abraham, "Electrical Breakdown and Electrolytic Coloration in MgO Single Crystals" (invited paper)

**European Materials Research Society Meeting, Strasbourg, France, May 28–31, 1991:**

A. Golanski, A. Grob, J. J. Grob, O. W. Holland, S. J. Pennycook, and C. W. White, "Dynamics of Lattice Damage Accumulation for MeV Ions in Silicon" (invited paper)

**Gordon Conference on High-Temperature Superconductivity, Wolfborough, Massachusetts, June 10–14, 1991:**

H. A. Mook, "Excitations in High-Temperature Superconductors" (invited paper)

**Cryogenic Engineering Conference and International Cryogenic Materials Conference, Huntsville, Alabama, June 11–14, 1991:**

H. R. Kerchner, J. O. Thomson, and R. Feenstra, "AC Susceptibility of Superconducting Thin Films"

**Symposium on the Structure and Dynamics of Supramolecular Aggregated and Strongly Interacting Colloids, NATO Advanced Study Institute, Acquafredda di Maratea, Italy, June 11–21, 1991:**

E. Y. Sheu, J. S. Lin, M. M. DeTar, M. Kotlarchyk, and D. A. Storm, "Structural Evolution and Transition of a Three-Component Densed Microemulsion System"

**Fifty-First Annual Conference on Physical Electronics, Piscataway, New Jersey, June 17–19, 1991:**

J.-K. Zuo, D. M. Zehner, and J. F. Wendelken, "The (1×*L*) Reconstruction of the TaC(110) Surface"

**Congrès ACP 1991 CAP Congress, Winnipeg, Manitoba, Canada, June 17–19, 1991:**

P. Grenier, S. Jandl, D. Houde, and L. A. Boatner, "Study of the Third-Order Nonlinear Susceptibility of $KTa_{0.94}Nb_{0.06}O_3$"

**Third Canadian Materials Science Conference, Kingston, Ontario, Canada, June 19–21, 1991:**

F. W. L. Fong and S. Spooner, "Small-Angle Neutron Scattering (SANS) from Zirconium Hydrides in Candu Reactor Zr-2.5-Nb Pressure Tube Materials" (invited paper)

**International Symposium on Metal/Ceramic Interfaces, Irsee, Germany, June 20–July 7, 1991:**

S. J. Pennycook, "Z-Contrast Imaging of Interfaces" (invited paper)

**6th International Conference on Radiation Effects in Insulators, Weimar, Germany, June 24–28, 1991:**

R. F. Haglund, Jr., R. H. Magruder, S. H. Morgan, D. O. Henderson, R. A. Weller, L. Yang, and R. A. Zuhr, "Nonlinear Optical Properties of Cu- and Pb-Implanted Fused Silica"

**Second International Conference on Surface X-Ray and Neutron Scattering, Bad Honnes, Germany, June 25–28, 1991:**

D. L. Abernathy, Doon Gibbs, G. Grübel, K. G. Huang, S. G. J. Mochrie, B. M. Ocko, A. R. Sandy, and D. M. Zehner, "X-Ray Reflectivity Studies of Au Surfaces"

**Strongly Correlated Electron Systems Gordon Godfrey Workshop on Condensed Matter Physics, Sydney, Australia, July 1–5, 1991:**

Mark Rasolt, "Superconductivity in a Very High Magnetic Field" (invited paper)

D. J. W. Geldart and M. Rasolt, "Energy Functionals for Inhomogeneous Many-Electron Systems," (invited paper)

**Seventeenth International Conference on the Physics of Electronic and Atomic Collisions, Brisbane, Australia, July 10–16, 1991:**

F. W. Meyer, S. H. Overbury, C. C. Havener, P. A. Zeijlmans van Emmichoven, and D. M. Zehner, "Above- and Below-Surface Auger Electron Emission During Interactions of Highly Charged Ions with Metal Surfaces"

P. A. Zeijlmans van Emmichoven, C. C. Havener, F. W. Meyer, and D. M. Zehner, "Measurements and Simulations of the Neutralization of Multicharged Ions Close to Metal Surfaces"

**Nineteenth Rare-Earth Research Conference, Lexington, Kentucky, July 14–19, 1991:**

W. K. Kot, N. M. Edelstein, M. M. Abraham, and L. A. Boatner, "Zero-Field Splitting of $Cm^{3+}$ in $LuPO_4$"

D. H. Lowndes, "Epitaxial Copper Oxide Superconductor Superlattices," (invited paper)

H. A. Mook, "Recent Neutron Scattering Measurements on High-Temperature Superconductors"

**Seventh International Conference on Surface Modification of Metals by Ion Beams, Washington, D.C., July 15–19, 1991:**

R. J. Hanrahan, M. P. Brady, J. C. Liu, S. P. Elder-Randall, E. D. Verink, Jr., and S. P. Withrow, "The Effect of Y Ion Implantation on the High-Temperature Oxidation Behavior of NbTiAl Alloys"

J. Rankin, P. Thevenard, L. J. Romana, L. A. Boatner, C. W. White, C. J. McHargue, and L. L. Horton, "Ion Bombardment, Ultrasonic, and Pulsed-Laser Beam Effects on Small Metallic Clusters of Potassium in MgO"

L. J. Romana, C. J. McHargue, P. S. Sklad, C. W. White, J. C. McCallum, and L. L. Horton, "Formation and Annealing Behavior of an Amorphous Layer Induced by Tin Implantation into Sapphire"

J. M. Williams, I. S. Lee, and R. A. Buchanan, "Production of Iridium Films on Ti and Ti-6Al-4V Alloy Substrates by Ion Beam Techniques"

**American Crystallographic Association Annual Meeting, Toledo, Ohio, July 21–26, 1991:**

B. C. Chakoumakos, G. A. Lager, and J. A. Fernandez-Baca, "Crystal Structure Refinements of $Sr_2Al_2O_6$ and the Hydrogarnet $Sr_3Al_2(D_4O_4)_3$"

**International Conference on Materials and Mechanisms of Superconductivity, Kanazawa, Japan, July 22–26, 1991:**

D. K. Christen, R. Feenstra, C. E. Klabunde, D. P. Norton, D. H. Lowndes, and J. D. Budai, "Effects of Thermal Processing and Oxygen Composition on Flux Pinning in High-$J_c$ Epitaxial $Y_2Ba_2CuO_{7-x}$ Thin Films"

R. Feenstra, D. K. Christen, T. B. Lindemer, J. D. Budai, S. J. Pennycook, and M. D. Galloway, "Properties of Low-Temperature, Low-Oxygen Pressure Post-Annealed $YBa_2CuO_{7-x}$ Films"

E. M. Forgan, D. McK. Paul, H. A. Mook, S. L. Lee, R. Cubitt, J. S. Abell, F. Gencer, and P. Timmins, "Neutron Diffraction from the Flux-Line Lattice" (invited paper)

D. McK. Paul, E. M. Forgan, H. A. Mook, R. Cubitt, S. L. Lee, M. L. Norton, H-Y Tang, and P. Timmins, "Anomalous Neutron Scattering from the Flux-Line Lattice in $K_{0.6}Ba_{0.4}BiO_3$" (invited paper)

**Symposium on Electron Correlation, Trieste, Italy, July 22–August 3, 1991:**

G. D. Mahan, "Electron Energies in Metals" (invited paper)

**Fourteenth International Conference on Atomic Collisions in Solids, Salford, United Kingdom, July 28–August 2, 1991:**

M. T. Robinson, "Computer Simulation Studies of High-Energy Collision Cascades"

S. H. Overbury, F. W. Meyer, and M. T. Robinson, "Computer Simulations of Relaxation Processes in Scattering of Multicharged Ions from Metal Surfaces"

**Electron Microscopy Society of America (EMSA) 49th Annual Meeting, San Jose, California, August 4–9, 1991:**

D. E. Jesson and S. J. Pennycook, "Structural and Compositional Mapping of Si-Ge Interfaces Using Z-Contrast STEM"

S. J. Pennycook and D. E. Jesson, "Compositional Mapping Using Large-Angle Electron Scattering" (invited paper)

**Physics and Materials Science of High-Temperature Superconductors—II, Porto Carras, Neos Marmaras, Hilkidiki, Greece, August 18–31, 1991**

J. R. Thomson, Y. R. Sun, D. K. Christen, H. R. Kerchner, A. P. Malozemoff, L. Civale, A. D. Marwick, T. K. Worthington, L. Krusin-Elbaum, and F. Holtzberg, "Magnetization Studies of Irradiated Single-Crystal $YBa_2CuO_7$ Superconductors: Flux Creep and Annealing Effects" (invited paper)

**Fourth International Conference on Energy Pulse and Particle Beam Modification of Materials, Dresden, Germany, August 19–23, 1991:**

A. Golanski, S. J. Pennycook, and C. W. White, "Radiation-Induced Effects in Ion Beam Synthesis of Erbium Silicide"

**Nineteenth International Conference on Positron Annihilation, Szombathely, Hungary, August 25–31, 1991:**

Bent Nielsen, O. W. Holland, T. C. Leung, and K. G. Lynn, "Defects in Si-Implanted Si"

**American Chemical Society Symposium on the Solid State Characterization of Multicomponent Systems, New York, New York, August 25–30, 1991:**

Kevin P. Gallagher, Zuifang Zhang, James P. Rung, Gia Huynh-ba, and J. S. Lin, "Cocrystallization in Blends of Poly(butylene terephthalate) and Poly(ester-ether) Segmented Block Copolymers"

**Course on Path Integration, International Center for Theoretical Physics, Trieste, Italy, August 26–September 2, 1991:**

G. S. Canright, "From Path Integrals to Anyons" (invited paper)

**International Conference on Neutron Scattering, Rutherford Appleton Laboratory, Chilton, Didcot, United Kingdom, August 27–30, 1991**

R. Cubitt, E. M. Forgan, D. McK. Paul, S. L. Lee, J. S. Abell, H. A. Mook, and P. Timmins, "Neutron Diffraction by the Flux Lattice in High-$T_c$ Superconductors" (invited paper)

T. Kanaya, M. Ohkura, H. Yamaoka, and G. D. Wignall, "Small-Angle Neutron Scattering from Poly(Vinyl Alchohol) Gells"

**International Conference on Magnetism, Edinburg, Scotland, September 2–6, 1991:**

P. Böni, G. Shirane, J. L. Martinez, and H. A. Mook, "Spin Fluctuations in Ni Above $T_c$: Comparison with RG" (invited paper)

A. T. Boothroyd, T. G. Perring, A. D. Taylor, D. McK. Paul, and H. A. Mook, "High Energy Spin Waves in Iron Measured by Neutron Scattering" (invited paper)

J. A. Fernandez-Baca, M. E. Hagen, R. M. Nicklow, Y. Tsunoda, and S. Hayden, "Magnetic Excitations in the Itinerant Antiferromagnet $Mn_{90}Cu_{10}$"

D. McK. Paul, E. M. Forgan, R. Cubitt, S. L. Lee, H. A. Mook, and P. Timmins, "Neutron Scattering from the Flux Lattice in High-Temperature Superconductors" (invited paper)

P. Radhakrishna and J. W. Cable, "Magnetic Excitations in the Triangular Antiferromagnet $Mn_3Sn$"

**Twelfth European Conference on Surface Science, Stockholm, Sweden, September 9–12, 1991:**

R. A. Bartynski, E. Jensen, S. Yang, S. L. Hulbert, C. C. Kao, M. Weinert, and D. M. Zehner, "Surface Electronic Structure and Interatomic Auger Transitions on the TaC(111) Surface Observed by Auger Photoelectron Coincidence Spectroscopy" (invited paper)

B. Blum, E. W. Plummer, H. L. Davis, and D. M. Zehner, "LEED-IV Investigation of Cu(100)-$c$(2×2)Bi"

B. Dötsch, K. Müller, H. L. Davis, and D. M. Zehner, "A LEED Determination of Layer Relaxations and Atom Concentrations of the Random Alloy Molybdenum/Rhenium"

**EMAG '91, Bristol, United Kingdom, September 10–13, 1991:**

S. J. Pennycook, "Z-Contrast STEM: Incoherent Imaging with Atomic Resolution" (invited paper)

**European Materials Research Society Meeting, Carcans-Maubuisson, France, September 16–19, 1991:**

D. B. Geohegan, "Effects of Ambient Background Gases on YBCO Plume Propagation Under Film Growth Conditions: Spectroscopic, Ion Probe, and Fast Photographic Studies" (invited paper)

D. H. Lowndes, D. P. Norton, S. Zhu, and X.-Y. Zheng, "Laser Ablation Synthesis and Properties of Epitaxial $YBa_2Cu_3O_{7-\delta}/PrBa_2Cu_3O_{7-\delta}$ Superconductor Superlattices" (invited paper)

**10th Pfefferkorn Conference on Signal and Image Processing, Cambridge, United Kingdom, September 16–19, 1991:**

S. J. Pennycook, D. E. Jesson, M. F. Chisholm, A. G. Ferridge, and M. J. Seddon, "Sub-Ångstrom Microscopy Through Incoherent Imaging and Image Reconstruction" (invited paper)

**Fifth Annual Conference on Superconductivity and Applications, Buffalo, New York, September 24–26, 1991:**

D. P. Norton, D. H. Lowndes, X.-Y. Zheng, R. Feenstra, and S. Zhu, "Properties of Epitaxial $YBa_2Cu_3O_{7-\delta}$-Based Superconducting Superlattices" (invited paper)

**International Workshop on Electron Microscopy in Materials Science, Brindisi, Italy, October 7–19, 1991:**

S. J. Pennycook, "Scanning Transmission Electron Microscopy" (invited paper)

**Second Workshop on Electro-Optical Materials for Tactical and Strategic Applications, Huntsville, Alabama, October 8–10, 1991:**

A. Erbil, B. S. Kwak, and L. A. Boatner, "Ferroelectric Nonlinear Optical Materials Grown by Metall-Organic Chemical Vapor Deposition"

**Conference on Physics and Chemistry of Finite Systems, Richmond, Virginia, October 8–12, 1991:**

R. F. Haglund, Jr., R. H. Magruder, L. Yang, J. E. Wittig, and R. A. Zuhr, "Optical Characteristics of Cu-Nanocluster Layers Assembled by Ion Implantation"

**Fourth International Symposium on Superconductivity, Tokyo, Japan, October 14–17, 1991:**

D. H. Lowndes, D. P. Norton, S. Zhu, and X.-Y. Zheng, "Superconducting Properties and Microstructure of Epitaxial $YBa_2Cu_3O_{7-\delta}/PrBa_2Cu_3O_{7-\delta}$ Superlattices" (invited paper)

**Department of Energy 17th Surface Studies Conference, Livermore, California, October 15–18, 1991:**

John Wendelken and Jiang-Kai Zuo, "Growth and Kinetics of Si(111)-$(\sqrt{3}\times\sqrt{3})$R30°-Ag Domains Studied with High-Resolution LEED"

**American Ceramic Society Meeting, Marco Island, Florida, October 15–18, 1991:**

L. A. Boatner and M. M. Abraham, "The Investigation of Ceramic Texturing by Electron Paramagnetic Resonance" (invited paper)

**44th Annual Gaseous Electronics Conference, Albuquerque, New Mexico, October 22–25, 1991:**

F. W. Meyer, S. H. Overbury, C. C. Havener, P. A. Zeijlmans van Emmichoven, and D. M. Zehner, "Evidence for Above- and Sub-Surface Neutralization During Interactions of Highly Charged Ions with a Metal Surface"

S. M. Gorbatkin and L. A. Berry, "Contamination by Sputtering in Mirror Field Electron Cyclotron Resonance Microwave Ion Plasmas"

**Eighth International Conference on Solid State Ionics, Lake Louise, Canada, October 20–26, 1991:**

J. B. Bates, N. J. Dudney, A. L. Wachs, R. A. Zuhr, B. C. Sales, and C. F. Luck, "Fabrication and Characterization of $Li_2O$:$SiO_2$:$P_2O_5$ Thin Films"

J. B. Bates, G. R. Gruzalski, N. J. Dudney, and C. F. Luck, "Lithium Oxynitride Electrolyte Thin Films"

J. B. Bates, N. J. Dudney, G. R. Gruzalski, and C. F. Luck, "Electrical Properties of Amorphous Lithium Electrolyte Thin Films"

N. J. Dudney and C. F. Luck, "Sputter Deposition of $CaF_2$ Thin Films"

N. J. Dudney, J. B. Bates, R. A. Zuhr, and J. D. Robertson, "Composition Analysis of $Li_2O$-$P_2O_5$-$SiO_2$ Electrolyte Thin Films"

N. J. Dudney, J. B. Bates, and J. D. Robertson, "Sputtering of Lithium Compounds for Preparation of Electrolyte Thin Films"

**The Fourth International Conference on Polyimides, Ellenville, New York, October 30–November 1, 1991:**

M. Ree, T. L. Nunes, and J. S. Lin, "X-Ray Scattering Studies of Polymide Thin Films from Poly(amic acids) Functionalized with a Methacrylate"

**Optical Society of America Annual Meeting, San Jose, California, November 3–8, 1991:**

J. Z. Tischler and B. C. Larson, "Time-Resolved X-Ray Scattering Using Synchrotron Sources" (invited paper)

**National Science Foundation Workshop on Epitaxy, Interfaces, Defects, and Processing of Electronic and Photonic Materials," Pittsburgh, Pennsylvania, November 4–7, 1991:**

S. J. Pennycook, "Z-Contrast Imaging of Interfaces" (invited paper)

**IEEE Nuclear Science Symposium, Santa Fe, New Mexico, November 5–8, 1991:**

S. H. Derenzo, W. W. Moses, T. A. DeVol, J. L. Cahoon, and L. A. Boatner, "X-Ray Fluorescence Measurements of 412 Inorganic Compounds"

**1991 Annual Meeting of the Southeastern Section of the American Physical Society, Durham, North Carolina, November 11–13, 1991:**

J. Sharp and D. Eres, "Optical Monitoring of Semiconductor Film-Growth Surfaces" (invited paper)

**Thirty-Eighth Annual American Vacuum Society Symposium and Topical Conference, Seattle, Washington, November 11–15, 1991:**

H. L. Davis, D. M. Zehner, B. Dötsch, and K. Müller, "Termination of the TaC(111) Surface"

S. M. Gorbatkin, L. A. Berry, and J. Swyers, "Poly-Si Etching Using an Electron Cyclotron Resonance Microwave Plasma Source with Multipole Confinement"

Q. T. Jiang, T. Gustafsson, P. Häberle, and D. M. Zehner, "Investigations of the Ca-Induced (1×2) Reconstruction of Au(113) Using Medium-Energy Ion Scattering"

J. R. Noonan and H. L. Davis, "Composition Gradient and Atomic Relaxations at the Surface of a Solid Solution Alloy: $Au_{0.62}Ag_{0.38}(111)$"

J.-K. Zuo and J. F. Wendelken, "Kinetics of the Initial Growth for Ag/Si(111)"

J.-K. Zuo, D. M. Zehner, and J. F. Wendelken, "Reconstruction of the TaC(110) Surface: Periodic Faceting"

**Materials Research Society Fall Meeting, Boston, Massachusetts, December 2–6, 1991:**

L. A. Boatner and M. M. Abraham, "The Formation of Textured Ceramics from Faceted, Nanophase Precursors and the Characterization of Preferred Orientations in Ceramic Microstructures by EPR Spectroscopy"

M. F. Chisholm and S. J. Pennycook, "Surface Nucleation Dislocation in Constrained High-Misfit Films of $Si_xGe_{1-x}$"

D. K. Christen, R. Feenstra, C. E. Klabunde, D. P. Norton, D. H. Lowndes, and J. D. Budai, "Effects of Oxygen Defects and Thermal Processing on Flux Pinning in High-$J_c$ $YBa_2Cu_3O_{7-\delta}$ Thin Films"

J. J. Dobbins, J. M. Williams, D. J. Birch, and B. L. Giammara, "Analysis of Nitrogen Ion-Implanted Titanium and the Effect on Bacterial Adherence"

D. Eres and J. W. Sharp, "Temperature-Dependent Evolution of Chemisorbed Layers of Digermane in Ge Thin-Film Growth"

R. Feenstra, D. K. Christen, D. P. Norton, D. H. Lowndes, S. J. Pennycook, and J. D. Budai, "Evidence for Doping Effects in $YBa_2Cu_3O_{7-\delta}$ Films Processed at Low-Oxygen Pressures"

B. L. Giammara, J. M. Williams, D. J. Birch, and J. J. Dobbins, "Quantitative Ruthenium Method for Analysis of Nitrogen Ion-Implanted Titanium Alloy (Ti-6Al-4V) and the Effect on Bacterial Adherence"

T. E. Haynes, O. W. Holland, and U. V. Desnica, "Damage Accumulation in Gallium Arsenide During Silicon Ion Implantation Near Room Temperature"

D. E. Jesson, S. J. Pennycook, and J.-M. Baribeau, "Lateral Segregation and Long-Range Ordering During MBE Growth of $Si_xGe_{1-x}$ Alloys"

H. R. Kerchner, D. K. Christen, C. E. Klabunde, D. H. Lowndes, and D. P. Norton, "Evidence of K-T Transition in $YBa_2Cu_3O_{7-\delta}/PrBa_2Cu_3O_{7-\delta}$ Superlattice Films"

R. H. Magruder, R. F. Haglund, L. Yang, J. E. Wittig, K. Becker, and R. A. Zuhr, "Picosecond Nonlinear Optical Response of Copper Clusters Created by Ion Implantation in Fused Silica"

J. C. McCallum, T. W. Simpson, I. V. Mitchell, J. Rankin, and L. A. Boatner, "Annealing of Pb-Implanted $SrTiO_3$ in the Presence of Water Vapor: A Study Using $D_2{}^{18}O$ Labeling"

J. W. McCamy, D. H. Lowndes, J. D. Budai, B. C. Chakoumakos, and R. A. Zuhr, "Growth of Epitaxial ZnS Films by Pulsed-Laser Ablation"

D. P. Norton, B. C. Chakoumakos, D. H. Lowndes, J. D. Budai, R. Feenstra, and D. K. Christen, "Epitaxial Growth and Properties of $Ba_{1-x}K_xBiO_3$ Thin Films Grown by Pulsed-Laser Deposition"

J. G. Ossandon, J. R. Thompson, D. K. Christen, B. C. Sales, H. R. Kerchner, J. O. Thompson, Y. R. Sun, and J. E. Tkaczyk, "Correlation Between Critical Current Density $J_c$ and Irreversibility Line in Magnetically Aligned Sintered Samples of $YBa_2Cu_3O_x$ with Various Oxygen Contents"

S. J. Pennycook, M. F. Chisholm, D. E. Jesson, D. P. Norton, D. H. Lowndes, and R. Feenstra, "Growth Mechanisms of $YBa_2Cu_3O_{7-x}$ Films and Superlattices Studied by Z-Contrast STEM"

D. B. Poker, D. G. Tonn, and U. B. Ramabadran, "Effect of Oxygen Implantation on the Thermal Stability of Ti-Implanted $LiNbO_3$"

J. Rankin, L. A. Boatner, and T. A. Nguyen, "In Situ TEM Study of the Sintering of Single-Crystal Nanoscale MgO Cubic Particles"

T. P. Sjoreen, A. Schuppen, S. Mantl, and L. Vescan, "Schottky Barrier Heights of Ion Beam Synthesized $Si/CoSi_2$ Diodes"

J. R. Thompson, A. P. Malozemoff, Y. R. Sun, M. W. McElfresh, L. Civale, A. D. Marwick, and F. Holtzberg, "Influence of Flux Creep on the Temperature Dependence of the Critical Current Density in $YBa_2Cu_3O_7$ Crystals"

D. G. Tonn and D. B. Poker, "Effect of Implantation Temperature on the Solid-Phase Epitaxy of Ti-Implanted $LiNbO_3$"

S. P. Withrow, C. W. White, R. A. Zuhr, J. McCamy, J. D. Budai, and D. M. Hembree, Jr., "Analysis of C Films Formed on Single-Crystal Cu by Ion Implantation and Laser Annealing"

S. Zhu, D. H. Lowndes, X.-Y. Zheng, D. P. Norton, and R. J. Warmack, "Epitaxial $YBa_2Cu_3O_{7-x}$ Thin Films: Scanning Tunneling Microscopy Study of the Initial Stages of Epitaxial Growth, Growth Mechanisms, and Effects of Substrate Temperature"

J.-K. Zuo, D. M. Zehner, and J. F. Wendelken, "Stability of Transition-Metal Carbide Surfaces: TaC"

**Condensed Matter and Materials Physics Conference and Exhibition, Birmingham, United Kingdom, December 17–19, 1991:**

L. Siller, J. F. Wendelken, and R. E. Palmer, "Resonance Scattering Study of Physisorbed and Chemisorbed $O_2$ on the Pt(111) Surface"

**Gordon Research Conference on Superconductivity, Oxnard, California, January 6–10, 1992:**

D. H. Lowndes, "Anisotropy and Reduced Dimensionality in Superconducting Superlattices" (invited paper)

H. A. Mook, "Phonon and Magnetic Excitations in High-Temperature Superconductors" (invited paper)

J. R. Thompson, "Influence of Flux Creep on the Temperature Dependence of the Critical Current Density in $YBa_2Cu_3O_7$ Crystals "

J. R. Thompson, "Correlation Between Critical Current Density $J_c$ and Irreversibility Line in Magnetically Aligned $YBa_2Cu_3O_{7-\delta}$ with Various Oxygen Contents $\delta$"

**2nd Williamsburg Conference on Ferroelectrics, Williamsburg, Virginia, February 3–4, 1992:**

G. D. Mahan, "Ionic Polarization" (invited paper)

**National Research Council 3rd Neutron Scattering Meeting, Rome, Italy, February 17–18, 1992:**

J. B. Hayter, "The Advanced Neutron Source" (invited paper)

**WATTec '92, Knoxville, Tennessee, February 18, 1992:**

J. B. Bates, G. R. Gruzalski, N. J. Dudney, A. Choudhury, and C. F. Luck, "New Amorphous Thin-Film Lithium Electrolyte and Rechargeable Microbattery" (invited paper)

**U.S. DOE HTS Wire Development Workshop, Richmond, Virginia, February 19–20, 1992:**

D. K. Christen, "Critical Currents in High-Temperature Superconductors: What are the Limits?" (invited paper)

**3rd European Expert Meeting on Neutron Sources, Science and Engineering Research Council, Abingdon, United Kingdom, February 24–28, 1992:**

J. B. Hayter, "Neutron Optical Insertion Devices" (invited paper)

**The Mining, Minerals, and Materials Society Meeting, San Diego, California, March 1–5, 1992**

H. R. Kerchner, C. E. Klabunde, and R. R. Coltman, "Low-Temperature Neutron Irradiation" (invited paper)

H. R. Kerchner, J. R. Thompson, Y. R. Sun, D. K. Christen, J. O. Thomson, B. C. Sales, B. C. Chakoumakos, L. Civale, and A. D. Marwick, "Enhanced Critical Current Density and Magnetic Irreversibility Line in Single-Crystal $Bi_2Sr_2CaCu_2O_8$ via Columnar Defects From Heavy Ion Irradiation"

R. M. Moon, "Neutron Scattering from Rare-Earth Materials" (invited paper)

**Joint TMS-Australian IMM Annual Meeting, San Diego, California, March 2–5, 1992:**

G. Sundar, J. J. Hoyt, and S. Spooner, "A Test of the Langer-Schwartz Model of Nucleation and Growth"

**Workshop on High-Energy Resolution X-Ray Scattering, Chicago, Illinois, March 6, 1992:**

J. Z. Tischler and B. C. Larson, "X-Ray Scattering with Nano-Electronvolt Resolution"

**Conference on Microelectronics Technology Transfer: "Exploring the Untapped Potential of the National Labs," March 12–13, 1992:**

J. B. Roberto, "Opportunities for Microelectronics R&D at Oak Ridge National Laboratory" (invited paper)

**Thirty-Second Sanibel Symposia, Gainsville, Florida, March 14–21, 1991:**

M. Rasolt, "Self-Induced Effective Gauge Fields and Spontaneous Generation of Currents in the Copper-Oxygen Plane of High-$T_c$ Perovskites" (invited paper)

**1992 March Meeting of the American Physical Society, Indianapolis, Indiana, March 16–20, 1992:**

D. L. Abernathy, S. G. J. Mochrie, D. M. Zehner, G. Grübel, and D. Gibbs, "Capillary Modes on a Close-Packed Metal Surface: Pt(001)" [*Bull. Am. Phys. Soc.* **37**, 57 (1992)]

A. P. Baddorf, G. Helgesen, D. Gibbs, A. R. Sandy, C. You, and S. G. J. Mochrie, "X-Ray Scattering Determination of Cu(110) (2×3)-N Structure" [*Bull. Am. Phys. Soc.* **37**, 695 (1992)]

G. Beaucage, W. Hamilton, D. Schaefer, and A. Hurd, "Off-Specular X-Ray Reflections From Etched and Sol-Coated Silicon Surfaces" [*Bull. Am. Phys. Soc.* **37**, 725 (1992)]

J. D. Budai, M. F. Chisholm, L. A. Boatner, B. S. Kwak, and A. Erbil, "Epitaxial Growth of $PbTiO_3$ Thin Films on Oxide Substrates" [*Bull. Am. Phys. Soc.* **37**, 797 (1992)]

D. K. Christen, C. E. Klabunde, S. Zhu, J. R. Thompson, L. Civale, A. D. Marwick, and J. D. Budai, "Asymmetric Angular Dependence in the Transport Critical Current and Flux Pinning of Epitaxial $YBa_2Cu_3O_7$ Thin Films" [*Bull. Am. Phys. Soc.* **37**, 173 (1992)]

J. F. Cooke, J. A. Blackman, and J. M. Bass, "Itinerant-Electron Analysis of Neutron Scattering Data from Transition-Metal Ferromagnets" [*Bull. Am. Phys. Soc.* **37**, 133 (1992)]

H. L. Davis, J. B. Hannon, K. B. Ray, and E. W. Plummer, "Anomalous Interlayer Expansion for the (0001) Surface of Be" [*Bull. Am. Phys. Soc.* **37**, 273 (1992)]

R. Feenstra, "Oxygen Vacancies in $YBa_2Cu_3O_{7-\delta}$ Thin Films: Growth Properties, Lattice Disorder, and Flux Pinning" [*Bull. Am. Phys. Soc.* **37**, 331 (1992)] (invited paper)

J. A. Fernandez-Baca, R. M. Nicklow, M. E. Hagen, and Y. Tsunoda, "Magnons in $Mn_{90}Cu_{10}$" [*Bull. Am. Phys. Soc.* **37**, 133 (1992)]

D. B. Geohegan, "Mechanisms of YBCO Plume Transport Through Background Gases Studied by Fast ICCD Photography" [*Bull. Am. Phys. Soc.* **37**, 248 (1992)]

B. S. Itchkawitz, P. F. Lyman, and D. M Zehner, "Photoemission Spectroscopy from Monolayer Graphite on the TaC(111) Surface" [*Bull. Am. Phys. Soc.* **37**, 639 (1992)]

D. E. Jesson, "Segregation and Ordering During Si-Ge MBE Growth" [*Bull. Am. Phys. Soc.* **37**, 734 (1992)] (invited paper)

E. C. Jones, D. K. Christen, J. R. Thompson, R. Feenstra, J. M. Phillips, M. P. Siegal, and S. Zhu, "Effects of Carrier Density on the Electrical Transport Properties of Epitaxial $YBa_2Cu_3O_{7-\delta}$ Thin Films" [*Bull. Am. Phys. Soc.* **37**, 278 (1992)]

T. Kyu, H. S. Lee, J. P. Kennedy, and J. S. Lin, "Structural Characterization of Multicomponent Networks" [*Bull. Am. Phys. Soc.* **37**, 675 (1992)]

B. C. Larson, M. D. Galloway, G. E. Ice, and P. Zschack, "X-Ray Bragg Diffuse Scattering for the Investigation of Precipitates in Dilute Alloys" [*Bull. Am. Phys. Soc.* **37**, 363 (1992)]

R. M. Nicklow, M. E. Mostoller, and M. L. Norton, "Neutron Scattering Study of Phonons in Superconducting $Ba_{0.6}K_{0.4}BiO_3$" [*Bull. Am. Phys. Soc.* **37**, 347 (1992)]

J. G. Ossandon, J. R. Thompson, D. K. Christen, and Y. R. Sun, "Flux Creep Studies in Grain-Aligned $YBa_2Cu_3O_{7-\delta}$ Oxygen vs Deficiency $\delta$" [*Bull. Am. Phys. Soc.* **37**, 118 (1992)]

R. B. Rogge, Y. S. Yang, R. M. Nicklow, B. Gaulin, J. A. Fernandez-Baca, and A. Harrison, "A Neutron Scattering Study of a Dilute Stacked Triangular Lattice Ising-Like Antiferromagnet" [*Bull. Am. Phys. Soc.* **37**, 603 (1992)]

P. K. Roy, A. T. Fiory, and G. E. Jellison, Jr., "Examination of Thin $SiO_2$ Films on Si(001) by Ion Channeling and Spectroscopic Ellipsometry"

B. C. Sales, R. A. Zuhr, J. C. McCallum, and L. A. Boatner, "Dominant Role of Electronic Energy Losses in the Ion Beam Amorphization of $Pb_2P_2O_7$" [*Bull. Am. Phys. Soc.* **37**, 672 (1992)]

B. C. Sales, "Structural Analysis of Amorphous Phosphates Using High-Performance Liquid Chromatography" [*Bull. Am. Phys. Soc.* **37**, 632 (1992)] (invited paper)

A. R. Sandy, D. L. Abernathy, S. G. J. Mochrie, D. M. Zehner, and D. Gibbs, "Au(113) Surface Studies" [*Bull. Am. Phys. Soc.* **37**, 274 (1992)]

H. G. Smith, R. Berliner, and J. Trivisonno, "Are There Precursor Effects Above the Martensitic Transformation in a Virgin Crystal of Li Metal?" [*Bull. Am. Phys. Soc.* **37**, 407 (1992)]

Y. R. Sun, J. R. Thompson, D. K. Christen, J. G. Ossandon, A. Goyal, and Y. J. Chen, "Effects of Magnetic Fields Sweeping Rate on Magnetization and Flux Creep in High-$T_c$ Superconductors" [*Bull. Am. Phys. Soc.* **37**, 118 (1992)]

J. R. Thompson, Y. R. Sun, H. R. Kerchner, D. K. Christen, J. O. Thomson, B. C. Sales, B. C. Chakoumakos, L. Civale, and A. D. Marwick, "Enhanced Current Density $J_c$ in Single-Crystal $Bi_2Sr_2Ca_2Cu_2O_8$ via Linear Defects from Heavy Ion Irradiation" [*Bull. Am. Phys. Soc.* **37**, 172 (1992)]

J. Z. Tischler, B. C. Larson, E. E. Alp, T. Mooney, and Q. Shen, "Measurements of the $BaTiO_3$ Phase Transision Using Resonant Nuclear Bragg Scattering" [*Bull. Am. Phys. Soc.* **37**, 790 (1992)]

J. F. Wendelken, L. Siller, and R. E. Palmer, "Resonance Scattering from Physisorbed Oxygen on Pt(111) Observed with HREELS" [*Bull. Am. Phys. Soc.* **37**, 328 (1992)]

G. D. Wignall, W. Wu, and L. Mandelkern, "A SANS Investigation into the Plastic Deformation Mechanisms of Polyethylene" [*Bull. Am. Phys. Soc.* **37**, 676 (1992)]

R. F. Wood, "Resistive Transition and Normal State Conductivity in YBCO/PBCO Superlattices" [*Bull. Am. Phys. Soc.* **37**, 479 (1992)]

S. Zhu, D. K. Christen, C. E. Klabunde, J. R. Thompson, E. C. Jones, R. Feenstra, D. H. Lowndes, and D. P. Norton, "Interpretation of Superconductive Transport Properties of Epitaxial $YBa_2Cu_3O_7$ Thin Films" [*Bull. Am. Phys. Soc.* **37**, 593 (1992)]

**SPIE Symposium on Compound Semiconductor Physics and Devices, Somerset, New Jersey, March 23–27, 1992:**

G. D. Mahan, B. A. Sanborn, and P. B. Allen, "Mobility of Electrons and Holes in Semiconductors" (invited paper)

# *Seminars*

## *SOLID STATE DIVISION SEMINARS AT ORNL*

During this period H. L. Davis served as Seminar Chairman October 1990–October 1991, and S. J. Pennycook, October 1991–continuing. The following seminars were held:

"Sputter-Assisted Plasma CVD of Ferroelectric Thin Films," Shoichi Mochizuki, GIRIO, Osaka, Japan

"The High-Temperature Superconducting Materials for Magnetic Bearing Applications," W.-K. Chu, Texas Center for Superconductivity, University of Houston, Houston, Tex.

"Thin-Film Growth from Gaseous Molecular Jets," Djula Eres, Solid State Division, ORNL

"Defect Production, Radiation Annealing, and Effects of Electron Excitation in Ion Irradiation of Ni and Cu," Tadao Iwata, Japan Atomic Energy Research Institute, Tokai, Japan

"Instabilities in Metal Surfaces," T.-M. Lu, Rensselaer Polytechnic Institute, Troy, N.Y.

"Crystal and Molecular Fields in Rare-Earth Iron Boron Compounds," Michael Loewenhaupt, Forschungszentrum, Jülich, Germany

"Growth and Properties of High-$T_c$ Superconducting 123 Compounds," J. M. Phillips, AT&T Bell Laboratories, Murray Hill, N.J.

"Specific Heat Measurements for $Ba_{1-x}K_xBiO_3$," R. G. Goodrich, Louisiana State University, Baton Rouge, La.

[1]"Surface Physics Studies at Harwell," Martin Murrell, Harwell Laboratory, Oxfordshire, United Kingdom

"Z-Contrast Imaging of Ultrahigh $(Si_mGe_m)_p$ Superlattices," D. E. Jesson, Solid State Division, ORNL

"Conventional LEED, Diffuse LEED, and Electron Holography," Klaus Heinz, University of Erlangen-Nürnberg, Erlangen, Germany

"New Insight into the Structure of Glass," B. C. Sales, Solid State Division, ORNL

"Electrical and Optical Properties of Y-Ba-Cu-O Superconducting Thin Films," Anatoly Frenkel, Bellcore, Red Bank, N.J.

"New Developments on Flux Creep in HTSC: The Vortex Glass Model and Quantum Tunneling," A. Malozemoff, American Superconductor Corporation, Boston, Mass.

[2]"Vibrational Anomalies in High-Temperature Superconductors," Nancy Hecker, Harvard University, Cambridge, Mass.

"Superconductivity and Hole Doping in $Pr_{0.5}Ca_{0.5}Ba_2Cu_3O_{7-\delta}$ Thin Films and $YBa_2Cu_3O_{7-\delta}/Pr_{0.5}Ca_{0.5}Ba_2O_{7-\delta}$ Superlattice Structures," D. P. Norton, Solid State Division, ORNL

"The Advanced Neutron Source Research and Development Program," J. B. Hayter, Solid State Division, ORNL

"National High-Magnetic Field Laboratory: Status and Future," Jack Crow, Florida State University, Tallahassee, Fla.

[3]"Structure, Formation, and Properties of Langmuir-Blodgett Films," L. A. Feigin, USSR Academy of Sciences, Moscow, Russian Providence

[4]"The Kumakhov Lens: A New Type of X-Ray and Neutron Optics," M. W. Gibson, State University of New York, Albany, N.Y., and M. A. Kumakhov, Institute for Roentgen Optical Systems, Moscow, Russian Providence

"Synthesis and Properties of High-$T_c$ Thin Films and Multilayers Grown by 90°-Off-Axis Sputtering," C.-B. Eom, Stanford University, Stanford, Calif.

"Excitations in Modulated Systems: Lattice Vibrations and Spin Waves," S. W. Lovesey, Rutherford Appleton Laboratory, Didcot, United Kingdom

"Characteristics of Laser-Produced Plasma Used for Thin-Film Growth," D. B. Geohegan, Solid State Division, ORNL

"Influence of the Accelerated Crucible Rotation Technique on the Directional Solidification of InSb-GaSb Alloys," R. T. Gray, Clarkson University, Potsdam, N.Y.

"Scaling Theory of Island Growth in Thin Films," J. A. Blackman, University of Reading, Reading, United Kingdom

"Progress on the Variable Reflectivity Electrochromic Window," R. B. Goldner, Tufts University, Medford, Mass.

"Metastable Liquid Immisicibility in Iron-Copper Alloys," S. P. E. Randall, University of Florida, Gainesville, Fla.

"Atomic Layer Epitaxy of Si on Si(001)-(2×1): Surface Reactions and Film-Growth Kinetics," Daniel Lubben, University of Illinois, Urbana, Ill.

"Simulation of Silicates: Molecular Polymerization, Surface Structure, and Absorption," S. H. Garofalini, Rutgers University, Piscataway, N.J.

"Ion Irradiation of the High-$T_c$ Superconductor $YBa_2Cu_3O_7$: Vortex Pinning via Tailored Defects," J. R. Thompson, The University of Tennessee, Knoxville, Tenn./Solid State Division, ORNL

"Time-Resolved X-Ray Scattering Investigation of Ordering Kinetics in a Second-Order Phase Transition," Byungwoo Park, IBM T. J. Watson Research Center, Murray Hill, N.J.

"Ion Beam Enhanced Adhesion of Metal Films on a Sapphire Substrate," J. E. Pawel, Vanderbilt University, Nashville, Tenn.

"Moment-Volume Coupling in Transition Metals and Alloys," M. Acet, Universität Duisburg, Duisburg, Germany

"The Interfacial Transition Region in Metal-Metal Overlayer Systems," J. E. Houston, Sandia National Laboratories, Albuquerque, N. Mex.

"Critical Current, Flux Motion, and Magnetization in High-$T_c$ Superconductors," M. N. Kunchur, University of Virginia, Charlottesville, Va.

"Characterization of Perovskite Thin Films by TEM," S. A. Rou, North Carolina State University, Raleigh, N.C.

"Tight-Binding Molecular Dynamics: From Melting Silicon to Making Buckyballs," C. Z. Wang, Iowa State University, Ames, Iowa

"Electronic and Atomic Structure of the Potassium(110) Surface," B. S. Itchkawitz, The University of Pennsylvania, Philadelphia, Pa.

"The Superconducting Phase Transition of Artificial Wire Networks," Fang Yu, University of Minnesota, Minneapolis, Minn.

"Current Status of Buckyballs ($C_{60}$)," Ward Plummer, The University of Pennsylvania, Philadelphia, Pa.

"Investigation of Semiconductor Surface Structures by Transmission Ion Channeling," Paul Lyman, University of Florida, Gainesville, Fla.

"NMR Studies of $YBa_2Cu_3O_7$ in the Superconducting State," S. E. Barrett, University of Illinois, Urbana, Ill.

"Characterization and Engineering of Semiconductor Heterostructures," Xiaohua Yu, University of Minnesota, Minneapolis, Minn.

"Plasma Synthesis of Fe-Containing Thin Films," J.-L. Li, University of Missouri, Rolla, Mo.

"Spectroscopic Measurements and Quantum Mechanical Modeling of Biologically Active Paramagnetic Sites," A. S. Brill, University of Virginia, Charlottesville, Va.

"TEM Study of Extended Defect Formation in Ion-Implanted Semiconductors," Kevin Jones, University of Florida, Gainesville, Fla.

"Microstress Distribution in Ceramic Heterostructures," S. S. Rao, Rutgers University, Piscataway, N.J.

"Superconductivity in Metals Containing Anderson Impurities with Strong Local Electron-Phonon Coupling," A. G. Malshukov, USSR Academy of Sciences, Moscow, Russian Providence

"Photoemission Studies of Fullerenes and Fullerides," J. H. Weaver, University of Minnesota, Minneapolis, Minn.

"Surfaces of Simple Metals: An Experimentalist in a Theorist's Playground," Ward Plummer, The University of Pennsylvania, Philadelphia, Pa.

"Defect Scattering of Neutrons from Antiferromagnetic Alloys," Trevor Hicks, Monash University, Clayton, Australia

"Ion Beam Erosion of Graphite at High Temperatures," J. Roth, Max-Planck-Institüt für Plasmaphysik, Garching, Germany

"Impurity States in Quantum Wells and Quantum Wires," L. E. Oliveira, State University of Campinas, Sao Paulo, Brazil

"Heat Capacity and Thermal Expansion Measurements of High-$T_c$ Superconductors," D. K. Wohlleben, University of Cologne, Cologne, Germany

"Vortex Fluctuations in Superconductors," P. Minnhagen, Umeå University, Umeå, Sweden

"The Story of Dr. A and Prof. B: An Introduction to Bayesian Model Selection," D. S. Sivia, Rutherford Appleton Laboratory, Chilton, United Kingdom

"Epitaxial Growth Dynamics: From Quantum Wires to the Renormalization Group," A. Zangwill, Georgia Institute of Technology, Atlanta, Ga.

"Growth Phenomena and Domain Formation in Ferroelectric Thin Films," B. S. Kwak, Georgia Institute of Technology, Atlanta, Ga.

"Grain and Crystal Growth in Thin Films," D. A. Smith, IBM T. J. Watson Research Center, Yorktown Heights, N.Y.

"Theoretical Studies of Semiconductor Epitaxial Growth on Stepped Si(100) Surfaces," D. Srivastava, The Pennsylvania State University, University Park, Pa.

"A Crack Propagation Model for Earthquakes," H.-J. Xu, University of British Columbia, Vancouver, British Columbia, Canada

"Lattice Damage in Ion-Implanted Semiconductors," T. E. Haynes, Solid State Division, ORNL

"Mathematical Methods for Problem Solving in Neutron and X-Ray Data Reduction via Perceptual Criteria," D. Svergun, Institute of Crystallography, Moscow, Russian Providence

"Laser Molecular Beam Epitaxy for the Construction of Superconducting Artificial Lattices," T. Kawai, Osaka University, Osaka, Japan

"Interfacial Dynamics at a Martensitic Phase Transition," G. S. Bales, Queen's University, Ontario, Canada

---

[1]Joint Solid State and Physics division sseminar

[2]Joint Solid State and Engineering Physics and Mathematics divisions seminar

[3]Joint Solid State and Chemical Technology divisions seminar

[4]Joint Solid State and Health & Safety Research divisions seminar

# *LECTURES AND SEMINARS BY DIVISION MEMBERS*

J. B. Bates—University of Kentucky, Lexington, Kentucky, "Amorphous Lithium Electrolyte Thin Films"; The University of Tennessee, Knoxville, Tennessee, "Amorphous Inorganic Thin-Film Lithium Electrolytes" and "Ceramic Thin Films and Thin-Film Batteries"; Eveready Battery Co., Cleveland, Ohio, "Amorphous Lithium Electrolyte Thin Films and Thin-Film Batteries"; Exxon Research and Engineering, Clinton, New Jersey, "Fabrication and Characterization of Amorphous Lithium Electrolyte Thin Films and Rechargeable Thin-Film Batteries"

L. A. Boatner—Alabama A&M University, Normal, Alabama, "The Growth of Single Crystals and Their Application in Materials Science"

B. C. Chakoumakos—University of New Mexico, Albuquerque, New Mexico, "Hole Filling and Hole Creation in the Superconducting Compound $Bi_{2-x}PbxSr_{2-y}La_yCuO_{6+z}$"; East Tennessee Public Schools Workshop, Oak Ridge, Tennessee, "Crystals & Symmetry"

Y. Chen—University of Florida, Gainesville, Florida, "Tunable Laser Based on Anion Vacancies in CaO Crystals: The Hydride Problem"; Virginia Commonwealth University, Richmond, Virginia, "Tunable Laser Based on Vacancies in MgO Crystals"

D. K. Christen—University of Kentucky, Lexington, Kentucky, "Studies of Flux Pinning and Critical Currents in High-Temperature Superconductors"

J. B. Hayter—State Department, Washington, D.C., "Neutron Scattering and Other Reactor-Based Research at ORNL"; Oak Ridge National Laboratory Showcase Lecture, Oak Ridge, Tennessee, "The Advanced Neutron Source—All Done With Mirrors?"; The University of Tennessee, Knoxville, Tennessee, "Uses of the Advanced Neutron Source"; University of Delaware, Newark, Delaware, "Neutron Scattering Studies of Sub-Micron Structures"; Johnson & Johnson Polymer Research Symposium, New Brunswick, New Jersey, "SANS Studies of Self-Assembling Structures"; EG&G ORTEC, Oak Ridge, Tennessee, "Neutron-Scattering Instrumentation"; University of Wisconsin, Madison, Wisconsin, "Small-Angle Neutron Scattering from Self-Assembling Systems"; University of Wisconsin, Madison, Wisconsin, "Some Research Applications of the Advanced Neutron Source"; Physics Division Seminar, Oak Ridge National Laboratory, Oak Ridge, Tennessee, "Nuclear Physics at the ANS"; University of Keele, Keele, United Kingdom, "Small-Angle Neutron Scattering Studies of Sub-Micron Structures"; State Department, Washington, D.C., "Research Reactors and Other Radiation Producing Devices"

D. E. Jesson—IBM, Yorktown Heights, New York, "Direct Imaging of Si-Ge Alloys, Superlattices, and Buried Ge Layers Using Z-Contrast STEM"; National Center for Electron Microscopy, Berkeley, California, "Z-Contrast Imaging"

B. C. Larson—University of Illinois, Urbana-Champaign, Illinois, "ORNL Synchrotron Research Program for the Advanced Photon Source"

S. H. Liu—Iowa State University, Ames, Iowa, National Taiwan University, Taiwan, China, and National Normal University, Taiwan, China, "Interlayer Pairing in Layered Superconductors"; Iowa State University, Ames, Iowa, and Argonne National Laboratory, Argonne, Illinois, 'Deterministic Sandpiles: Route to Chaos in Large Systems"; National Tsing-Hua University, Taiwan, China, Sun Yat-sen University, Taiwan, China, and National Central University, Taiwan, China, "Fractals and Their Applications in Physics"; National Normal University, Taiwan, China, "Heavy Fermion Materials"

D. H. Lowndes—University of Florida, Gainesville, Florida, "Copper Oxide Superconducting Superlattices"; Argonne National Laboratory, Argonne, Illinois, "Superconductivity in Epitaxial Copper Oxide Superlattices"; Louisiana State University, Baton Rouge, Louisiana, "Superconductivity in Epitaxial High-$T_c$ Superlattices: Effects of Hole Filling and of Reduced Dimensionality"; Oak Ridge National Laboratory, Oak Ridge, Tennessee, "Reduced Dimensionality and Doping Effects in High-$T_c$ Superconducting Films and Superlattices"; Oak Ridge National Laboratory, Oak Ridge, Tennessee, "Scanning Tunneling Microscope Studies of $YBa_2Cu_3O_{7-x}$ Film-Growth Mechanisms and Surface Microstructure"; Swiss Federal Institute of Technology, Lausanne, Switzerland, and University of Geneva, Geneva, Switzerland, "Microstructure and Superconducting Properties of Epitaxial $YBa_2Cu_3O_{7-x}/PrBa_2Cu_3O_{7-x}$ Superlattices"; Hitachi Central Research Laboratory, Tokyo, Japan, Matsushita Industrial Electric Co., Ltd., Osaka, Japan, and University of Tsukuba, Tsukuba, Japan, "Laser Ablation Synthesis and Properties of Epitaxial Copper Oxide Superlattices"

G. D. Mahan—International Centre Theoretical Physics, Trieste, Italy (4 lectures), "Electron Correlation in Simple Metals"; International Centre Condensed Matter Physics, Brazil (4 lectures) "Many-Body Theory"; Linköping University, Lingköping, Sweden, Chalmers Technical University, Göteborg, Sweden, and Pennsylvania State University, University Park, Pennsylvania, "Current Drag on Semiconductors"

J. W. McCamy—The University of Tennessee, Knoxville, Tennessee, "Growth of ZnS and ZnSe Epilayers by Pulsed-Laser Ablation"

S. J. Pennycook—Max-Planck Institut für Metallforschung, Stuttgart, Germany, and National Research Council of Canada, Institute for Microstructural Sciences, Ottawa, Canada, "Compositional Imaging of Interfaces in Semiconductors and Superconductors by Z-Contrast STEM"; Conductus, Inc., Sunnyvale, California, "Z-Contrast Imaging of High-$T_c$ Films and Superlattices"; The University of Tennessee, Knoxville, Tennessee, "Z-Contrast STEM: Visualizing Materials on the Atomic Scale"; Michigan State University, Lansing, Michigan, "Z-Contrast Imaging of Semiconducting and Superconducting Superlattices"; Harvard University, Boston, Massachusetts, "Direct Imaging of Materials Through Z-Contrast STEM"

D. B. Poker—Alabama A&M University, Normal, Alabama, "Ion-Implanted Optical Waveguides in $LiNbO_3$"

M. Rasolt—University of Tokyo, Tokyo, Japan, "Superconductivity Induced by Very Strong Magnetic Fields"; IBM T. J. Watson Research Center, Yorktown Heights, New York, "Kosterlitz-Thouless Theory of Resistive Transitions in High-$T_c$ Superlattices and Spontaneously Broken Chiral States"; Johns Hopkins University, Baltimore, Maryland, "Kosterlitz-Thouless Theory of Resistive Transitions in High-$T_c$ Superlattices"

H. G. Smith—University of South Florida, Tampa, Florida "Applications of Neutron Scattering to Problems in Materials Sciences"

J. R. Thompson—University of Louisville, Louisville, Kentucky, "Magnetic and Transport Studies of High-Temperature Superconductors"; IBM T. J. Watson Research Center, Yorktown Heights, New York, "DC Magnetization Studies of High-Temperature Superconductors: Reversible, Irreversible, and Flux Creep Properties"; Pusan National University, Pusan, South Korea, "Magnetic Studies of High-$T_c$ Superconductors: Equilibrium and Irreversible Properties"; National Research Institute for Metals: Tsukuba Laboratories, Tsukuba, Japan, "Irreversibility and Flux Creep in High-Temperature Superconductors"; Physics Division, Oak Ridge National Laboratory, Oak Ridge, Tennessee, "Better High-$T_c$ Superconducting Materials with Ion-Induced Defects"

# *Scientific Activities, Awards, and Honors*

| | |
|---|---|
| A. P. Baddorf | President, Tennessee Valley Chapter, American Vacuum Society, 1991–1992<br>Vice-President, Tennessee Valley Chapter, American Vacuum Society, 1990–1991 |
| J. B. Bates | Co-Chairman, Thin-Film Ionics Session, Eighth International Conference on Solid State Ionics, Lake Geneva, Canada, October 1991<br>Co-Organizer, Symposium on Solid Electrolytes, The Electrochemical Society Meeting, Seattle, Washington, October 1990 |
| L. A. Boatner | Recipient, ASM International Fellowship, 1991<br>Associate Editor, *Optical Materials*, 1990–1992<br>Executive Secretary, Materials Research Society, 1992–1993<br>Co-Chairman, Eighth International Summer School on Crystal Growth (to be held in 1992)<br>Co-Editor, *The Journal of Crystal Growth*, Special Issue<br>Recipient, Second Place Award, Optical Micrographs Category, 1991 Ceramographic Competition of the American Ceramic Society<br>Chairman, ORNL-Universidad Nacional Autonoma de Mexico Joint Steering Committee<br>Member, Executive Committee, American Association for Crystal Growth<br>Member, Membership Committee, Materials Research Society, 1991<br>Session Chairman, American Physical Society Meeting, Cincinnati, Ohio, March 1991<br>Session Chairman, Materials Research Society Symposium, Boston, Massachusetts, November 1991<br>Session Chairman, American Ceramic Society, Basic Sciences Division Meeting, Marco Island, Florida, October 1991<br>Special Graduate Faculty Member, Alabama A&M University 1991<br>Research Advisor, ORNL/SERS Program, 1991–1992<br>Thesis Advisor, ORAU Graduate Research Program ,1992<br>Member, ORNL Showcase Talk Selection Committee, 1991–1992 |
| J. D. Budai | Recipient, Martin Marietta Energy Systems Technical Achievement Award for Publication, 1991 |
| B. C. Chakoumakos | Traveling Lecturer, Oak Ridge Associated Universities, 1991–1992 |

| | |
|---|---|
| Y. Chen | Session Chairman, American Physical Society Meeting, Cincinnati, Ohio, March 1991<br>Co-Chairman, Materials Research Society Symposium on Synthesis and Processing of Ceramics: Scientific Issues, Boston, Massachusetts, November 1991<br>Advisor, Superconducting Supercollider GEM $BaF_2$ Panel, 1991–1992<br>Co-Chairman, DOE Research Assistance Task Force Meeting on Electrical Breakdown of Insulating Ceramics in a High-Radiation Field, Vail, Colorado, May 1991<br>Co-Chairman, MPTG Symposium on Optical Materials, American Physical Society, Cincinnati, Ohio, March 1991<br>Chairman, DOE Research Assistance Task Force Meeting on the Application of Positron Spectroscopy to Materials Sciences (to be held in 1992) |
| M. F. Chisholm | Traveling Lecturer, Oak Ridge Associated Universities, 1992–1993 |
| D. K. Christen | Recipient, DOE/DMS 1991 Materials Sciences Research Competition Award for Significant Implication for Energy-Related Technology Category, 1991<br>Panel Chairman, ONR/NSF Workshop on New Research Opportunities in Superconductivity (to be held in 1992 |
| J. F. Cooke | Member, Advisory Committee, *Journal of Physics, Condensed Matter* |
| H. L. Davis | Traveling Lecturer, Oak Ridge Associated Universities, 1991–1992 |
| N. J. Dudney | Associate Editor, *Journal of the American Ceramic Society*<br>Abstracter, American Ceramic Society<br>Judge, Annual Southern Appalachian Science and Engineering Fairs |
| R. Feenstra | Recipient, DOE/DMS 1991 Materials Sciences Research Competition Award for Significant Implication for Energy-Related Technology Category, 1991<br>Traveling Lecturer, Oak Ridge Associated Universities, 1992–1993 |
| S. M. Gorbatkin | Member, Plasma Science and Technology Program Committee, and Session Chairman, 38th Annual American Vacuum Society Symposium, Seattle, Washington, November 1991<br>Session Chairman, 37th American Vacuum Society Symposium, Toronto, Canada, October 1990<br>Co-Organizer, and Session Chairman, Symposium on Beam and Plasma Modification of Materials, Materials Research Society, Anaheim, California, April 1991<br>Co-Editor, *Beam and Plasma Modification of Materials*, Materials Research Society, Philadelphia, Pennsylvania, 1991<br>Secretary, Plasma Science and Technology Division, American Vacuum Society, 1991–1992<br>Member, Plasma Science and Technology Division Student Award Committee, American Vacuum Society, 1991 |

| | |
|---|---|
| P. H. Green | Secretary/Treasurer, DOE Basic Energy Sciences/Materials Sciences Five Laboratory Information Meeting on Synthesis and Processing of Tailored Materials (to be held in 1992)<br>Secretary/Treasurer, DOE/OBES Workshop on Environmental, Safety, and Health Requirements, Gatlinburg, Tennessee, May 1991<br>Secretary/Treasurer, DOE Research Assistance Task Force Meeting on Electrical Breakdown of Insulating Ceramics in a High-Radiation Field, Vail, Colorado, May 1991<br>Secretary/Treasurer, DOE/DMS Workshop on Future Synchrotron VUV and X-Ray Beam Lines, Gatlinburg, Tennessee, October 1991 |
| W. A. Hamilton | Traveling Lecturer, Oak Ridge Associated Universities, 1992–1993 |
| T. E. Haynes | Member, Executive Board, Tennessee Valley Chapter, American Vacuum Society<br>Co-Chairman, 11th Annual Symposium of Tennessee Valley Chapter, American Vacuum Society, Oak Ridge, Tennessee, May 1991 |
| J. B. Hayter | Recipient, American Physical Society Fellowship, 1992<br>Discussion Leader, National Institute of Standards and Technology Workshop on Applications of Cold Neutron Spectroscopy, Gaithersburg, Maryland, June 1991<br>Member, Executive Committee, National Steering Committee for the Advanced Neutron Source, 1990–1992<br>Member, National Steering Committee, Advanced Neutron Source, 1990–1992<br>Chairman, Data Analysis Workshop, LANSCE, Los Alamos, New Mexico, January 1992<br>Member, Working Group on Large Scale Structures, 3rd European Expert Meeting on Neutron Sources, Science and Engineering Council, Abingdon, England, February 1992<br>Chairman, Program Advisory Committee on Reflectometry and Small-Angle Scattering, LANSCE, Los Alamos, New Mexico, March 1992<br>Recipient, ANS Extra Kilometer Award for "extra efforts and outstanding contributions to the preparation of system design descriptions for the Advanced Neutron Source Project's Conceptual Design," 1991<br>Technical Communication Award for "Achievement in Design Graphics, Presentations," Society for Technical Communication (East Tennessee Chapter), 1991<br>Technical Communication Award for "Merit in Design Graphics, Covers," Society for Technical Communication (East Tennessee Chapter), 1991 |
| G. E. Jellison, Jr. | Editorial Board, *Applied Physics Communications* |
| T. Kaplan | Member, ORNL Proposal Review Committee<br>Traveling Lecturer, Oak Ridge Associated Universities, 1992–1993 |
| H. R. Kerchner | Recipient, DOE/DMS 1991 Materials Sciences Research Competition Award for Significant Implication for Energy-Related Technology Category, 1991 |

| | |
|---|---|
| C. E. Klabunde | Recipient, DOE/DMS 1991 Materials Sciences Research Competition Award for Significant Implication for Energy-Related Technology Category, 1991 |
| B. C. Larson | Co-Chairman, DOE/DMS Workshop on Future Synchrotron VUV and X-Ray Beam Lines, Gatlinburg, Tennessee, October 1991 |
| J. S. Lin | Adjunct Professor, Department of Materials Science and Engineering, The University of Tennessee, Knoxville, Tennessee<br>Chairman, American Crystallographic Association, Small-Angle Scattering Special Interest Group, 1989–1991<br>Chairman, Symposium Organizing Committee for 40th ACA Annual Meeting, Small-Angle Scattering Special Session, 1990 |
| S. H. Liu | Member, Advisory Board, Center of Condensed Matter Science, National Taiwan University, Taiwan, China, 1991–present<br>Charter Member, Physics and Astronomy Council, Iowa State University, 1992 |
| D. H. Lowndes | Co-Chairman, Focused Session on Epitaxial Layers of High-$T_c$ Superconductors, American Physical Society, Cincinnati, Ohio, 1991<br>Program Committee, Workshop on Pulsed Laser Ablation, Oak Ridge, Tennessee, April 1991.<br>Program Committee, International Conference on Laser Ablation (COLA-93) (to be held in 1993)<br>Adjunct Professor of Materials Science and Engineering, The University of Tennessee, Knoxville, Tennessee<br>Recipient, Martin Marietta Energy Systems Technical Achievement Award for Publication, 1991<br>Co-Editor, *Surface Chemistry and Beam-Solid Interactions*, Materials Research Society, Pittsburgh, Pennsylvania, 1991 |
| G. D. Mahan | Member, Selection Committee to Choose Professorships, Umeå University, Umeå, Sweden; Royal Institute of Technology; Chalmers Technical University<br>Member, Review Committee, Vanderbilt University, Nashville, Tennessee<br>Chairman, Scientific Committee, International Center of Condensed Matter Physics, Brasilia<br>Member, Executive Committee, Division of Condensed Matter Physics, American Physical Society, 1990–1992<br>Co-Editor, Plenum Publishing Company Book Series |
| R. M. Moon | Recipient, Martin Marietta Corporate Fellowship, 1991<br>Executive Secretary, National Steering Committee for the Advanced Neutron Source<br>Advisor, Steering Committee for the U.S.–Japan Cooperative Program on Neutron Scattering |
| D. P. Norton | Recipient, Martin Marietta Energy Systems Technical Achievement Award for Publication, 1991 |

| | |
|---|---|
| S. J. Pennycook | Recipient, American Physical Society Fellowship, 1992<br>Member, Materials Research Society Publications Committee<br>Meeting Co-Chairman, Materials Research Society Fall Meeting (to be held in 1992)<br>Guest Editor, *MRS Bulletin*, March 1991<br>Member, Organizing Committee, International Workshop on Electron Microscopy in Materials Science, Brindisi, Italy |
| D. B. Poker | Meeting Co-Chairman, Materials Research Society (to be held in 1993)<br>Member, Editorial Board, *Nuclear Insturments and Methods in Physics Research Section B*<br>Member, Materials Research Society Publications Committee<br>Co-Editor, *Ion Beam Modification of Materials*, North-Holland, Amsterdam, 1991<br>Session Chair, Materials Research Society, Anaheim, California, April 1991 |
| J. B. Roberto | President, Materials Research Society, 1991<br>Past President, Materials Research Society, 1992<br>Recipient, Martin Marietta Energy Systems President's Award, "Image of ORNL," 1991<br>Co-Chairman, Washington Materials Forum, Washington, D.C., February 1991<br>Co-Chairman, DOE Basic Energy Sciences/Materials Sciences Five Laboratory Information Meeting on Synthesis and Processing of Tailored Materials (to be held in 1992)<br>Co-Organizer, Forum on Advanced Materials and Processing: The 1993 Presidential Initiative in Materials Science and Technology, Materials Research Society (to be held in 1992)<br>Member, Technology Area Coordination Team for Microelectronics and Photonics, DOE Technology Commercialization Initiative, 1991–1992<br>Focus Area Coordinator, Advanced Ceramics and Ceramic Thin Films, DOE-BES Center of Excellence in Synthesis and Processing, 1991–1992<br>Working Group Chairman, DOE/OBES Workshop on Environmental, Safety, and Health Requirements, Gatlinburg, Tennessee, May 1991<br>Organizer, Congressional Advanced Materials Caucus Meeting, Washington, D.C., July 1991<br>Chairman, Nominating Committee and Von Hippel Award Subcommittee, Materials Research Society, 1992<br>Member, Long-Range Planning Committee, Materials Research Society, 1991–1992<br>Subcommittee Chairman, ORNL Overhead Oversight Committee, 1991<br>Member, ORNL Strategic Research and Development Planning Committee, 1991–1992<br>Member, ORNL Waste Management Operations Committee, 1991–1992<br>Member, ORNL Facility Management Committee, 1991 |
| M. T. Robinson | Member, International Advisory Committee, Symposium on Fundamental Processes in Sputtering, Danish Academy of Sciences and Letters, Copenhagen (to be held in 1992) |

| | |
|---|---|
| H. G. Smith | Correspondent, *Neutron News*<br>Consulting Member, Neutron Diffraction Commission of the International Union of Crystallography, 1990–1993<br>Traveling Lecturer, Oak Ridge Associated Universities, 1991–1992<br>Member, Program Committee, Neutron Scattering Satellite Meeting of the General Assembly of the International Union of Crystallography (to be held in 1993) |
| S. Spooner | Chairman, The Physics and Chemistry of Materials Committee, The Metals Society, American Institute of Mining, Petroleum, and Metallurgical Engineers |
| J. R. Thompson | Recipient, DOE/DMS 1991 Materials Sciences Research Competition Award for Significant Implication for Energy-Related Technology Category, 1991<br>Martin Marietta Energy Systems Significant Achievement Award, June 1991<br>Session Organizer, Symposium on Vortices in High-$T_c$ Superconductors, Nineteenth Rare-Earth Research Conference, Lexington, Kentucky, July 1991.<br>International Advisory Committee, International Symposium on Mechanical Alloying, Kyoto, Japan, May 1991<br>Session Chairman, American Physical Society, Indianapolis, Indiana, March 1992 |
| J. F. Wendelken | Short Course Chairman, Tennessee Valley Chapter, American Vacuum Society<br>Co-Chairman, Future Sites Committee, American Vacuum Society<br>Traveling Lecturer, Oak Ridge Associated Universities, 1992–1993 |
| C. W. White | Councillor, Materials Research Society, 1990–1991<br>Principal Editor, *Journal of Materials Research*, 1990–June 1991 |
| M. K. Wilkinson | Recipient, DOE Distinguished Associate Award, 1991<br>Executive Secretary, DOE Basic Energy Sciences Laboratory Program Panel<br>Adjunct Professsor, School of Physics, Georgia Institute of Technology, Atlanta, Georgia<br>Member, ORNL Steering Committee, Advanced Neutron Source<br>Secretary, National Steering Committee for the Advanced Neutron Source (NSCANS)<br>Secretary, NSCANS Executive Committee<br>Member, ORNL Stage II Budget Review Committee<br>Chairman, Evaluation Panel for Reactor Radiation Division, National Institute of Standards and Technology<br>Member, Evaluation Panel for Materials Science and Engineering Laboratory, National Institute of Standards and Technology<br>Member, ORNL 50th Year Celebration Committee |

| | |
|---|---|
| J. M. Williams | Vice-President, Executive Committee, Oak Ridge Chapter, ASM International<br>Member, International Committee, Seventh International Conference on Surface Modification of Metals by Ion Beams, Washington, D.C., July 1991 |
| S. P. Withrow | Co-Editor, *Ion Beam Modification of Materials*, North-Holland, Amsterdam, 1991 |
| R. F. Wood | Member, ORNL Wigner Fellowship Committee<br>Member, ORNL-UT Distinguished Scientist Committee<br>Chairman, Corporate Fellows Committee for a New ORNL Postdoctoral Program, 1991–1992<br>Chairman, Search Committee for Director of the ORNL Center for Computational Science, 1992<br>Co-Chairman, ORNL/EPRI Committee for White Paper Assessment of Opportunities in Thin-Film Silicon Photovoltaics<br>Chairman, Oversight Committee for ORNL Postdoctoral Program |
| F. W. Young | Executive Secretary, Division of Materials Physics, American Physical Society, 1990–1992<br>Member, Materials Sciences Advisory Board, Southeastern Universitites Research Association |
| D. M. Zehner | Member, User Executive Committee, National Synchrotron Light Source, 1989–1992<br>Member, Oak Ridge Associated Universities Graduate Fellow Selection Panel<br>Session Chairman, American Physical Society Meeting, Indianapolis, Indiana, March 1992 |

# *Personnel Changes*

## New Staff Members

**A.** ***Scientific Staff***

W. A. Hamilton, Los Alamos National Laboratory, Los Alamos, New Mexico
D. E. Jesson, University of Bristol, Bristol, United Kingdom
D. C. Lubben, University of Illinois, Urbana, Illinois

**B.** ***Administrative and Technical Support Staff***

L. S. Crawley, Senior Secretary
S. B. Hannon, Secretary
D. K. Hensley, Senior Laboratory Technician
S. L. Stairs, Secretary
G. B. Taylor, Senior Laboratory Technician

## Staff Transfers and Terminations

**A.** ***Scientific Staff***

J. R. Noonan (voluntary resignation)
J. Rankin (completion of temporary employment)
A. L. Wachs (transferred to Quality Division)
M. K. Wilkinson (retirement)
F. W. Young, Jr. (retirement)

**B.** ***Administrative and Technical Support Staff***

B. E. Gray (transferred to Office of Waste Management and Remedial Actions)
A. M. Keesee (retirement)
J. L. Moore (transferred to Instrumentation and Controls Division)
S. L. Stairs (voluntary resignation)

## Guest Assignments

**A.** ***Scientific Staff***

G. S. Canwright, The University of Tennessee, Knoxville, Tennessee
A. L. Claesson, University of Umea, Umea, Sweden
B. Dötsch, Universitat Erlangen-Nürnberg, Erlangen, Germany
H. O. da Frota, The University of Tennessee, Knoxville, Tennessee
T. J. Hicks, Monash University, Clayton, Victoria, Australia
M. Karimi, Alabama A&M University, Normal, Alabama
S. Katano, Japan Atomic Energy Research Institute, Tokai, Japan

A. *Scientific Staff* (cont'd)

G. D. Mahan*, The University of Tennessee, Knoxville, Tennessee
A. Malchoukov, The University of Tennessee, Knoxville, Tennessee
Y. Morii, Japan Atomic Energy Research Institute, Tokai, Japan
H. Naramoto, Japan Atomic Energy Research Institute, Tokai, Japan
J. L. Park, North Carolina State University, Raleigh, North Carolina
A. Rojo, The University of Tennessee, Knoxville, Tennessee
B. Sernelius, The University of Tennessee, Knoxville, Tennessee
J. Sofo, The University of Tennessee, Knoxville, Tennessee
E. Takasuka, Sumitomo Metal Industries, Ltd., Amagasaki, Japan
R. Triolo, University of Palermo, Palermo, Italy
G. Watson, The University of Tennessee, Knoxville, Tennessee
H. Wenzl, Forschungszentrum, Jülich, Germany
J. L. Zarestky, Ames Laboratory/Iowa State University, Ames, Iowa

*ORNL/UT Distinguished Scientist

B. *Postgraduate Research Participation Program*

J. R. Brewster, The University of Tennessee, Knoxville, Tennessee
N. Browning, University of Cambridge, Cambridge, United Kingdom
D. E. Jesson, University of Bristol, Bristol, United Kingdom
M. N. Kunchur, Rutgers University, Piscataway, New Jersey
P. F. Lyman, University of Pennsylvania, Philadelphia, Pennsylvania
L. Romana, Université Claude Bernard, Lyon, France
M. Yethiraj, University of Missouri, Columbia, Missouri
S. Y. Zheng, The University of Tennessee, Knoxville, Tennessee
J. K. Zuo, Renssealear Polytechnic Institute, Troy, New York

C. *Graduate Students*

H. H. Burke, Columbia University, New York, New York
Y. J. Chen, The University of Tennessee, Knoxville, Tennessee
E. C. Jones, The University of Tennessee, Knoxville, Tennessee
J. W. McCamy, The University of Tennessee, Knoxville, Tennessee
J. Ossandon, The University of Tennessee, Knoxville, Tennessee
J. Sharp, The University of Tennessee, Knoxville, Tennessee
Y. R. Sun, The University of Tennessee, Knoxville, Tennessee
C. Walters, University of Pennsylvania, Philadelphia, Pennsylvania
S. Zhu, The University of Tennessee, Knoxville, Tennessee

D. *Undergraduate Students*

R. Boekenhauer, Coe College, Cedar Rapids, Iowa
R. Burgie, Alfred University, Alfred, New York
S. Graber, The University of Tennessee, Knoxville, Tennessee
H. Fujita, Monmouth College, Monmouth, Illinois
J. Paul, The University of Tennessee, Knoxville, Tennessee
Y. Powell, Alabama A&M University, Normal, Alabama
G. Steadman, University of Southern Colorado, Pueblo, Colorado
A. Wong, Princeton University, Princeton, New Jersey

## Summer Assignments (1991)

**A.** ***Scientific Staff***

R. S. Fishman, North Dakota State University, Fargo, North Dakota
L. Hammer, University of Erlangen–Nürenberg, Erlangen, Germany
T. Motooka, University of Tsukuba, Tsukuba, Japan
R. Triolo, University of Palermo, Palermo, Italy
N. Wakabayashi, Keio University, Yokohama, Japan

**B.** ***Technical Support Staff***

D. Gilmore, California Institute of Technology, Pasadena, California

**C.** ***Oak Ridge Associated Universities—Faculty Research Participants***

M. J. Aziz, Harvard University, Cambridge, Massachusetts
E. W. Plummer, University of Pennsylvania, Philadelphia, Pennsylvania
D. G. Tonn, Wooster College, Wooster, Ohio

**D.** ***Oak Ridge Associated Universities—Student Research Participants***

A. Watson, University of Illinois, Urbana, Illinois
L. Murphy, State University of New York, Albany, New York

**E.** ***Graduate Student***

L. Siller, University of Cambridge, Cambridge, United Kingdom

# SOLID STATE DIVISION

*April 1, 1992*

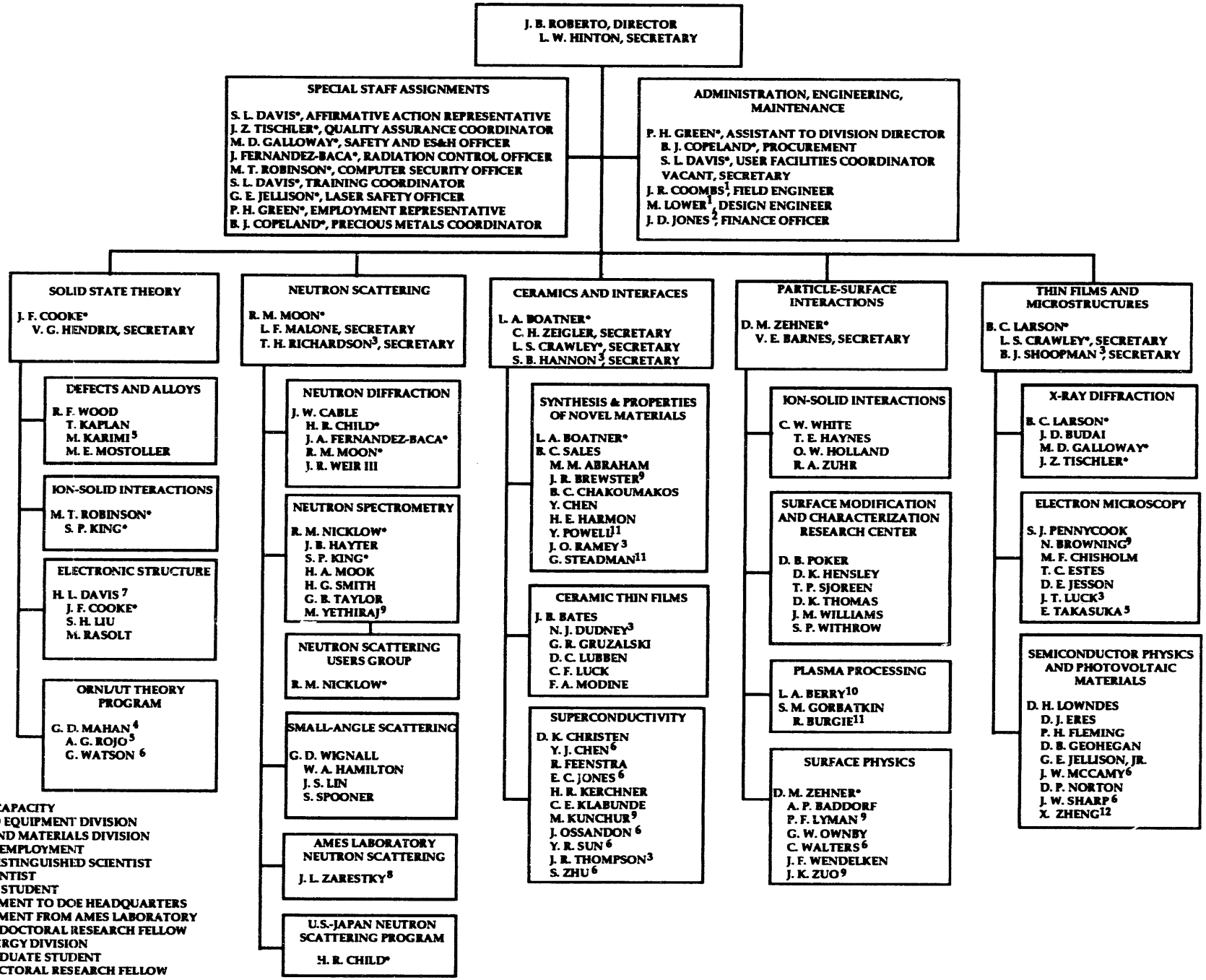


*MULTIPLE CAPACITY
[1]PLANT AND EQUIPMENT DIVISION
[2]FINANCE AND MATERIALS DIVISION
[3]PART-TIME EMPLOYMENT
[4]ORNL/UT DISTINGUISHED SCIENTIST
[5]GUEST SCIENTIST
[6]GRADUATE STUDENT
[7]ON ASSIGNMENT TO DOE HEADQUARTERS
[8]ON ASSIGNMENT FROM AMES LABORATORY
[9]ORAU POSTDOCTORAL RESEARCH FELLOW
[10]FUSION ENERGY DIVISION
[11]UNDERGRADUATE STUDENT
[12]UT POSTDOCTORAL RESEARCH FELLOW

# *Author Index*

# *Internal Distribution*

1. M. M. Abraham
2. B. R. Appleton
3. A. P. Baddorf
4. J. B. Ball
5. V. E. Barnes
6. J. B. Bates
7. L. E. Berry
8. E. E. Bloom
9–13. L. A. Boatner
14. J. Brewster
15. N. Browning
16. J. D. Budai
17. G. J. Bunick
18. W. H. Butler
19. J. W. Cable
20. J. Canright
21. R. S. Carlsmith
22. B. C. Chakoumakos
23. Y. Chen
24. H. R. Child
25. M. F. Chisholm
26. D. K. Christen
27–31. J. F. Cooke
32. B. J. Copeland
33–36. S. J. Cox
37. D. F. Craig
38. L. S. Crawley
39. H. L. Davis
40. S. L. Davis
41. N. J. Dudney
42. D. Eres
43. T. C. Estes
44. G. G. Fee
45. R. Feenstra
46. R. E. Fenstermaker
47. J. A. Fernandez-Baca
48. P. H. Fleming
49. W. Fulkerson
51. M. D. Galloway
52. R. K. Genung
53. D. B. Geohegan
54. H. A. Glovier
55. S. M. Gorbatkin
56. C. A. Grametbauer
57–61. P. H. Green
62. G. R. Gruzalski
63. W. A. Hamilton
64. H. E. Harmon
65. F. C. Hartman
67. T. E. Haynes
68. J. B. Hayter
69. V. G. Hendrix
70–75. L. W. Hinton
76. O. W. Holland
77. R. B. Honea
78. C. C. Hopkins
79. L. L. Horton
80. D. W. Jared
81. G. E. Jellison, Jr.
82. D. E. Jesson
83. E. Jones
84–87. J. D. Jones
89. J. E. Jones, Jr.
90. T. Kaplan
91. S. V. Kaye
93. H. R. Kerchner
94. S. P. King
95. P. W. King
96. C. E. Klabunde
97. E. H. Krieg
98. M. N. Kunchur
100. B. S. Kwak
101–105. B. C. Larson
106. R. P. Leinius
107. J. S. Lin
108. S. H. Liu
109. D. H. Lowndes
110. D. Lubben
111. C. F. Luck
112. J. T. Luck
113. G. D. Mahan
114. L. F. Malone
115. L. K. Mansur
116. R. G. Maples
117. J. W. McCamy
118. S. A. Meacham
119. F. A. Modine
120. H. A. Mook
121–125. R. M. Moon
126. O. B. Morgan
127. M. E. Mostoller
128. R. M. Nicklow
129. D. P. Norton
130. G. E. Oliphant
131. C. E. Oliver
132. G. W. Ownby
133. S. J. Pennycook
134. D. B. Poker
135. M. L. Poutsma
136. J. O. Ramey

137. M. Rasolt
138. D. E. Reichle
139. J. B. Richard
140. T. H. Richardson
141. C. R. Richmond
142–217. J. B. Roberto
218. M. T. Robinson
219. M. W. Rosenthal
220. T. H. Row
221. B. C. Sales
222. A. C. Schaffhauser
223. J. W. Sharp
224. J. Sheffield
225. R. B. Shelton
226. B. J. Shoopman
227. W. D. Shults
228. W. D. Siemens
229. T. P. Sjoreen
230. H. G. Smith
232. E. J. Soderstrom
233. E. Sonder
234. S. Spooner
235. J. O. Stiegler
236. G. B. Taylor
238. D. K. Thomas
239. J. R. Thompson
240. J. Z. Tischler
241. D. B. Trauger
242. A. W. Trivelpiece
243. R. I. Van Hook
244. R. C. Ward
245. D. A. Waters
246. G. I. Watson
247. J. R. Weir III
248. J. F. Wendelken
249. C. D. West
250. C. W. White
251. G. D. Wignall
252. M. K. Wilkinson
253. B. Y. Wilkes
254. J. M. Williams
255. S. P. Withrow
256. R. F. Wood
257. M. Yethiraj
258. J. L. Zarestky
259–263. D. M. Zehner
264. C. H. Zeigler
265. R. A. Zuhr
266. Biology Library
267–268. Central Research Library
269. ORNL Y-12 Technical Library
270. Document Reference Section
271–275. Laboratory Records Department
276. Laboratory Records, ORNL–RC

# *External Distribution*

277. Dr. A.A.Z. Ahmad, Chief Scientific Officer, Institute of Nuclear Science and Technology, Atomic Energy Research Establishment, Ganakbari, Savar, Dhaka, G.P.O. Box 3787, Dhaka, Bangladesh

278. Dr. Craig Allison, Department of Physics, Oklahoma State University, Stillwater, OK 74078

279. Dr. S. Amelinckx, SCK/CEN, B 2400-Mol, Belgium

280. Dr. Marcello Antonini, Physics Division, Building 44, Joint Research Centre, Euratom 21020 ISPRA (Varese) Italy

281. Dr. R. R. Arons, Institut für Festkörperforschung, Forschungszentrum, Postfach 1913, D-5170, Jülich, Germany

282. Dr. Neil W. Ashcroft, Laboratory of Atomic and Solid State Physics, Clark Hall, Cornell University, Ithaca, NY 14853-2501

283. Prof. Frank Avignone, Chairman, Department of Physics, University of South Carolina, Columbia, SC 29208

284. Dr. John Axe, Associate Director, Brookhaven National Laboratory, Upton, NY 11973

285. Dr. Michael J. Aziz, Department of Applied Science, Harvard University, Cambridge, MA 02138

286. Dr. K. J. Bachmann, Department of Chemistry, North Carolina State University, Box 5247, Raleigh, NC 27650

287. Dr. R. W. Balluffi, Department of Materials Science and Engineering, Massachusetts Institute of Technology, 77 Massachusetts Avenue, Cambridge, MA 02139

288. Dr. G. M. Bancroft, Department of Chemistry, Chemistry Building, The University of Western Ontario, London, N6A 5B7, Canada

289. Dr. J. H. Barrett, 827 W. Outer Drive, Oak Ridge, TN 37830

290. Dr. F. S. Bates, 151 Amundson Hall, Department of Chemical Engineering, University of Minnesota, Minneapolis, MN 55455

291. Dr. Edwin V. Beebe, Chemicals and Pigments Department, Research and Development Division, E.I. du Pont de Nemours and Company, Wilmington, DE 19898

292. Prof. Boris W. Batterman, Applied and Engineering Physics, 227 Clark Hall, Cornell University, Ithaca, NY 14853

293. Dr. Walter Bauer, Physical Research Division, Department 8340, Sandia National Laboratories, P.O. Box 969, Livermore, CA 94550

294. Dr. Rainer Behrisch, Max-Planck-Institut für Plasmaphysik, D-8046 Garching bei München, Germany

295. Dr. Ronald R. Berliner, Assistant Professor of Physics, University of Missouri, Research Reactor Facility, Columbia, MO 65211

296. Bibliotheque, Institut Max von Laue–Paul Langevin, 156 X 38042 Grenoble, Cedex, France

297. Dr. A. I. Bienenstock, Stanford Synchrotron Radiation Laboratory, Stanford University, P.O. Box 4349, Bin 69, Stanford, CA 94305

298. Prof. H. Birnbaum, University of Illinois, Materials Research Laboratory, 104 South Goodwin, Urbana, IL 61801

299. Dr. N. Bloembergen, Gordon McKay Laboratory, 9 Oxford Street, Cambridge, MA 02138

300. Dr. M. Blume, Brookhaven National Laboratory, Upton, NY 11973

301. Dr. Dawn Bonnell, Department of Materials Science, University of Pennsylvania, 3231 Walnut Street, Philadelphia, PA 19104

302. Dr. J. L. Boldu O., Instituto de Física, Universidad Nacional Autonoma de Mexico, Apartado Postal 20-364, 01000 Mexico, D.F.

303. Prof. Walter Borst, Chairman, Department of Physics, Texas Technology University, Box 4180, Lubbock, TX 79409-1051

304. Dr. William F. Brinkman, Room 1C-224, AT&T Bell Laboratories, 600 Mountain Avenue, Murray Hill, NJ 07974

305. Dr. Bruce Brown, PNS-372, Argonne National Laboratory, 9700 South Cass Avenue, Argonne, IL 60439

306. Dr. F. C. Brown, Department of Physics, University of Illinois, Urbana, IL 61801

307. Dr. Walter Brown, Room IE-452, AT&T Bell Laboratories, 600 Mountain Avenue, Murray Hill, NJ 07974

308. Dr. Christoph J. Buchal, Kernforschungsanlage, Postfach 1913, 5170 Jülich 1, Germany

309. Dr. R. Bullough, Atomic Energy Research Establishment, Harwell, Didcot, Oxon OX11 ORA, United Kingdom

310. Dr. John L. Burnett, Division of Chemical Sciences, ER-142, Office of Basic Energy Sciences, Office of Energy Research, Department of Energy, Washington, DC 20585

311. Prof. W.J.I Buyers, Atomic Energy of Canada Limited, Chalk River Nuclear Laboratories, Chalk River, Ontario KOJ 1JO, Canada

312. Prof. Nicolas Cabrera, Departamento de Fisica Fundamental, Facultad de Ciencias, Universidad Autonoma de Madrid, Canto-Blanco, Madrid 34, Spain

313. Prof. Robert W. Cahn, Department of Materials Science and Metallurgy, Cambridge University, Pembroke Street, Cambridge CB2 3Q2, United Kingdom

314. Dr. D. J. Campbell, L-209, Lawrence Livermore National Laboratory, P.O. Box 808, Livermore, CA 94550

315. Dr. J. M. Carpenter, Argonne National Laboratory, 9700 South Cass Avenue, Argonne, IL 60439

316. Prof. Ray W. Carpenter, Center for Solid State Science, Arizona State University, Tempe, AZ 85287

317. Dr. R. L. Chaplin, Department of Physics, Clemson University, Clemson, SC 29631

318. Prof. Girish Chandra,Tata Institute of Fundamental Research, National Centre of the Government of India for Nuclear Science and Mathematics, Homi Bhabha Road, Colaba, Bombay 400 005, India

319. Dr. Lloyd Chase, MS L-490, Lawrence Livermore National Laboratory, P.O. Box 808, Livermore, CA 94550

320. Dr. Andre Chatelain, Lab. Phys. Exp., Federal Institute of Technology, PH Ecublens, 1015 Lausanne, Switerland

321. Dr. D. S. Chemla, Lawrence Berkeley Laboratory, MS-66, 1 Cyclotron Road, Berkeley, CA 94720
322. Dr. W. J. Choyke, Westinghouse R&D Center, 1310 Beulah Road, Pittsburgh, PA 15235
323. Dr. Wei-Kan Chu, Texas Center for Superconductivity, University of Houston, Science and Research 1, Houston, TX 77204-5506
324. Dr. C. B. Clark, Department of Physics, University of North Carolina, Greensboro, NC 27412
325. Francisco H. Claro, Catholic University of Chile, Casilla 6177, Santiago, Chile
326. Dr. Frank Clinard, MS-546, Los Alamos National Laboratory, Los Alamos, NM 87545
327. Prof. Marvin Cohen, Department of Physics, University of California, Berkeley, CA 94720
328. Dr. Morrel H. Cohen, Corporate Research Science Laboratories, Exxon Research and Engineering Company, Clinton Township, Route 22 East, Annandale, NJ 08801
329. Mr. Ralph R. Coltman, Jr., 7905 Wiebelo Drive, Knoxville, TN 37931
330. Prof. James W. Corbett, Department of Physics, State University of New York at Albany, Albany, NY 12222
331. Dr. Roger A. Cowley, Department of Physics, Clarendon Laboratory, University of Oxford, Parks Road, Oxford, OX1 3PU, United Kingdom
332. Dr. Juan C. Crespi, Comision Nacional de Energía Atómica, Gerencia Desarrollo-Dto. Materiales, Avenida del Libertador 8250, 1429 Buenos Aires, Argentina
333. Dr. Gordon Czjzek, Kernforschungszentrum Karlsruhe, INFP, Postfach 3640, D-7500 Karlsruhe 1, Germany
334. Dr. L. S. Darken, Tennelec, Inc., 601 Oak Ridge Turnpike, Oak Ridge, TN 37830
335. Dr. Lubomir David, Director, Centro de Física, Instituto Venezolano de Investigaciones Cientificas (IVIC), Apartado 1827, Caracas 1010-A, Venezuela
336. Dr. Robert F. Davis, Department of Materials Science & Engineering, North Carolina State University, Box 7907, Raleigh, NC 27695
337. Prof. Dr. P. H. Dederichs, Institut für Festkörperforschung der Forschungszentrum Jülich GmbH, Postfach 1913, 5170 Jülich 1, Germany
338. Dr. Steven Derenzo, MS-55-121, 1 Cyclotron Road, Lawrence Berkeley Laboratory, Berkeley, CA 94720
339. Dr. Adriaan M. de Graaf, Division of Materials Research, National Science Foundation, 1800 G Street NW, Washington, DC 20550
340. Dr. J. Diehl, Max-Planck-Institut für Metallforschung, Institut für Werkstoffwissenschaften, Sestrasse 92/BRD, D-7000 Stuttgart 1, Germany
341. Dr. J. Dienes, Department of Physics 510B, Brookhaven National Laboratory, Upton, NY 11973
342. Prof. Dr. H.-D. Dietze, Institut fur Theoretische Physik C, RWTH Aachen, 5100 Aachen, Germany
343. Dr. Sam Divita, U.S. Army Communications, Electronics Command, AMSEL-COM-RM1, Fiber Optics Team, Ft. Monmouth, NJ 07703
344. Dr. G. Dolling, Atomic Energy of Canada Limited, Chalk River Nuclear Laboratories, Chalk River, Ontario KOJ 1JO, Canada
345. Dr. D. G. Doran, Hanford Engineering Development Laboratory, P.O. Box 1970, Richland, WA 99352
346. Dr. Mildred Dresselhaus, Rm. 13-2090, Massachusetts Institute of Technology, Cambridge, MA 02139
347. Dr. C. B. Duke, Xerox Webster Research Center, 800 Phillips Rd 0114-38D, Webster, NY 14850
348. Dr. B. D. Dunlap, Argonne National Laboratory, MSD-212, 9700 South Cass Avenue, Argonne, IL 60439
349. Dr. Robert C. Dynes, Department of Physics, 0319, University of California-San Diego, La Jolla, CA 92093
350. Dr. Dean E. Eastman, Vice-President of Logic, Memory, and Packaging, International Business Machines Corporation, P.O. Box 218, Yorktown Heights, NY 10598
351. Dr. Norman Edelstein, MMRD/Bldg. 70A/Room 1115, Lawrence Berkeley Laboratory, Berkeley, CA 94720

352. Prof. Henry Ehrenreich, Division of Engineering and Applied Physics, Pierce Hall 205A, Harvard University, Cambridge, MA 02138
353. Dr. Vic Emery, Department of Physics, Brookhaven National Laboratory, Upton, NY 11973
354. Dr. Ahmet Erbil, School of Physics, Georgia Institute of Technology, 225 North Avenue, Atlanta, GA 30332-0430
355. Prof. T. L. Estle, Physics Department, Rice University, Houston, TX 77001
356. Dr. Peder J. Estrup, Department of Physics, Brown University, Providence, RI 02912
357. Dr. R. C. Ewing, Department of Geology, University of New Mexico, Albuquerque, NM 87131
358. Ms. Harriet L. Fadem, Librarian, National Synchrotron Light Source, Brookhaven National Laboratory, Upton, Long Island, NY 11973
359. Dr. G. C. Farlow, Physics Department, Wright State University, Dayton, OH 45435
360. Dr. G. C. Farrington, Department of Materials Science and Engineering, University of Pennsylvania, 3231 Walnut Street, LSRM Building K-1, Philadelphia, PA 19104
360. Prof. Robert S. Feigelson, Center for Materials Research, Stanford University, 105 McCullough Building, Stanford, CA 94305
361. Dr. Jack Feinberg, Department of Physics, SSC-421, University of Southern California, Los Angeles, CA 90089-0484
362. Dr. G. P. Felcher, Argonne National Laboratory, 9700 South Cass Avenue, Argonne, IL 60439
363. Dr. Trevor R. Finlayson, Department of Physics, Monash University, Clayton, Victoria, 3168, Australia
364. Mr. David Fitzgerald, President, Tennessee Innovation Center, Inc., 120 Badger Avenue, P.O. Box 607, Oak Ridge, TN 37830
365. Dr. Robert Fleischer, General Electric Research & Development Center, P. O. Box 8, Schenectady, NY 12301
366. Dr. M. Fluss, Lawrence Livermore National Laboratory, L-326, P. O. Box 808, Livermore, CA 94550
367. Dr. C. Peter Flynn, Materials Research Laboratory, University of Illinois, 104 S. Goodwin, Urbana, IL 61801
368. Dr. F. Y. Fradin, Associate Laboratory Director for Physical Sciences, Argonne National Laboratory, Building 221, 9700 South Cass Avenue, Argonne, IL 60439
369. Prof. Dr. Werner Frank, Max-Planck-Institut für Metallforschung, Institut für Physik, Heisenbergstrasse 1, D-7000, Stuttgart 80, Germany
370. Dr. Roger Frech, Department of Chemistry, University of Oklahoma, Norman, OK 73019
371. Prof. Arthur Freeman, Physics Department, Northwestern University, Evanston, IL 60201
372. Dr. Roger H. French, Central Research & Development Department, E.I. du Pont de Nemours & Co., Experimental Station, E356-323, Wilmington, DE 19898
373. Dr. J. Friedel, Physique des Solides, Universite Paris Sud, 91405 Orsay, France
374. Dr. A. T. Fromhold, Department of Physics, Auburn University, Auburn, AL 36849
375. Dr. Noboru Fukuoka, Division of Science, Naruto University of Teacher Education, Naruto, Tokushima 772, Japan
676. Dr. Y. Fujii, Institute of Solid State Physics, University of Tokyo, Roppongi Minato-ku, Tokyo 106, Japan
377. Dr. S. Funahashi, Japan Atomic Energy Research Institute, Tokai-mura, Naka-gun, Ibaraki-ken, Japan
378. Dr. B. Gaulin, McMaster University, Dept. of Physics, 1280 Main Street West, Hamilton, Ontario, L8S 4M1, Canada
379. Dr. J. F. Gibbons, Stanford Electronics Laboratories, McCullough 220, Stanford University, Stanford, CA 94305
380. Dr. Doon Gibbs, Brookhaven National Laboratory, Upton, NY 11973
381. Dr. A. N. Goland, Associate Chairman for Energy Sciences, Department of Applied Sciences, Bldg. 179A, Brookhaven National Laboratory, Upton, NY 11973
382. Dr. A. Golanski, C.N.E.T.-R.P.T., B.P. 98, 38240 Meylan, France
383. Dr. R. J. Gottschall, Metallurgy & Ceramics Branch, Division of Materials Sciences, Office of Basic Energy Sciences, ER-131, Washington, D.C. 20585

384. Dr. M. Guinan, Lawrence Livermore National Laboratory, P.O. Box 808, Livermore, CA 94550

385. Dr. Mark Hagen, Neutron Division, Rutherford Appleton Laboratory, Chilton, Didcot OXON OX11 OQX, United Kingdom

386. Dr. B. N. Harmon, Ames Laboratory, Iowa State University, Ames, IA 50011

387. Dr. Craig S. Hartley, Department of Materials Engineering, University of Alabama at Birmingham, Birmingham, AL 35294

388. Dr. Werner Heiland, Fachbereich Physik, Universität Osnabrück, Postfach 4469, D-4500 Osnabrück, Germany

389. Dr. T. J. Hicks, Department of Physics, Monash University, Clayton, Victoria, Australia 3168

390. Dr. W. O. Hofer, Forschungszentrum, Postfach 1913, D-5170, Jülich, Germany

391–395. Dr. William A. Hoffman, Jr., Director, Oak Ridge Science Semester, GLCA, Denison University, Main Street, Granville, OH 43023

396. Dr. P. H. Holloway, Department of Materials Sciences and Engineering, University of Florida, Gainesville, FL 32601

397. Dr. Marc Hou, Physique des Surfaces, Faculté des Sciences, Université Libre de Bruxelles, Campus de la Plaine (C.P. 234), Boulevard de Triomphe, B-1050 Bruxelles, Belgium

398. Dr. John J. Hren, North Carolina State University, Raleigh, NC 27607

399. Dr. A. E. Hughes, Materials Development Division B552, Atomic Energy Research Establishment, Harwell, Didcot, Oxon OX11 ORA, United Kingdom

400. Dr. Tom Hutchinson, A114 Thornton Hall, University of Virginia, Charlottesville, VA 22901

401. Dr. Louis C. Ianniello, Deputy Associate Director for Basic Energy Sciences, Office of Energy Research, ER-11, Department of Energy, Washington, DC 20585

402. Dr. M. Iizumi, Deputy Director General, Tokai Research Establishment, Japan Atomic Energy Research Institute, Tokai-mura, Naka-gun, Ibaraki-ken, Japan

403. Dr. Tadao Iwata, Division of Physics, Japan Atomic Energy Research Institute, Tokai-mura, Naka-gun, Ibaraki-ken 319-11, Japan

404. Dr. P. K. Iyengar, Director, Physics and Chemical Groups, Bhabha Atomic Research Centre, Bombay 400 085, India

405. Dr. Vincent Jaccarino, Department of Physics, University of California, Santa Barbara, CA 93106

406. Dr. Leslie H. Jenkins, 817 Whirlaway Circle, Knoxville, TN 37923

407. Ms. Beth Jinkerson, University Programs Division, Oak Ridge Associated Universities, P.O. Box 117, Oak Ridge, TN 37830

408. Dr. A. Wayne Johnson, Division 5126, Sandia National Laboratories, Albuquerque, NM 87185

409. Dr. Pierre H. Jourde, Charge du Centre d'Information sur les Déchets Nucléaires, CEA/DCAEA/CIDN, CEN/CADARACHE, B.P. 1, F 13115 Saint Paul lez Durance, France

410. Dr. S. Katono, Japan Atomic Energy Research Institute, Tokai-mura, Naka-gun, Iboraki-ken, Japan

411. Dr. W. A. Kamitakahara, Division of Materials Sciences, Office of Basic Energy Sciences, Office of Energy Research, ER-132, Department of Energy, Washington, DC 20585

412. Dr. Takaji Kaneda, Research Laboratories, Ashigara, Fuji Photo Film Company, Ltd., Minami-Ashigara, Kanagawa, 250-01 Japan

413. Dr. Elton N. Kaufmann, Building 207 (TTC), Argonne National Laboratory, 9700 South Cass Avenue, Argonne, IL 60439

414. Dr. Shinji Katano, Research Reactor Institute, Kyoto University, Kumatori, Sennan, Osaka 590-04, Japan

415. Dr. Fred Keller, Department of Physics, Clemson University, Clemson, SC 29631

416. Dr. Richard D. Kelley, Division of Materials Sciences, Office of Basic Energy Sciences, Office of Energy Research, ER-132, Department of Energy, Washington, DC 20585

417. Dr. Q. H. Khan, N.P.D., PINSTECH, P.O. Nilore, Rawalpindi, Pakistan

418. Dr. J. K. Kjems, Risø National Laboratory, DK-4000 Roskilde, Denmark

419. Dr. J. S. Koehler, Physics Department, University of Illinois, Urbana, IL 61801

420. Prof. Walter Kohn, Physics Department, University of California, Santa Barbara, CA 93106

421. Dr. Daniel E. Koshland, Jr., Editor, *Science*, 1515 Massachusetts Avenue N.W., Washington, DC 20005

422. Prof. Eckhard Krätzig, Universitat Osnabrück, Fachbereich Physik, Postfach 4469, 4500 Osnabrück, Germany

423. Prof. J. Kübler, Theoretische Physik, Institut für Festkörperphysik, Technische Hochschule Darmstadt, Hochschulstrasse 2, 6100 Darmstadt, Germany

424. Dr. Gerard H. Lander, Tu-Euratom, Postfach 2340, D7500, Karlsruhe, Germany

425. Dr. S. S. Lau, Department of EECS, C-014, University of California at San Diego, La Jolla, CA 92093

426. Dr. R. A. Laudise, Director, Materials and Processing Research Laboratory, AT&T Bell Laboratories, 600 Mountain Avenue, Murray Hill, NJ 07974

427. Library, Building 465, Atomic Energy Research Establishment, Harwell, Didcot, Oxon OX11 ORB, United Kingdom

428. Library, Department of Physics, Quaid-I-Azam, University Islamabad, Pakistan

429. Dr. A. B. Lidiard, Theoretical Physics Division, Building 424.4, Atomic Energy Research Establishment, Harwell, Didcot, Oxon OX11 ORA, United Kingdom

430. Prof. Per-Anker Lindgård, Physics Department, Risø National Laboratory, DK-4000 Roskilde, Denmark

431. Dr. W. M. Lomer, Director, UKAEA Culham Laboratory, Abingdon, Oxon OX14 3DB, United Kingdom

432. Dr. C.-K. Loong, Argonne National Laboratory, 9700 S. Cass Avenue, Argonne, IL 60439

433. Dr. Stephen W. Lovesey, Rutherford Appleton Laboratory, Chilton, Didcot, Oxon OX11 OQX, United Kingdom

434. Dr. G. Lucovsky, Department of Physics, North Carolina State University, Raleigh, NC 27650

435. Dr. Siu-Ching Lui, 2403 Merrywood Drive, Edison, NJ 08817

436. Dr. W. Lutze, Hahn-Meitner-Institut für Kernforschung, Gleinicker Strasse 100, D1000, Berlin 39, Germany

437. Dr. D. W. Lynch, Department of Physics, Iowa State University, Ames, IA 50011

438. Dr. J. W. Lynn, Department of Physics, University of Maryland, College Park, MD 20742

439. Prof. Allan R. Mackintosh, Physics Laboratory, H. C. Oersted Institute, Universitetsparken 5, DK 2100 Copenhagen, Denmark

440. Dr. R. W. Major, Department of Physics, University of Richmond, Richmond, VA 23173

441. Dr. W. C. Mallard, Department of Physics and Astronomy, Georgia State University, Atlanta, GA 30303

442. Dr. P. M. Marcus, T. J. Watson Research Center, International Business Machines Corporation, P.O. Box 218, Yorktown Heights, NY 10598

443. Dr. J. W. Mayer, Department of Materials Sciences, Cornell University, Ithaca, NY 14853

444. Dr. G. L. McVay, Battelle-Pacific Northwest Laboratories, Richland, WA 99352

445. Dr. James L. Merz, Electrical and Computer Engineering Department, University of California, Santa Barbara, CA 93106

446. Dr. I. V. Mitchell, Department of Physics, Physics and Astronomy Building, University of Western Ontario, London, Ontario N6A 3K7, Canada

447. Dr. Y. Morii, Japan Atomic Energy Research Institute, Tokai-mura, Naka-gun, Ibaraki-ken 319-11, Japan

448. Prof. K. A. Müller, Manager, Physics Department, International Business Machines Corporation, Forschungslaboratorium Zurich, CH-8803 Rüschlikon, Saumerstrasse 4, Switzerland

449. Prof. Klaus E. Müller, University of Erlangen–Nürnberg, Institut für Angewandt Physik, Lehrstuhl für Festkörperphysik, Erwin-Rommel-Str 1, D-8520 Erlangen, Germany

450. Dr. R. B. Murray, Office of Graduate Studies, University of Delaware, Newark, DE 19711

451. Dr. H. Naramoto, Department of Physics, Japan Atomic Energy Research Institute, Tokai, Ibaraki, Japan

452. Dr. Jagdish Narayan, Division of Materials Research, National Science Foundation, 1800 G Street NW, Washington, DC 20550

453. Dr. Stuart Nelson, Director, Northern Research Laboratories, UK Atomic Energy Authority, Risley, Warrington, Cheshire WA3 6AT, United Kingdom
454. Dr. M.-A. Nicolet, Department of Electrical Engineering, 116–81, California Institute of Technology, Pasadena, CA 91125
455. Dr. A. S. Nowick, Columbia University, 1146 S. W. Mudd Building, New York, NY 10027
456. Oak Ridge Institute for Science and Education (ORISE), DOE/Oak Ridge Associated Universities, ATTN: H. T. Burn, Librarian, Information Center/EES, P. O. Box 117, Oak Ridge, TN 37831-0117
457. Office of Assistant Manager for Energy Research and Development, Department of Energy, Oak Ridge Operations Office, Oak Ridge, TN 37831
458–557. Office of Information Services, Oak Ridge Associated Universities, P.O. Box 117, Oak Ridge, TN 37831 (100 copies)
558. Dr. O. S. Oen, 119 Lehigh Lane, Oak Ridge, TN 37830
559. Dr. D. N. Olson, Department of Physics, St. Olaf College, Northfield, MN 55057
560. Dr. W. T. Oosterhuis, Chief, Solid State Sciences Branch, Division of Materials Sciences, Office of Basic Energy Sciences, ER-132, Washington, D.C. 20585
561. Dr. V. M. Orera, Departamento de Optica, Facultad de Ciencias, Universidad de Zaragoza, Zaragoza, Spain
562. Dr. A. W. Overhauser, Department of Physics, Purdue University, West Lafayette, IN 47907
563. Dr. Robert L. Park, Director, Center for Materials Research, University of Maryland, College Park, MD 20742
564. Dr. D. Parkin, Los Alamos National Laboratory, MS-K765, P. O. Box 1663, Los Alamos, NM 87545
565. Dr. P. S. Peercy, Division 5112, Sandia National Laboratories, Albuquerque, NM 87115
566. Dr. Hans Peisl, Sektion Physik, Universitat München, Geschwister-Scholl-Platz 1, 8000 München 22, Germany
567. Dr. Norman E. Phillips, Lawrence Berkeley Laboratory, Cyclotron Road, Berkeley, CA 94720
568. Physics/Optics/Astronomy Library, 374 Bausch and Lomb Building, University of Rochester, Rochester, NY 14627
569. Dr. Lothar A. R. Pintschovius, Kernforschungszentrum Karlsruhe GmbH, Postfach 3640, D-7500 Karlsruhe 1, Germany
570. Dr. E. W. Plummer, Department of Physics, University of Pennsylvania, Philadelphia, PA 19104
571. Dr. J. M. Poate, AT&T Bell Laboratories, 600 Mountain Avenue. Murray Hill, NJ 07974
572. Dr. C. P. Poole, Department of Physics, University of South Carolina, Columbia, SC 29208
573. Dr. Richard C. Powell, Physics Department, Oklahoma State University, Stillwater, OK 44078
574. Dr. Rene Pretorius, Head, Ion-Solid Interaction Division, National Accelerator Centre, P.O. Box 72, Faure 7131, South Africa
575. Dr. P. P. Pronko, Universal Energy Systems, 3195 Plainfield Road, Dayton, OH 45432
576. Dr. Roger Pynn, LANSCE, MS H805, Los Alamos National Laboratory, Los Alamos, NM 87545
577. Dr. Y. Quéré, Centre d'Études Nucléaires de Fontenay-aux-Roses, B.P. No. 6, 92260 Fontenay-aux-Roses (Seine), France
578. Dr. John J. Quinn, Department of Physics and Astronomy, The University of Tennessee, 200 South College, Knoxville, TN 37996-1501
579. Dr. V. R. Ramakrishnan, Biology Department, Brookhaven National Laboratory, Upton, NY 11973
580. Dr. Michel Rappaz, Ecole Polytechnique Fédérale de Lausanne, Department des Matériaux, 34 ch. de Bellerive, CH-1007, Lausanne, Switzerland
581. Dr. W. Reichardt, Kernforschungszentrum Karlsruhe GmbH, Institut für Angewandte Kernphysik 1, Postfach 3640, D-7500 Karlsruhe, Germany
582. Dr. James Rhyne, Research Reactor Facility, University of Missouri, Columbia, MO 65211
583. Dr. James R. Rice, Division of Applied Sciences, Rm 224, Pierce Hall, Harvard University, 29 Oxford Street, Cambridge, MA 02138

End Date
12/30/92